Modeling of electrons in the heliosphere

R R Nndanganeni

20884648

Thesis submitted for the degree *Philosophiae Doctor* in Space Physics at the Potchefstroom Campus of the North-West University

Promoter: Prof M S Potgieter

May 2016

Abstract

The propagation and modulation of electrons in the heliosphere play an important part in improving our understanding and assessment of the processes of solar modulation. A locally developed, full three-dimensional, numerical model is used to study the modulation of Jovian and galactic electrons from 1 MeV to 50 GeV, and from the Earth into the heliosheath. Modeling results are compared with Voyager 1 observations in the outer heliosphere, including the heliosheath, as well as observations at or near the Earth, in particular the 2009 spectrum from the PAMELA space mission and from Voyager 1 for 1977. First, new heliopause spectra for galactic electrons are established. The issue of the intensity levels and the spectral shape of the local interstellar spectrum at lower energies is specifically addressed. The heliopause is assumed at 122 AU in the model. The extra-ordinary large increase of galactic electrons in the 5 MeV to 50 MeV range in the heliosheath is investigated. The modeling confirms that the heliosheath acts as a most effective modulation barrier for these low energy electrons. This is followed by establishing new Jovian electron source functions, also addressing its level of intensity and its spectral shape. Modulated electron spectra from the inner to the outer heliosphere are computed, first separately for Jovian and galactic electrons and then for the combined modulation. After combining these results, the intensity levels of galactic and Jovian electrons at the Earth below 50 MeV could be estimated. The energy range could be established over which the Jovian electrons dominate over galactic electrons in the inner heliosphere, a process which depends strongly on what is assumed for the Jovian electron source function. Conclusions are made about diffusion and drift theory as applicable to electrons in the heliosphere. Ways of reducing particle drifts explicitly and implicitly are investigated with interesting results. Increasing the rigidity dependence of the drift coefficient at lower energies very effectively reduces the extent to which particle drifts play a role in the modulation process. Concerning diffusion, a general result is that the rigidity dependence of both the parallel and perpendicular diffusion coefficients needs to be constant below ~0.4 GV, but to increase above this rigidity to assure compatibility between the modeling and observations at the Earth, and especially in the outer heliosphere. A modification in the radial dependence of the diffusion coefficients in the inner heliosheath is required to compute modulation that is compatible with observations in this region.

Keywords: Cosmic rays, galactic electrons, Jovian electrons, particle drifts, galactic spectra, heliospheric modulation, solar modulation, very local interstellar spectrum

Samevatting

Die transport en modulasie van elektrone in die heliosfeer speel 'n belangrike rol in die verbetering van ons begrip en assessering van die prosesse verantwoordelik vir modulasie. 'n Drie-dimensionele numeriese model wat plaaslik ontwikkel is, word gebruik vir die studie van joviaanse en galaktiese elektrone, van 1 MeV tot 50 GeV, en vanaf die Aarde tot in die heliomantel. Modelresultate word vergelyk met waarnemings wat met die ruimtetuig Voyager 1 in die buitenste heliosfeer en in 1977 naby die Aarde gemaak is. Dit sluit ook die elektronspektrum vir 2009 van die PAMELA ruimtemissie in. Eerstens is nuwe heliopouse spektra vir galaktiese elektrone bepaal. Die intensiteitvlak en spektraalvorm van hierdie spektra by lae energie is spesifiek ondersoek. Die heliopouse is by 122 astronomiese eenhede (AE) geplaas. Die buitengewone groot toename van galaktiese elektrone in die heliomantel in die 5 tot 50 MeV gebied is ondersoek. Die modelering bevestig dat die heliomantel as 'n hoogs effektiewe modulasie hindernis vir hierdie lae energie elektrone optree. Die navorsing is opgevolg deur die vasstel van nuwe bronfunksies vir joviaanse elektrone, waarin ook die intensiteitsvlakke en spektraalvorms ondersoek is. Moduleerde elektronspektra is bereken van die binneste tot die buitenste heliosfeer, eerstens afsonderlik vir joviaanse en galaktiese elektrone, en dan vir die gekombineerde spektra. Daarna is die intensiteitvlakke van hierdie soort elektrone onder 50 MeV by die Aarde bepaal, en die energie-grense bereken waar die joviaans elektrone die galaktiese elektrone oorskadu. Hierdie proses hang sterk af van die bronfunksie wat gebruik word. Gevolgtrekkings word gemaak oor diffusie- en dryfteorie soos van toepassing op elektrone in die heliosfeer. Metodes om die vermindering van dryf te bewerkstellig op eksplisiete en implisiete wyse word illustreer, met interessante resultate. Die toename in die styfheidsafhanklikheid van die dryfkoëffisient by lae energie is hoogs effektief om die modulasie-effekte van dryf daar te verminder. Wat diffusie betref is die algemene resultaat verkry dat die styfheidsafhanklikheid van beide die parallelle en loodregte diffusiekoëffisiente onder ~0.4 GV konstant moet wees, maar toeneem bokant hierdie waarde om ooreenstemming met genoemde waarnemings te verkry. Modifikasie van die radiale afhanklikheid van die diffusiekoëffisiente in die binneste heliomantel is nodig om elektron-waarnemings daar te verklaar.

Nomenclature

2D	Two-dimensional
3D	Three-dimensional
ACRs	Anomalous Cosmic Rays
AMS	Alpha Magnetic Spectrometer
AU	Astronomical units = 1.49×10^{8} km
CIRs	Corotating Interaction Regions
CMEs	Coronal Mass Ejections
CRs	Cosmic Rays
DCs	Diffusion Coefficients
DR	Distributed re-acceleration
DRD	Diffusive re-acceleration with damping
ESA	European Space Agency
GCRs	Galactic Cosmic Rays
GS	Galactic Spectra
HCS	Heliospheric Current Sheet
HMF	Heliospheric Magnetic Field
HP	Heliopause
HPS	Heliopause Spectrum/Spectra
IS	Interstellar Spectrum/Spectra
LIS	Local Interstellar Spectrum/Spectra
LISM	Local Interstellar Medium
MFP	Mean Free Path
NASA	National Aeronautic and Space Administration
PAMELA	Payload for Antimatter/ Matter Exploration and Light-nuclei Astrophysics
PD	Plain Diffusion
QLT	Quasi-Linear Theory
SEPs	Solar Energetic Particles
SOHO	Solar and Heliospheric Observatory
TPE	Transport Equation
TS	Termination Shock
V1	Voyager 1
V2	Voyager 2

Table of Contents

Chapter 1

Introduction

Cosmic rays (CRs) are charged particles, which, after being accelerated to very high energies in galactic space and beyond, propagate towards the solar system. As they propagate from the local interstellar medium into the heliosphere and up to the Earth, their intensity changes as a function of position, time and energy, following a process that is called the solar modulation of CRs. In this thesis the modulation of two populations of the CRs are studied; galactic electrons and electrons of Jovian origin. The main focus is on their global features as obtained with numerical modeling of which the results are compared to sets of selected observations relevant to each population. The computed intensities up to the Earth and out into the heliosheath are of particular importance. The latter is done to determine a heliopause spectrum (HPS) for galactic electrons while the first study is used to determine the Jovian electron intensity in the inner heliosphere and then predict the intensity of galactic electrons at the Earth.

The transport and propagation processes of these particles inside the heliosphere are described by a basic transport equation (Parker 1965), with several important mechanisms included, and which needs to be studied systematically to fully understand the solar modulation of these particles. This equation, applied to a three-dimensional (3D) heliosphere, is complex, and as such it must be solved numerically. In this study a 3D numerical model, developed by Ferreira (2002), is used and applied to study these electrons in terms of their spectra and radial profiles at selected energy ranges.

The first main objective of this study is to determine new very local interstellar spectra (LIS), or alternatively called HPS specifically for low energy electrons (1-100 MeV) by comparing numerical results to recent Voyager 1 observations. The second objective is to revisit the issue of determining a source function for Jovian electrons, in terms of its spectral index and intensity level. Two new alternative source functions are presented and investigated.

A second main objective is to use the comparison between the model and the available observations to determine the rigidity dependence of the relevant diffusion coefficients at these low energies, and to establish how this may change from the inner to the outer heliosphere. The role of particle drifts is revisited as applied to electrons in order to establish

over which energy range drifts effectively influence their modulation. Ways of reducing drifts explicitly and implicitly are investigated.
From the combined modulation of these particles, the energy range where each of them dominates can be determined from a spectral point of view. Subsequently, the model is used to predict the intensity of these low energy galactic electrons at Earth, and the results are compared to the previous results that were calculated from the radial dependent point of view (Potgieter and Nndanganeni 2013a).

The structure of this thesis is as follows:

Chapter 2 provides the basic concepts about CRs, the heliosphere and the solar modulation of CRs. This includes a brief discussion of the solar wind, the heliospheric magnetic field (HMF), the heliospheric current sheet (HCS), the geometry of the heliosphere, solar cycle variations and some aspects of charged particles in the heliosphere, but in particular galactic and Jovian electrons. The chapter ends with a brief description of selected spacecraft missions, which provide important observations used in comparison with the results from numerical modeling.

Chapter 3 gives a brief discussion of the basic modulation theory, the relevant transport equation and modulation processes. This is followed by a short review of the comprehensive full 3D numerical model in a steady state. The relevant modulation coefficients, for diffusion and drifts, are given with specific attention to their radial, and the rigidity dependence and the values assumed.

Chapter 4 is devoted to establishing the new HPS or very LIS for galactic electrons over an energy range from 1 MeV to 50 GeV which is an important requirement for studying the solar modulation of electrons with numerical modeling. A HPS needs to be specified at the heliospheric modulation boundary, usually taken as the heliopause (HP), as an input spectrum (initial condition) to be modulated inside the heliosphere as a function of energy and position. First, the background and information about published galactic electron spectra are given, including various approaches that have been presented in the literature on the topic of galactic and local interstellar electron spectra. This chapter is focused on the heliospheric modulation of galactic electrons, using two particular HPS as input for the 3D modulation model. It will be shown that the two HPS selected give good compatibility with the Voyager 1 observations in the outer heliosphere and beyond the HP, while also reproducing the PAMELA

observations at the Earth. The consequence for the diffusion coefficients required in the numerical model is shown and its implication on the modulated spectra is briefly discussed.

Chapter 5 is focused on the modulation of Jovian electrons in the inner heliosphere. First, the controversy is addressed concerning the spectral index of the Jovian electron source function and the level of its intensity, from the lowest to the highest energies of relevance. Both the modulation model and observations are used to investigate these aspects. In the process two new alternative source functions are computed so that the energy range where the Jovian electron intensity dominates the total electron intensity in the heliosphere could be estimated. The effects of these two new source functions on the Jovian electron modulation and on total electron modulation are investigated.

Chapter 6 is devoted to studying the effects of gradient, curvature and HCS drifts on the modulation of galactic electrons. The effects on the global modulation of electrons and how its reduction influences these effects are revisited by studying different modulation scenarios using the numerical model. Ways of reducing drifts explicitly and implicitly are illustrated, and the consequences are discussed. It will be shown how reducing the drift coefficient with decreasing rigidity can reduce the extent to which drifts play a role in the modulation process in the heliosphere. The energy range is shown where drifts are most effective and where they completely dissipates.

Chapter 7 is focused on the total electron modulation that occurs in the heliosheath, motivated by the electron observations from Voyager 1. The main purpose is to gain a better understanding of how low energy electrons get modulated in this region, which is different from the rest of the heliosphere. This is done by comparing the model's output to these observations. The spectra in the heliosheath are computed along the Voyager 1 trajectory, followed by studying the effects of the thickness of the heliosheath and the effects of using different HPS. It is shown that modulation in this region affects the transport of CRs electrons differently and should be recognized as an eminent feature of the heliosphere that contributes to the overall modulation of CRs, especially at lower energies.

Chapter 8 is focused on the combined modulation of the Jovian and the galactic electrons in the heliosphere, from both experimental and modeling points of view. This is motivated by the PAMELA electron observations during the unusual solar minimum of 2009, together with the Voyager 1 observations made in 1977 close to the Earth. The first objective is to establish the energy range where the Jovian electrons dominate over the galactic electrons in the inner

heliosphere using computations based on the different scenarios presented for the Jovian source functions. Secondly, with the HPS established, a prediction is made of what the galactic electron intensity could be at the Earth, as a part of a long missing piece of the modulation puzzle.

Chapter 9 is a summary of the thesis work, along with the main results and conclusions. Pending aspects and future prospects related to this study are listed.

The published manuscripts in science journals partially based on the work presented in this thesis are:

1. Potgieter, M. S, Nndanganeni, R. R., The solar modulation of electrons in the heliosphere, Astrophys Space. Sci., 345, 33-40, 2013.
2. Potgieter, M. S., Nndanganeni, R. R., A local interstellar spectrum for galactic electrons, Astropart. Phys., 48, 25-29, 2013.

The published manuscripts in the proceedings of the International Cosmic Ray Conferences and other conferences based on the work presented in this thesis are:

1. Nndanganeni, R. R., Potgieter, M. S., The solar modulation of electrons in the heliosphere, Proc. 33rd Inter. Cosmic Ray Conf. (Rio de Janeiro, Brazil), icrc2013-0033, 2013.
2. Potgieter, M. S., Vos, E. E., Nndanganeni, R. R., Boezio, M., Munini, R., A very local interstellar spectrum for galactic electrons, Proc. 33rd Inter. Cosmic Ray Conf. (Rio de Janeiro, Brazil), icrc2013-0056, 2013.
3. Potgieter, M. S., Nndanganeni, R. R., Vos, E. E., Boezio, M., A heliopause spectrum for electrons, Proc. 33rd Inter. Cosmic Ray Conf. (Rio de Janeiro, Brazil), icrc2013-0070, 2013.
4. Potgieter, M. S., Vos, E. E., Nndanganeni, R. R., The first very local interstellar spectra for galactic protons, helium and electrons. Proc. 14th ICATPP Conference on Cosmic Rays for Particle and Astroparticle Physics, (Como, Italy), 8, 204-211, 2014.
5. Nndanganeni, R. R., Potgieter, M.S., Modelling of the solar modulation of Jovian electrons in the inner heliosphere, Proc. 34th Inter. Cosmic Ray Conf. (The Hague, The Netherlands), POS(ICRC2015) 165.
6. Nndanganeni, R. R., Potgieter, M. S., The effects of particle drifts on the modulation of galactic electrons in the global heliosphere, Proc. 34th Inter. Cosmic Ray Conf., (The Hague, The Netherlands), POS(ICRC2015) 166.

Chapter 2

Cosmic rays and the heliosphere

2.1 Introduction

This chapter is devoted to a discussion of the concepts and terminology important to cosmic ray electrons and their modulation in the heliosphere. An overview will be given of solar activity and how this is related to the solar wind and the heliospheric magnetic field (HMF), the two concepts of importance to cosmic ray modulation. The heliosphere, its geometry, plasmatic structure and features such as the termination shock (TS), heliosheath and heliopause (HP) will be briefly discussed. All these aspects are discussed in the context of what is relevant to the solar modulation of cosmic rays, with the emphasis on their global features. The chapter is concluded by a discussion of selected spacecraft missions, which provides relevant *in situ* observations and insight for modulation studies.

2.2 Solar activity

The Sun is the nearest star and it is on average 1 astronomical unit (AU) away from the Earth. It contains about ~ 98% of the total mass of the solar system and consists of ~90% Hydrogen and ~10% Helium with a small fraction of heavier elements (see e.g. Lodders 2003). The output of the Sun in all forms of light, the solar wind and energetic particles is not constant. It varies with both time and with position on the Sun (e.g. Jones et al. 2008). These changes collectively are called solar activity and are a reflection of changes below the Sunôs surface. Sunspots, as a visible example of solar activity, are temporary disturbances in the Sunôs photosphere. They appear dark because temperatures are considerably lower than the surrounding areas, and occur where magnetic field lines emerge from inside of the Sun to form expanding loops above its surface.

They may last for months and overall vary with an average of 11 years, which means they increase up to solar maximum, to decline afterwards to become rare during solar quiet times and are as such a direct indication of the level of solar activity (see e.g. Cliver 2015, Clette et al. 2015 and Bazilevskaya et al. 2015). A record of sunspot numbers is shown in Figure 2.1,

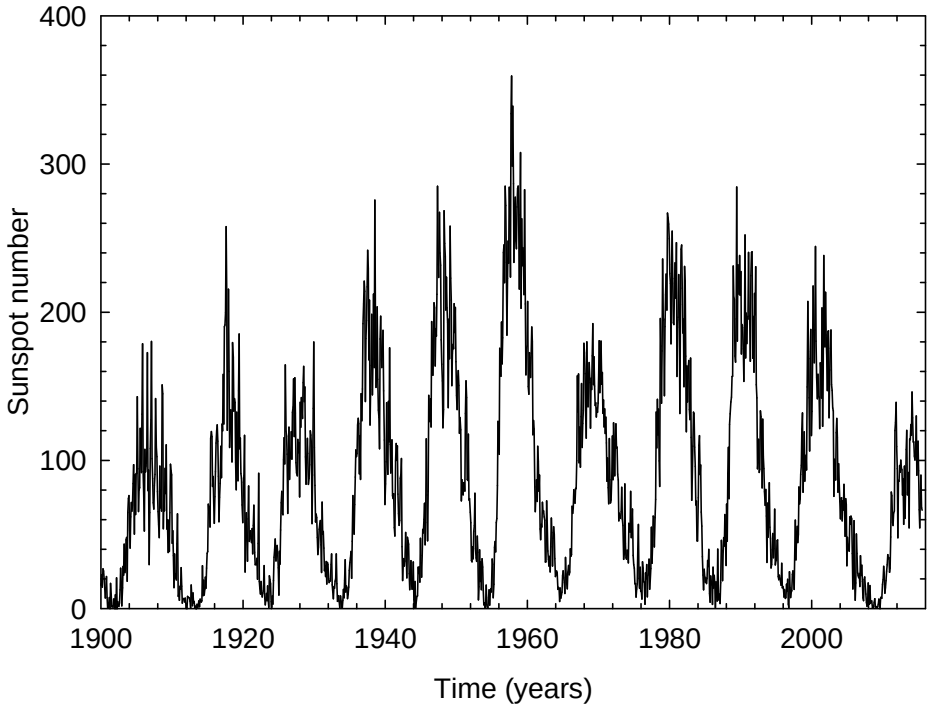

Figure 2.1: Monthly averaged sunspot number from the year 1900 to early 2015 as an illustration of the quasi-periodic behaviour of solar activity. Data from http://www.sidc.oma.be/.

as monthly averaged values, from the year 1900 up to early 2015 as an illustration of that theyhave a quasi-periodic 11 year cycle. See also the reviews by Hathaway (2010) and Usoskin (2013).

Solar activity produces space weather and even space climate that can affect the Earth in various ways. For comprehensive reviews on these interesting topics, see Scherer et al. (2006a) and reference therein; also Scherer et al. (2007); Schrijver et al. (2015) and Shea and Smart (2012).

2.3 The solar wind

The Sun gradually loses mass in the form of a flux of high speed protons and electrons leaking away from the Sunôs outer layer, called the solar wind (http://hyperphysics.phy-astr.gsu.edu/hbase/solar/solwin.html/, see also McComas et al. 2007). This plasmatic wind carries with it the imbedded magnetic field. The existence of the solar wind was predicted by Ludwig Biermann in 1951, from studying the shape of comets' tails as described in the review by Fichtner (2001). A theory and mathematical model explaining the solar wind and its characteristics was first introduced by Eugene Parker (Parker 1958).

The source of the solar wind is the Sun's hot corona; the temperature of the corona is so high that the Sun's gravity cannot hold on to it. The solar wind flows in an outward direction and carries magnetic clouds and interaction regions with it. Interaction regions can form when the high solar wind stream catches up with the slow solar wind. The high and slow speed streams interact with each other and pass by the Earth as the Sun rotates. The origin and the acceleration of the fast and slow solar wind are not well understood (e.g. Wang 2012) but observations from SOHO (e.g. Cranmer et al. 2007) have provided new insight. Among the important results obtained from these observations are that the fast and slow wind originates and accelerates in very different ways, related to the global structure of the corona. The bimodal solar wind flow is most evident near solar minimum. The fast solar wind is characterized by speeds of ~750-800 km.s^{-1} with relatively small fluctuations, and is directly associated with coronal holes and polar coronal holes and are often stable over long periods of time. The high speed solar wind is dominant during periods of low solar activity, and occupies the whole heliosphere at solar latitude larger than 20^{o}. The slow solar wind originates from equatorial coronal holes located in the vicinity of active regions and is characterized by an average speed of ~450 km.s^{-1} but with very large fluctuations.

(See the reviews by Cranmer (2012) and for Voyager observations, see http://solarscience.msfc.nasa.gov/SolarWind.shtml/), see also Richardson and Burlaga (2011). Figure 2.2 shows first the observed latitudinal dependence of the solar wind speed V (Philips et al. 1995) for solar minimum (solid black curve) and solar maximum (dashed dot) conditions for three fast latitudinal scans (FLS) that Ulysses made, indicated in the figure as FLS1 (cyan curve), FLS2 (red curve) and FLS3 (grey). The FLS1 and FLS3 occurred during solar minimum period whereas FLS2 occurred during solar maximum period (McComas et al. 2001, 2002, 2008). For the solar minimum period there is a clear dependence of V on latitude. During such conditions V can be divided into two distinct regions, namely a slow equatorial stream between ~20 ^{o} S and ~20 ^{o} N with an average speed of ~450 km.s^{-1} and a fast wind stream with an average of ~800 km.s^{-1} at a heliolatitude $\geq 20^{\circ}$ in the Northern and Southern hemisphere. FLS2 occurred during solar maximum and during this time the latitudinal dependence structure is not well defined, so that there is a mixture of fast and slow wind streams. During solar maximum conditions, the coronal holes are smaller and more or less uniformly distributed in the corona, so that this latitude dependence dissipates. In this context, see also e.g. Heber et al. (2003a); and the reviews by Heber and Potgieter (2006, 2008) and Heber (2013).

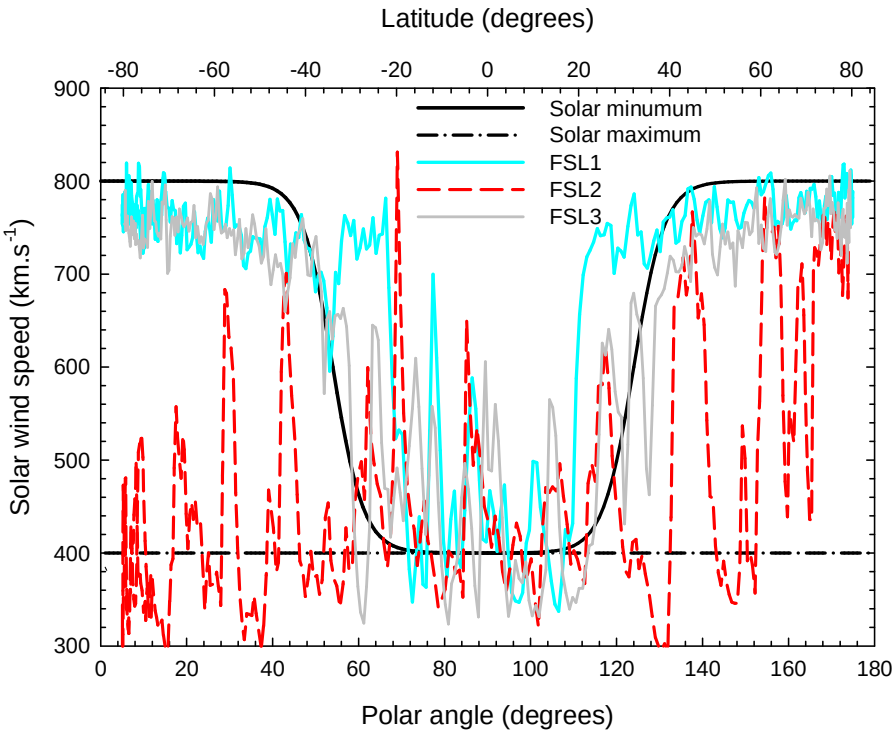

Figure 2.2: Solar wind speed measurements from Ulysses as a function of heliolatitude (top scale) for three fast latitude scans as indicated: FLS1 during July 1994-July 1995, FLS2 during October 2000-September 2000 and FLS3 during February 2007-January 2008 (McComas et al. 2002, 2008). The data obtained from http://cohoweb.gsfc.nasa.gov/. Also shown are the computed solar wind speed approximations as a function of polar angle θ for solar minimum (black solid curve; see Eq. 2.3) and solar maximum conditions (dash-dotted line; see Eq. 2.4).

On a global scale, thus neglecting smaller scale variations, the solar wind velocity **V** is assumed, for the purpose of cosmic ray numerical modeling as

$$\mathbf{V}(r,\theta) = V(r,\theta)\mathbf{e}_r = V(r)V(\theta)\mathbf{e}_r, \tag{2.1}$$

where r is radial distance in AU, θ the polar angle, and $\mathbf{e}_r$ the unit vector component in the radial direction. The radial dependence of the solar wind speed is approximated by

$$V(r) = V_0\left\{1-\exp\left[\frac{40}{3}\left(\frac{r_\odot - r}{r_0}\right)\right]\right\}, \tag{2.2}$$

with $V_0 = 400\,\mathrm{km.s^{-1}}, r_\odot$ the solar radius and $r_0 = 1$ AU (see e.g. Potgieter 1984).

The latitude dependence of the solar wind speed $V(\theta)$ during solar minimum conditions is given by

$$V(\theta) = 1.5 \mp 0.5 \tanh\left[\frac{2\pi}{45^{\circ}}\left(\theta - 90^{\circ} \pm \varphi\right)\right], \quad (2.3)$$

where the top and bottom signs correspond to the Northern $\left(0 \le \theta \le \pi/2\right)$ and Southern $\left(\pi/2 < \theta \le \pi\right)$ hemisphere respectively (see also e.g. Hattingh 1998; Langner 2004). For solar maximum conditions it is assumed to be independent of latitude so that

$$V(\theta) = 1. \quad (2.4)$$

Recently, Strauss (2010), Vos (2011) and Ngobeni (2015) followed a similar approach to model these basic features of the solar wind speed. These approximations are plotted in Figure 2.2 in comparison with the Ulysses solar wind observations.

2.4 The heliospheric magnetic field

The Sunôs magnetic field is embedded in the solar wind and is carried off into heliospheric space forming the HMF which is the physical framework in which charged energetic particles and all cosmic rays propagate. During solar minimum the HMF at Earth has an average magnitude of ~5 nT and this increases to be between 10 nT and 12 nT during solar maximum conditions. During the solar minimum of 2009 this value dropped to below 4 nT which has profound effects on solar modulation (see e.g. Cliver et al. 2013; Potgieter et al. 2014b).

Several space missions have provided a large amount of magnetic field observations (e.g. Balogh et al. 1995, Heber and Potgieter 2008) which have allowed testing Parkerôs (1958) basic approach. This has also provided a realistic framework for discussing the effects of the HMF on the propagation of CRs in the heliosphere. At solar minimum the HMF can be represented by a dominant dipole term so that a uniformly distributed magnetic field dominates. Heliospheric conditions around solar maximum are dominated by solar transients that occur at all heliolatitude and introduce a very large degree of unpredictability in the observed solar wind and corresponding HMF at all locations in the heliosphere. The HMF is clearly very dynamic, as controlled by the solar wind variability. Around solar minimum, the pattern of high speed solar wind streams and open magnetic field lines from the large polar coronal holes with the slow solar wind are associated with the near equatorial streamer belt. Resulting interaction creates well-known patterns of co-rotating interaction regions (CIRs) as one of the most prominent features of the inner heliosphere around solar minimum. For

reviews, see e.g. Smith et al. (2000a); Smith (2008); Solanki et al. (2006); Balogh and Erdõs (2013).

The Parkerõs HMF exhibits a spiral structure caused by the Sun rotating about an axis almost perpendicular to the equatorial plane and has become known as the Parker spiral field (Parker 1958, 1963). This spiral is shown in Figure 2.3. A mathematical model to describe the Parker spiral for radial distance $r \geq r_{\odot}$, as derived by Parker (1958), is given by the expression

$$\mathbf{B} = B_0 \left(\frac{r_0}{r} \right)^2 \left(\mathbf{e}_r - \tan\psi \mathbf{e}_\phi \right), \tag{2.5}$$

where $\mathbf{e}_r$ and $\mathbf{e}_\phi$ are unit vectors in the radial and azimuthal direction respectively, B_0 is the magnitude of HMF which have an average of ~5 nT at Earth, $r_0 = 1$ AU and ψ is the spiral angle defined as the average angle between the radial direction and the average HMF direction at a certain position. This spiral angle is expressed as

$$\psi = \arctan\left[\frac{\Omega\left(r - r_{\odot}\right)\sin\theta}{V} \right], \tag{2.6}$$

with Ω the angular velocity of the Sun about its rotation axis, $r_{\odot}$ the solar radius and V the solar wind speed. The spiral angle indicates how tightly wound is the spiral structure of the HMF lines. At very high latitudes the spiral angle is less tightly wound and the field lines are nearly radial. Substituting Eq. (2.6) into Eq. (2.5) yields for the HMF magnitude

$$B = \frac{B_0 r_0^2}{r^2} \sqrt{1 + \left(\frac{\Omega\left(r - r_{\odot}\right)\sin\theta}{V} \right)^2}, \tag{2.7}$$

throughout the heliosphere. The polar angle θ is measured from 0° at the polar axis of the Sun with $\theta = 90^{\circ}$ in the equatorial plane. Eq. (2.7) gives that B decreases as r^{-2} in the polar regions, thus overestimating drift effects in these regions. It was later realized that some modification was necessary, such that B will have to decrease like r^{-1} instead. Jokipii and Kóta (1989) proposed a modification, with their expression for the modified HMF magnitude given as

$$B = \frac{B_0 r_0^2}{r^2} \sqrt{1 + \left(\frac{\Omega\left(r - r_{\odot}\right)\sin\theta}{V} \right)^2 + \left(\frac{r\delta_m}{r_{\odot}} \right)}. \tag{2.8}$$

Steenberg (1998) and Langner (2004) improved on this using a modification

$$\delta(\theta) = \frac{\delta_m}{\sin\theta}, \tag{2. 9}$$

with $\delta_m = 8.7 \times 10^{-5}$ so that $\delta(\theta) = 0.002$ near the poles and $\delta(\theta) \approx 0$ in the equatorial plane. This type of modification is qualitatively supported by Ulyssesô HMF measurements over the polar regions (e.g. Balogh et al. 1995) and has been applied in many numerical models; see e.g. Haasbroek and Potgieter (1995), Potgieter and Ferreira (1999). See also the recent work by Raath (2014) and Raath et al. (2015) who have shown how these modifications affect the modulation of CRs by using alternative approaches.

Beside the Parker field and its modifications, more complex fields may exist e.g. Fisk type fields (Fisk 1996). Unfortunately this field is too complex to deal with straightforwardly in standard modulation codes, but progress has been made from a cosmic ray point of view; see e.g. Engelbrecht (2008). Sternal et al. (2011) presented a study which supports the existence of a Fisk-type field based on Ulysses/KET electron observations. However, for the purpose of this thesis the modified Parker HMF as described above, is used.

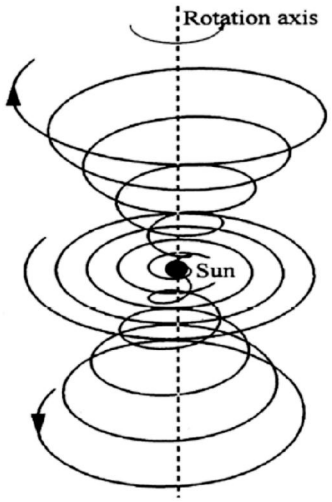

Figure 2.3: A 3D representation of the Parker HMF spiral structure with the Sun at the origin. Spirals rotate around the polar axis, here with polar angles of θ = 45°, θ = 90° and θ = 135°. From Hattingh (1998).

2.5 The heliospheric current sheet

Heliospheric current sheet (HCS) is the surface where the polarity of the Sunôs magnetic field changes direction locally. It is tilted by an angle α because the magnetic axis of the Sun is tilted relative to the Sunôs rotational axis (Hoeksema 1992). The HMF is divided into two sectors with opposite magnetic field polarities, separated by the HCS (Wilcox and Ness 1965; Smith et al. 2000b). The shape of the HCS results from the influence of the Sunôs rotating magnetic field on the plasma in the interplanetary medium, in essence determined by the combined effect of the tilt angle, solar rotation and the solar wind speed. It was later realised that the polarity jumps were due to the spacecraft crossing the HCS. Observations by e.g. Burlaga and Ness (1993) suggested that the HCS might cover the entire extent of the heliosphere; see also Smith (2001) for a detailed review of the HCS. The HCS has turned out to be one of the most successful modulation parameters when it was realized that the gradient and curvature drifts of cosmic ray particles should play an important role (Jokipii et al. 1977). Figure 2.4 depicts the averaged tilt angle α as a function of time as computed with the newer approach as described by T.J Hoeksema on http://wso.stanford.edu/. This new HCS model uses radial boundary conditions at the photosphere of the Sun to calculate these values. The α varies from a minimum value of $\sim 5^\circ$ at solar minimum activity to higher values of $\alpha = 75^\circ$ with increased solar activity. It is regarded as a good proxy for solar activity in CRs modulation studies because it is a prime indicator of solar magnetic activity from a drift-modulation point of view, and it is widely used in CRs data interpretation and modeling. The modulation effects of the HCS and global drifts, the subsequent 22-year cycle and charged-sign dependence have been studied in detail (e.g. Ferreira and Potgieter 2003; Ferreira et al. 2003a,b; Potgieter 2013a,b; Potgieter et al. 2014b). However, it is not known how the waviness is preserved throughout the outer heliosphere, especially what happens to it in the heliosheath (see e.g. Opher et al. 2009; Florinski 2011; Pogorelov et al. 2013; Strauss 2013) and needs to be studied in detail which is beyond the scope of this study.

For numerical modeling purposes, an expression for this wavy HCS was derived by Jokipii and Thomas (1981), given by

$$\theta' = \frac{\pi}{2} + \sin^{-1}\left(\sin\alpha \sin\left[\phi + \frac{\Omega(r - r_0)}{V} \right] \right), \tag{2.10}$$

with θ' the polar extent of the HCS and ϕ the azimuthal angle. For small values of α, the above equation reduces to

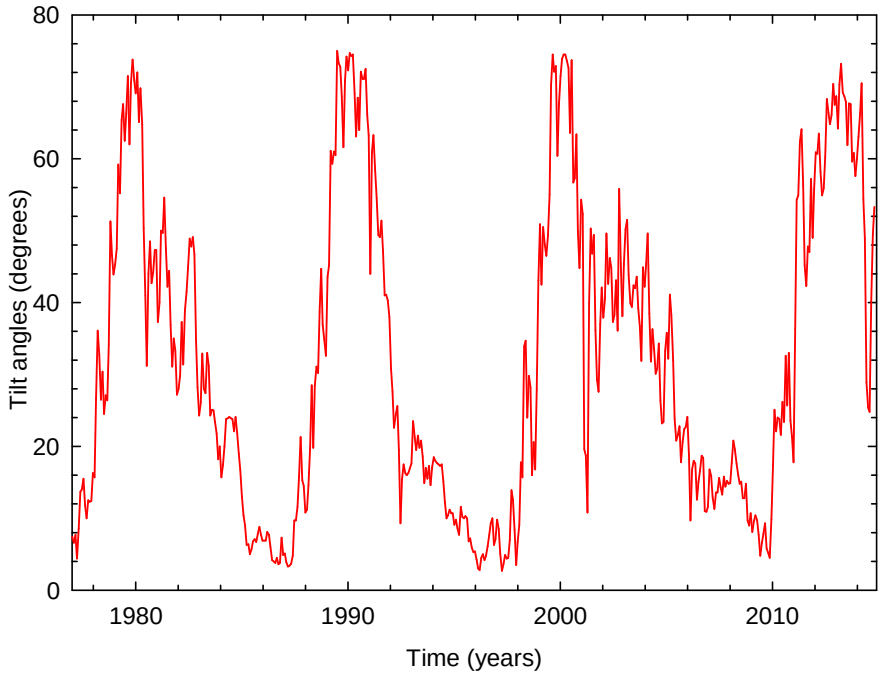

Figure 2.4: The HCS tilt angle as calculated since 1976 as a function of time. Maximum values indicate extreme solar activity when the polarity of the solar magnetic field changes and the minimum values indicate when solar activity is at its minimum. Data is from Wilcox Solar observatory: http://wso.stanford.edu/, courtesy of T.J Hoeksema.

$$\theta' \cong \frac{\pi}{2} + \alpha \sin\left[\phi + \frac{\Omega\left(r - r_0\right)}{V}\right]. \tag{2.11}$$

In order to incorporate the HCS into the HMF, it must be modified to

$$\mathbf{B} = A_c B_0 \left(\frac{r_0}{r}\right)^2 \left(\mathbf{e}_r - \tan\psi \mathbf{e}_\phi\right)\left[1 - 2H\left(\theta - \theta'\right)\right], \tag{2.12}$$

with $A_c \pm 1$ and $H(\theta - \theta')$ the Heaviside step function. The constant A_c determines the polarity of the HMF with $A_c \equiv +1$ for the $qA > 0$ polarity cycle and $A_c \equiv -1$ for the $qA < 0$ epochs.

The Heaviside step function is given by

$$H\left(\theta - \theta'\right) = \begin{cases} 0 \text{ when } \theta < \theta' \\ 1 \text{ when } \theta > \theta' \end{cases}, \tag{2.13}$$

and causes the HMF polarity to change across the HCS. If this function is used directly in numerical modeling it causes severe numerical problems (Langner 2004), so the Heaviside function is approximated by

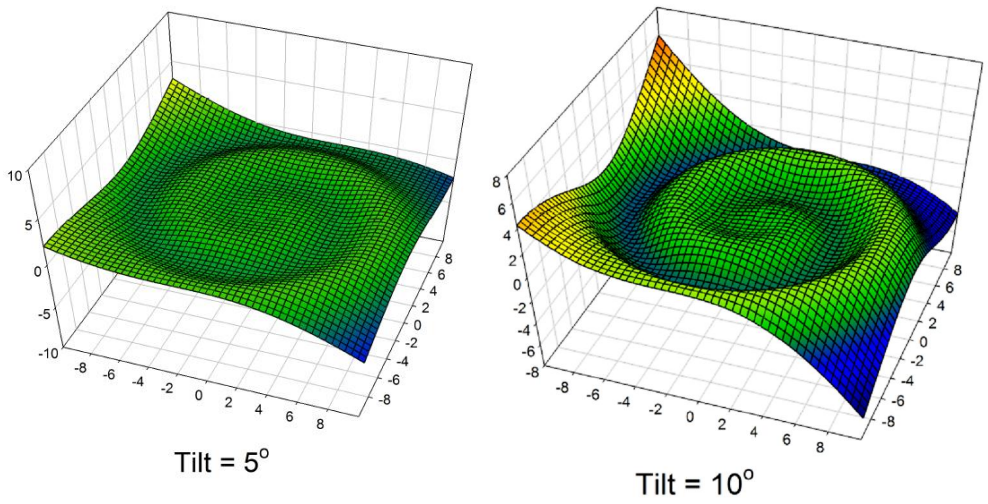

Figure 2.5: Simulations of the HCS for two different tilt angles with the Sun at the centre. The simulations are done for tilt angle $\alpha = 5^{\circ}$ (left panel) and $\alpha = 10^{\circ}$ (right panel). Figure adapted from Raath (2014).

$$H(\theta - \theta') \cong \tanh\left[2.75\left(\theta - \theta'\right)\right]. \tag{2.14}$$

Figure 2.5 shows an illustrative 3D simulation of the wavy structure of the HCS for the first 10 AU in the heliosphere with $\alpha = 5^{\circ}$ and $\alpha = 10^{\circ}$; see e.g. also Strauss et al. (2012); Strauss (2013) and Raath (2014).

2.6 The heliosphere

The heliosphere is the region surrounding the Sun, including the solar system, that is filled with the solar wind and the solar magnetic field. It moves through the local interstellar medium (LISM) with a speed between ~23 km s^{-1} and ~26 km s^{-1} (Zieger et al. 2013; Scherer and Fichtner 2014) so that a heliospheric interface is formed caused by the interaction of the solar and interstellar plasmas. This interface consists of a termination shock (TS), a heliopause (HP) and a bow wave or bow shock (BS). The region between the TS and HP is

defined as the inner heliosheath and the region between the HP and BS as the outer heliosheath. In CRs modulation studies the term heliosheath is frequently used to refer to the inner heliosheath.

The geometry and main features of the heliospheric boundaries are illustrated in Figure 2.6 in terms of proton number density as done by Scherer et al. (2008) using hydrodynamic (HD) model. For reviews and further detail, see also Fahr et al. (2000); Malama et al. (2006); Ferreira and Scherer (2006); Richardson et al. (2009) and Pogorelov et al. (2008, 2009).

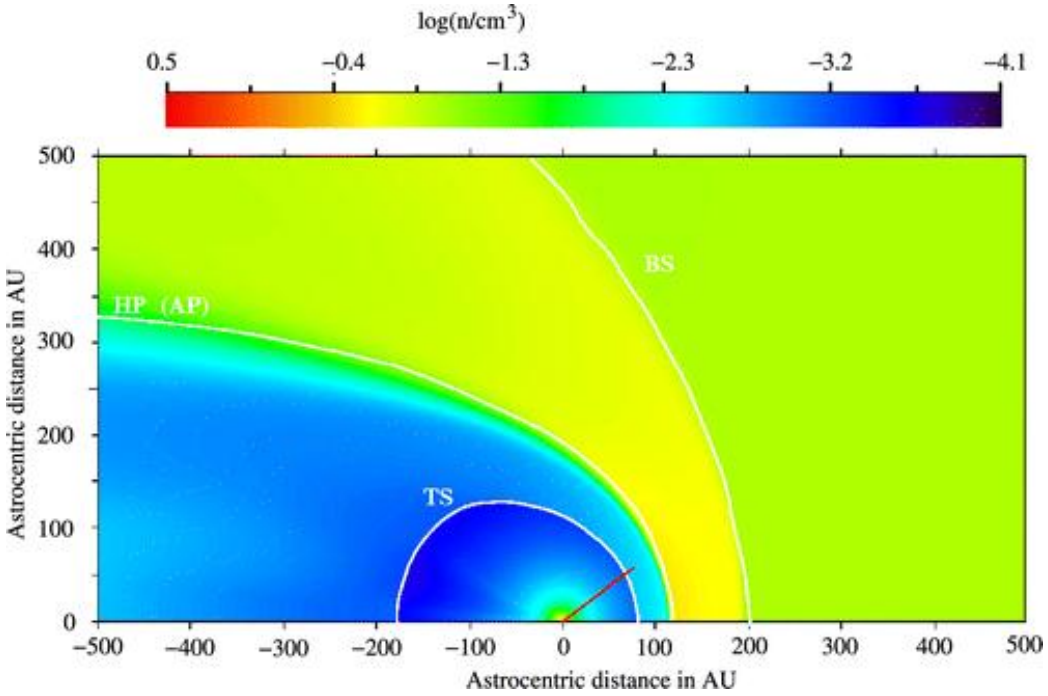

Figure 2.6: A hydrodynamic (HD) simulation of heliosphere visualized in the rest frame of the Sun with the colour-coded proton number density. The interstellar flow is from the right. Respectively, the white lines indicate the termination shock (TS), the heliopause (HP) and the bow shock (BS). The red line indicates the trajectory of Voyager 1. Figure adapted from Scherer et al. (2008).

2.6.1 The solar wind termination shock

The region in the heliosphere where the solar wind changes from supersonic speeds to subsonic speeds is called the termination shock (TS), which could be considered as the first heliospheric boundary away from the Sun, with the main feature that the Sunôs supermagnetosonically expanding solar wind almost abruptly slows down. The existence of the TS was first suggested in 1961 by Parker (Parker 1961). Later, its position was estimated

to vary between ~ 80 AU and ~ 100 AU (e.g. Stone et al. 1996, Whang and Burlaga 2000). Voyager 1 found the position of the TS to be at 94 AU in 2004 when it crossed into the heliosheath region (Stone et al. 2005) and Voyager 2 did the same in 2007 at 84 AU (Stone et al. 2008). This indicated that the position of the TS is dynamic, moving in and out with the solar activity cycle, which affects the modulation of CRs; see e.g. Manuel et al. (2015).

In the inner heliosheath region beyond the TS, the solar wind is slower, hotter and denser as it interacts with the surrounding interstellar matter. Across the TS the solar wind flow speed drops by a factor s called the TS compression ratio. It is essentially defined by $s = V_1 / V_2$, with V_1 the flow in the upstream region and V_2 the flow in the downstream region. For a detailed discussion about the properties of the TS see e.g. Li et al. (2008). This coincides with the increase in the solar wind density and also in the HMF magnitude. For non-relativistic flow, it follows that a maximum value of $s = 4$ is possible for a strong shock. The TS crossing of Voyager 2 confirmed that the TS is much weaker than anticipated with a compression ratio of $s = 2.4$ (Richardson et al. 2008).

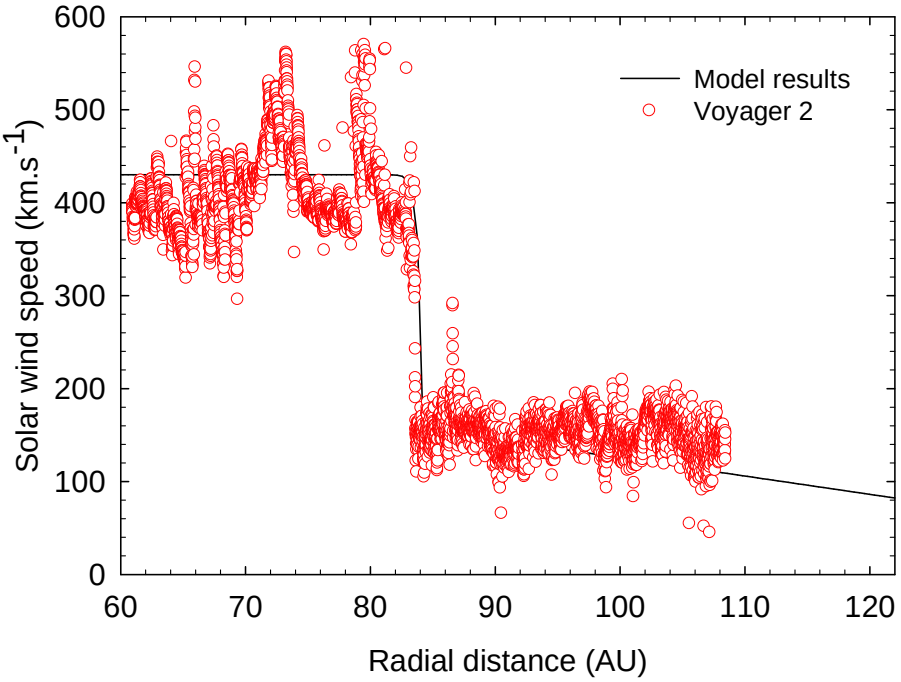

Figure 2.7: Radial component of the solar wind velocity modelled as a function of radial distance for $r \geq 60$ AU (black line). The position of TS is at 84 AU with $s = 2.0$ in Eq. (2.15) and the HP at 122 AU. This is compared to the solar wind speed observations from Voyager 2 taken ahead and beyond the TS. The solar wind data is from: http://cohoweb.gsfc.nasa.gov/.

Figure 2.7 shows observations of the solar wind speed from Voyager 2 taken ahead and beyond the TS (respectively, upstream and downstream). The speed varied much upstream of the TS, but less inside the heliosheath. At ~84 AU the measurements show a sudden decrease in speed, corresponding to the TS crossing (Stone et al. 2008, Richardson et al. 2008) and serve as a beautiful example of a stellar wind TS. This is compared to the approximation of the solar wind speed as is used in the numerical modeling in this work. It shows how the radial component of the velocity $V(r)$ changes as a function of distances across the TS and how it then decreases proportionally to r^{-2} from a few AU beyond the TS to the HP, computed by using Eq. (2.15) given below.

Eq. (2.2) gives the radial dependence of solar wind that does not include the TS. If this TS is included, the radial dependence for the solar wind speed is given as

$$V_{\mathrm{sw}}(r,\theta) = \frac{V_{\mathrm{sw}}(r_{\mathrm{ts}},\theta)(s+1)}{2s} - \frac{V_{\mathrm{sw}}(r_{\mathrm{ts}},\theta)(s-1)}{2s}\tanh\left(\frac{r-r_{\mathrm{ts}}}{L}\right), \qquad (2.15)$$

with r_{ts} the radial position of the TS, L =1.2 AU is the shock precursor scale length and with $s = 2.5$ the shock compression ratio (le Roux et al. 1996; Langner et al. 2003; Potgieter et al. 2014c).

2.6.2 The heliosheath and heliopause

The heliosheath is the region of the shocked solar wind between the TS and the heliopause. Voyager 1 has been exploring this region since 2005, until recently when it crossed the HP (Stone et al. 2013; Burlaga et al. 2013), considered as the boundary between the local interstellar medium and the solar wind medium. The plasma properties and geometry of the heliosheath region are still not well understood; in particular how turbulent it is inside this region, and what the corresponding transport mechanisms are for charged particles.

The shape of the HP is highly asymmetrical, as shown in Figure 2.6, from the nose to the tail. It is well defined in the nose direction, predicted to be about 40-50 AU beyond the TS, but it is ill defined in the tail direction, so more modeling is required to understand it (e.g. Opher et al. 2009). It has been widely considered as the outer boundary of the heliosphere and is mostly applied as such in CRs modulation models. However, based on MHD modeling it is known and expected that a BS or perhaps just a bow wave should occur well beyond the HP in the nose direction of the heliosphere. Whether a BS or bow wave exists in reality, has become somewhat controversial as argued by McComas et al. (2012) and Scherer and

Fichtner (2014). The heliosheath is different from the region up-wind of the TS and several theoretical and observational publications, since the launch of the two Voyager spacecraft have emphasised the importance of this region to CRs modulation.

Voyager 1 crossed the HP at ~ 121.7 AU in August 2012 (e.g. Stone et al. 2013; Krimigis et al. 2013; Gurnett et al. 2013) and is now at ~132 AU from the Sun. Remarkably, the magnetic field on both sides of the HP were found to be similar, although theoretically they are assumed to be independent of each other (Burlaga et al. 2013). This delayed the identification of the boundary as the HP and led to many alternative explanations and controversy, created mostly by Fisk and Gloeckler (2014) and Gloeckler and Fisk (2014). Recent publications by Gurnett et al. (2013), Burlaga et al. (2014) and Burlaga and Ness (2014a, b) largely settled these arguments, so that it is now widely accepted that Voyager 1 is well beyond the HP and in the very local interstellar medium (LISM).

The heliosheath may have an average width of ~28 AU from Voyager 1's point of view. Obviously, this number changes over the solar cycle because the TS is not stationary (e.g. Manuel et al. 2015, and references therein). Voyager 2 has not yet reached the HP, so that only estimates are made based on assumptions that the heliosheath may be less wide along the Voyager 2 trajectory (see also Ngobeni and Potgieter 2011), influenced by MHD modeling (e.g. Opher et al. 2009). Considering the present position of Voyager 2, the thickness of the heliosheath in that direction could be ~25 AU or less with an uncertainty of ~2.5 AU caused by possible solar wind pressure differences. If this kind of prediction is correct, Voyager 2 might reach the HP as early as in the second semester of 2015; see e.g. Webber and Intriligator (2014) for these estimates and mostly speculative arguments. What will happen when Voyager 2 crosses the HP is eagerly awaited.

The role of the heliosheath in the modulation of CRs will be further discussed in a later chapter. Recently, the observational data from Voyager 1 have stimulated several theoretical investigations of GCRs transport near the HP. Scherer et al. (2011) and Strauss et al. (2013a) argued that the HP is not the modulation boundary for GCRs and that there should be some modulation happening beyond the HP. On the other hand, Kóta and Jokipii (2014) expressed the opinion that GCRs modulation may not exist beyond the HP. Later, Guo and Florinski (2014) shared the same opinion. Lou et al. (2015) convincingly showed that it can exist, but depends strongly on what is assumed for the diffusion coefficients beyond the HP.

In this work, the HP is assumed to be the CRs modulation boundary so that no further attention is given to the outer heliosheath and BS.

2.7 Cosmic rays in the heliosphere

Cosmic rays (CRs) are charged particles (not rays) which, after being accelerated to very high energies at e.g. supernova shocks, propagate through the galaxy towards the solar system. These particles were discovered by Victor Hess during the historic balloon flights between 1911 and 1912, when it was established that these particles were from an extra-terrestrial origin (see e.g. Carlson 2012). They were later called cosmic rays by Millikan. As reviewed by e.g. Simpson (1997), Fichtner (2001) and Carlson (2012), Compton and Clay had already shown in 1930 that these particles were electrically charged (fully ionized). Today it is known that they have kinetic energy E ranging from ~ 1 MeV to as high as 10^{21} eV . Those that are detected at Earth around a few GeV consist of ~ 97 % protons, ~ 2 % electrons and positrons, and ~ 1 % heavier elements (Mewaldt et al. 2010). In the heliosphere charged particles of different origin can be identified. Generally they can be classified into four populations, based on their origin, as will be briefly discussed below, but with the focus on only two populations that are important to carry out the objectives of this study.

The first group is galactic cosmic rays (GCRs), as mentioned above. It is believed that they are accelerated in galactic space, and beyond, through various mechanisms; see the review by e.g. Jones and Ellison (1991). These charged particles experience the galactic wind and magnetic field before entering heliospheric space so that their original position of creation is hidden. At energies below a few GeV influence of solar modulation becomes important. The focus in this study is on GCRs, but in particular on galactic electrons and how they are modulated in the heliosphere. Galactic electrons originate as primary GCRs from astrophysical phenomena distributed throughout the galaxy. It is assumed that they penetrate the heliosphere isotropically to be modulated by essentially four physical processes that will be briefly discussed in Chapter 3. They differ from the nuclei in the sense that they are oppositely charged and far less massive, making it significantly more difficult to measure their intensities. Until recently, space experiments could not distinguish between electrons and positrons and thus presented observations as the sum of electrons and positrons, as is the case for Voyager 1 and Voyager 2.

The second important group for this study is the Jovian electrons which originate from Jupiter's magnetosphere and was discovered as early as 1973 during the Pioneer 10 Jupiter fly-by. This large magnetosphere was recognized to be a relatively strong source of electrons at energies up to ~30 MeV (e.g. Simpson et al. 1974; Chenette et al. 1974). They dominate the low energy electron spectrum within the first 15-20 AU from the Sun (see e.g. Ferreira

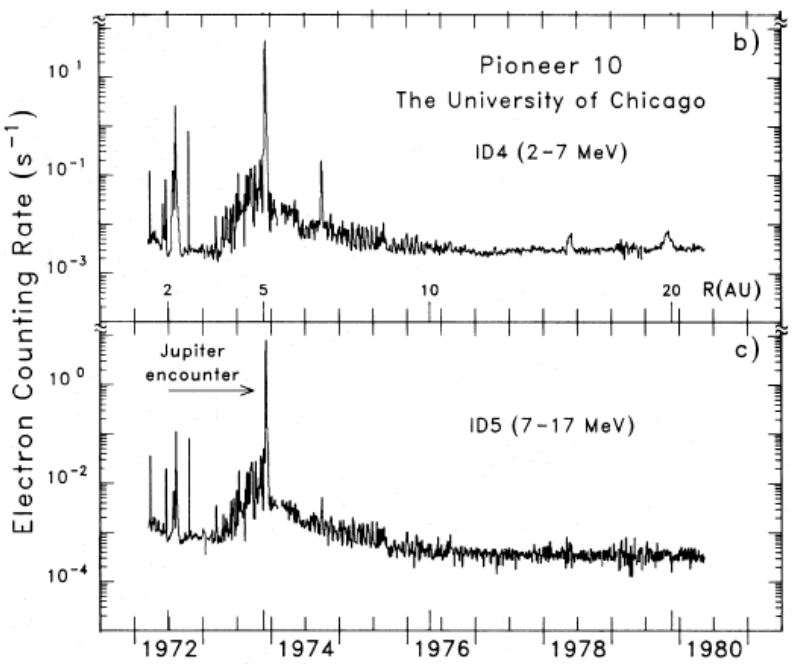

Figure 2.8: The electron count rate measured by the Pioneer 10 spacecraft as a function of time and radial distance for two energy channels. The figure is from Eraker (1982.)

2002; Ferreira and Potgieter 2004a; Potgieter and Nndanganeni 2013a; Ferreira 2005; Heber et al. 2007 and reviews by Heber and Potgieter 2006, 2008). The study of these Jovian electrons resulted in the first observational evidence for diffusive transport of electrons perpendicular to the mean HMF (Chenette et al. 1974; Hamilton and Simpson 1979).

Figure 2.8 shows the Pioneer 10 observed electron counting rate in terms of time and also in terms of radial distance (Eraker 1982). From the figure it is evident that the intensity of the Jovian electrons is a maximum at Jupiterôs position. Modeling the modulation of these Jovian electrons will be further discussed in Chapter 5 and in Chapter 8, in particular up to what kinetic energy they can dominate over galactic electrons in the inner heliosphere and to what radial distances away from the Sun.

Other CRs populations include Solar Energetic Particles (SEPs) and the Anomalous Cosmic Rays (ACRs). The SEPs originate from solar flares, especially when the Sun gets more active (see Schröter et al. 2006; Malandraki et al. 2009, the review by Klecker et al. 2006; McComas et al. 2014). SEPs usually have energies up to several hundred MeV, but are observed at the Earth only for a few hours before they dissipate (see also e.g. Cliver 2000, 2008). The last group to mention here, is the so-called Anomalous Cosmic Rays (ACRs) which are primarily formed because of the ionization of interstellar neutral atoms relatively

close to the Sun, which then, as charged particles, get picked-up by the solar wind and transported outwards (away from the Sun) to be accelerated at and beyond the solar wind TS (Garcia-Munoz et al. 1973; Pesses et al. 1981; see the reviews by Fichtner 2001; Giacalone et al. 2012 and Leske et al. 2013). The process of their acceleration in the outer heliosphere has recently become highly controversial (see e.g. Potgieter 2008a, b, 2013a, b; Potgieter and Strauss 2010; Strauss et al. 2010). These two groups are not studied in this thesis.

2.8 The solar modulation of cosmic rays

Figure 2.9 shows an example of the long term modulation of GCRs as measured at sea-level by the Hermanus neutron monitor (See also e.g. Flückiger and Bütikofer 2009). The count rate was normalized to 100 % in March 1987. Two long term cycles are evident in this figure; the 11-year cycle and the 22-year cycle. The GCRs intensity profiles reach maximum values in 1965, 1976-77, 1987, 1998 and 2009, corresponding to solar minimum activity conditions. The alternating $A > 0$ and $A < 0$ magnetic polarity cycles are indicated in this figure.

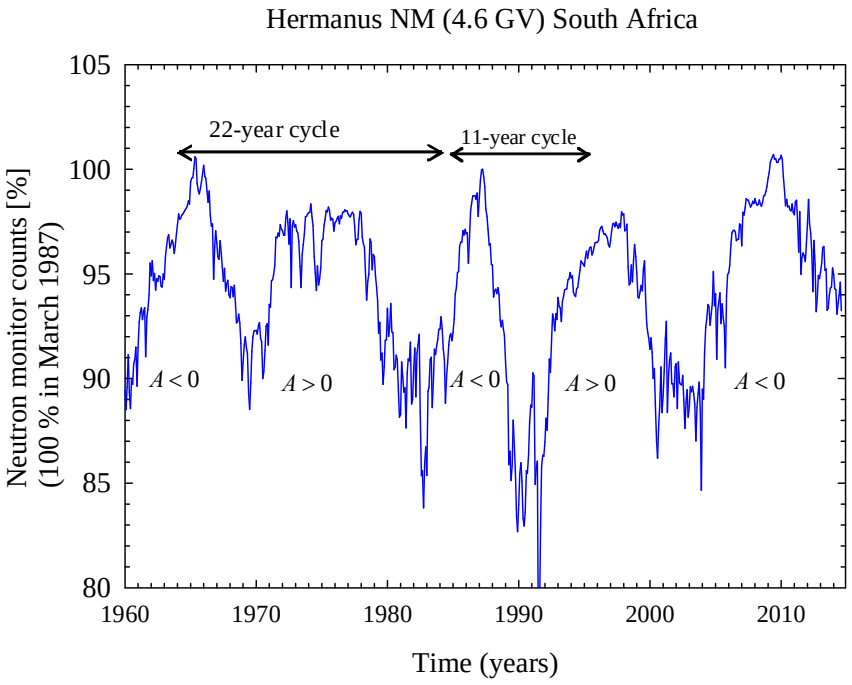

Figure 2.9: The count rate of the Hermanus neutron monitor (NM), normalized to 100% in March 1987, as a function of time since 1958. The present cut-off rigidity for CRs at this NM in South Africa is 4.6 GV. Pressure corrected data is obtained from http://www.nwu.ac.za/content/neutron-monitor-data. The alternating HMF polarity cycles are indicated by $A > 0$ and $A < 0$.

During the $A < 0$ polarity cycles, peaks are formed through heliospheric modulation, whereas for $A > 0$ polarity cycles the modulated flux has plateau-like shapes, as an illustration of the observed 22-year cycle. The modulation effects of this alternating HMF direction will be discussed in Chapter 6. For recent reviews, see Potgieter (2010, 2013a, b) and Kóta (2013).

Also evident are large step-like decreases and increases which are believed to occur as a result of solar transient events known as global merged interaction regions. For reviews on these phenomena see e.g. Fujii and McDonald (1995), le Roux and Potgieter (1991, 1995) and Potgieter and Ferreira (2001). See the reviews by Potgieter (1995, 1997). These interaction regions are not considered in this thesis.

2.9 Selected spacecraft missions

The Voyager 1 spacecraft mission and the PAMELA space mission are briefly discussed in this section. For reviews of the Ulysses mission, see Wenzel et al. (1992); Heber and Marsden (2001); Heber and Potgieter (2006) and Heber (2013). Possible future space missions are discussed by Mewaldt (2013).

2.9.1 The Voyager mission

The Voyager twin spacecraft, called Voyager 1 and Voyager 2, have made CRs, solar wind and magnetic field observations, amongst others, for more than three decades. These observations have been used to study the spatial and temporal variations of GCRs and ACRs at distances now extending to beyond the HP. The two spacecraft were launched in 1977, Voyager 2 first in August, and Voyager 1 in September. They have thus been in flight for 38 years and are the first to study the outer solar system, the TS, the heliosheath and now the interstellar medium in case of Voyager 1.

The first objectives were to explore and study the planets Jupiter and Saturn, but Voyager 2 also went by the giant planets Uranus and Neptune. Voyager 1 is speeding away at ~ 3.5 AU per year, out of the ecliptic plane at a heliolatitude of 34.4°, whereas Voyager 2 travels at ~3.3 AU per year out of the ecliptic plane at a heliolatitude of -28.8° (i.e. below the equatorial plane). Voyager 1 was the first to cross the TS in 2004 at a distance of 94 AU. It then explored the inner heliosheath. Voyager 2 crossed the TS in 2007 at 84 AU, that is 10 AU closer to the Sun than Voyager 1. This is confirmation that the shock is not stationary, it

moves inwards and outwards depending on solar activity (see e.g. Snyman 2007 and Intriligator and Webber 2011).

Voyager 1 crossed the HP in August 2012 at ~122 AU, and it is now exploring the interstellar medium, and it is currently at 132.3 AU. Voyager 2 is still in the heliosheath with its current position at 108.8 AU. Voyager 1 made unexpected discoveries in terms of the CRs intensity of the ACRs when it crossed the HP and this gave new perspective regarding the outer regions of the heliosphere (Stone et al. 2013; Krimigis et al. 2013; Gurnett et al. 2013; Burlaga et al. 2013). This knowledge has been very handy in modeling modulation studies and will continue to be so for another decade.

The crossing of the HP by Voyager 2 is eagerly awaited. The two spacecraft are expected to operate until at least 2020. For the vast number of discoveries and accomplishments of this mission, see reviews by Stone et al. (2008), Richardson et al. (2008) and Krimigis et al. (2011). More information about the Voyager mission can be found at: http://voyager.jpl.nasa.gov/mission/intersterllar.html/. For specifically CRs data, see http://voyager.gsfc.nasa.gov/heliopause/data.html/.

2.9.2 The PAMELA mission

This is a satellite-borne experiment making long duration measurements of CRs particularly optimized for their antiparticles such as positrons and anti-protons. It was launched on 15 June 2006 from the Baikonur cosmodrome on board of the Russian Resurs DK1 satellite, following a high inclination elliptical orbit with a period of 90 minutes. It is also suited to study particles of solar origin and particles trapped in the Earthôs magnetosphere.

The main scientific objective is the simultaneous observations of CRs protons, electrons, antiprotons and positrons, performed in the extended energy range, 80 MeV to at least 200 GeV. A major discovery was the large positron excess with respect to electrons between 10 GeV and 100 GeV as well as the discovery of antiprotons being trapped in the radiation belts around the Earth (Adriani et al. 2011). The advantage is that PAMELA has data collected over a relatively long time, and as such the spectral time evolution can be monitored and the short and the long term effects can be studied. The mission will continue until the satellite fails, hopefully not soon.

For other accomplishments of this mission, see publications and reviews by Picozza.et al. (2007); Adriani et al. (2009); Boezio et al. (2009, 2011); Mocchiutti et al. (2009) and Adriani et al. (2014, 2015). For more detailed information, and data sets, about the PAMELA mission visit its official website, http://pamela.roma2.infn.it/.

A new experiment making similar observations as PAMELA is AMS2 (Gaggero et al. 2014, Aguilar et al. 2014 and see: www.ams02.org/). Since CRs data down to only 1 GeV have been published so far, it is not used in this modeling study.

2.10 Summary

In this chapter a brief overview about the basic concepts important to the heliospheric modulation of CRs were discussed, including the solar wind, the HMF, the HCS, the solar cycle and the heliosphere and its geometry. The Voyager and the PAMELA space missions were briefly discussed.

In the next chapter an overview of modulation theory is given, particularly concerning the transport equation and the diffusion tensor, and also a brief overview of the modulation models relevant to this study.

Chapter 3

Heliospheric modulation of cosmic rays: Theory and models

3.1 Introduction

The modulation of cosmic rays (CRs) is the process by which their intensities change as a function of position, time and energy as they propagate from the local interstellar medium into the heliosphere. These fully charged galactic particles have to cross various heliospheric boundaries and regions, as described in the previous chapter, on their way to the point of observation. The transport and propagation processes are described by a basic transport equation with several important mechanisms: convection due to the expanding solar wind, diffusion caused by the irregular heliospheric magnetic field (HMF) through the diffusion tensor, gradient, curvature and heliospheric current sheet (HCS) drifts and adiabatic cooling (or heating) as discussed below. This equation was developed by Eugene Parker in the early 1960s (Parker 1965), verified by Gleeson and Axford (1967) and Fisk et al. (1974), and refined by Gleeson and Axford (1968) and Jokipii and Parker (1970)

3.2 The Parker transport equation

The modulation processes given above were combined into the Parker transport equation (TPE) which is given by:

$$\frac{\partial f}{\partial t} = -\left(\mathbf{V} + \left\langle \mathbf{v}_A \right\rangle\right).\nabla f + \nabla.\left(\mathbf{K}_s.\nabla f\right) + \frac{1}{3}\left(\nabla.\mathbf{V}\right)\frac{\partial f}{\partial \ln P} + Q \qquad (3.1)$$

where $f(\mathbf{r}, P, t)$ is the omni-directional CRs distribution function dependent on position **r**, rigidity P and time *t*; $\mathbf{V}$ is the solar wind velocity, $\mathbf{v}_A$ is the pitch angle averaged guiding centre drift velocity and $\mathbf{K}_s$ is the diffusion tensor. This TPE includes the following modulation mechanisms

i. The term on the left side describes the change in the CRs distribution with time.

ii. The first term on the right describes the outward directed particle convection caused by the expanding solar wind.

iii. The second term on the right side describes the gradient and curvature drifts of CRs, including any abrupt change in the HMF direction such as the HCS.

iv. The third term on the right side describes the spatial diffusion parallel and perpendicular to the average HMF.

v. The fourth term describes energy changes in the form of adiabatic cooling $\left(\nabla.\mathbf{V}>0\right)$ or heating $\left(\nabla.\mathbf{V}<0\right)$.

vi. The last term describes possible sources of CRs inside the heliosphere, e.g. the Jovian electron source.

These processes combine to give a descriptive picture of the modulation of CRs in the heliosphere. Because of small scale irregularities in the HMF comparable with the gyro-radii, CRs are resonantly scattered to form an inward diffusive flux component. The outward convection due to the solar wind forms a convection flux component with corresponding adiabatic energy changes. The density gradients and curvature in the background HMF result in a drift flux component of which the direction depends on the polarity of the HMF epoch. With a solar magnetic field directed outward from the Sun in the northern polar region and inward in the southern polar region, positively charge particles are expected to drift into the inner heliosphere mainly over the solar poles and out along the HCS. This period is known as the $A>0$ magnetic polarity epoch. In this phase of the solar cycle, the drift pattern of negatively charged particles is in the opposite direction.

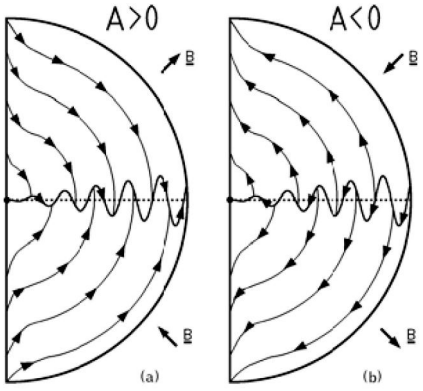

Figure 3.1: The global drifts pattern of positively charged particles in an $A>0$ and $A<0$ solar magnetic epoch, together with a wavy current sheet. Figure adapted from Heber and Potgieter (2006). See also Jokipii and Thomas (1981).

This is shown in Figure 3.1 (a) and (b) respectively. The period in which the HMF is directed inward in the northern polar region and outward in the southern polar region, is called $A<0$.

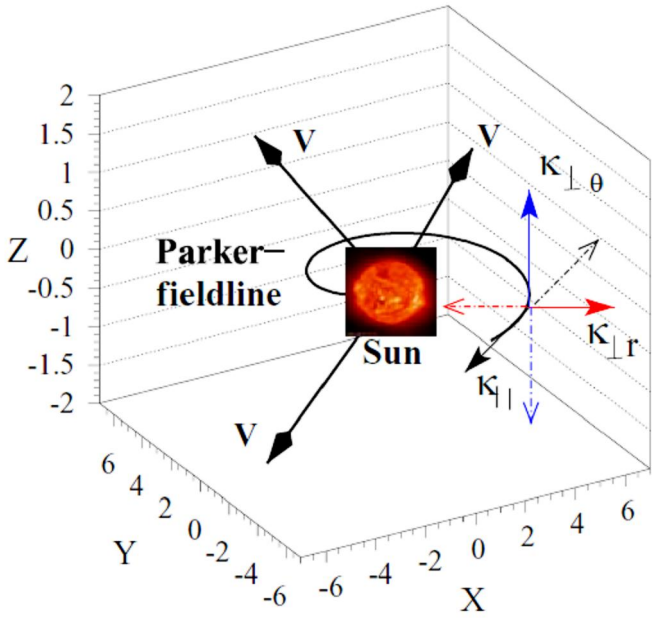

Figure 3.2: An illustration of the three elements of the diffusion tensor with respect to the direction of the Parker-HMF spiral. The expanding solar wind velocity (**V**) is indicated by the arrows emanating from the Sun in the centre of the figure. Figure adapted from Heber and Potgieter (2006).

3.2.1 The heliospheric propagation tensor

An asymmetrical tensor, consisting of a symmetrical diffusion tensor and an asymmetrical drift tensor, which contains the three diffusion coefficients and one drift coefficient in a HMF aligned coordinates, is given by:

$$\begin{aligned}\mathbf{K} &= \mathbf{K}_S + \mathbf{K}_A \\ &= \begin{pmatrix} K_{\parallel} & 0 & 0 \\ 0 & K_{\perp\theta} & 0 \\ 0 & 0 & K_{\perp r} \end{pmatrix} + \begin{pmatrix} 0 & 0 & 0 \\ 0 & 0 & K_A \\ 0 & -K_A & 0 \end{pmatrix}, \\ &= \begin{pmatrix} K_{\parallel} & 0 & 0 \\ 0 & K_{\perp\theta} & K_A \\ 0 & -K_A & 0 \end{pmatrix}.\end{aligned} \tag{3.2}$$

The diffusion coefficients in the symmetrical tensor describe particle diffusion parallel to the average HMF $\left(K_{\parallel}\right)$ as well as in the polar $\left(K_{\perp\theta}\right)$ and radial $\left(K_{\perp r}\right)$ directions perpendicular to it. The coefficients in the asymmetrical tensor describe gradient, curvature and current sheet drifts experienced by the CRs particles. Figures 3.1 and 3.2 give a schematic representation of the direction in which drifts and the diffusion coefficients operate with respect to the background HMF.

Using the full tensor, the TPE can be rewritten in a more compact form as

$$\frac{\partial f}{\partial t} = -\mathbf{V}.\nabla f + \nabla.\left(\mathbf{K}.\nabla f\right) + \frac{1}{3}\left(\nabla.\mathbf{V}\right)\frac{\partial f}{\partial \ln P} + Q. \tag{3.3}$$

The geometry of the heliosphere is assumed to be of a spherical nature, and as such it is convenient to write the tensor in Eq. (3.3) in terms of heliocentric spherical coordinates. The HMF aligned coordinate system is related to the spherical coordinate system through the HMF spiral angle ψ as

$$\begin{aligned}
&\mathbf{e}_{\parallel} = \cos\psi\mathbf{e}_r - \sin\psi\mathbf{e}_{\phi} \\
&\mathbf{e}_{\perp\theta} = \mathbf{e}_{\theta} \\
&\mathbf{e}_{\perp r} = \mathbf{e}_{\parallel} \times \mathbf{e}_{\perp\theta} = \sin\psi\mathbf{e}_r + \cos\psi\mathbf{e}_{\phi},
\end{aligned} \tag{3.4}$$

where ψ is defined as the average angle between the parallel component of the HMF and the radial direction. The tensor $\mathbf{K}$ can therefore also be written in terms of spherical coordinates by specifying the correct matrix transformation $\mathbf{T}$, for which is required that $\det\left(\mathbf{T}\right) = 1$. This matrix is given by

$$\mathbf{T} = \begin{bmatrix} \cos\psi & 0 & \sin\psi \\ 0 & 1 & 0 \\ -\sin\psi & 0 & \cos\psi \end{bmatrix}. \tag{3.5}$$

This allows the diffusion tensor in Eq. (3.3) to be written in spherical coordinates as

$$\begin{bmatrix} K_{rr} & K_{r\theta} & K_{r\phi} \\ K_{\theta r} & K_{\theta\theta} & K_{\theta\phi} \\ K_{\phi r} & K_{\phi\theta} & K_{\phi\phi} \end{bmatrix} = \mathbf{T}\mathbf{K}\mathbf{T}^{T} \tag{3.6}$$

$$= \begin{pmatrix} \cos\psi & 0 & \sin\psi \\ 0 & 1 & 0 \\ -\sin\psi & 0 & \cos\psi \end{pmatrix} \begin{pmatrix} K_{\parallel} & 0 & 0 \\ 0 & K_{\perp\theta} & K_A \\ 0 & -K_A & K_{\perp r} \end{pmatrix} \begin{pmatrix} \cos\psi & 0 & -\sin\psi \\ 0 & 1 & 0 \\ \sin\psi & 0 & \cos\psi \end{pmatrix}$$

$$= \begin{pmatrix} K_{\parallel}\cos^2\psi + K_{\perp r}\sin^2\psi & -K_A\sin\psi & \left(K_{\perp r}-K_{\parallel}\right)\cos\psi\sin\psi \\ K_A\sin\psi & K_{\perp\theta} & K_A\cos\psi \\ \left(K_{\perp r}-K_{\parallel}\right)\sin\psi\cos\psi & -K_A\cos\psi & K_{\perp r}\cos^2\psi + K_{\parallel}\sin^2\psi \end{pmatrix} . \tag{3.7}$$

Eq. (3.3) can now be written in terms of heliocentric spherical coordinates (r,ϕ,θ) as

$$\begin{aligned} \frac{\partial f}{\partial t} = & \left[\frac{1}{r^2}\frac{\partial}{\partial r}\left(r^2K_{rr}\right)+\frac{1}{r\sin\theta}\frac{\partial}{\partial\theta}\left(K_{\theta r}\sin\theta\right)+\frac{1}{r\sin\theta}\frac{\partial K_{\phi r}}{\partial\phi}-V\right]\frac{\partial f}{\partial r} \\ & + \left[\frac{1}{r^2}\frac{\partial}{\partial r}\left(rK_{r\theta}\right)+\frac{1}{r^2\sin\theta}\frac{\partial}{\partial\theta}\left(K_{\theta\theta}\sin\theta\right)+\frac{1}{r^2\sin\theta}\frac{\partial K_{\phi\theta}}{\partial\phi}\right]\frac{\partial f}{\partial\theta} \\ & + \left[\frac{1}{r^2\sin\theta}\frac{\partial}{\partial r}\left(rK_{r\phi}\right)+\frac{1}{r^2\sin\theta}\frac{\partial K_{\theta\phi}}{\partial\theta}+\frac{1}{r^2\sin^2\theta}\frac{\partial K_{\phi\phi}}{\partial\phi}-\Omega\right]\frac{\partial f}{\partial\phi} \\ & + K_{rr}\frac{\partial^2 f}{\partial r^2}+\frac{K_{\theta\theta}}{r^2}\frac{\partial^2 f}{\partial\theta^2}+\frac{K_{\phi\phi}}{r^2\sin^2\theta}\frac{\partial^2 f}{\partial\phi^2}+\frac{2K_{r\phi}}{r\sin\theta}\frac{\partial^2 f}{\partial r\partial\phi} \\ & + \frac{1}{3r^2}\frac{\partial}{\partial r}\left(r^2V\right)\frac{\partial f}{\partial\ln p}+Q. \end{aligned} \tag{3.8}$$

Grouping the terms that contribute to diffusion, drifts, convection and adiabatic energy losses, Eq. (3.8) becomes

$$\begin{aligned} & \overbrace{\left[\frac{1}{r^2}\frac{\partial}{\partial r}(r^2K_{rr})+\frac{1}{r\sin\theta}\frac{\partial K_{\phi r}}{\partial\phi}\right]\frac{\partial f}{\partial r}+\left[\frac{1}{r^2\sin\theta}\frac{\partial}{\partial\theta}(K_{\theta\theta}\sin\theta)\right]\frac{\partial f}{\partial\theta}}^{\text{diffusion}} \\ & +\overbrace{\left[\frac{1}{r^2\sin\theta}\frac{\partial}{\partial r}(rK_{r\phi})+\frac{1}{r^2\sin^2\theta}\frac{\partial K_{\phi\phi}}{\partial\phi}-\Omega\right]\frac{\partial f}{\partial\phi}}^{\text{diffusion}} \\ & +\overbrace{K_{rr}\frac{\partial^2 f}{\partial r^2}+\frac{K_{\theta\theta}}{r^2}\frac{\partial^2 f}{\partial\theta^2}+\frac{K_{\phi\phi}}{r^2\sin^2\theta}\frac{\partial^2 f}{\partial\phi^2}+\frac{2K_{r\phi}}{r\sin\theta}\frac{\partial^2 f}{\partial r\partial\phi}}^{\text{diffusion}} \\ & +\overbrace{\left[-\left\langle \mathbf{v}_A\right\rangle_r\right]\frac{\partial f}{\partial r}+\left[-\frac{1}{r}\left\langle \mathbf{v}_A\right\rangle_\theta\right]\frac{\partial f}{\partial\theta}+\left[-\frac{1}{r\sin\theta}\left\langle \mathbf{v}_A\right\rangle_\phi\right]\frac{\partial f}{\partial\phi}}^{\text{drift}} \\ & -\overbrace{V\frac{\partial f}{\partial r}}^{\text{convection}}\ \overbrace{+\frac{1}{3r^2}\frac{\partial}{\partial r}(r^2V)\frac{\partial f}{\partial\ln P}}^{\text{adiabatic energy change}} \\ & =-\overbrace{Q}^{\text{sources}}, \end{aligned} \tag{3.9}$$

where $K_{rr,}K_{r\theta},K_{r\phi},K_{\theta r},K_{\theta\theta},K_{\theta\phi},K_{\phi r},K_{\phi\theta}$ and $K_{\phi\phi}$ are the nine elements of the 3D tensor based on a Parkerian HMF. The terms that describe the diffusion process are $K_{rr},K_{r\phi},K_{\theta\theta},K_{\phi r},K_{\phi\phi}$ and those that describe the gradient, curvature and current sheet drifts are $K_{r\theta},K_{\theta r},K_{\theta\phi},K_{\phi\theta}$.

The differential intensity of CRs is computed as a function of kinetic energy to obtain the spectra which can be compared to observations. The TPE can also be written in terms of momentum, but is solved in this work in terms of rigidity in the numerical modulation models. This rigidity is defined as

$$P=\frac{pc}{q}=\frac{mvc}{Ze}, \tag{3.10}$$

where

$$p=mv=\frac{m_0 v}{\sqrt{1-v^2/c^2}},$$

is the magnitude of the particleôs relativistic momentum, $q=Ze$ its charge, v its speed, m its relativistic mass with c the speed of light in outer space.

For relativistic particles, the total energy in terms of momentum is given as

$$E_t^2=\left(E+E_0\right)^2=p^2c^2+m_0^2c^4, \tag{3.11}$$

with E the kinetic energy and E_0 the rest mass energy of the particles $\left(\text{e.g. } E_0=0.938 \text{ GeV for protons and } E_0=5.11\times10^{-4} \text{ GeV for electrons}\right)$ and m_0 the particleôs rest mass.

The kinetic energy per nucleon in terms of particle rigidity is then

$$E=\sqrt{P^2\left(\frac{Ze}{A}\right)^2+E_0^2}-E_0, \tag{3.12}$$

so that the rigidity can be written in terms of kinetic energy per nucleon as

$$P=\left(\frac{A}{Ze}\right)\sqrt{E\left(E+2E_0\right)}, \tag{3.13}$$

with Z the atomic number and A the mass number of the CRs particle. The ratio of a particleôs speed to the speed of light can be defined from the above relation and is given as

$$\beta=\frac{v}{c}=\frac{P}{\sqrt{P^2+\left(\frac{A}{Ze}\right)^2E_0^2}}, \tag{3.14}$$

in terms of rigidity, and in terms of kinetic energy it is written as

$$\beta = \frac{v}{c} = \frac{\sqrt{E\left(E+2E_0\right)}}{E+E_0}. \tag{3.15}$$

The relation between rigidity, kinetic energy and β is therefore

$$P = \frac{A}{Z}\sqrt{E\left(E+2E_0\right)} = \left(\frac{A}{Z}\right)\beta\left(E+E_0\right). \tag{3.16}$$

For galactic protons and electrons $A/Z = 1.0,$ but for fully charged galactic nuclei $A/Z = 2.0$, but this changes for different isotopes and for the anomalous component.

Moreover, the particle density within the region $d^3r,$ for particles with momenta between $\mathbf{p}$ and $\mathbf{p}+d\ \mathbf{p},$ is related to the full CRs distribution function (which includes a pitch angle distribution) by

$$n = \int F\left(\mathbf{r},\mathbf{p},t\right)d^3p = \int_p p^2\left[\int_\Omega F\left(\mathbf{r},\mathbf{p},t\right)d\Omega\right]dp, \tag{3.17}$$

where $d^3p = p^2dpd\Omega.$ The differential particle density, $U_p,$ is related to n by

$$n = \int U_p\left(\mathbf{r},p,t\right)dp, \tag{3.18}$$

which gives

$$U\left(r,p,t\right) = \int_\Omega p^2F\left(\mathbf{r},\mathbf{p},t\right)d\Omega. \tag{3.19}$$

The omni-directional average of $F(\mathbf{r},\mathbf{p},t)$ is calculated as

$$f\left(\mathbf{r},p,t\right) = \frac{\int_\Omega F\left(\mathbf{r},\mathbf{p},t\right)d\Omega}{\int_\Omega d\Omega} = \frac{1}{4\pi}\int_\Omega F\left(\mathbf{r},\mathbf{p},t\right)d\Omega, \tag{3.20}$$

which leads to

$$U_p\left(r,p,t\right) = 4\pi p^2 f\left(\mathbf{r},p,t\right). \tag{3.21}$$

The differential intensity in units of particles/unit area/unit time/unit solid angle/unit momentum, is

$$j_p = \frac{vU_p(\mathbf{r},\mathrm{p},t)}{\int_\Omega d\Omega} = \frac{vU_p(\mathbf{r},p,t)}{4\pi} = vp^2 f(\mathbf{r},p,t), \tag{3.22}$$

so that

$$j(\mathbf{r},p,t) = \frac{v}{4\pi}U_p \frac{dp}{dE_t} = \frac{1}{4\pi}U_p = p^2 f(\mathbf{r},p,t), \tag{3.23}$$

where $j(\mathbf{r},p,t)$ is the differential intensity in units of particles/area/time/solid angle/energy. The relation between j and f is simply $(p)^2$ or $(P)^2$.

3.3 Basic diffusion coefficients

The diffusion coefficients of special interest in a 3D heliocentric coordinate system are

$$\begin{aligned} K_{rr} &= K_{\parallel}\cos^2\psi + K_{\perp r}\sin^2\psi, \\ K_{\perp\theta} &= K_{\theta\theta}, \\ K_{\phi\phi} &= K_{\perp r}\cos^2\psi + K_{\parallel}\sin^2\psi, \\ K_{\phi r} &= \left(K_{\perp r} - K_{\parallel}\right)\cos\psi\sin\psi = K_{r\phi}, \end{aligned} \tag{3.24}$$

where K_{rr} is the effective radial diffusion coefficient, a combination of the parallel diffusion coefficient $K_{\parallel}$ and the radial perpendicular diffusion coefficient $K_{\perp r}$ with ψ the spiral angle of the average HMF; $K_{\theta\theta} = K_{\perp\theta}$ is the effective diffusion coefficient perpendicular to the HMF in polar direction. Here, $K_{\phi\phi}$ describes the effective diffusion in the azimuthal direction and $K_{\phi r}$ is the diffusion coefficient in the $\phi r-$plane. Both are determined by the choice for $K_{\parallel}$ and $K_{\perp}$. Beyond ~20 AU in the equatorial plane $\psi \to 90^\circ$, so that K_{rr} is dominated by $K_{\perp r}$ but by $K_{\parallel}$ in the polar regions of the heliosphere, whereas $K_{\phi\phi}$ is dominated by $K_{\parallel}$, but only if the HMF is Parkerian in its geometry. If the type of HMF assumed is non-Parkerian, the expressions in Eq. (3.24) become much more complicated (see e.g. Burger et al. (2008), Sternal et al. (2011) and Effenberger et al. (2012) for a detailed discussion).

3.3.1 Parallel diffusion

The diffusion coefficient parallel to the HMF plays an important role in transporting the CRs along the HMF lines. This diffusion is mainly due to the pitch angle scattering caused by the turbulent HMF. This basic transport mechanism is described by the quasi-linear theory (QLT) (e.g. Jokipii 1966; 1971; Bieber et al. 1994; Dröge 2000), with the parallel mean free path $(\lambda_{\parallel})$ given by

$$\lambda_{\parallel} = \frac{3v}{2}\int_0^1 \frac{\left(1-\mu^2\right)^2}{\Phi(\mu)}d\mu, \tag{3.25}$$

with v the speed of light and μ the cosine of the pitch angle and $\Phi(\mu)$ the Fokker-Planck coefficient for pitch-angle scattering (see e.g. Hasselmann and Wibberenz 1970; Jokipii 1971; Earl 1974). For a comprehensive review, see Teufel and Schlickeiser (2003) and Shalchi (2009).

The relationship between the parallel mean free path $(\lambda_{\parallel})$ and the parallel diffusion coefficient $K_{\parallel}$ is given by

$$\lambda_{\parallel} = K_{\parallel}\frac{3}{v}. \tag{3.26}$$

The calculation of $\Phi(\mu)$ in Eq. (3.25) is needed as an input power spectrum of the magnetic field fluctuations which can be divided into three ranges e.g. Bieber et al. (1994). The ranges are : the energy range, where the power spectrum is independent of the wave number k, the inertial range where it is proportional to $k^{-5/3}$; and the dissipation range where it is proportional to k^{-3}. The dissipation range plays an important role in the resonant scattering of low energy particles where the pitch angles of these particles approach 90°. QLT predicts that $\lambda_{\parallel}$ becomes infinite if the dissipation range is included in the calculation of Eq. (3.25). This is because $\Phi(\mu)$ goes to zero in the dissipation range as pitch angle approaches 90°. In contrast, if the dissipation is neglected, $\lambda_{\parallel}$ becomes too small for lower rigidities and gives a wrong rigidity dependence. However, this small $\lambda_{\parallel}$ can be applied when calculating high energy proton modulation, since protons experience large adiabatic energy changes below ~300 MeV and the change in $\lambda_{\parallel}$ will not have any effect on proton modulation (see e.g.

Potgieter 1984). Knowledge of $\lambda_{\|}$ is quite important for electron modulation because electrons with energies (rigidities) below ~300 MeV (300 MV) are diffusion dominated and respond directly to any changes in $\lambda_{\|}$ for rigidities $P < 100$ MV. A higher order theory, which is beyond the scope of this study, is needed to fully understand these issues.

Taking into account theoretical arguments by Burger et al. (2000), $K_{\|}$ was constructed by Ferreira (2002) for computing CRs electron modulation in the heliosphere. This complex coefficient is given by

$$K_{\|} = K_0 \beta f_1(r, P), \tag{3.27}$$

where

$$f_1(r, P) = 0.2 g(P) c(r) h(r, P), \tag{3.28}$$

with

$$h(r, P) = 0.02\left(\frac{P}{P_0}\right)^2\left(\frac{r}{r_0}\right)^{1.7} + 0.02\left(\frac{P}{P_0}\right)\left(\frac{r}{r_0}\right)^{2.2} + 0.2\left(\frac{P}{P_0}\right)^{1/3}\left(\frac{r}{r_0}\right) + 7.0e(r), \tag{3.29}$$

$$c(r) = \begin{Bmatrix} 1.0 \text{ if } r > r_c \\ m(r) \text{ if } r \le r_c \end{Bmatrix}, \tag{3.30}$$

$$m(r) = \frac{r_0}{r_c}\xi\left(\frac{r}{r_0}\right)^{\xi}, \tag{3.31}$$

and

$$g(P) = \left(\frac{P_0}{P_s}\right)^{0.6}, \tag{3.32}$$

$$\text{where} \quad \xi = \left(\frac{r}{r_c}\right)^{x},\ x = \left(\frac{0.016}{P/P_0}\right)^{0.2},\ r_c = \frac{r_0}{0.1 + \left(P_s/P_0\right)^{1.4}}, \tag{3.33}$$

and

$$e(r) = \begin{Bmatrix} \left(10 r_0 / r\right)^k \text{ if } r > 10 \text{ AU} \\ 1.0 \text{ if } r \le 10 \text{ AU} \end{Bmatrix}, \tag{3.34}$$

with $k = 1.25\times10^{-4}\left(r/r_0\right)^2$, $K_0 = 4.5\times10^{22}$ cm^{2}s^{-1}, $P_0 = 1$ GV, $r_0 = 1$ AU and $P_s = P$ when $P < 1$ GV and $P_s = 1$ GV when $P \ge 1$ GV.

Ndiitwani (2005) constructed a different $\lambda_{||}$, especially in terms of its rigidity dependence, based on the theoretical turbulence work done for $\lambda_{||}$ at Earth by Teufel and Schlickeiser (2002). In addition, a radial dependence was constructed in order to have a $\lambda_{||}$ which produces realistic modulation in the heliosphere. This parallel mean free path is given by

$$\lambda_{||} = \lambda_1(r,P)\lambda_2(r,P), \tag{3.35}$$

where

$$\lambda_1(r,P) = \frac{5}{3}\left(0.0106\left(\left(P/P_0\right)^{1/3} + \frac{3.57}{\left(0.511^2 + \left(P/P_0\right)^2\right)^{1/4}} \right) + (r/r_0)^{1.4}\times 10^{-9}\left(P/P_0\right)^2 \right), \tag{3.36}$$

and

$$\lambda_2(r,P) = \frac{c_1(P) + 0.08}{c_1(P)(r/r_0)^{-2.30} + 0.08(r/r_0)^{0.37}}, \tag{3.37}$$

with

$$c_1(P) = 83.0\left(\frac{0.02}{1000P}\right)^{0.75}. \tag{3.38}$$

In general terms, the parallel diffusion coefficient is then

$$K_{||} = \frac{v}{3}\lambda_{||}(r,P). \tag{3.39}$$

This implies that $\lambda_{||}$ for low energy electrons has almost no rigidity dependence, which is required, as will be illustrated in the following chapters.

This mean free path was also used by Nkosi (2006) and Nkosi et al. (2008) to compute modulation for electrons in terms of its rigidity and radial dependence as will be shown below.

3.3.2 Perpendicular diffusion

The diffusion coefficients perpendicular to the HMF play a crucial role in the transportation and modulation of the CRs particles in the heliosphere. The role becomes directly evident from latitude-dependent modulation first studied by Fisk (1976). Even after the inclusion of the drifts in the models, the importance of the perpendicular diffusion remains. It is expected

that in the polar regions, the perpendicular diffusion should be larger, even extremely so in the polar direction, than in the radial/azimuthal direction. Therefore it is subdivided into two coefficients, perpendicular to the HMF in the radial direction given by $K_{\perp r}$ and perpendicular to the HMF in the polar direction, given by $K_{\perp\theta}$. A straightforward practical approach has been to scale $K_{\perp}$ spatially as $K_{||}$. It then follows that

$$K_{\perp r} = aK_{||}, \tag{3.40}$$

and

$$K_{\perp\theta} = bK_{||}. \tag{3.41}$$

Here, a and b are constants which determine the values of $K_{\perp r}$ and $K_{\perp\theta}$ in terms of $K_{||}$ respectively (see also Ferreira 2002; Nkosi 2006; Moeketsi 2004 and Ngobeni 2006).

In this work, as done by Ferreira (2002) and Nkosi (2006), it is assumed that

$$K_{\perp\theta} = bK_{||}F(\theta), \tag{3.42}$$

with

$$F(\theta) = A^{+} \pm A^{-}\tanh\left[\frac{1}{\Delta\theta}\left(\theta_A - 90^{\circ} + \theta_F\right)\right], \tag{3.43}$$

where $A^{\pm} = \dfrac{1}{2\left(d \pm 1\right)}$, $\Delta\theta = \dfrac{1}{8}, \theta_A = \theta$ and $\theta_F = 35^{\circ}$ for $\theta \le 90^{\circ}$ whereas for $\theta \ge 90^{\circ}$, $\theta_A = 180^{\circ} - \theta$ and $\theta_F = -35^{\circ}$. This signifies that $K_{\theta\theta} = K_{\perp\theta}$ is enhanced toward the poles by a factor *d* with respect to the value of $K_{||}$ in the equatorial regions as is required to explain Ulysses observations (see Potgieter 1996, 2000; Ferreira et al. 2001a; Heber and Potgieter 2006).

In Figure 3.3 the function $F(\theta)$ in Eq. (3.43) is shown in terms of polar angle with $d = 1.0,\ 3.5,\ 7.0$ and 13.0 respectively. It is enhancing $K_{\perp\theta}$ up to a maximum value at the poles as determined by the value of *d*, with no enhancement in the equatorial plane. The region over which the function increases can also be changed to be less steep and to cover a broader range of polar angles. An additional justification for such an increase in $K_{\perp\theta}$ could be to compensate for a HMF with a meridional component. For solar minimum, a Fisk-type HMF (Burger et al. 2008) is probably more realistic, resulting in a different latitudinal transport than for the Parker HMF, and which could affect drifts. To account for such a

process, $K_{\perp\theta}$ needs to be enhanced towards the poles when a Parker HMF is used (Ferreira and Potgieter 2004a, b), as in this work. However, there is not yet enough convincing evidence for the existence of such a Fisk-type field (Sternal et al. 2011).

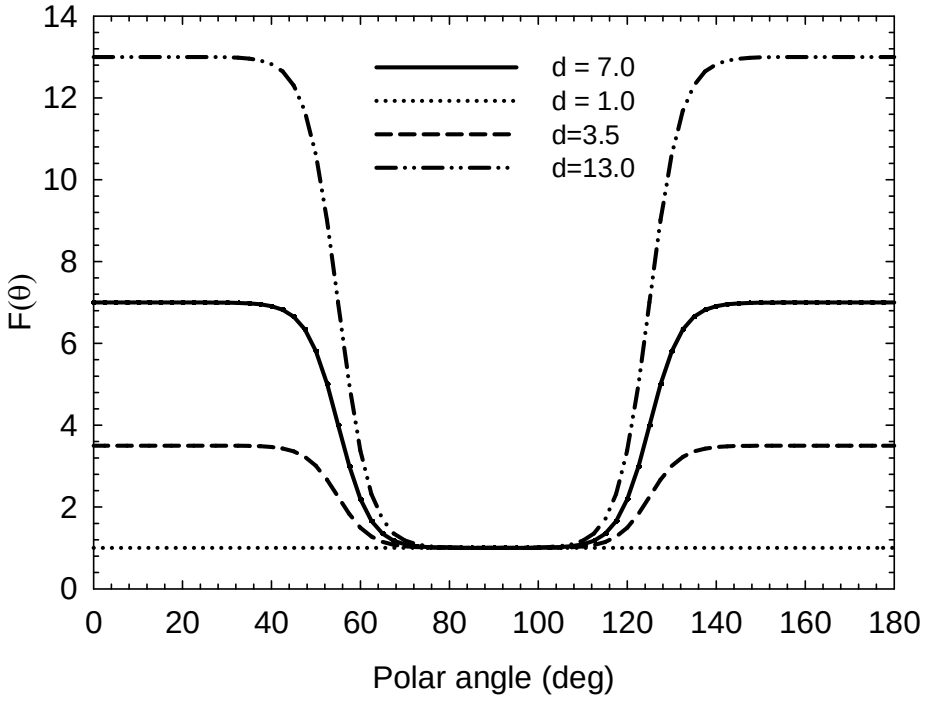

Figure 3.3: Illustration of $F(\theta)$ in Eq. (3.43) as a function of polar angle θ for four different d scenarios, that is $d = 1.0,\ 3.5,\ 7.0$ and 13.0 respectively.

Figure 3.4 shows the rigidity dependence of $K_{\parallel}, K_{\perp r}$ and $K_{\perp\theta}$ for 12 MeV electrons at 1 AU and 110 AU with $\theta = 60^{\circ}$. The DCs are in units of $6\times10^{20}\,\mathrm{cm^2 s^{-1}}$ in all the figures.

This rigidity dependence corresponds to the mean free path given by Eq. (3.36). At 1 AU, all the DCs are almost constant at low rigidity, but increase rapidly for $P > 0.1$ GV. At 110 AU, the DCs have a different rigidity dependence than at Earth, with a stronger rigidity dependence for all rigidities. Despite its complexity, applying these values in the numerical model in comparison with electron observations from Voyager 1 could not reproduce all aspects of these observations, so that an alternative, simpler approach was used instead, with a constant rigidity dependence below $P \le 0.1$ GV. This is discussed further below.

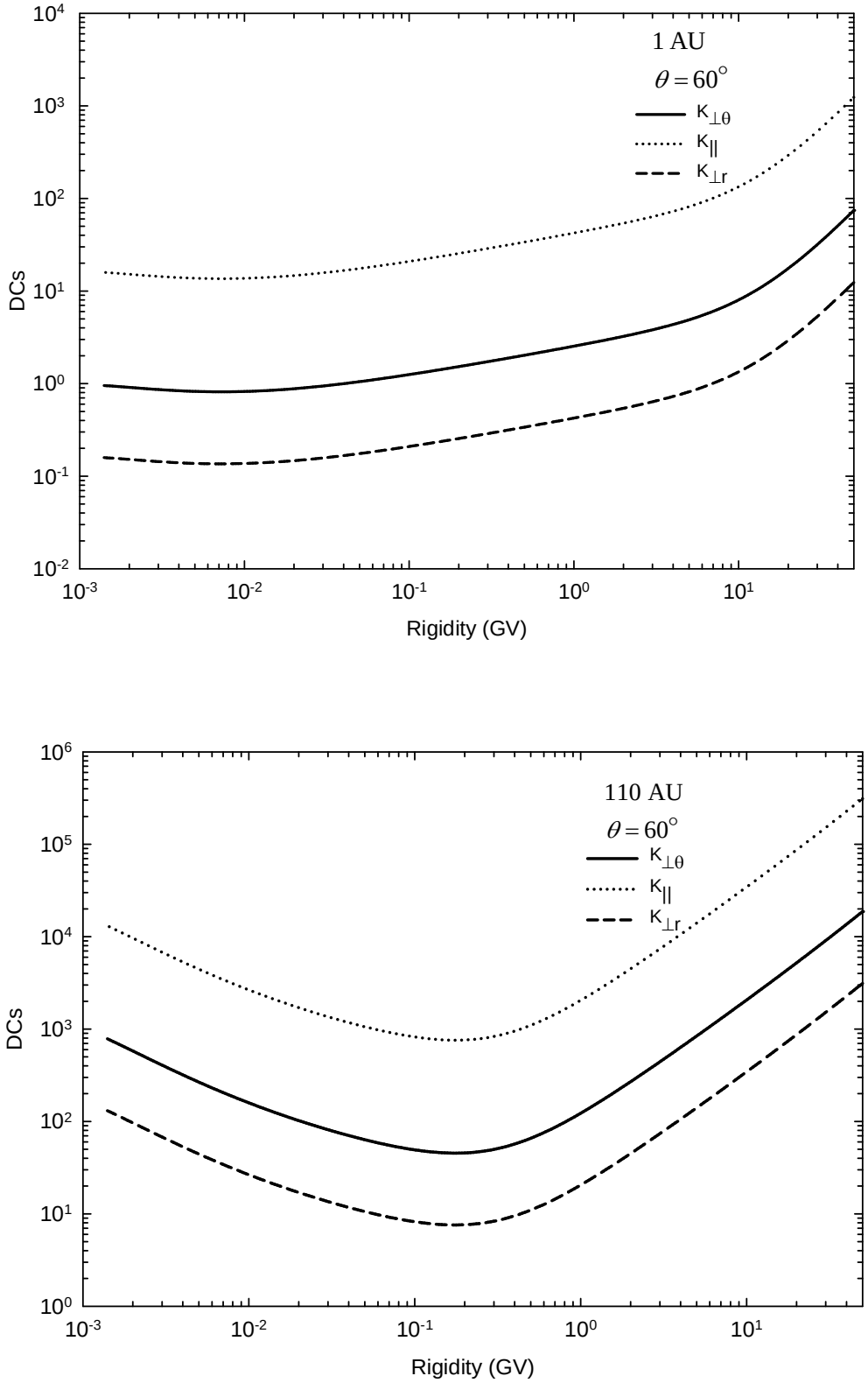

Figure 3.4: The assumed rigidity dependence of $K_{\parallel}, K_{\perp r}$ and $K_{\perp \theta}$ for 12 MeV electrons at 1 AU (top panel) and 110 AU (bottom panel) respectively, computed with $\theta = 60^{\circ}$. The DCs are in units of 6×10^{20} cm^2 s^{-1} in all the figures.

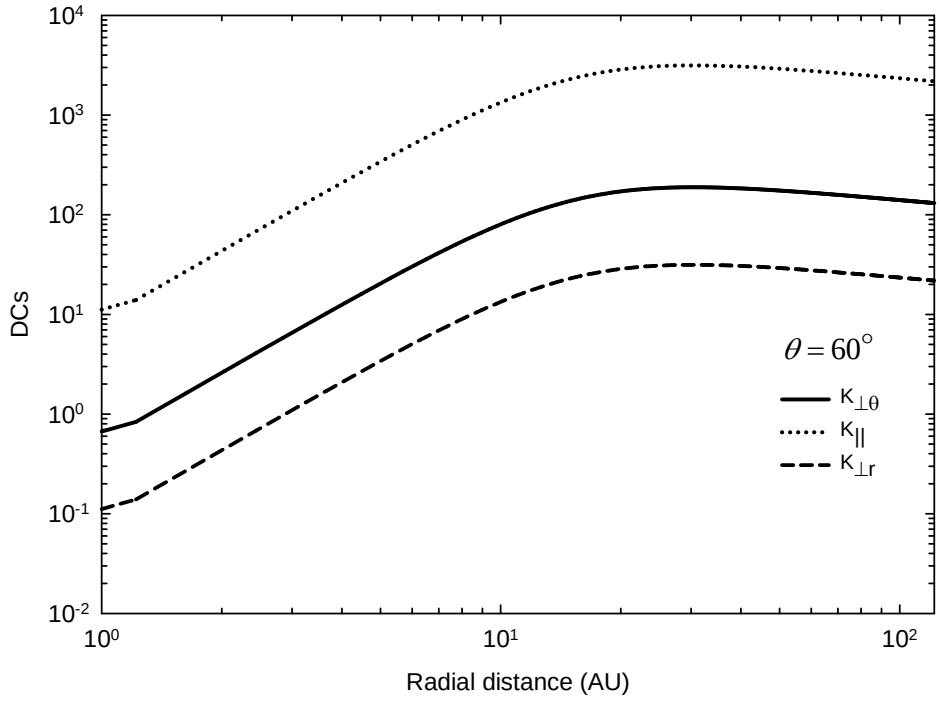

Figure 3.5: Computed radial dependence of $K_{\parallel}, K_{\perp r}$ and $K_{\theta\theta}$ for 12 MeV electrons with $\theta = 60^{\circ}$ based on Eq. (3.37).

Figure 3.5 shows the corresponding computed radial dependence based on Eq. (3.37). This is based on the assumption that $K_{\parallel} > K_{\perp r}$ throughout the heliosphere, so that both increase from 1 AU to 10 AU, then to remain constant. According to the first term in Eq. (3.24), K_{rr} is dominated by $K_{\parallel}$ in the inner heliosphere, whereas $K_{\perp r}$ dominates in the outer heliosphere (except at and near the poles). Essentially this is determined by the combination of $K_{\parallel}$ and $K_{\perp r}$, and the geometry of the assumed HMF (the term depending on the spiral angle). $K_{\perp\theta}$ also increases rapidly within the first 10 AU to remain constant.

The DCs as computed by Ferreira et al. (2000), Ndiitwani (2005) and Nkosi (2006) do not reproduce all aspects of observed electrons in the heliosphere (e.g. the radial intensity profile as observed by Voyager 1). These DCs are complex to the extent that it becomes rather difficult to keep the numerical ADI solving procedure stable. As such it has become necessary to re-evaluate these complex DCs and to rather use a simpler approach and make comparison between the results obtained using these different DCs.

To compute electron modulation in the heliosheath, a simpler approach is to assume, for example: $K_{||} = K_0 \beta f_1(P) f_2(r,\theta)$ with $f_1(P)$ giving the rigidity dependence and $f_2(r,\theta)$ the spatial dependent of $K_{||}$. This approach, which separates the rigidity dependence from the spatial dependence, will be used to compute the modulation of 12 MeV electrons. Following Potgieter and Ferreira (1999), the assumptions made in Eqs. (3.44) to (3.47) are used. It will be illustrated in that such a simplified approach is adequate to obtain compatibility with Voyager 1 observations in the outer heliosphere. In order to be able to achieve this compatibility, a constant rigidity dependence below $P < 0.4$ GV is needed, but changing significantly when $P > 0.4$ GV. A similar approach was used by Potgieter (1984).

The parallel and the perpendicular diffusion coefficient used here are similar to those from Nndanganeni (2012), but were adjusted to reproduce the latest Voyager 1 observations in the outer heliosphere and PAMELA observations at Earth. These coefficients have a different radial dependence in the inner heliosphere than in the outer heliosphere. In order to assure compatibility with Voyager 1 electron observations, it is necessary to specify the DCs differently over the first 84 AU than in the outer heliosphere with r > 84 AU.

The parallel, two perpendicular DCs and the drift coefficient, in terms of P, with $P_0 = 1$ GV, and radial distance r, with $r_e = 1$ AU, are as follows.

In the inner heliosphere, with $r < 84$ AU:

if $P < 0.4$ GV:

$$K_{||} = K_0 \beta \left(1 + \left(\frac{r}{r_e} \right)^c \right), \tag{3.44}$$

if $P \geq 0.4$ GV:

$$\mathrm{K}_{||} = K_0 \beta \left(P / P_0 \right) \left(1 + \left(r / r_e \right)^c \right), \tag{3.45}$$

with $c = 1.25$. Here, β is the ratio of the particle's speed to the speed of light.

In the outer heliosphere, with $r \geq 84$ AU, the radial dependence changes, with $c = 0.6$. The constant $K_0 = 70$ is in units of 6 x 10^{20} cm^2 s^{-1}.

In all cases

$$K_{\perp r} = a K_{||}, \tag{3.46}$$

with $a = 0.02$. Furthermore,

$$K_{\perp\theta} = K_{\perp r} F(\theta), \tag{3.47}$$

with $F(\theta)$ given by Eq. (3.43).

Figure 3.6 shows the corresponding rigidity dependence of $K_{\perp\theta}, K_{\perp r}$, and $K_{\parallel}$ at 1 AU (top panel), and 110 AU (bottom panel) with $\theta = 60^{\circ}$. These diffusion coefficients are rigidity independent at low energies. The choice to use this straightforward rigidity dependence is based on turbulence theory (Teufel and Schlickeiser 2002, 2003) as developed for the innermost heliosphere, assuming it to be applicable also to the outer heliosphere. Evidently, all the diffusion coefficients are constant below $P < 0.4$ GV, increasing proportional to P above 0.4 GV. In this case both the perpendicular DCs have the same rigidity dependence as $K_{\parallel}$ but with $K_{\perp r}$ and $K_{\perp\theta} < K_{\parallel}$.

Figure 3.7 shows the radial dependence of the same set of DCs for 12 MeV electrons with $\theta = 60^{\circ}$ and from 1 AU to 122 AU, which is the position of the HP. Each one increases steadily with increasing radial distances for $r \leq 84$ AU, as expected from Eqs. (3.44) and (3.45). With $r > 84$ AU, all the DCs decrease abruptly and continue to do so with less strong radial dependence to the HP, according to Eqs. (3.46) and (3.47). This jump in the DCs to the lower values in the heliosheath is introduced so that the radial profile intensities observed by Voyager 1 beyond the TS at 94 AU can be reproduced, as will be shown in Chapter 7. It is expected that the turbulence beyond the TS and inside the heliosheath will increase, resulting in the DCs dropping significantly over the TS and staying small up to the HP.

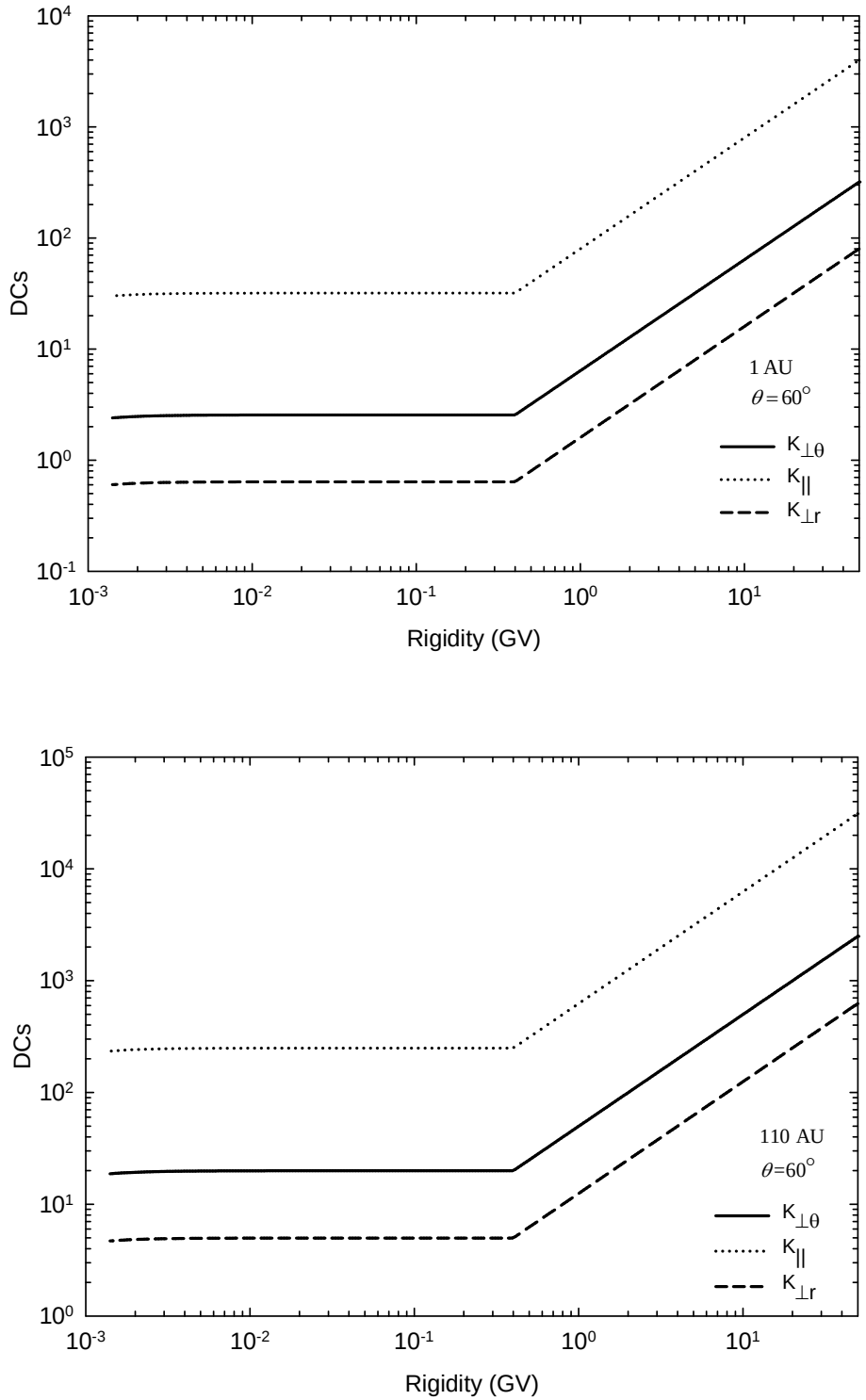

Figure 3.6: Computed rigidity dependence of $K_{\perp\theta}, K_{\perp r}$, and $K_{\parallel}$ for 12 MeV electrons at 1 AU (top panel) and 110 AU (bottom panel) with $\theta = 60^{\circ}$ as given by Eq. (3.44 to 3.47). The DCs are in units of 6×10^{20} cm^2 s^{-1} in all the figures.

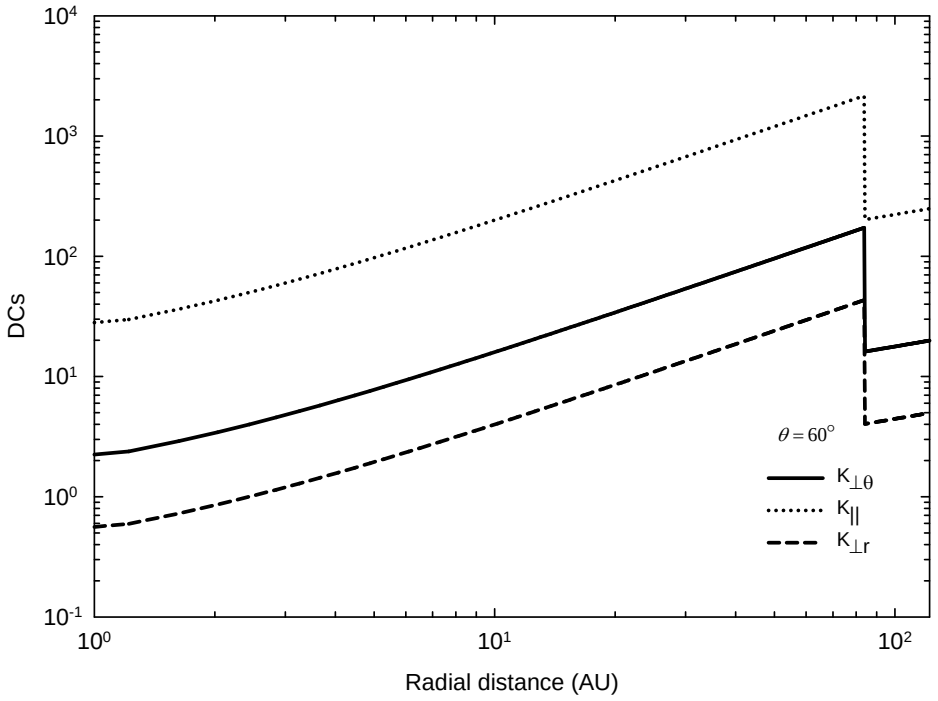

Figure 3.7: Computed radial dependence of the DCs for 12 MeV electrons with $\theta = 60^{\circ}$ for $K_{\parallel}, K_{\perp r}$ and $K_{\perp \theta}$ based on Eqs. (3.44 to 3.47). In this case, a TS is assumed at 94 AU, with the HP at 122 AU.

3.4 The drift coefficient

Gradients and curvature in the background HMF result in CRs having a drift velocity of which the direction depends on the magnetic polarity of the HMF epoch. Drifts effects in solar modulation studies were neglected until Jokipii et al. (1977) pointed out that particle drifts are an important mechanism of CRs modulation. Global drifts affect CRs transport through contributing drift motions associated with gradients and the curvature of the field and any abrupt change in the field direction, such as HCS. Drifts are sensitive to the polarity of the HMF and lead to a charge-sign asymmetry between oppositely charged CRs. For example, electrons will drift primarily inwards through the equatorial regions of the heliosphere along the HCS during $A>0$ polarity cycles, but they drift primarily through the polar regions, down to the equatorial regions and then outwards along the HCS during $A<0$ cycles.

The three components of the drift velocity in terms of $K_{r\theta}, K_{\theta r}, K_{\phi\theta}, K_{\theta\phi}$ in three dimensions are:

$$\langle v_A \rangle_r = -\frac{A}{r\sin\theta}\frac{\partial}{\partial\theta}\left(\sin\theta K_{\theta r}\right), \tag{3.48}$$

$$\langle v_A \rangle_\theta = -\frac{A}{r}\left[\frac{1}{\sin\theta}\frac{\partial}{\partial\phi}\left(K_{\phi\theta}\right)+\frac{\partial}{\partial r}\left(rK_{r\theta}\right)\right], \tag{3.49}$$

$$\langle v_A \rangle_\phi = -\frac{A}{r}\frac{\partial}{\partial\theta}\left(K_{\theta\phi}\right), \tag{3.50}$$

with $A = \pm 1;$ which determines the drift direction of the charged particles in the heliosphere according to the magnetic polarity. For this study only electrons are studied and hence:

$$A = \begin{cases} -1 \text{ for an } A > 0 \text{ cycle} \\ +1 \text{ for an } A < 0 \text{ cycle.} \end{cases}$$

The pitch angle averaged guiding centre drift velocity for a near isotropic CR distribution is given by:

$$\langle \mathbf{v}_A \rangle = \nabla \times \left(K_A \mathbf{e}_B\right), \tag{3. 51}$$

with $\mathbf{e}_B = \mathbf{B}/B$ where B is the magnitude of the background HMF, usually assumed to have a basic Parkerian geometry; see Eq. (2.7) or a modified version of the Parkerian HMF; see Eq. (2.8). The Parkerian geometry, as described in Chapter 2, however, gives very large particle drifts over the polar regions of the heliosphere so that it is a standard practice to modify it in the polar regions of the heliosphere (see e.g. Potgieter 1996, 2000; Ferreira 2002; Langner 2004; Ngobeni 2015 and Raath 2014, who did a detailed study of these modifications). This is in fact a procedure through which unrealistic large drift velocities over the poles of the heliosphere, under certain modulation conditions, can be reduced. Drift models without this reduction could not reproduce the very small latitudinal gradients observed by Ulysses (Heber and Potgieter 2006).

Under the assumption of weak scattering, the drift coefficient is given by

$$\left(K_A\right) = \frac{\beta P}{3B_m} f_s, \tag{3.52}$$

where f_s is considered to be a drift reduction function. Potgieter (2013b) gives an overview of the reasons why the reduction of particle drift is required in the heliosphere. It can be done explicitly, for example, by making $f_s < 1.0,$ both in terms of its rigidity dependence and/or its spatial dependence, and through modifying the HMF geometry. Reducing drifts implicitly by changing the CR intensity gradients in the TPE is more complicated, for example, by

enhancing perpendicular diffusion in the polar direction through Eq. (3.43). In Chapter 6 illustrations will be given of what the modulation effects are when this drift coefficient is reduced explicitly and implicitly.

Ngobeni (2015) revisited this issue, following on the theoretical work that was done by Bieber and Matthaeus (1997) and Burger and Visser (2010). He gave an expression for f_s as follows:

$$f_s = \frac{(\omega\tau)^2}{1+(\omega\tau)^2}, \tag{3.53}$$

where ω is the gyro-frequency of a CR particle in the HMF and τ represents a typical time scale defined by the scattering of CRs (see also Potgieter 1984). Determining the latter is of essence in diffusion and drift theory and the major uncertainty in solar modulation studies; for example, is it constant throughout the heliosphere, or changing with rigidity and/or space and with time, depending on solar activity? In the case of weak scattering, $\omega\tau \gg 1.0$, so that $f_s = 1.0$ and the drift coefficient becomes a maximum throughout the heliosphere. Then Eq. (3.52) reduces to the standard and straight forward equation that has been used in numerous numerical drift models, starting from Jokipii and Kopriva (1979); see also e.g. Potgieter and Moraal (1985) and Potgieter (1996, 2000) and the references therein. This approach has become known as full drifts, with modulation models to be drift dominated.

The reduction of drift is in agreement with what Potgieter et al. (1989); Webber et al. (1990); Ferreira and Potgieter (2004a, b); Langner et al. (2003, 2004, 2006) and Ngobeni and Potgieter (2010, 2014, 2015) found when they were reporting on the comparison of modeling results and observations throughout the heliosphere. In most of these models, it was required to make $f_s \approx 0.5$, and to reduce the rigidity dependence at lower energies, as will be discussed next. The implication then is that $\omega\tau \approx 1.0$ if assuming it to be a constant.

Taking the above-mentioned into account, Eq. (3.51) can be generalized and re-written as

$$\langle \mathbf{v}_A \rangle = \frac{\beta P}{3}\left[f_s \nabla \times \frac{\mathbf{B}}{B_m^2} + \nabla f_s \times \frac{\mathbf{B}}{B_m^2} \right]. \tag{3.54}$$

From Burger et al. (2000), an expression for $\omega\tau$ that depends only on rigidity was constructed by Ngobeni (2015) and is given as:

$$\omega\tau = \sqrt{\left(K_A\right)_0 \frac{\left(P/P_0^{'}\right)^2}{1+\left(1-\left(K_A\right)_0\right)\left(P/P_0^{'}\right)^2}}, \tag{3.55}$$

with $\left(K_A\right)_0$ a dimensionless constant ranging from 0 to 1.0 and $P_0^{'} = \frac{1}{\sqrt{10}}$ GV. Making use of Eq. (3.55), the drift coefficient given by Eq. (3.52) and the drift reduction function given by Eq. (3.53) respectively become

$$\left(K_A\right) = \left(K_A\right)_0 \frac{\beta P}{3B_m} \frac{\left(P/P_0^{'}\right)^2}{1+\left(P/P_0^{'}\right)^2}, \tag{3.56}$$

with

$$f_s = \left(K_A\right)_0 \frac{\left(P/P_0^{'}\right)^2}{1+\left(P/P_0^{'}\right)^2}. \tag{3.57}$$

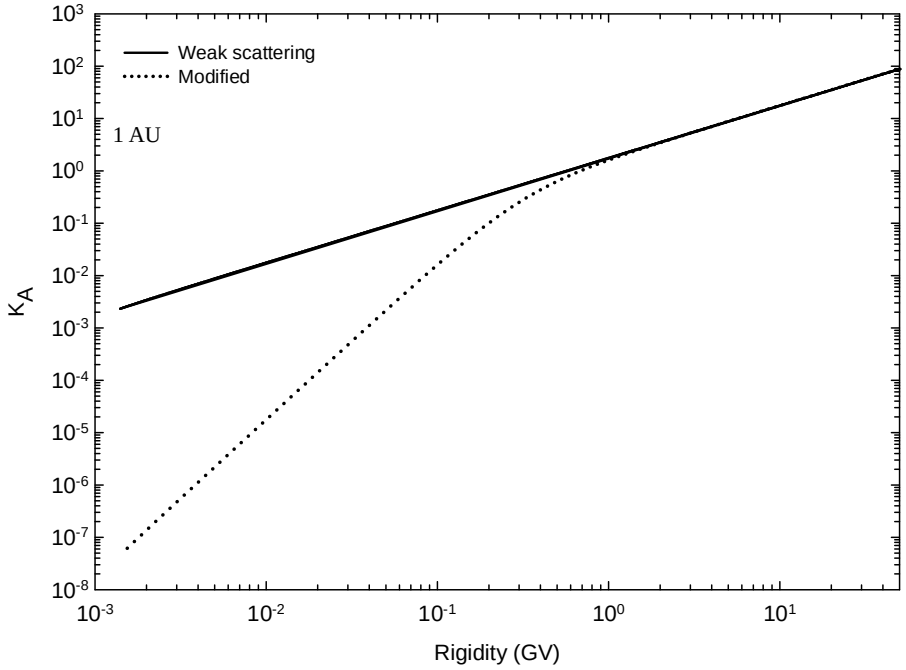

Figure 3.8: Computed rigidity dependence of K_A at Earth (1 AU with $\theta = 90^{\circ}$). The solid line is for weak scattering as in Eq. (3.52) and the dotted line is for the modified drifts drift coefficient as in Eq. (3.56).

This rigidity dependence is shown in Figure 3.8, together with the weak scattering case as given by Eq. (3.52). The stronger decrease in the rigidity dependence below $P \simeq 0.1\,\mathrm{GV}$ is the direct result of the reduction (or scaling) factor f_s as in Eq. (3.57). The implication is that for low energy electrons, drifts become negligible so that the transport and modulation of these particles become dominated by the diffusion process, as will be illustrated in Chapter 6. This is not the case for protons and CRs nuclei. Above 1 GV the weak scattering and the modified drifts coefficient have the same rigidity dependence.

3.5 Turbulence theory relevant to solar modulation

Turbulence is a universal phenomenon and also exists everywhere in the solar wind plasma. This means that solar wind may be regarded as a huge laboratory for studying turbulence. Turbulence is important to multiple problems in the solar wind, such as the scattering of solar energetic particles (Li et al. 2008, Zank et al. 2007) and heating of the solar wind (Matthaeus et al. 1995; Zank et al. 1999; Smith 2001). The heliosphere is filled with the magnetized, supersonically expanding solar wind which is highly fluctuating and turbulent. The modulation of cosmic rays in the heliosphere cannot be fully understood from first principles without studying the inclusion of the magnetic field fluctuation in the solar wind plasma. This is, however, work in progress and of a very sophisticated theoretical nature so that it is not pursued in this thesis. It suffices to say that over the last decade, progress has been made to improve the understanding of the heliospheric turbulence, and in particular to address some of the shortcomings of the standard scattering (diffusion) theories, of which the Quasi-Linear Theory (QLT) is the best known. See e.g. the comprehensive review by Shalchi (2009). These new advancements have taken into account the characteristics of turbulent changes in the solar wind and HMF. Originally, Bieber et al. (1994) lobbied for a composite model for turbulence which consists of ~20% slab and ~80% 2D fluctuation in order to get compatibility between the calculated mean free path and the corresponding observations. At low rigidities the dynamical theory predicts more efficient scattering, which in turn reduces the parallel mean free path, whereas at high rigidities the simple theory is used to describe the particle transport parallel to the average magnetic field. Drogë (2005) showed that QLT underestimated the parallel mean free path of electrons by almost two orders of magnitude, even with a corrected slab fraction for magnetic turbulence.

Shalchi (2006), for example, derived an expression for the mean free path from the extended non-linear guiding centre theory using the 2D turbulence power spectrum, and their results produce a fair to good agreement with spacecraft observations of turbulence quantities throughout the heliosphere. Recently, Shalchi (2010) proposed a nonlinear diffusion theory for perpendicular transport, but this theory contains previous theories as special cases and limits, and it was found that it agrees well with the non-linear guiding centre theory of Matthaeus et al. (2003) for 2D turbulence. The perpendicular diffusion coefficient for the 2D turbulence based on the unified non-linear transport theory for different spectra and found that this theory yields the same results as those obtained when using the non-linear guiding centre theory; it was also also found that the inertial range of the spectrum does not have a strong influence on perpendicular mean free path. The application of these new theories to solar modulation has been carried out recently by Engelbrecht (2012) and an ab initio approach for solar modulation of cosmic ray modulation and for galactic electrons is given by Engelbrecht and Burger (2013a, b).

In this thesis the in-depth study of turbulence and its application to the solar modulation was not pursued and is considered beyond the scope of this numerical modeling study.

3.6 Numerical models

For the past four decades CRs models, in particular numerical models, have been developed with increasing complexity, from steady state to comprehensive time dependent models, including the TS with diffusive shock acceleration. The observations have always been limited, as such numerical modeling plays a crucial role in enhancing our understanding of solar modulation. See the reviews by Potgieter (1998, 2013a), Potgieter and Ferreira (2001) and Heber and Potgieter (2006).

3.6.1 A short overview of numerical models

The first numerical solution of the TPE was developed by Fisk (1971), where he assumed a steady state and spherical symmetry in a 1D model with radial distance as the only spatial variable. Fisk (1976) developed a 2D steady state model without drifts, but it included a polar angle dependence. The first numerical model which includes gradient and curvature drifts for a flat HCS was developed by Jokipii and Kopriva (1979) and Moraal et al. (1979)

respectively. The first 2D numerical models simulating the waviness of the HCS were developed by Potgieter and Moraal (1985) and Burger and Potgieter (1989).

Kóta and Jokipii (1983) were the first to develop a full 3D steady state drift model, followed by Williams (1990); Hattingh (1998), and Gil and Alania (2001). Fichtner et al. (2000) developed a 3D steady state non-drift model which included the Jovian magnetosphere as a source for low energy electrons. In 2001, Ferreira et al. (2001a, b) developed a 3D steady state drift model which included gradient, curvature and current sheet drifts and the Jovian magnetosphere as a source of low energy electrons. The motivation for developing this model was the Ulysses observations which revealed 3D modulation effects in the inner heliosphere. These steady state models describe solar cycle effects as a series of steady solutions with each solution containing solar activity related changes in the modulation parameters such as the solar wind, the various diffusion coefficients and the Jovian electron source, neglecting strong time dependent effects such as the re-acceleration of GCRs at the TS. This model is the departure point of this study. The Ferreira model as well as improvements thereof was applied by Moeketsi (2004) and Nkosi (2006), see also Moeketsi et al. (2005) and Nkosi et al. (2008). For this thesis, the focus is on the modulation of CRs electrons in the heliosphere. The section that follows gives a brief overview of the applied numerical scheme. For a more elaborative discussion of this scheme, see Hattingh (1998).

3.6.2 The numerical scheme

The TPE as in Eq. (3.8) is solved in terms of the distribution function which is normalized to the CRs input spectrum, in other words, the galactic or local interstellar spectrum f_g so that

$$f(\mathbf{r},P)=\frac{f_0(\mathbf{r},P)}{f_g(P)} \tag{3.58}$$

The following boundary conditions are implemented:

i. At the outer modulation boundary $(r=r_b)$, typically assumed to be the HP, the distribution function is equal to the LIS

$$f(r_b,\theta,\phi,P)=f_g(P). \tag{3.59}$$

ii. At the inner boundary $(r=r_1)$ it is assumed that the gradient of the distribution function relative to r is the same just outside the boundary than just inside, so that

$$\left.\frac{\partial f}{\partial r}\right|_{r=r_0} = \left.\frac{\partial f}{\partial r}\right|_{r=r_1}. \tag{3.60}$$

iii. On the polar lines, the partial derivative of the distribution function relative to the polar angle is zero

$$\left.\frac{\partial f}{\partial \theta}\right|_{\theta=0,\pi} = 0. \tag{3.61}$$

iv. The grid line at $\phi = 0^\circ$ is the same as the grid at $\phi = 360^\circ$.

In order to solve the TPE in Eq. (3.8) numerically, it is re-written as

$$\begin{aligned} &a'(r,\theta,\phi,P)\frac{\partial f}{\partial r} + b'(r,\theta,\phi,P)\frac{\partial f}{\partial \theta} + c'(r,\theta,\phi,P)\frac{\partial f}{\partial \phi} \\ &+d'(r,\theta,\phi,P)\frac{\partial^2 f}{\partial r \partial \phi} + e'(r,\theta,\phi,P)\frac{\partial^2 f}{\partial r^2} + l'(r,\theta,\phi,P)\frac{\partial^2 f}{\partial \theta^2} \\ &+m'(r,\theta,\phi,P)\frac{\partial^2 f}{\partial \phi^2} + s'(r,\theta,\phi,P)\frac{\partial f}{\partial \ln p} = 0, \end{aligned} \tag{3.62}$$

where

$$\begin{aligned} a'(r,\theta,\phi,P) &= \frac{1}{r^2}\frac{\partial}{\partial r}\left(r^2 K_{rr}\right) + \frac{1}{r\sin\theta}\frac{\partial}{\partial \theta}\left(K_{\theta r}\sin\theta\right) + \frac{1}{r\sin\theta}\frac{\partial K_{\phi r}}{\partial \phi} - V \\ b'(r,\theta,\phi,P) &= \frac{1}{r^2}\frac{\partial}{\partial r}\left(rK_{r\theta}\right) + \frac{1}{r^2\sin\theta}\frac{\partial}{\partial \theta}\left(K_{\theta\theta}\sin\theta\right) + \frac{1}{r^2\sin\theta}\frac{\partial K_{\phi\theta}}{\partial \phi} \\ c'(r,\theta,\phi,P) &= \frac{1}{r^2\sin\theta}\frac{\partial}{\partial r}\left(rK_{r\phi}\right) + \frac{1}{r^2\sin\theta}\frac{\partial K_{\theta\phi}}{\partial \theta} + \frac{1}{r^2\sin^2\theta}\frac{\partial K_{\phi\phi}}{\partial \phi} - \Omega \end{aligned} \tag{3.63}$$

$$d'(r,\theta,\phi,P) = \frac{2K_{r\phi}}{r\sin\theta}$$

$$e'(r,\theta,\phi,P) = K_{rr}$$

$$l'(r,\theta,\phi,P) = \frac{K_{\theta\theta}}{r^2}$$

$$m'(r,\theta,\phi,P) = \frac{K_{\phi\phi}}{r^2\sin^2\theta}$$

$$s'(r,\theta,\phi,P) = \frac{1}{3r^2}\frac{\partial}{\partial r}\left(r^2 V\right).$$

The TPE is a parabolic differential equation and can be solved for three spatial coordinates, radial distance r, polar angle θ and azimuthal angle ϕ, in terms of rigidity starting from an

assumed maximum rigidity, where no modulation is assumed, working downwards to a sp ecified minimum rigidity. In this work the ADI method is used to solve the TPE for three spatial coordinates and rigidity. See Potgieter (1984) and Hattingh (1998) for full discussions of this method. Unfortunately, having four numerical dimensions to handle, the ADI method is not always stable and strict precaution must be applied to avoid large intensity gradients. This is also a serious inhibiting factor, contributing to why the ADI is unsuited for adding a fifth numerical dimension, such as a time-dependence. Most time-dependent models for solar modulation studies have therefore only two spatial dimensions (e.g. Ngobeni 2015). Recently, this obstacle was overcome by using the so-called Stochastic Differential Equation (SDE) method of solving the TPE, but with its own set of complications; see e.g. Kopp et al. (2012, 2014); Strauss (2013); Strauss et al. (2012) and Lou et al. (2013).

In this study, the HPS is taken as an input spectrum at the outer boundary of the heliosphere; the HP, located at $r_b = 122$ AU for all values of θ and ϕ. The solution is obtained as follows: A solution is then obtained by first calculating an initial solution at one third of a rigidity step backward by solving the differential equation implicit in the direction of r. A second solution is determined at another third of a rigidity step backward in terms of θ, and the process is repeated for ϕ to determine a solution at the third rigidity step in terms of the two previous solutions. As a result, a system of linear equations is obtained which can be solved using the Thomas algorithm (Lapidus and Pinder 1982). For locally developed models, Williams (1990) was the first to implement this numerical scheme in order to solve the TPE in three spatial coordinates, with rigidity as a fourth numerical coordinate, but only for a flat HCS, after which Hattingh (1998) applied it to the wavy HCS model. The latter still forms the basis of the numerical scheme as used here. See also Ferreira et al. (2000).

The TPE is solved numerically for a 3D grid with radial grid points $r_i = (i-1)\Delta r + r_1$ for $i = 1, 2, ..., N_r$ running from $r = r_1$ at the inner boundary to $r = r_b$ at the outer boundary with the radial increments $\Delta r = (r_b - r_1)/(N_r - 1)$. The polar grid points are $\theta_j = (j-1)\Delta\theta$ for $j = 1, 2, ..., N_\theta$ running from the north pole at $\theta = 0^\circ$ to the south pole at $\theta = 180^\circ$, with the polar increments $\Delta\theta = \pi/(N_\theta - 1)$. The azimuthal grid points are $\phi_k = (k-1)\Delta\phi$ for $k = 1, 2, ..., N_\phi$ running from $\phi = 0^\circ$ to $\phi = 360^\circ$, for one rotation of the Sun, where the azimuthal increments are $\Delta\phi = 2\pi/(N_\phi - 1)$. The rigidity decreases logarithmically from an initial maximum value where the modulation is negligible.

The distribution function *f* is related to the differential intensity by $j = P^2 f$.

The distribution function in terms of the grid points is

$$f\left(r_i,\theta_i,\phi_{k,}P_n\right)=f\left(i\Delta r,\,j\Delta\theta,k\Delta\phi,n\Delta\ln P\right)=f_{i,j,k,n,} \tag{3.64}$$

so that, from a Taylor series expansion, the central finite difference approximation for the first, second and mixed derivatives of f, given in general terms here as a function of *x* and *y,* is given by

$$\begin{aligned}
\frac{\partial f}{\partial x}&=\frac{f\left(x+\Delta x\right)-f\left(x-\Delta x\right)}{\Delta x}\\
\frac{\partial^2 f\left(x\right)}{\partial x^2}&=\frac{f\left(x+\Delta x\right)-2f\left(x\right)+f\left(x-\Delta x\right)}{\left(\Delta x\right)^2}\\
\frac{\partial^2 f\left(x\right)}{\partial x\partial y}&=\frac{f\left(x+\Delta x,y+\Delta y\right)-f\left(x+\Delta x,y-\Delta y\right)-f\left(x-\Delta x,y+\Delta y\right)}{4\Delta x\Delta y}\\
&\quad+\frac{f\left(x-\Delta x,y-\Delta y\right)}{4\Delta x\Delta y}.
\end{aligned} \tag{3.65}$$

The error on the first two equations is $\left(\Delta x\right)^2$, and on the third it is $\Delta x\Delta y$. In terms of the grid points these equations are re-written as

$$\begin{aligned}
\frac{\partial f}{\partial x}&=\frac{f_{i+1}-f_{i-1}}{2\Delta x}\\
\frac{\partial^2 f}{\partial x^2}&=\frac{f_{i+1}-2f_i+f_{i-1}}{\left(\Delta x\right)^2}\\
\frac{\partial^2 f}{\partial x\partial y}&=\frac{f_{i+1,j+1}-f_{i+1,j-1}-f_{i-1,j+1}+f_{i-1,j-1}}{4\Delta x\Delta y}.
\end{aligned} \tag{3.66}$$

The respective solutions for f at different rigidity steps are

$$\begin{aligned}
f_{i,j,k,n}&=f_{i,j,k}\\
f_{i,j,k,n+\frac{1}{3}}&=f^*_{i,j,k}\\
f_{i,j,k,n+\frac{2}{3}}&=g_{i,j,k}\\
f_{i,j,k,n+1}&=h_{i,j,k}.
\end{aligned} \tag{3.67}$$

The boundary condition (3.59) at r_b in terms of the grid points is

$$f_{N,j,k}=f_g, \tag{3.68}$$

for $j = 1, 2, ..., N_\theta$ and $k = 1, 2, ..., N_\phi$. At r_1 the slope of f between r_0 and r_1 is taken to be equal to the slope between r_1 and r_2 so that

$$f_{0,j,k} = 2f_{1,j,k} - f_{2,j,k}, \tag{3. 69}$$

for $j = 1, 2, ..., N_\theta$ and $k = 1, 2, ..., N_\phi$. The boundary condition in Eq. (3.61) at the poles is

$$f_{i,0,k} = f_{i,2,k}, \tag{3.70}$$

$$f_{i,N_\theta+1,k} = f_{i,N_\theta-1,k}, \tag{3.71}$$

for $i = 1, 2, ..., N_r$ and $k = 1, 2, ..., N_\phi$. At $\phi = 0^\circ, 360^\circ$

$$f_{i,j,0} = f_{i,j,N_\phi-1}, \tag{3.72}$$

$$f_{i,j,N_\phi} = f_{i,j,1}, \tag{3.73}$$

$$f_{i,j,N_\phi+1} = f_{i,j,2}, \tag{3.74}$$

for $i = 1, 2, ..., N_r$ and $j = 1, 2, ..., N_\theta$. This last set of boundary conditions ensures the continuity at the edges of the ϕ-grid.

The first solution $f^*_{i,j,k}$ is calculated by solving Eq. (3.62) implicitly in the radial direction at one third of a rigidity step backward. This is achieved by evaluating half of the central difference Eq. (3.66) in r at the present rigidity step and half of them at the third of a rigidity step backwards. For the second solution, $g_{i,j,k}$ this process is repeated by once again solving Eq. (3.63) implicitly, in terms of $f^*_{i,j,k}$, in the θ direction. Similarly, the third solution, $h_{i,j,k}$ in terms of $f^*_{i,j,k}$ and $g_{i,j,k}$ is obtained at one full rigidity step backward by solving Eq. (3.63) implicitly in ϕ-direction. This process is repeated for all rigidity values in order to obtain a solution for the final distribution function f, which is related to the differential intensity j as $j = P^2 f$.

3.7 Summary

This chapter was devoted to the theoretical and numerical aspects of the CRs modulation model as used in this study. A brief background on the TPE, the 3D modulation model and aspects of the diffusion and drift tensors were given. In particular, the rigidity dependence of all the diffusion coefficients and the drift coefficient was discussed and illustrated. The consequences of these aspects will be discussed further in later chapters. A brief overview was given of the numerical scheme.

The next chapter is devoted to computing the heliopause spectrum for electrons.

Chapter 4

Interstellar spectra for electrons

4.1 Introduction

The local interstellar spectrum (LIS) for galactic electrons is one of the important aspects of solar modulation studies because it is specified as an input spectrum for modulation models. In the literature various authors have tried to explain what this spectrum is and what it should look like. At high energies this is less problematic since observations from various spacecraft and balloon flights have shed light on this aspect. The problem occurs at lower kinetic energies (E < ~1 GeV), because of solar modulation and the fact that the diffusion coefficients throughout the heliosphere are not well established, so that the issue about interstellar spectra has remained controversial for a long time. This issue, concerning both the spectral shape of the spectrum and the value of the differential intensity, was partially resolved, as recently as 2010, when Voyager 1 returned observations indicating that this spectrum is a power law in terms of kinetic energy. In this section the issue pertaining to the interstellar spectrum for electrons is further discussed. The main purpose is to find through this research the most reasonable very LIS for electrons and to use those in this modeling approach to the solar modulation of electrons.

4.2 Galactic spectra as local interstellar spectra

For a long time the science community in this field has simply accepted the concepts like galactic spectra (GS), interstellar spectra (IS) and local interstellar spectra (LIS) to have the same meaning and values. Potgieter and Nndanganeni (2013a, b) introduced the concept of a heliopause spectrum (HPS) as an input spectrum required for modulation models. They argue that this HPS should be seen as the lowest possible very LIS which may or may not be identical to a LIS. This can of course only be verified once Voyager 1 is deeper into the interstellar medium. It is believed, however, that the latest observed spectra from Voyager 1 can be considered as HPS, since now it is widely accepted that Voyager 1 indeed crossed the HP during August 2012 (Stone et al. 2013; Burlaga et al. 2013; Gurnett et al. 2013).

From a solar modulation point of view, GS at low energies are referred to as mostly computed spectra based on astrophysical sources, usually assumed to be evenly distributed through the Galaxy and relatively far away from the heliosphere. They may be different from LIS, which are regarded as spectra thousands of AU away from the Sun, which may be different from a very LIS, say within ~200 AU from the Sun, which may be quite similar to a HPS. The HPS is the ideal choice to use in solar modulation models. In this study the latest Voyager 1 observations are used together with modulation models to compute such electron spectra, to be followed by computing the total solar modulation. First a short review is given of the progress that has been made in computing GS, presented as LIS, over the last decade or so.

4.3 Computed galactic electron spectra

Below a few GeV, down to a few MeV, the effects of solar modulation in the heliosphere greatly change the shape of electron spectra, and are difficult to correct for. In the literature published by different authors, computed LIS follow from different types of galactic propagation models. The best known are those computed from an astrophysical point of view, using mostly the openly available GALPROP model (Strong et al. 1994, 2000; Ptuskin et al. 2006) or modified GALPROP models such as DRAGON (e.g. Gaggero et al. 2013) or the new generation PICARD code (Kissmann 2014) as well as Monte Carlo-type models (e.g. Webber 1993), together with different heliospheric modulation models, but mainly the simple force-field model (Strong et al. 2007, 2011).

Electrons produce synchrotron radiation so that radio data can be used in estimating the electron GS at very low energies. Strong et al. (1994, 2000) and Langner et al. (2001), for example, did some work on this approach and computed GS used as LIS in early modulation models. Since then they and others have made improvements to the models as new observational data became available.

More sophisticated galactic propagation models, including updated physics, have been developed, and corresponding computations have been done over the years. For example, Ptuskin et al. (2006) investigated and re-examined some of the physical turbulence processes in galactic space, involving the rigidity dependence of the diffusion of cosmic rays through the galaxy. They applied three theoretical approaches in the GALPROP code: re-acceleration with damping (DRD); plain diffusion (PD) with a break in the diffusion coefficient, and an approach with distributed re-acceleration (DR), and power law diffusion with no breaks.

These different models and examples of their computed spectra were also shown and discussed by Nndanganeni (2012) and will be referred to again briefly below.

A different method to determine the very LIS is to do so from a modulation point of view, which made significant progress when Voyager 1 crossed the TS and entered the inner heliosheath. Webber and Higbie (2008) derived such a LIS which is lower than all the previous LIS over the entire range of measurements. They used a Monte Carlo Diffusion Model for electron propagation in the Galaxy to calculate alternative electron LIS below ~1 GeV. They also used the out dated force-field modulation approach but pointed out that solar modulation effects should be properly handled at low energies in the outer heliosphere. This was the first attempt to compute the LIS that is constraint to Voyager 1 data. They calculated a few plausible electron LIS and found most of them to be lower than the one from Langner et al. (2001). They also critically evaluated the computed electron spectra presented by Ptuskin et al. (2006) and found most of them to be lower than the one from Langner et al. (2001). Three of the Webber and Higbie (2008) spectra, identified as IS 2.2, IS 2.3 and IS 2.4, are basically the same down to ~500 MeV, but with their IS 2.3 similar to the one by Langner et al. (2001). When these LIS were evaluated by comparing them to observations in the heliosphere, it was found that some of them were not compatible to these observations and were eliminated, as discussed by Nndanganeni (2012).

In what follows, these aspects are discussed and emphasized further. Figure 4.1 is taken from Webber and Higbie (2008). The two panels show several computed LIS, together with the LIS from Langner et al. (2001) and Ptuskin et al. (2006), in comparison with observations near Earth and from Voyager 1. The top panel shows three of their spectra IS 2.4, IS 2.3 and IS 2.2, together with the PD and DRD approaches of Ptuskin et al. (2006), and also the LIS from Langner et al. (2001). The bottom panel shows the results from Webber and Higbie (2008) where they followed the Ptuskin approaches, but used a Monte Carlo Diffusion model to compute the LIS. The peculiar forms of spectra PD, DRD, IS-7 and IS-11 are caused by differences in the rigidity dependence of the galactic diffusion coefficient.

Strong et al. (2011) re-analysed synchrotron radiation data, using various radio surveys to constrain the low energy electron LIS in combination with the Fermi-LAT and other experiments. They applied two different theoretical approaches in the GALPROP code: a plain diffusion model, and a re-acceleration model. Their main objective was to reproduce the observations at high energy, but they also used the synchrotron data as a constraint at low energies when computing the interstellar spectra. They preferred the plain diffusion model because the re-acceleration model reproduces too high intensities at the energy range of

interest and as such could not reproduce the direct measurements or the synchrotron data. They also computed the modulated spectra at Earth, using a simple force field modulation model, which is strictly speaking not valid for electron modulation at E < ~1 GeV because it deals with adiabatic energy losses as if electrons are losing as much energy as protons, which is not the case. Despite this latest improvement in determining the electron LIS, they still experienced difficulties regarding how to deal with the effects of solar modulation.

Figure 4.2 shows two examples of computed GS, presented as LIS, from Strong et al. (2011), together with a large set of data and several modulated spectra using various force-field modulation model options, as indicated in the figures. All these LIS were computed using the pure diffusion model in GALPROP. At high energies they all reproduce the measurements fairly well and also seem to give a reasonable representation of the synchrotron data. The main conclusion drawn from their work is that the LIS must turn below a few GeV, that is, exhibit a spectral break. In addition, they state that the LIS below few GeV has to be lower than what standard galactic propagation models predict.

Figure 4.3 displays a compilation of various computed GS, presented as LIS. These spectra are from Langner et al. (2001), Webber and Higbie (2008) and Strong et al. (2011), indicated in the figure. The main objective here is to make a direct comparison of the spectral shapes between these computed spectra that were done over the years to see how they have evolved. For this reason they are normalised at the highest possible energy. The Langner 2001 spectrum has been used for many years as the preferred LIS in modulation models by the local research group (in the Centre for Space Research).

Webber and Higbie (2008) were motivated by the new experimental and theoretical developments related to both electron propagation in the Galaxy and to the electron spectra observed by Voyager 1. They argued that the Langner 2001 LIS was too high at low energies although their option, IS-2.3, was almost identical to Langner 2001. This is to be expected since both authors used the observed radio data to improve the spectral shape below 50 MeV. On the other hand, their IS-7 option, influenced by the Voyager 1 observations, was considerable lower than Langner 2001, but quite in agreement with the two options from Strong et al. (2011). For E > 1 GeV these spectra are quite similar, but not identical, most likely because of the large number of data sets they could be tuned to. It became obvious that the large differences at the low energies could only be resolved if direct electron observations were made in this energy range in the outer heliosphere.

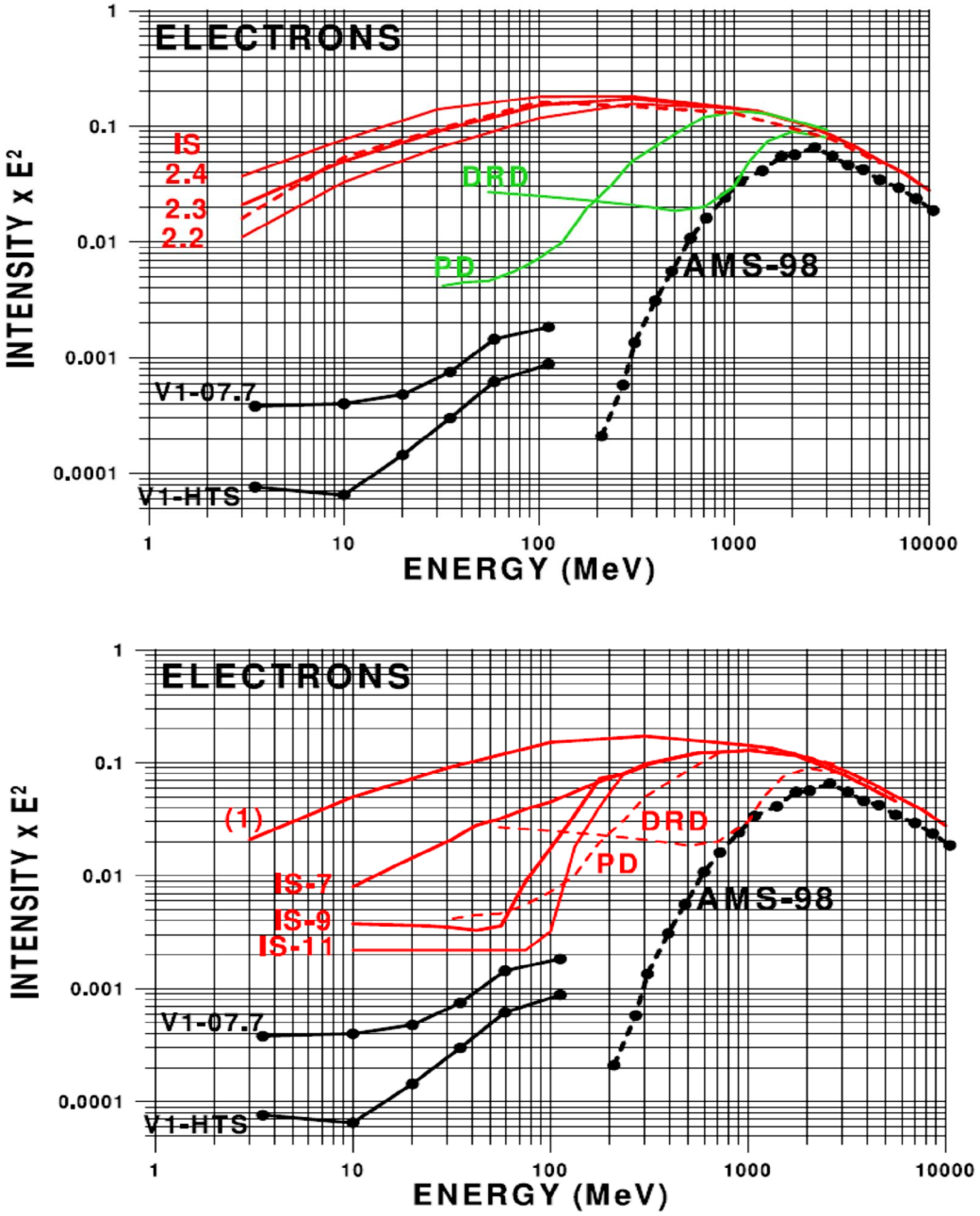

Figure 4.1: The top panel shows various computed electron LIS (red lines) from Webber and Higbie (2008), indicated by IS 2.4, 2.3 and 2.2 in comparison with two LIS calculated by Ptuskin et al. (2006), and indicated by DRD and PD (two green lines). The red dashed line is the LIS from Langner et al. (2001). The data points (in black) are AMS-1 electron measurements (Alcaraz et al. 2000) at Earth at the time of the 1998 modulation minimum (AMS-98) and Voyager 1 electron measurements (McDonald et al. 2007) at the time of its TS crossing (V1-HTS) and ~3 years later (V1-07.7). The bottom panel shows these observations and the mentioned PD and DRD models with the various attempts from Webber and Higbie (2008) at computing the LIS using their Monte Carlo Diffusion model. Here (1) indicates a reference LIS based on a source spectral index of -2.3 and a constant galactic diffusion coefficient below ~3.0 GV. The other three computed spectra (IS-7, IS-9 and IS-11) each has a different rigidity dependence for the galactic diffusion coefficient.

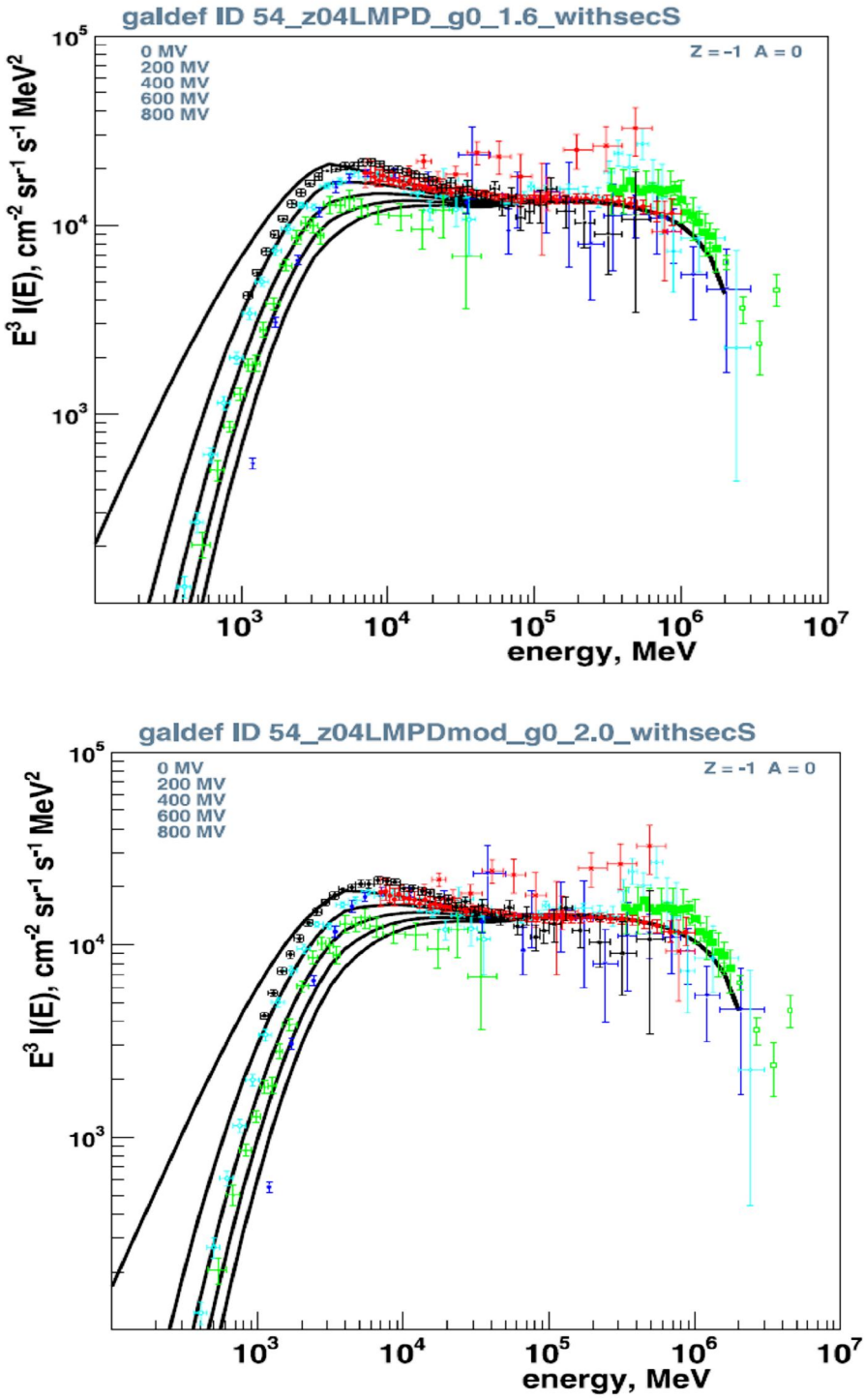

Figure 4.2: Two examples of computed galactic electron spectra from Strong et al. (2011) shown as the upper black curve in both panels together with several modulated spectra, using various force field model options as indicated. All these spectra were computed using a pure diffusion model in GALPROP. The data points, as listed and referenced by Strong et al. (2011), are from various experiments: Cyan open circle: AMS01; green crosses and filled circles: CAPRICE: blue squares: HEAT; red filled circle: Fermi-LAT; black filled circles: PAMELA; blue triangles: SANRIKU; red crosses: BETS, PPT-BETS; cyan open circles: ATIC-1-2; green filled and open squares: H.E.S.S.

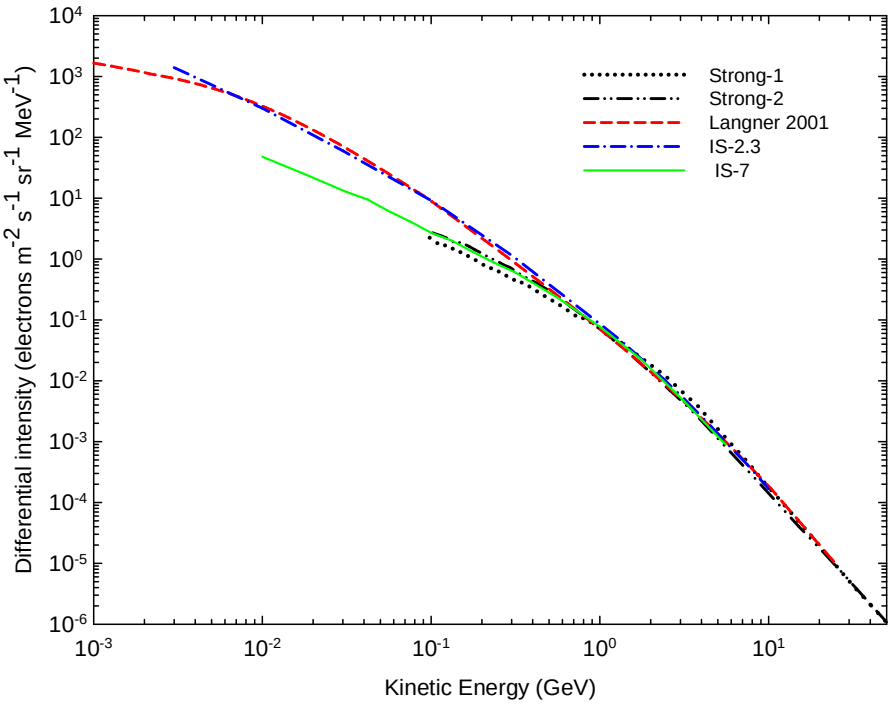

Figure 4.3: A compilation of various computed GS, presented as LIS; from Langner et al. (2001) indicated as Langner 2001; from Webber and Higbie (2008) indicated as IS-7 and IS-2.3, together with two LIS from Strong et al. (2011) indicated as Strong-1 and Strong -2.

In 2010, Voyager 1 returned exactly the observations that were needed and gave an answer to the long outstanding question regarding the spectral shape (energy dependence) and the value of the LIS at these low energies. For the first time, these observations gave an indication that the electron LIS at these energies (E < 100 MeV) could be a power law. None of the computed spectra shown in Figure 4.3 could reproduce observed spectrum from Voyager 1 and hence it was necessary to reinvestigate the issue further as is done and discussed below. Nndanganeni (2012) and Vos (2011), motivated by the work of Webber and Higbie (2008), used a 3D modulation model as described in this work to compute a LIS or what can be referred to as the HPS for electrons by using Voyager 1 spectra at low energies (~6-120 MeV) observed during 2010 and the PAMELA yearly averaged spectrum for 2009. Based on this study, it was concluded that the HPS has a power law form $E^{(-1.5\pm0.1)}$ below ~0.8 GeV but $E^{(-3.13\pm0.05)}$ above ~2 GeV. This HPS was used by Potgieter and Nndanganeni (2013a) to compute the total modulation of galactic electrons from the inner to the outer heliosphere, emphasizing the importance of determining such a HPS. An important assumption was that for electron modulation in the heliosphere the basic diffusion coefficients should be

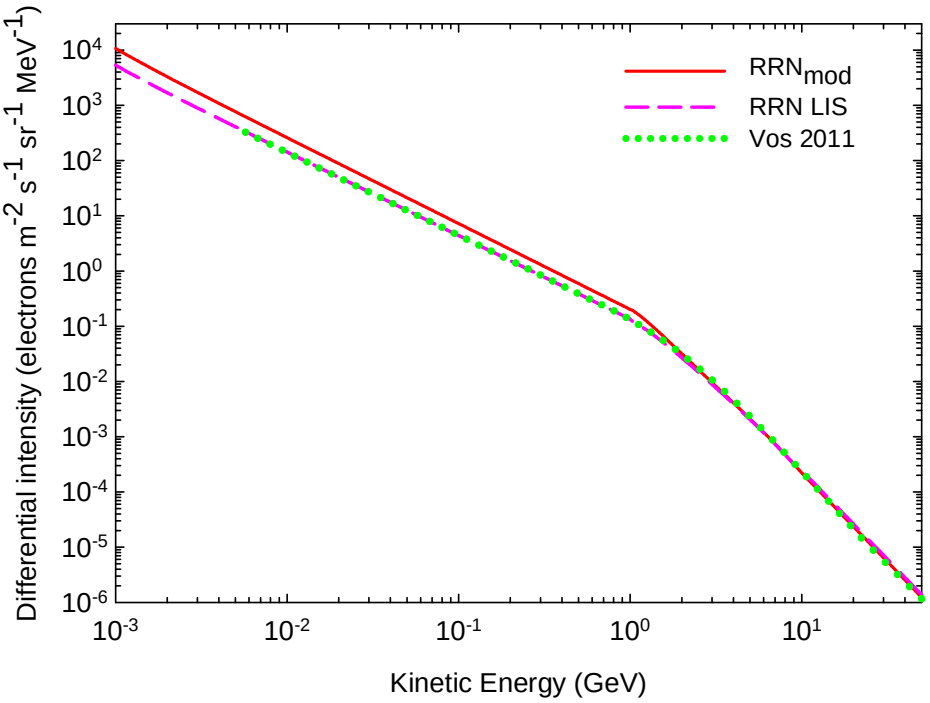

Figure 4.4: Computed electron heliopause spectra (HPS) based on previous work from Nndanganeni (2012) indicated as RRN LIS, from Vos (2011) indicated as Vos 2011 and as RRN_{mod} from Potgieter and Nndanganeni (2013b). Below 800 MeV, the latter has the form $E^{(-1.55\pm0.05)}$ whereas above ~2 GeV it becomes $E^{(-3.13\pm0.05)}$. However, note the slight 'bump' in the Vos 2011 LIS between ~2 GeV and ~ 15 GeV, which requires the spectral shape to change to $E^{-(3.13\pm0.05)}$.

independent of rigidity at these low energies, essentially as predicted by turbulence theory applicable at Earth (e.g. Potgieter 1996).

Potgieter and Nndanganeni (2013b) went on to refine the RRN LIS, which has $E^{-1.5}$, to RRN_{mod} with $E^{-1.55}$, by taking statistical and systematic uncertainties into account. This HPS was then used in the modulation of galactic electrons in the heliosphere, until recently when Voyager 1 crossed the HP and returned what could be regarded as the 'true' HPS, the highest observed electron spectrum in and beyond the heliosheath. See also the progress report by Nndanganeni and Potgieter (2013a). An effect that was unknown to Nndanganeni (2012), was that the PAMELA electron observations for the period of 2006 to 2009 (Adriani et al. 2015) exhibit a spectral feature (a bump) between ~ 2 GeV and ~ 15 GeV, as a complication to the picture presented by Potgieter and Nndanganeni (2013a, b). This seemingly important feature was first illustrated in the Masterôs thesis of Vos (2011), and later reported by Vos et al. (2013); see also Potgieter et al. (2014b). This means that above ~2 GeV but below ~ 20 GeV,

the spectral shape has to change to $E^{-(3.13\pm0.05)}$, indicative of a second break in the very LIS for galactic electrons. Figure 4.4 shows the three computed HPS, from Vos (2011), Nndanganeni (2012) and Potgieter and Nndanganeni (2013b). The issue about the highest computed HPS based on the latest Voyager 1 observations will be addressed in section 4.5 where new HPS will be presented.

4.4 Modulation implication of different LIS

In the preceding section, the different computed LIS were discussed, and several examples were shown, differing greatly from one another. The main aim of this section is to show how different LIS, and also changing the rigidity dependence of the diffusion coefficients in the model, affect the modulation of electrons from the inner heliosphere to the outer heliosphere. The purpose is to emphasize how important the choice of the LIS is in numerical modeling and how significantly the spectral shape of modulated spectra is changed when making these changes.

For this purpose, the computations were done with the 3D model as described in Chapter 3, from the inner to the outer heliosphere at the following radial distances: 1 AU, 5 AU, 60 AU, 90 AU and 110 AU, in the equatorial plane. The heliopause in the modulation model was specified at 120 AU with the TS at 94 AU in this case. These illustrative computations were done using the Langner 2001 and RRN LIS as discussed above; using the diffusion coefficients as given by Ndiitwani (2005), and later with the diffusion coefficients as given by Nndanganeni (2012). See Eqs. (3.35-3.39) and Eqs. (3.44-3.47) respectively shown in Chapter 3.

4.4.1 Illustrative modeling examples

Figure 4.5 shows computed spectra at 1 AU, 5 AU, 60 AU, 90 AU and 110 AU, in the equatorial plane. The top panel shows computed spectra with respect to the Langer 2001 LIS, and the bottom panel shows the spectra computed with respect to the RRN LIS. To recap, the Langner 2001 LIS (Langner et al. 2001) was used extensively in the past, for almost a decade, as the preferred LIS in modulation studies by the members of the local Heliophysics Group (e.g. Ferreira 2002; Langner 2004; Moeketsi 2004 and Nkosi 2006). The RNN LIS by Nndanganeni (2012) was applied to the modeling of the modulation of galactic electron in the heliosphere also by Potgieter and Nndanganeni (2013a). This particular LIS was thus

considered as the replacement of the Langner 2001 LIS. First, it will be illustrated why it matters and also what the general features are of modulated electron spectra.

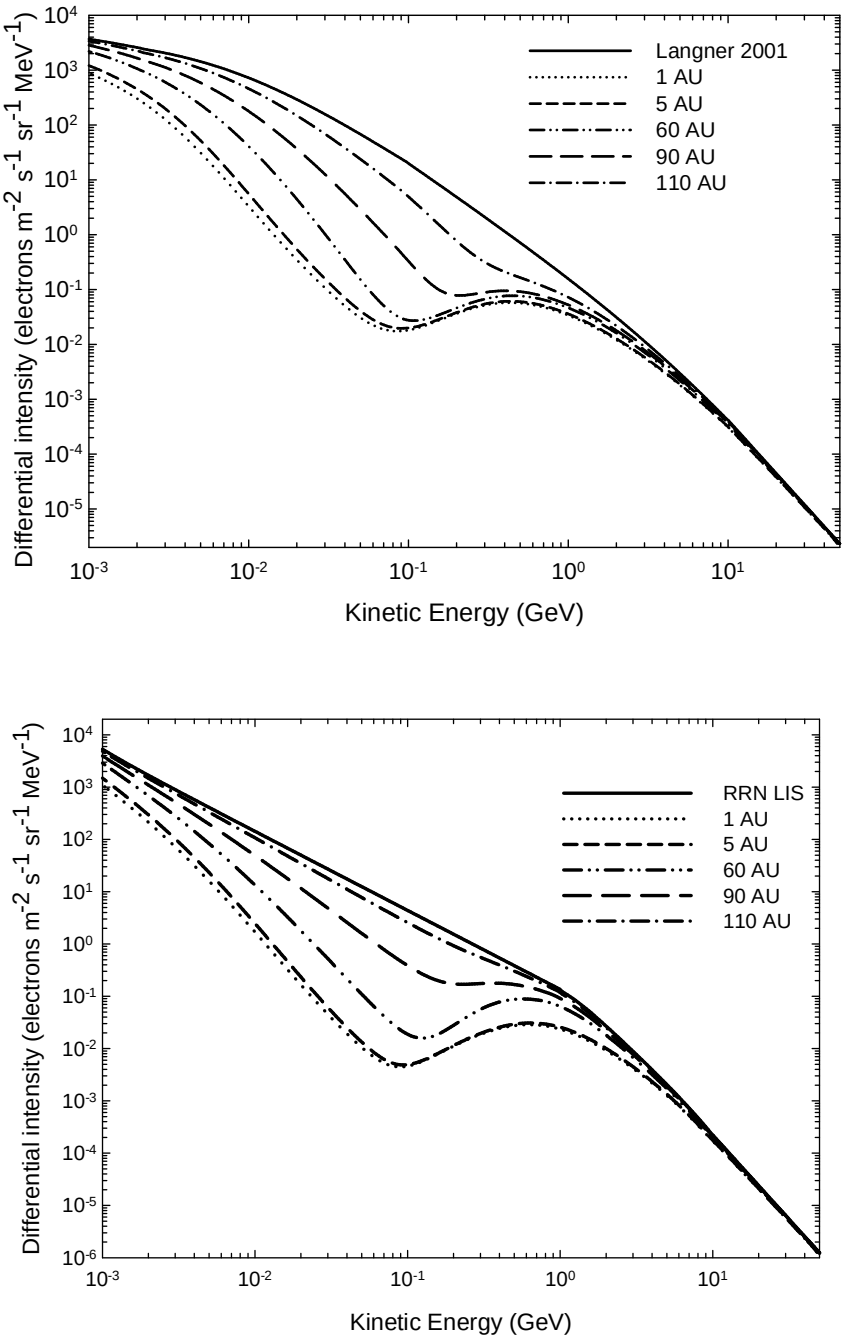

Figure 4.5: Computed modulated spectra at radial distance of 1 AU, 5 AU, 60 AU, 90 AU and 110 AU in the equatorial plane. These spectra are computed with respect to the Langner 2001 LIS (top panel) and the RRN LIS (bottom panel). The diffusion coefficients used in the model are from Ndiitwani (2005) as shown in Figure 3.4 in Chapter 3. The heliopause is at 120 AU.

In both cases, the LIS are normalized at 50 GeV, the energy above which it is assumed that no heliospheric modulation occurs. In this context, see also Strauss and Potgieter (2014).

It follows from this figure that the modulated spectra exhibits characteristic features, such as reaching a local peak, around ~500 MeV, gradually decreasing to around 50 MeV with increasing distance from the Sun. Closer to the HP this peak gradually subsides. Below these peaks, the modulated intensity decreases with decreasing energy to produce a clear local minimum just below 100 MeV in the inner heliosphere. These minima also move up in energy with increasing radial distance from the Sun. This phenomenon is the result of electron modulation, with nothing in the shape of the LIS resembling it. Below ~100 MeV, the modulated intensities always increase sharply, to follow the increasing trend of the spectral shape of the assumed LIS. At the lowest energy, around 1 MeV, the modulation for this choice of diffusion coefficients, produce little modulation. This is the direct consequence of assuming the rigidity dependence of the diffusion coefficients to change, making them larger with decreasing energy. (See Figure 3.4 in Chapter 3 and Eqs. 3.35-3.39). The consequence is that the total modulation at these low energies is getting rather small.

Figure 4.6 shows the changes in the modulated spectra related to changes in the rigidity dependence of the diffusion coefficients (see Eqs. 3.44-3.47 and Figures 3.6). The top panel is for the computation done with respect to the Langner 2001 LIS, and the bottom panel is with respect to the RRN LIS. The basic difference is that the diffusion coefficients are assumed to be constant below $P \leq 0.4$ GV, but to increase above $P > 0.4$ GV.

The consequence is that below $E < 50$ MeV at Earth, the total modulation becomes constant with decreasing E, with the modulated spectra having the same slope (spectral index) as the LIS down to 1 MeV. The same features, with subtle differences, are displayed as in the previous figure but mostly not as pronounced. The 1 AU and 5 AU spectra show significant modulation already at ~5 GeV, as compared to the spectra at larger radial distances. With $E > 100$ MeV, the 1 AU and 5 AU spectra are almost indistinguishable, as is the case for the 60 AU and 90 AU spectra. At 110 AU the modulation is still significant, with the heliopause at 120 AU.

Assuming the diffusion coefficients independent of rigidity below 0.4 GV is in line with the basic prediction of turbulence theory applicable in the inner heliosphere (e.g. Potgieter 1996; Burger et al. 2000) and in sharp contrast to the situation for protons (e.g. Potgieter 2000). This aspect and the main modulation features evident here will be discussed further in coming chapters.

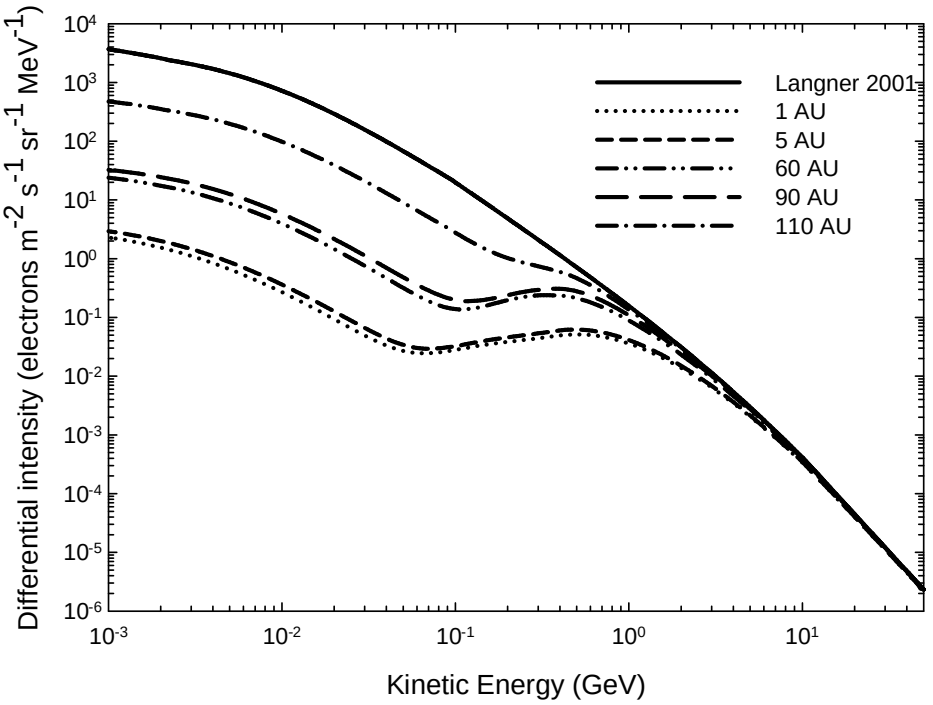

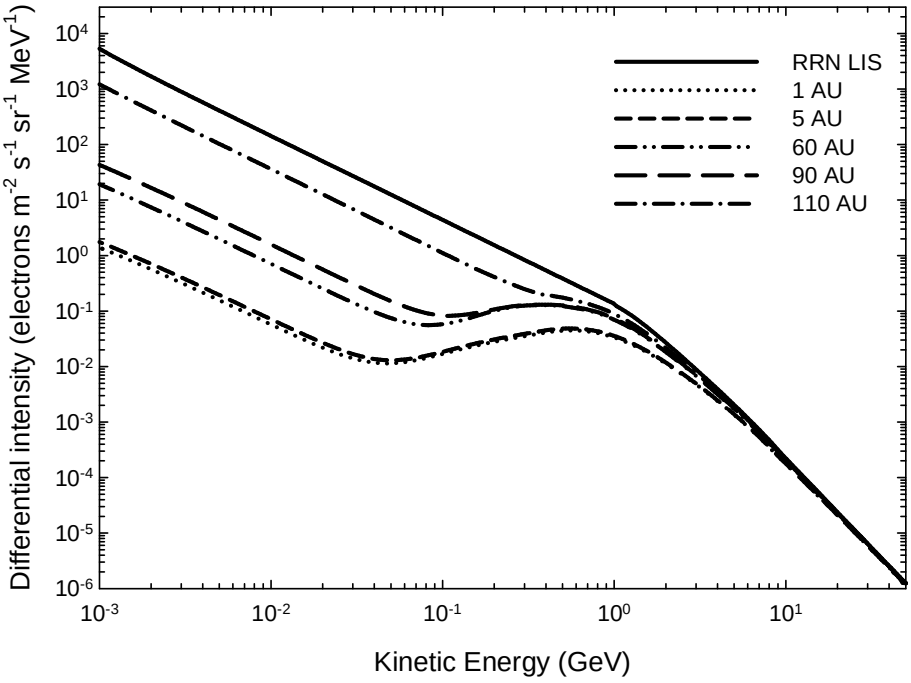

Figure 4.6: Similar to Figure 4.5, again with respect to the Langner 2001 LIS (top panel) and the RRN LIS (bottom panel), but now with a constant rigidity dependence of the diffusion coefficients as shown in Figures 3.6.

The main effect shown here is that if the diffusion coefficients are independent of rigidity at these low energies, then the modulated spectra throughout the heliosphere follow the spectral shape of the LIS at these low energies, again in sharp contrast to proton modulation where the modulated spectra in the inner heliosphere at low energies are dominantly determined by adiabatic energy loses so that the spectral shape of the proton LIS is then completely obscured.

4.5 The new electron HPS

As stated in the beginning of this chapter, a HPS is one of the most important aspects of modulation modeling, so that the most appropriate and up-to-date one is required. As mentioned, the issue about the spectral shape of the HPS at low energies has been under debate for a long time. This changed in 2010 when Voyager 1 returned observations convincingly indicating for the first time that this spectrum is a power law. This issue has already been addressed in section 4.3 and will not be repeated here. However, based on the latest Voyager 1 observations beyond the HP (Stone et al. 2013), the spectral form of $E^{-(1.5\pm0.1)}$ evident from the 2010 Voyager 1 observations, needs to be adjusted to $E^{-(1.45\pm0.09)}$ below ~0.8 GeV. The margin of uncertainty here is simply because of the two different techniques that the Voyager team followed in calculating the differential intensity from the observed counts per second (Stone et al. 2013). Their new approach also produces higher differential intensities at these low energies in the outer heliosphere than what was published before, e.g. by Webber and Higbie (2008); McDonald et al. (2013); Webber and Higbie (2009) and Webber and McDonald (2013). Potgieter and Nndanganeni (2013b) thus had to modify their electron HPS in terms of intensity values to incorporate this adjustment.

Consequently, two modified HPS have been constructed and are shown in Figure 4.7, as HPS $\left(E^{-1.55}\right)$ and HPS $\left(E^{-1.35}\right)$, together with the $\mathrm{RRN_{mod}}$ HPS as a reference HPS, that is, without taking into account the mentioned bump in the PAMELA data. The effect of including this bump is evident between ~1 GeV and ~15 GeV where this HPS is slightly lower than the other two HPS. These constructed HPS match the Voyager 1 observations as well as the PAMELA observations.

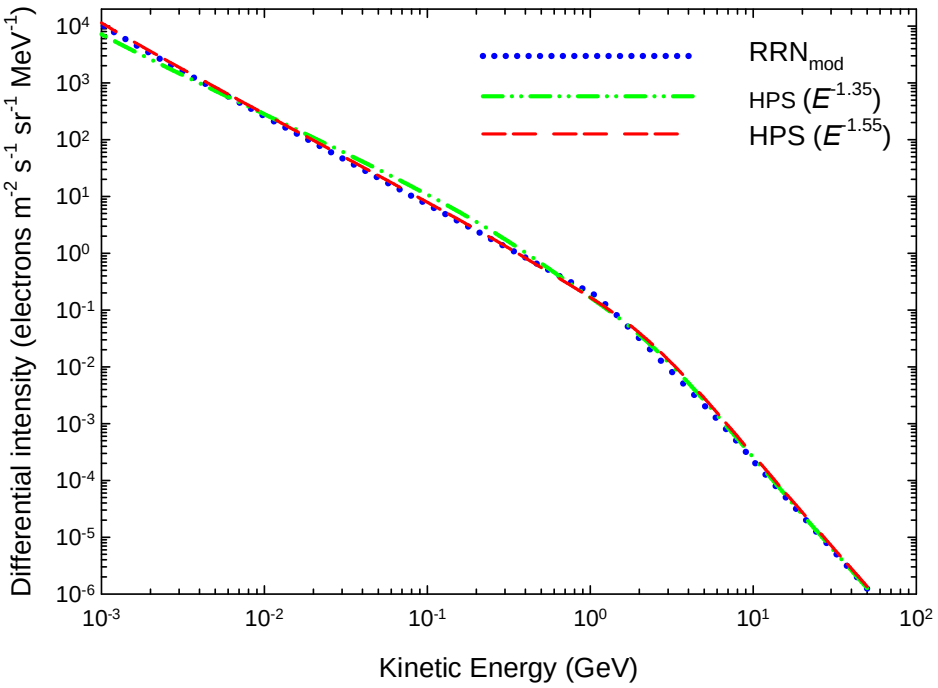

Figure 4.7: Three computed HPS for galactic electrons as a function of kinetic energy. The blue dotted line gives RRN_{mod} (Potgieter and Nndanganeni 2013b) as a reference HPS, without taking the bump into account as described in the text. The red dashed line and the green dashed double dot line show HPS $\left(E^{-1.55}\right)$ and HPS $\left(E^{-1.35}\right)$ respectively; they are computationally constructed based on the latest Voyager 1 observations (Stone et al. 2013) and the PAMELA observations (e.g. Vos et al. 2013), thus also taking into account the bump in the PAMELA data.

Since the difference between these HPS is not that clear on the scale of Figure 4.7, the corresponding ratios are computed and shown in Figure 4.8 in terms of value and spectral slope. The ratio of RRN_{mod} to HPS $\left(E^{-1.35}\right)$ is shown in the top panel and the ratio of HPS $\left(E^{-1.55}\right)$ to HPS $\left(E^{-1.35}\right)$ in the bottom panel. In the top panel the effect of including the bump is now clearly seen between 1 GeV and 10 GeV. However, the sharp changes in the ratios at ~1 GeV and ~10 GeV are technical, caused by the RRN_{mod} not being smooth properly in the transition between the two power-laws. Above ~2 GeV the ratio is less than unity because the RRN_{mod} HPS is lower than the HPS$\left(E^{-1.35}\right)$. Below ~7 MeV the ratio is larger than unity and it increases as a function of decreasing energy, because the RRN_{mod} HPS is higher than HPS $\left(E^{-1.35}\right)$ down to 1 MeV. The largest difference occurs around 100 MeV, where the ratio is the smallest.

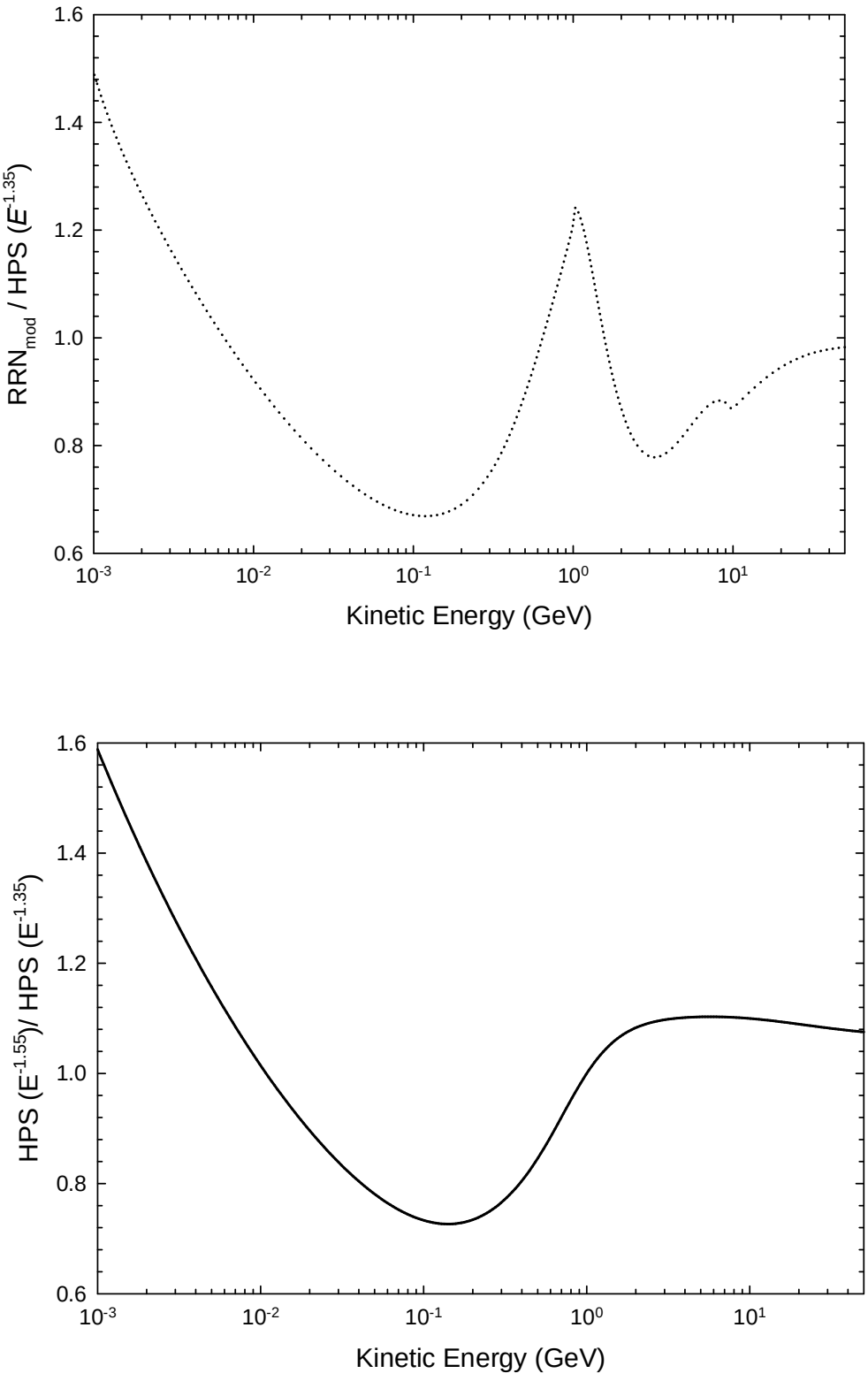

Figure 4.8: Computed ratios between the HPS shown in Figure 4.7. The top panel is the ratio between $\mathrm{RRN_{mod}}$ and $\mathrm{HPS}\left(E^{-1.35}\right)$. The $\mathrm{RRN_{mod}}$ HPS does not include the bump in the PAMELA data. The bottom panel shows the ratio between $\mathrm{HPS}\left(E^{-1.55}\right)$ and $\mathrm{HPS}\left(E^{-1.35}\right)$, where both of these HPS take into account the bump in the PAMELA data.

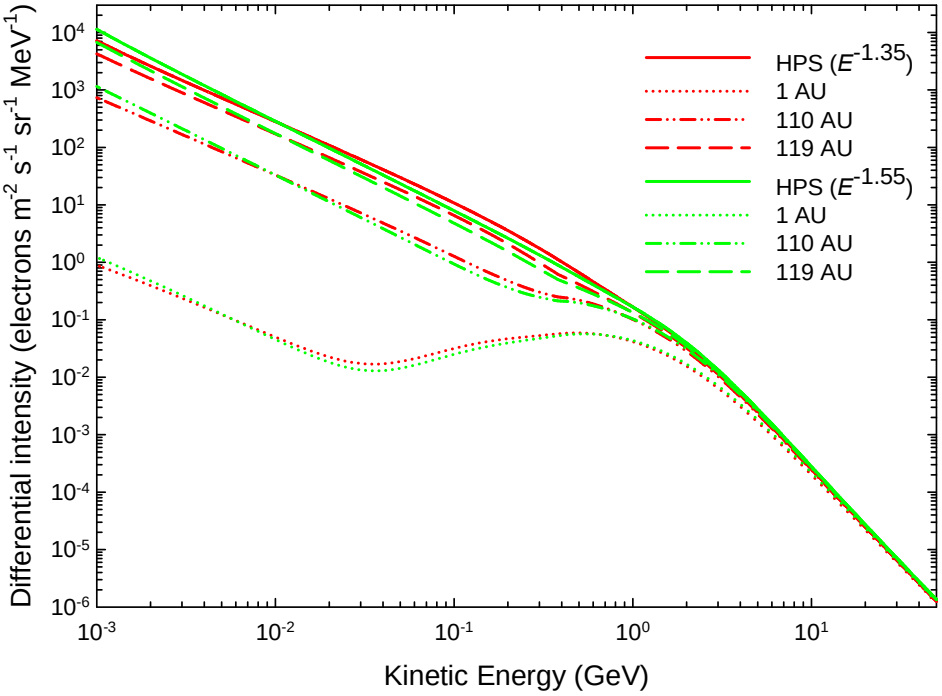

Figure 4.9: Computed modulated spectra as a function of kinetic energy, with respect to HPS$\left(E^{-1.55}\right)$ and HPS$\left(E^{-1.35}\right)$ respectively. The spectra are computed at 1 AU (with $\theta = 90^{\circ}$, 110 AU and 119 AU (with $\theta = 60^{\circ}$).

The bottom panel shows the computed ratio of HPS$\left(E^{-1.55}\right)$ to HPS $\left(E^{-1.35}\right)$, and as expected, the ratio is larger than one at E < 10 MeV, with the largest difference at 100 MeV. The smaller ratio above 10 GeV illustrates that the spectral slopes are getting to be the same as they should be, because these HPS are adjusted to the PAMELA data at higher energies. Like in the top panel, the ratio also increases as a function of decreasing energy with the maximum value at 1 MeV.

Figure 4.9 shows illustrative examples of computed modulated spectra at 1 AU (with $\theta = 90^{\circ}$), 110 AU and 119 AU (with $\theta = 60^{\circ}$) resulting from HPS$\left(E^{-1.55}\right)$ and HPS$\left(E^{-1.35}\right)$ respectively. The heliopause in this case was specified at 122 AU with the TS at 94 AU. The diffusion coefficients (see Eqs. 3.44-3.47) used here are similar to those from Nndanganeni (2012), but were adjusted to reproduce the Voyager 1 spectra observed between 2011 and 2012 in terms of differential intensity values between 1 MeV and 100 MeV, and also above ~1 GeV to reproduce the PAMELA data at Earth. This will be discussed further in Chapter 8. The two HPS have the same values down to ~700 MeV, because they are both adjusted to the

PAMELA data. Between ~5 MeV and ~20 MeV they were both adjusted to the Voyager 1 observations. This means that between 700 MeV and ~ 20 MeV, the HPS$\left(E^{-1.35}\right)$ is higher than the HPS$\left(E^{-1.55}\right)$, and below ~ 5 MeV the HPS$\left(E^{-1.55}\right)$ is higher than the HPS$\left(E^{-1.35}\right)$ because of the difference in the spectral indices.

The results in Figure 4.9 look qualitatively similar with the same main modulation features. The modulation process for low energy electrons is diffusion dominated, and since the diffusion coefficients are independent of rigidity, the modulated spectra at these low energies follow the spectral shape of the HPS, in both cases. These main features were discussed in Section 4.4. Quantitatively, the results are different, and although seemingly insignificant, they remain important. These differences are emphasized in Figure 4.10.

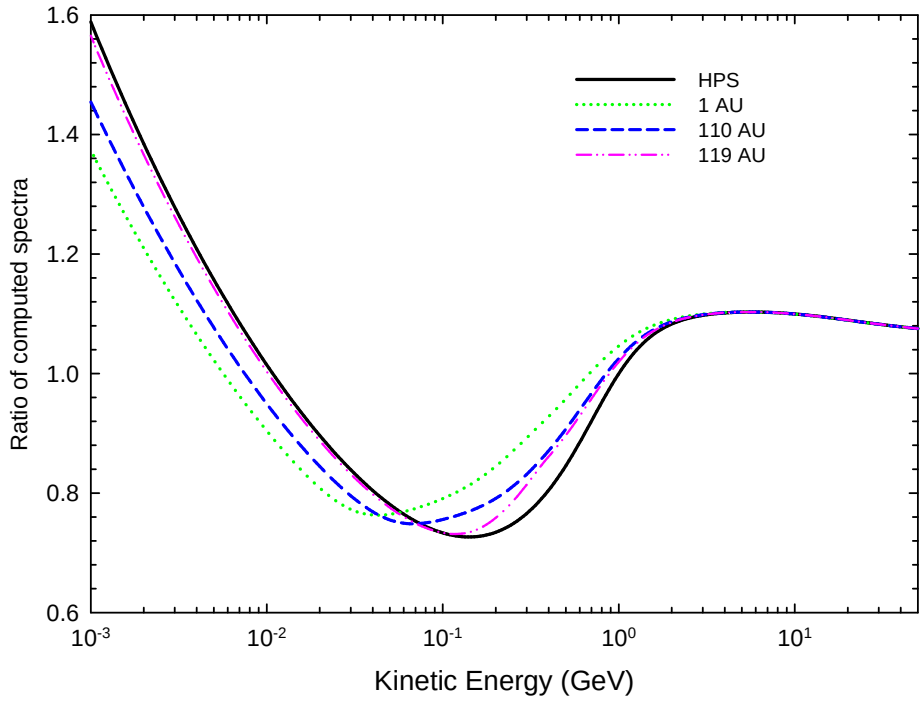

Figure 4.10: Computed ratios of the two sets of spectra shown in Figure 4.9 as a function of kinetic energy. The ratio between the two HPS $\left(E^{-1.55}\right.$ to $\left.E^{-1.35}\right)$ is shown at 122 AU as the black solid line compared to the ratios between the modulated spectra at 1 AU, 110 AU and 119 AU.

Figure 4.10 shows the computed ratios of the two sets of spectra shown in Figure 4.9 as a function of kinetic energy. The ratio between the two HPS $\left(E^{-1.55}\right.$ to $\left.E^{-1.35}\right)$ is shown at 122 AU compared to the ratios between the modulated spectra at 1 AU, 110 AU and 119 AU.

Above ~10 GeV the ratio approaches unity, as it should because the two HPS are then becoming identical. Below 10 MeV the ratio is greater than unity, because the $\mathrm{HPS}\left(E^{-1.55}\right)$ is higher than the $\mathrm{HPS}\left(E^{-1.35}\right)$. Between 10 MeV and 1 GeV the ratio is less than unity because $\mathrm{HPS}\left(E^{-1.35}\right)$ is higher than the $\mathrm{HPS}\left(E^{-1.55}\right)$. Clearly emphasized here is that the modulated spectra follow the spectral trends of the HPS.

The implication of this is that the spectral form of modulated electron spectra, even at Earth, can in principle show the spectral shape of the HPS, as long as the rigidity dependence of the diffusion coefficients is known at these low energies. Of course, in reality, the Jovian electrons prevent this to be done with spectra inside 20 AU (e.g. Ferreira et al. 2001a, b; Ferreira 2002; see also review by Potgieter 2008b, and Ferreira and Potgieter 2004a).

4.5.1 Comparison with observations

In this section, the three HPS shown and discussed in section 4.5, are used to compute modulated spectra at various positions in the heliosphere, and compared to available observations. For this purpose, electron observations at Earth from PAMELA (Adriani et al. 2015, see also Potgieter et al. 2015) and in the outer heliosphere from Voyager 1 (e.g. Webber et al. 2012; Webber and McDonald 2013; Stone et al. 2013; Webber private communication, 2014) are used. Voyager 1 observations are available from a few MeV and up to ~100 MeV but rarely published so that most of the data used for this work were obtained through private communication with W.R. Webber.

The published PAMELA data cover the energy range from 80 MeV to at least 40 GeV (even higher if required). The PAMELA observations shown in this work are obtained from Adriani et al. (2015); see also Potgieter et al. (2015).

In the inner heliosphere, the electron spectra below 50 MeV are dominated by Jovian electrons, as will be illustrated and discussed in Chapter 5 and again in Chapter 8. This is a crucial part of the modeled electron spectra, because this is the energy range where diffusion starts to play an increasingly important role with decreasing energy, an aspect that cannot be tested rigorously for galactic electrons in the inner heliosphere.

Figure 4.11 shows the computed modulated spectra from the inner to the outer heliosphere with respect to the $\mathrm{RRN}_{\mathrm{mod}}$ HPS from Potgieter and Nndanganeni (2013b). These spectra are shown at the same radial distances as in Figure 4.9. The spectra are shown together with the observations at Earth (indicated as PAMELA 2009, Boezio private communication, 2014; see

also Adriani et al. 2015, Potgieter et al. 2015) and for the outer heliosphere (V1 2010, Webber, private communication, 2014; Caballero et al. 2010; V1 2011/274, 2012/121, 2012/303 and 2012/366, respectively, Stone et al. 2013). To recap, between ~2 GeV and ~10 GeV, this HPS is below the PAMELA observations at Earth, because of the bump-effect mentioned above, which is not acceptable from a modulation point of view. This requires that the HPS needs to be adjusted in terms of its spectral index at the above mentioned energies as was discussed in the previous sections of this chapter. Furthermore, the model reproduces the V1 2010 observations in the energy range of ~6-100 MeV quite well, as it was the main purpose of the study by Potgieter and Nndanganeni (2013a, b), that is before the 2011 to 2012 electron data became available.

Figures 4.12 and 4.13 show the computed spectra as a function of kinetic energy at similar radial distance as in Figure 4.11. These spectra are compared to the same set of observations shown in Figure 4.11. In terms of compatibility between the model and observations, results at Earth are shown in Figure 4.11, 4.12 and 4.13, giving overall good compatibility down to 80 MeV.

This is due to the fact that $\mathrm{HPS}\left(E^{-1.35}\right)$ is little bit higher than the other two HPS in this energy range. In the outer heliosphere, comparing the results from Figure 4.11 to those in Figure 4.12 and 4.13, the latter show good compatibility between model result and observations between ~6 MeV and ~100 MeV. The main reason, of course, is that the HPS in Figure 4.11 when constructed, undermined a little the jump that was observed in the data in terms of count rates in the late 2012 (Stone et al. 2013 see their Figure 1). Qualitatively all three HPS are good, and as such there is no compelling reason why one should be selected above the other. All three will be used in this study unless otherwise stated. However, in later chapters preference is given to $\mathrm{HPS}\left(E^{-1.35}\right)$ and especially $\mathrm{HPS}\left(E^{-1.55}\right)$.

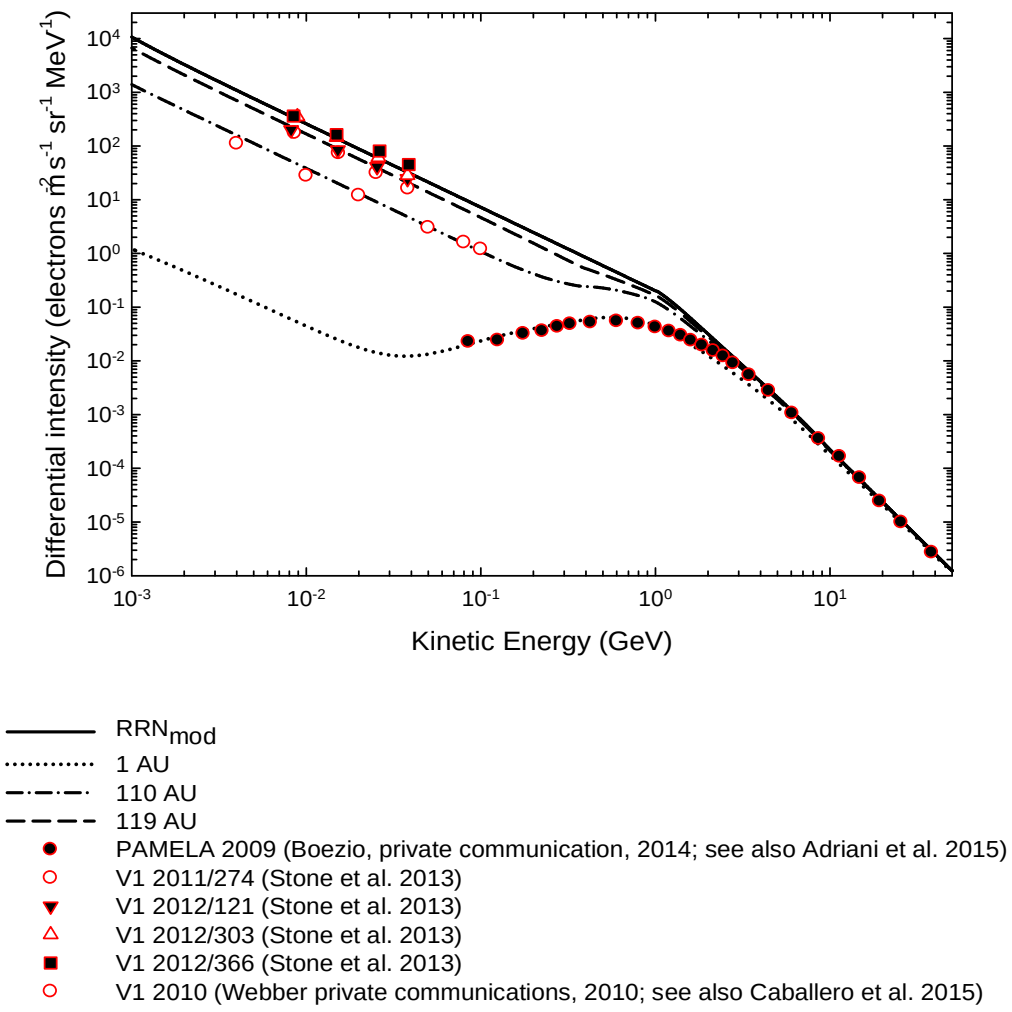

Figure 4.11: Computed electron spectra at 1 AU (with $\theta = 90^{\circ}$), 110 AU and 119 AU (with $\theta = 60^{\circ}$) as a function of kinetic energy with respect to the RRN_{mod} at 122 AU from Potgieter and Nndanganeni (2013b) and with Voyager 1 observations in the heliosheath from 2010 to 2012 as indicated in the legend.

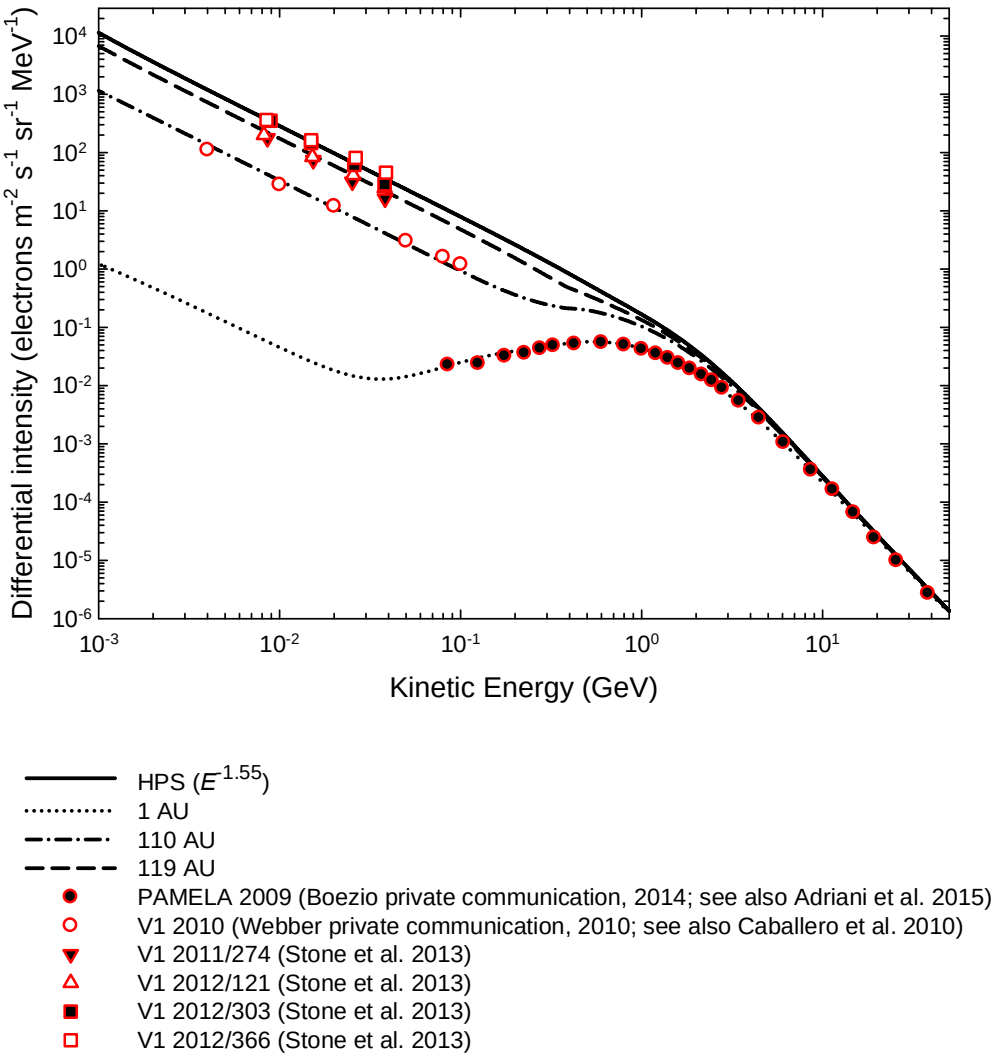

Figure 4.12: Computed electron spectra at 1 AU (with $\theta = 90^{\circ}$), 110 AU and 119 AU (with $\theta = 60^{\circ}$) as a function of kinetic energy. The modulated spectra are computed with respect to the $\mathrm{HPS}\left(E^{-1.55}\right)$, and are compared to the observations as given in the figure legend.

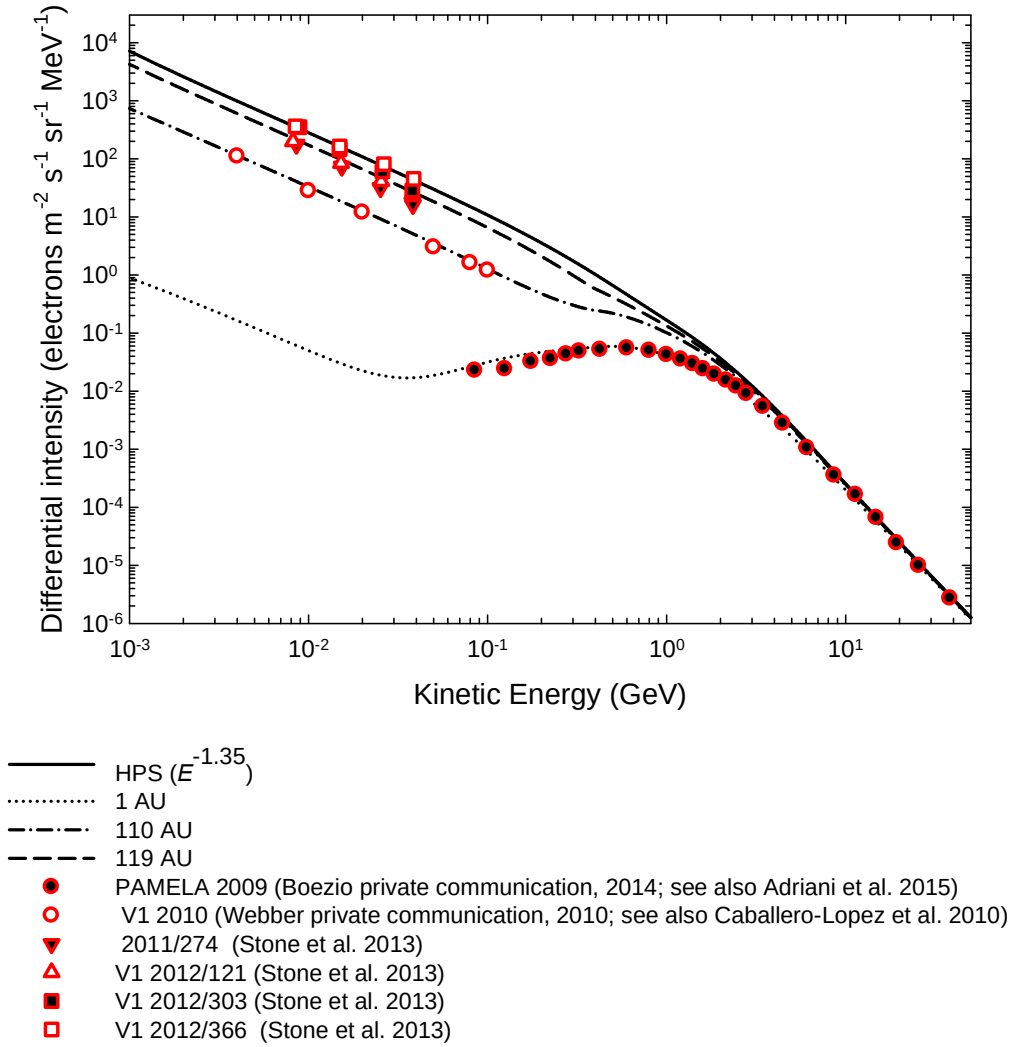

Figure 4.13: Computed electron spectra at 1 AU (with $\theta = 90^{\circ}$), 110 AU and 119 AU (with $\theta = 60^{\circ}$) as a function of kinetic energy. The modulated spectra are computed with respect to the HPS$\left(E^{-1.35}\right)$ and are compared to the observations as given in the figure legend.

4.6 Mathematical description of different HPS

This section gives the mathematical expressions for the three HPS, that is, RRN_{mod} , HPS $\left(E^{-1.55}\right)$ and HPS$\left(E^{-1.35}\right)$ as discussed above. The equations are as follows:

The expression for RRN_{mod} from Potgieter and Nndanganeni (2013b) is given as follows:

if $(1.0\ \text{MeV} \le E \le 1.0\ \text{GeV})$: $j_{LIS} = \exp\left[-2.0 - 1.5511(\ln E)\right]$,

if $(1.0\ \text{GeV} < E \le 10.0\ \text{GeV})$:

$$j_{LIS} = \frac{0.1349 - \left(6.6\times10^{-3}\right)E + \left(15.49\times10^{-5}\right)E^2}{1 - (1.3187)E + (1.0810)E^2 + (0.2327)E^3}, \tag{4.1}$$

and if $E > 10.0$ GeV : $j_{LIS} = \exp\left[-0.89 - 3.262(\ln E)\right]$.

The expression for HPS$\left(E^{-1.55}\right)$ is given as:

For $500\ \text{MeV} \le E \le 2.0$ GeV:

$$j_{LIS} = \frac{0.14}{\beta^2}\left[\frac{\left(\frac{E}{E_L}\right)^{1.6} + \left(\frac{E_{k1}}{E_L}\right)^{1.6}}{1 + \left(\frac{E_{k1}}{E_L}\right)^{1.6}}\right]^{\frac{b_1 - a_1}{1.6}} \left(\frac{E}{E_L}\right)^{a_1} \tag{4.2}$$

and

$$j_{LIS} = \left[4.0\exp\left(3.0 - 5.5\ln\left(E_{k1}\right) - 8.0E_{k1}{}^{(-0.7)}\right)\right], \tag{4.3}$$

elsewhere, with $E_L = 1$ GeV taking care of the units, $E_{k1} = 1.4$ GeV, $a_1 = -1.55$, $b_1 = -3.22$.

The expression for HPS$\left(E^{-1.35}\right)$ is given as:

For $500\ \text{MeV} \le E \le 2.0$ GeV:

$$j_{LIS} = \frac{0.14}{\beta^2}\left[\frac{\left(\frac{E}{E_L}\right)^{1.6} + \left(\frac{E_{k2}}{E_L}\right)^{1.6}}{1 + \left(\frac{E_{k2}}{E_L}\right)^{1.6}}\right]^{\frac{b_2 - a_2}{1.6}} \left(\frac{E}{E_L}\right)^{a_2} \tag{4.4}$$

and

$$j_{LIS} = \left[4.0\exp\left(3.0 - 5.5\ln\left(E_{k2}\right) - 8.0E_{k2}{}^{(-0.7)}\right)\right], \tag{4. 5}$$

elsewhere, now with $E_L = 1$ GeV, $E_{k2} = 0.8$ GeV, $a_2 = -1.35$, $b_2 = -3.22$. In these equations, j_{LIS} is the differential intensity in units of particles $\text{m}^{-2}\ \text{s}^{-1}\ \text{sr}^{-1}\ \text{MeV}^{-1}$, and $P = pc/q$ as the rigidity in units of GV, where p is the momentum of the galactic electrons, with charge q and c the speed of light.

4.7 Summary and conclusions

This chapter was devoted to establishing new HPS for galactic electrons which is an important requirement for studying the solar modulation of electrons with numerical modeling. This HPS is specified at the heliospheric modulation boundary, usually taken as the HP, as an input spectrum (as an initial condition) to be modulated inside the heliosphere as a function of energy and spatial position.

The value of this LIS below a few GeV has always been rather contentious. Langner et al. (2001) computed a LIS that was lower than the one computed by Moskalenko et al. (2002). Langner et al. (2001) recalculated the electron spectrum using a phenomenological approach, including also the radio data for calculations at lower energies and found that their LIS value was between the spectra computed by Strong et al. (1994, 2000). The LIS by Langner et al. (2001) was used extensively in the past, for almost a decade, as the preferred LIS in modulation studies by the members of the local Heliophysics Group (e.g. Ferreira 2002; Langner 2004; Moeketsi 2004; Nkosi 2006 and Nkosi et al. 2011).

Over the last decade, theoretical advancement was made concerning the galactic propagation of cosmic rays in finding a GS which could be used as a LIS by using increasingly more sophisticated models, together with different heliospheric modulation models, but mainly the simple force-field model (Strong et al. 2006, 2011). Webber and Higbie (2008), motivated by data in the outer heliosphere from the Voyager spacecraft, calculated new GS, in particular below a few GeV for electrons. Strong et al. (2011) re-analysed synchrotron radiation data, using various radio surveys to constrain the low energy LIS in combination with the Fermi-Lat and other experiments. Figure 4.2 shows two examples of their computed electron GS for the plain diffusion model, which these authors favoured.

Nndanganeni (2012), motivated by the 2010 Voyager 1 and PAMELA 2009 observations, computed a LIS that has a power law form with $E^{-1.5}$ below ~1 GeV and $E^{-3.15}$ at higher energies. This was the first time that it was realized that the LIS, over the full range of energies of interest to solar modulation studies, basically consists of two power-laws. This LIS was used by Potgieter and Nndanganeni (2013a) to compute the total solar modulation of the galactic electrons in the heliosphere. These authors argue that this LIS should rather be seen as a HPS, which is the lowest presentation of an LIS. Potgieter and Nndanganeni (2013b) continued the study and refined this HPS to obtain $E^{-(1.55\pm0.5)}$ for the lower energy part. At this stage the Voyager 1 observations beyond the HP (Stone et al. 2013) were not yet published, so that these authors underestimated the differential intensity at these low energies,

and also did not take into account the featured bump in the PAMELA data as was illustrated in Figure 4.7. This important feature was first illustrated by Vos (2011) and reported by Vos et al. (2013). See also Potgieter (2014a) and Potgieter et al. (2014b). This means that above ~2 GeV but below ~ 20 GeV, the spectral shape has to change to $E^{-(3.13\pm0.05)}$.

When Voyager 1 crossed the heliopause in August 2012 it measured the spectra at the modulation boundary (HP) which can be regarded as the HPS for the galactic electrons. This leads to the computation of two new HPS with two different spectral indices $\left(E^{-1.35}\right.$ and $\left.E^{-1.55}\right)$. This difference is the result of the different techniques that were used in the process of analysing the observations. Since there is no compelling reason why one of these HPS should be neglected, all will be used in this study unless otherwise stated. However, in later chapters preference is given to $\mathrm{HPS}\left(E^{-1.35}\right)$ and especially to $\mathrm{HPS}\left(E^{-1.55}\right)$.

The next chapter is devoted to the modulation of the Jovian electrons in the inner heliosphere.

Chapter 5

Modulation of Jovian electrons in the heliosphere

5.1 Introduction

It has been well established that the Jupiter magnetosphere is an important and relatively continuous source of relativistic electrons in interplanetary space (e.g. Simpson et al. 1974). Electrons of solar energetic particles (SEPs) events are also observed in the interplanetary medium, but as sudden and intense increases in their intensity in connection with the occurrence of solar flares or coronal mass ejections (CMEs). During solar quiet times the dominant electron population with kinetic energy E < 30 MeV is of Jovian origin. These Jovian electrons are emitted from Jupiterôs magnetosphere and are observed from inside the orbit of the Earth to a distance as far as 40 AU in the inner heliosphere. They effectively dominate the low energy electron spectrum within the first 20 AU from the Sun. Since they mostly follow the interplanetary magnetic field lines, their intensities observed near the Earth fluctuate, depending on the magnetic connection between the Earth and Jupiter with a 13 month periodicity caused by the relative position between Jupiter and the Earth (e.g. Chenette et al. 1974; Conlon and Simpson 1977; Heber et al. 2001, 2003a, 2007; del Peral et al. 2003). During solar quiet periods, Jovian electrons detected at Earth also exhibit a 27 day periodicity which corresponds to the modulation produced by the co-rotating interaction regions (CIRs). Apart from the mentioned periodicities, Jovian electrons otherwise do not show a significant variation under solar modulation (see e.g. McKibben et al. 1985; Gómez-Herrero et al. 2001). In addition to the mentioned periodicities and quiet time electron increases, Ferrando et al. (1993) reported very short duration electron events in the ecliptic plane at ~ 0.4 AU from Jupiter during the fly-by by the Ulysses spacecraft in 1992, and up to 0.9 AU out of the ecliptic. These events, with a strong first order anisotropy, are called ójetsô or óburstsó and are characterized by sharp intensity increases and decreases, with a spectrum identical to the Jovian electron spectrum. These very short-term events are still not fully understood (see e.g. Dunzlaff et al. 2010, 2013) and will not be discussed further in this study. See also the overviews by Heber and Potgieter (2006) and Heber et al. (2007) and references therein.

In this chapter, the focus is on the modeling of the global (large-scale) modulation of Jovian electrons in the inner heliosphere. Original observational details were extensively reported in

the literature (e.g. Teegarden et al. 1974; McDonald et al. 1972; L'Heureux and Meyer 1976) and will not be repeated here. The modeling work that was done by Ferreira et al. (2001a, b) and Ferreira (2002), will be used as a departure point, especially that pertaining to the spectral shape and intensity of the Jovian electron source function. This and other source functions will be revised and modified to see if these modifications to the modeling will be able to give improved compatibility with major observations as well as new insights, for example, if it is possible to give an estimate of the minimum and the maximum intensities that these Jovian electrons may have at Earth. A compilation of low-energy electron spectra as observed and reported over five decades will be shown, as well as some new observations from the Voyager spacecraft.

5.2 Electron flux observations at Earth

First, a compilation of observed electron spectra at Earth is shown to illustrate the characteristic spectral forms for all electrons between ~1 MeV and ~1 GeV. The observed radial profile for both galactic and Jovian electrons will also be shown.

In Figure 5.1 an illustrative selection of observed electron spectra from different spacecraft missions and balloon flights are illustrated: IMP 1 (Cline et al. 1964), OGO-V (L'Heureux et al. 1972), V1 1977 (Webber, 2014, private communication), IMP IV (Simnett and McDonald 1969), ISEE 3 (Moses 1987), LEE 1977 (Evenson et al. 1983), LEE 2002 (Evenson and Clem 2004) and LEE 2009 (Evenson and Clem 2011). The data were observed from ~ 2 MeV up to ~3 GeV. Below ~100 MeV, the spectral shape changes from being dominated by galactic electrons to being increasingly dominated by the Jovian electrons. Even though these observations were obtained at different times, they exhibit the same general characteristics in terms of their spectral slope. For example, below ~10 MeV, a power law shape appears in the spectra, in the form of a typical source function. It was reported by e.g. Moses (1987) that the Jovian electron flux has a simple power law at these energies. This will be discussed in detail in the section that follows (e.g. in Figure 5.7). Between ~10 MeV and ~30 MeV this spectral shape clearly changes to become steeper. Above this energy range, from a Jovian source point of view, one expects to see a rapid fall off as the Jovian electron contribution dissipates, eventually yielding a negligible flux of Jovian electrons, but instead the slope gets flatter as the contribution of the galactic electrons increases. At higher energies, E > ~100 MeV, the spectral form becomes typical that of modulated galactic electrons as will be illustrated with the model in Chapter 8.

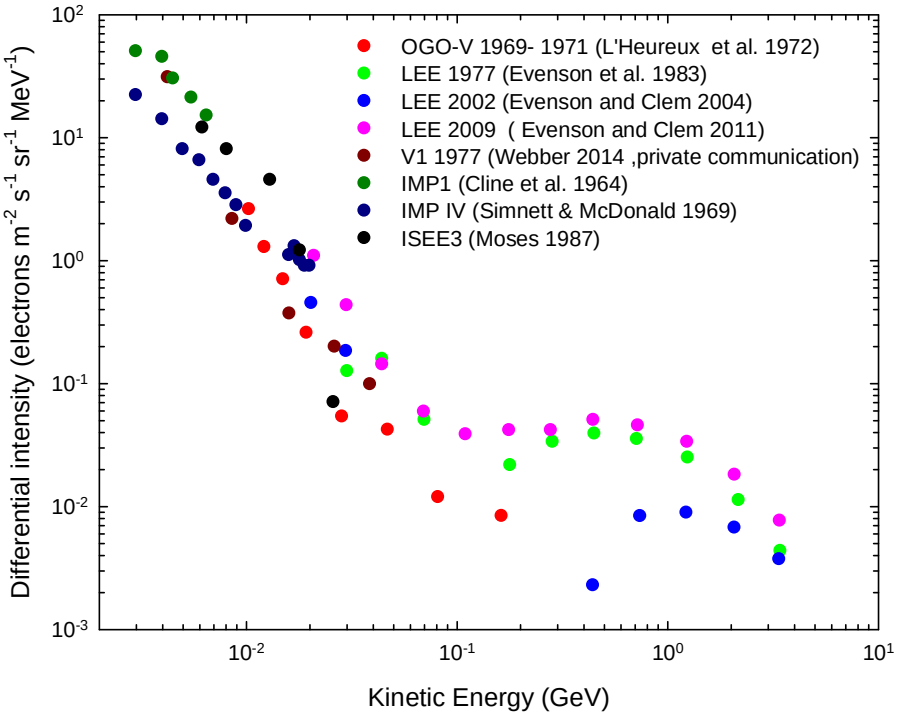

Figure 5.1: A compilation of electron spectra observed over the years at or close to the Earth for the energy range from ~2 MeV to as high as ~3 GeV. These spectra clearly show the transition from being galactic electron dominated above ~100 MeV to being Jovian electron dominated around 10 MeV. These observations are from different spacecraft missions and balloon flights as indicated in the accompanying legend.

The top panel of Figure 5.2 shows the observed radial intensity profiles for electrons for five different energy channels from Voyager 1 (Webber 2014, private communication). The emphasis here is rather on the energy dependence of the Jovian electron intensity at or very close to the source (~5 AU), and not on the radial profiles as such. It follows from these observations how the intensity at the source is decreasing as a function of increasing energy. The intensity is the highest for the energy channel of 5-12 MeV, and the smallest for 34-46 MeV, consistent with what was reported earlier (e.g. Chenette et al. 1974, Teegarden et al. 1974). Comparing the intensity at 5-12 MeV to that of 34-46 MeV a decrease by a factor of ~ 726 is found, confirming that the contribution of Jovian electrons to the total electron intensity becomes relatively small and eventually negligible as a function of the increasing energy.

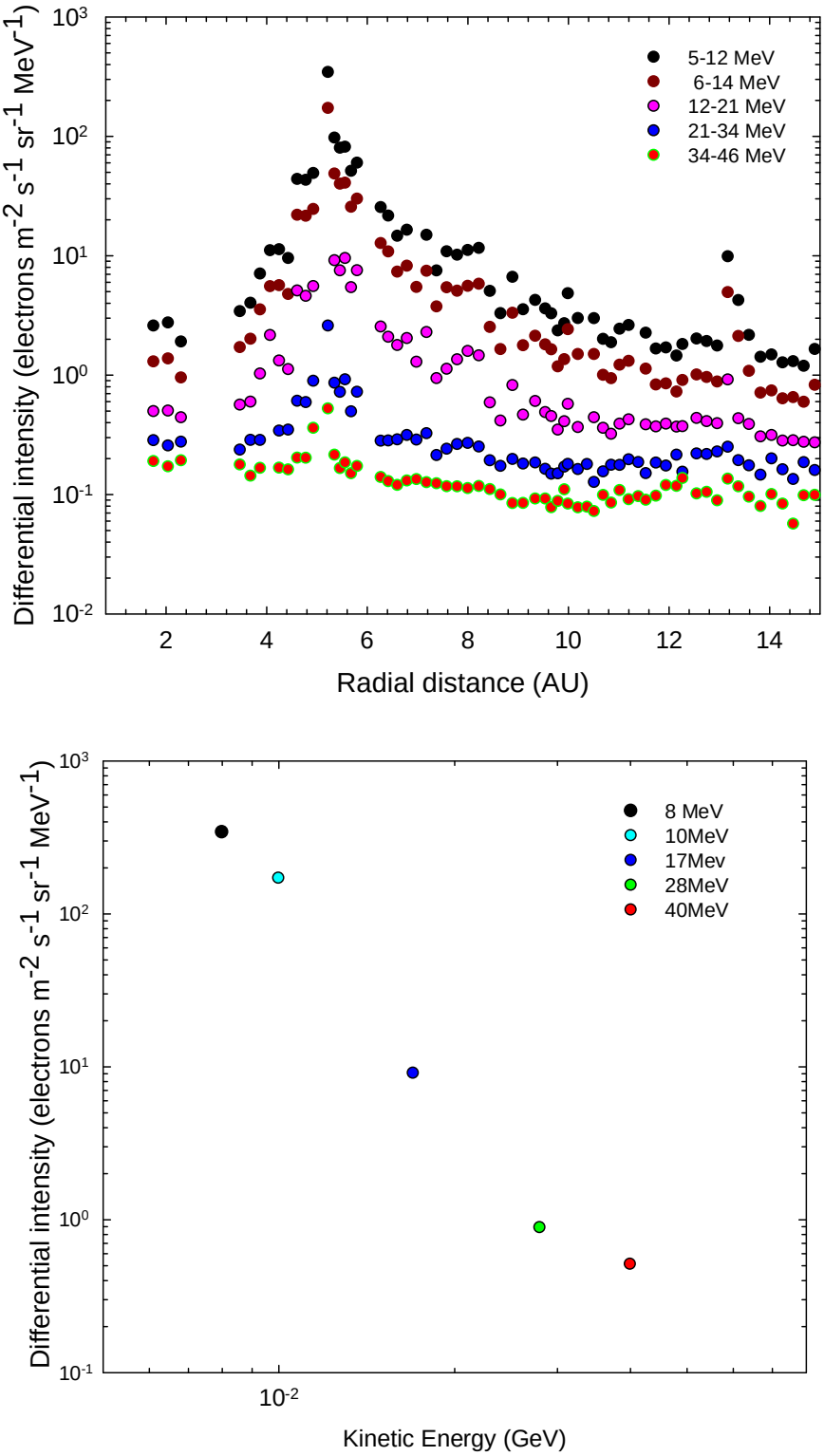

Figure 5.2: Observed electron differential intensity at and relatively close to Jupiter for different energies as indicated. The top panel shows the intensity for five different energy channels from Voyager 1 as a function of radial distance. The bottom panel is the averaged intensity taken very close to the source (~5 AU) as a function of kinetic energy. These observations were obtained from Webber (2014, private communication).

The bottom panel gives the averaged intensity as a function of kinetic energy taken at the source (highest intensities at ~5 AU) for each energy channel shown in the top panel. This confirms that the Jovian electron intensity dissipates quickly as a function of increasing energy, following an apparent power-law shape, with E^{-4}, which differs from what was reported before. It will be argued later on that the observed intensities beyond ~30 MeV probably contain a meaningful contribution from galactic electrons, and that this steep power-law cannot be maintained by Jovian electrons to these higher energies, but should rather exhibit an exponential cut-off. This particular set of data dictates that the Jovian source function should be revisited and further investigated.

5.3 Modulation model and parameters

In this section the 3D numerical model for the modulation of Jovian and galactic electrons is briefly discussed. The original model/code was developed by Ferreira (2002); see also Ferreira et al. (2001a, b) with applications by e.g. Ferreira and Potgieter (2002) and Moeketsi et al. (2005).

5.3.1 Jovian electron modulation model

Ferreira et al. (2001a, b) developed an advanced, 3D steady state, Jovian electron modulation model which is based on the transport equation by Parker (1965). This model describes the relevant physics of the heliospheric transport of low energy (E < 100 MeV) Jovian and galactic electrons. This was motivated by Ulysses observations (e.g. Simpson et al. 1993; Ferrando et al. 1993) of Jovian electrons, emphasizing that the transport of these electrons is truly three dimensional and should be treated as such in numerical models. A complementary model developed by Fichtner et al. (2001) yielded similar results when the same sets of transport parameters were used. Here, the numerical model from Ferreira et al. (2001a, b) is revised and further utilised to compute the modulation of Jovian electrons. The main difference will be in the assumed set of diffusion coefficients, and that the Jovian electron source function is modified to carry out the objectives set out in this study.

5.3.2 Basic modulation parameters

Elaborating on what was presented in Chapter 3, the model is based on the numerical solution of the steady state transport equation (Parker 1965),

$$\left(\mathbf{V}+\left\langle \mathbf{v}_A \right\rangle\right).\nabla f-\nabla .\left(\mathbf{K}_s .\nabla f\right)-\frac{1}{3}\left(\nabla .\mathbf{V}\right)\frac{\partial f}{\partial \ln P}=Q, \tag{5.1}$$

by following the approach of Ferreira (2002) as mentioned. Here, $f\left(\mathbf{r},P\right)$ is the cosmic ray distribution function, P is rigidity (in GV) and **r** (in AU) is the position vector, with r,θ,φ the radial, polar and azimuthal coordinates respectively in a 3D heliocentric spherical coordinate system. Terms on the right hand side respectively represent convection, gradient and curvature drifts, diffusion, and adiabatic energy changes, with Q being the Jovian electron source function. This term is of importance, since the modulation of the Jovian electrons observed at and near Earth is determined through this function; see also Ferreira and Potgieter (2002) and Moeketsi et al. (2005). The diffusion coefficients (DCs) used here are similar to those motivated and used by Nndanganeni (2012), but with small adjustments in order to obtain improved compatibility between the model and observations. The emphasis here is on simplicity and practicality rather than elaborate arguments based on turbulence theory.

To recap, the parallel, two perpendicular diffusion coefficients and the drift coefficient, in terms of *P*, with P_0 = 1 GV, and radial distance *r*, with r_e = 1 AU, are as follows:

In the inner heliosphere, with $r<84$ AU:

if $P<0.4$ GV:

$$K_{\parallel}=K_0\beta\left(1+\left(r/r_e\right)^c\right), \tag{5.2}$$

if $P\geq 0.4$ GV:

$$\mathrm{K}_{\parallel}=K_0\beta\left(P/P_0\right)\left(1+\left(r/r_e\right)^c\right), \tag{5.3}$$

with $c=1.25$. As before, β is the ratio of the particleôs speed to the speed of light.

In the outer heliosphere, with $r\geq 84$ AU, the radial dependence changes, with $c=0.6$. The constant $K_0=70$ in units of 6 x 10^{20} cm^2 s^{-1}.

In all cases

$$K_{\perp r}=aK_{\parallel}, \tag{5.4}$$

with a = 0.02 . Furthermore,

$$K_{\perp\theta} = K_{\perp r} F(\theta), \tag{5.5}$$

with $F(\theta)$ as in Eq. (3.43) .

The drift coefficient is given by

$$K_A = (K_A)_0 \frac{\beta P}{3B_m} K_{drift}(P), \tag{5.6}$$

with $K_{drift}(P) = \frac{10P^2}{1+10P^2}$.

Here, $(K_A)_0$, is a dimensionless constant, specifying the amount of drifts allowed, with $(K_A)_0 = 1.0$ giving maximum drifts as defined by Potgieter et al. (1989). This aspect will be addressed further in Chapter 6. The HMF magnitude, B_m is modified according to Jokipii and Kóta (1989) as in Eq. (2.8)

The model is applied to solar minimum modulation conditions with the tilt angle $\alpha = 5^\circ$ during $A > 0$ magnetic polarity epochs. However, it should be noted that at low electron energies the drift effects become negligible, as is illustrated in the next chapter. The outer boundary of the simulated heliosphere is set at 122 AU which is the known HP position. This model and some aspects of this chapter were published by Potgieter and Nndanganeni (2013a).

5.4 Jovian electron source function

5.4.1 Some historic source functions

Based on observations done at or near Jupiter, but mostly close to and at Earth, source functions for Jovian electrons were constructed which could reproduce these observations and reported in the literature, with a few examples given below. It seems that some of these reports were somewhat controversial, so that consensus about what a Jovian electron source function (the intensity when these electrons had already escaped the Jovian magnetosphere) exactly looks like, still appears elusive, as will briefly be discussed below.

Moses (1987) reported and commented on such a Jovian source spectrum between 5 MeV and 30 MeV, as measured at Earth by the University of Chicago instrument on board ISEE 3,

during a period of best magnetic connection between Jupiter and the Earth. A figure, adapted from his work, is shown in Figure 5.3, illustrating the Pioneer 10 electron spectrum obtained within the Jovian magnetosphere (Baker and Van Allen 1976), together with the normalized ISEE 3 data. It was argued that this source spectrum can be best fitted with a simple power law given as

$$j \propto E^{-\gamma} \tag{5.7}$$

at low energies, with j the differential intensity in units of particles m^{-2} s^{-1} sr^{-1} MeV^{-1} and γ the spectral index which may increase from $\gamma \approx 1.5$ at low energies to $\gamma \leq 6$ at higher energies. In essence, it is a power-law with an exponential cut-off, typically as one would expect from electrons been accelerated at a source. This was in general agreement with observed electron spectra reported by other authors (e.g. Teegarden et al. 1974; Eraker 1982; Eraker and Simpson 1979). However, Ferrando et al. (1991) and Rastoin (1995) analysed and simulated Jovian electrons spectra for periods of best magnetic connection between Jupiter and Earth and came to the conclusion that $\gamma = 2.5$ rather than $\gamma = 1.5$. The controversy thus lies in the index of 1.5: how is it possible for the Jovian magnetosphere to produce such a flat source spectrum if known much stronger sources cannot? This aspect, as well as the maximum value of the source intensity, is further investigated, as reported below.

Figure 5.4 shows a source function as constructed by Haasbroek (1997) for solar modulation purposes, which is given in terms of the differential intensity as a function of kinetic energy E:

$$j_{\text{source}}(E) = C_c \left(\frac{E}{E_0} \right)^{-1.5} \left(1 + \frac{E}{h_c} \right)^{-n_c}, \tag{5.8}$$

with the spectral index rolling over from $\gamma = 1.5$ to $\gamma = 3.5$ with $C_c = 4 \times 10^8$ particles m^{-2} s^{-1} sr^{-1} MeV^{-1}, $n_c = 3.5$, $h_c = 5.0$ MeV and $E_0 = 1.0$ MeV.

Shown together with this source function is the Pioneer 10 and ISEE 3 low energy electron observations (Eraker 1982; Lopate 1991). It is clear from the figure that this function does not really reproduce this specific set of observational data because it decreases much faster as a function of increasing energy, and the roll over from $\gamma = 1.5$ to $\gamma = 3.5$ occurs at a too low energy.

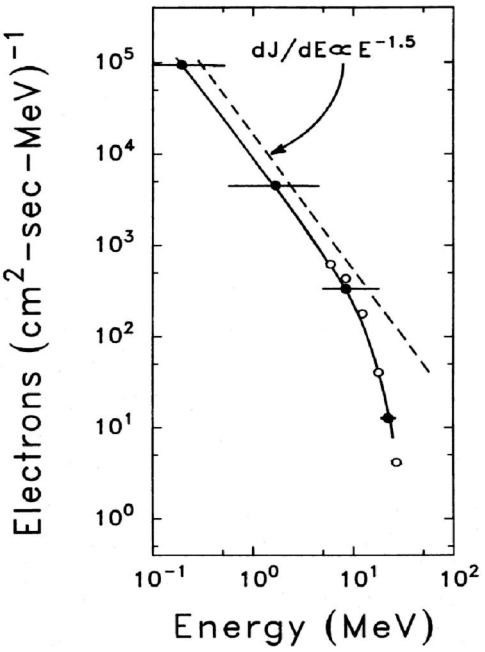

Figure 5.3: A comparison of the Pioneer 10 electron spectrum (filled circles) observed within the Jovian magnetosphere (Baker and Van Allen 1976) and the ISEE 3 spectrum (open circles) observed at Earth during a period of maximum flux as adapted from Moses (1987). The normalization of the ISEE 3 data was done arbitrary. The conclusion was made evidently that the Jovian source function could have a spectral slope as flat as of $E^{-1.5}$ below ~10 MeV.

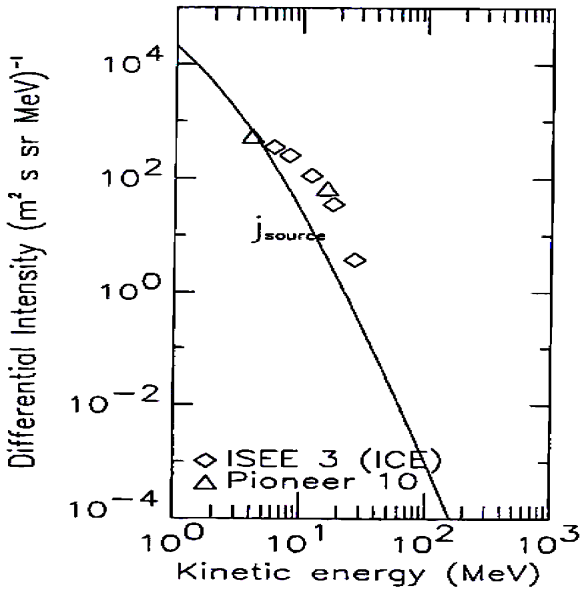

Figure 5.4: The source function (solid line) as used by Haasbroek (1997) together with the low energy Jovian electron observations from ISEE 3 (e.g. Evenson et al. 1979; Moses 1987) and Pioneer 10 (e.g. Eraker 1982; Lopate 1991). Figure adapted from Ferreira (2002).

5.4.2 Ferreira's source function

Ferreira (2002) set out to construct a source function that could reproduce the mentioned observations better, based on the reports from Eraker (1982) and Lopate (1991), assuming that the observations are trustworthy. His source function j_{source} is given as a superposition of $j(E) \propto E^{-1.5}$ and $j(E) \propto E^{-6.0}$ and is

$$Q = j_{\text{source}}(E) = 1.5\left(\frac{c_k j_{1.5} d_k j_{6.0}}{c_k j_{1.5} + d_k j_{6.0}}\right), \tag{5.9}$$

with

$$j_{1.5} = 5.0\times10^{3}\left(\frac{E}{E_0}\right)^{-1.5}, j_{6.0} = 10^{9}\left(\frac{E}{E_0}\right)^{-6.0}, \tag{5.10}$$

$$c_k = 0.6, d_k = 5.0,$$

with j_{source} again in units of particles m^{-2} s^{-1} sr^{-1} MeV^{-1}. He was not too concerned about the normalization of the ISEE 3 data to the Pioneer 10 data, the value of the intensities or the spectral index of 1.5. This function has been used in several numerical modulation studies by Ferreira et al. (2001a, b; 2003a), Ferreira and Potgieter (2002) and recently also by Strauss et al. (2013b). It is shown in Figure 5.5, illustrating the required roll over from $\gamma = 1.5$ to $\gamma = 6.0$

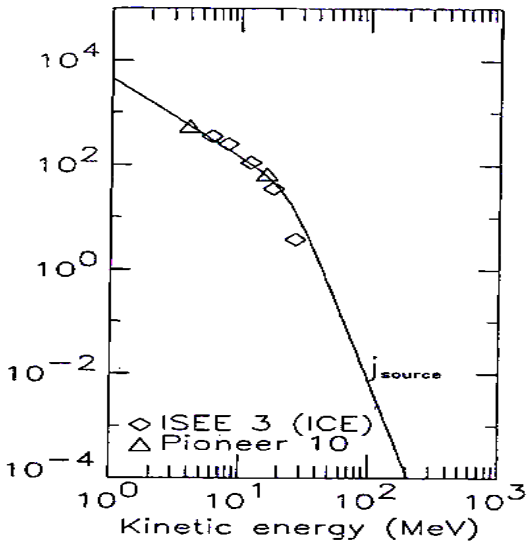

Figure 5.5: The constructed source function from Ferreira (2002) together with the same set of observations as those shown in Figure 5.4. Figure is adapted from Ferreira (2002).

5.4.3 Modifications to Ferreira's source function

The main objective of this section is to make modifications to the source function reported by Ferreira et al. (2001a, b) and Ferreira (2002), in particular to the level of the maximum intensity from the source based on observations at and close to the Earth, first, without changing the spectral indices. These observations are of course influenced by the modulation conditions between the source and the Earth. Even if periods of good magnetic connections are studied, the intensity at Earth is still determined by mostly diffusion which must be set through the diffusion coefficients in a numerical modulation model. Moeketsi et al. (2005) also suggested that Ferreira's source function (Eq. 5.9) gives too low intensities at the lower energy range. The observations from Voyager 1 discussed above, suggest that $\gamma = 1.5$ has to be changed.

The modification to the intensity value of the source function is done through changing the constant c_k when using the same set of diffusion coefficients as given in Eqs. (5.2 to 5.5). Firstly, c_k was changed from 0.6 to 2.3 to give the first modified source function referred to as $j_{\text{modified}}(\text{black line})$, and secondly c_k was changed from 0.6 to 5.5 to compute the second modified source function referred to as $j_{\text{modified1}}(\text{green line})$, all with corresponding modulated spectra at Earth, based on the DCs described above. The new functions are shown in Figure 5.6 together with Ferreira's original source function (solid red line).

It is evident from the figure that Ferreira's source function is modified through the mentioned adjustments only below 30 MeV, and that the two modifications make the intensity higher at lower energies, but retain the slope of the source function. The computed modulated spectra at Earth clearly follow these reductions while maintaining the spectral slope of the source functions, because of the assumed constant rigidity dependence of the diffusion coefficients at these energies which were given in Section 5.3.

These source functions, considered to give the minimum and the maximum intensities, are shown in Figure 5.7 where these modulated spectra at Earth (1 AU) are compared to observations in order to establish if reasonable compatibility could be established with these observations from different space missions: V1 1977 (Webber 2014, private communication; IMP 1 (Cline et al. 1964); IMP IV (Simnett and McDonald 1969); ISEE 3 (Moses 1987); OGO-V (L'Heureux and Meyer 1976) and Ulysses (Potgieter et al. 1999). The same set of diffusion coefficients as mentioned above was used. Modifying the source through the constant c_k from $c_k = 0.6$ to 2.3 improved the compatibility between the model and the observations.

This source function seems fairly compatible to the minimum observed flux between 5 MeV and 30 MeV, whereas modifying the constant c_k from 0.6 to 5.5 is compatible to the highest observed fluxes between 2 MeV and 30 MeV.

Based on these observations, which vary easily by a factor of 10, in conjunction with the numerical model, it is evidently not possible to find a unique source function, but simply establishing lower and upper limits for the intensity of these electrons. However, the modifications to Ferreira's source function do improve the compatibility between the modelled results and the reported observations. Alternative source functions will be further investigated below.

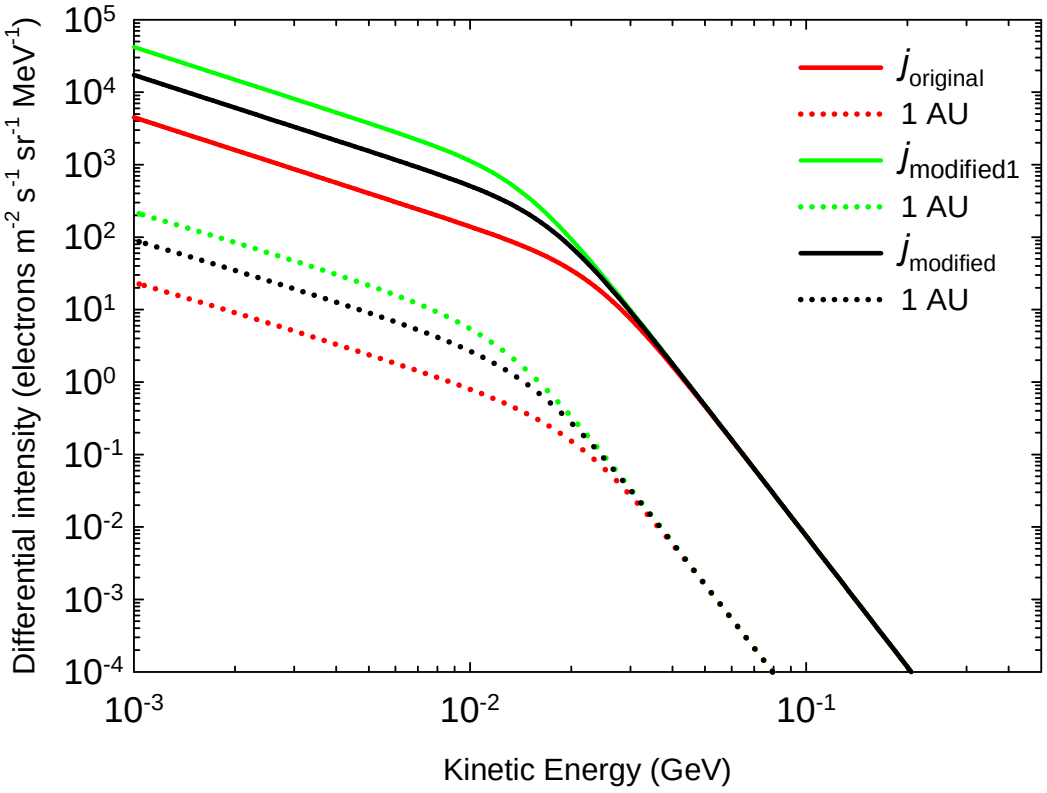

Figure 5.6: The source functions for Jovian electrons (at 5 AU) by Ferreira et al. (2001a, b) and Ferreira (2002) as a function of kinetic energy plotted together with its modifications which are done by changing the constant c_k in Eq. (5.9) from 0.6 (solid red line) to 2.3 (solid black line) and then to 5.5 (solid green line). Also shown are the computed modulated spectra (dotted lines) at Earth (1 AU), corresponding to each source function.

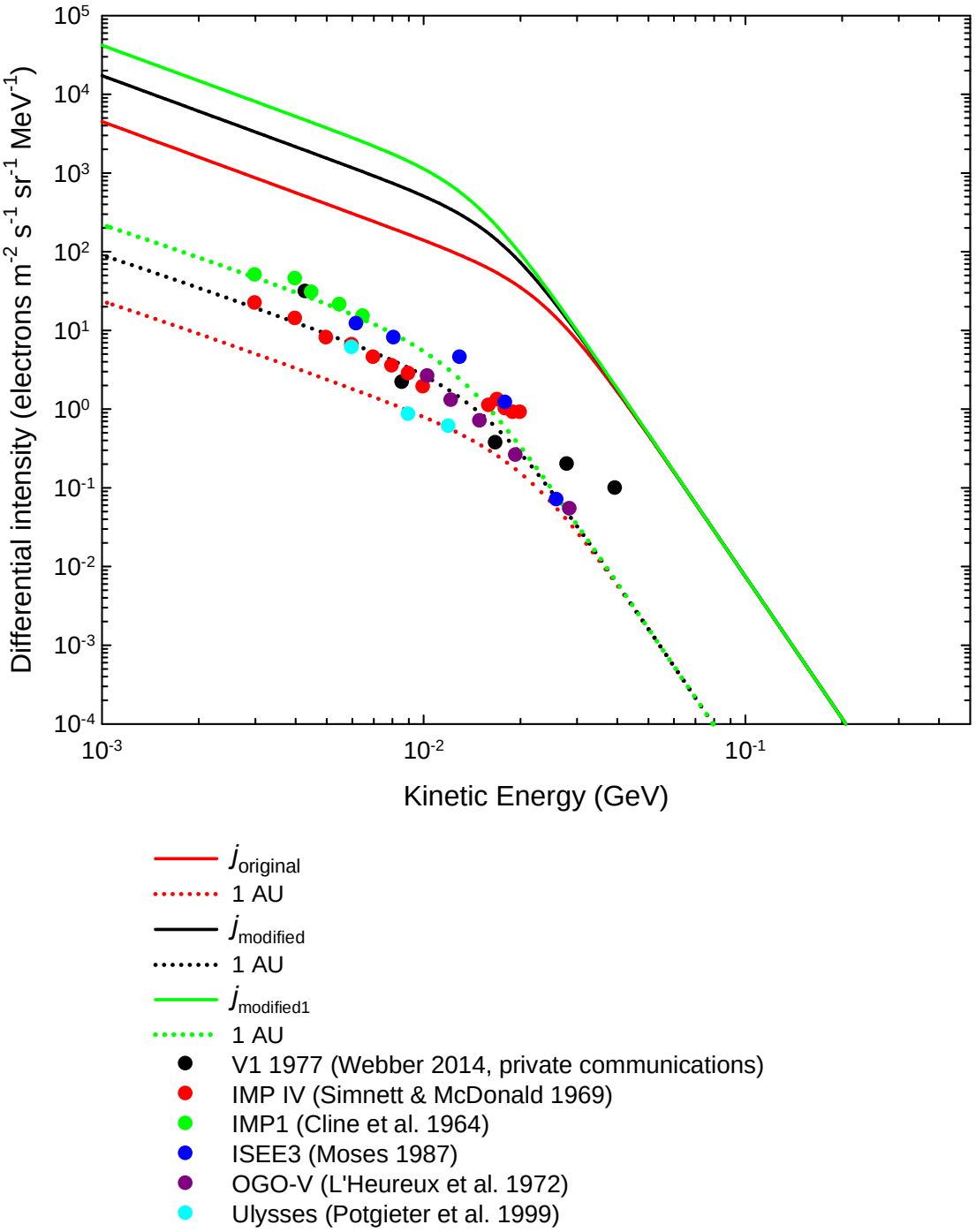

Figure 5.7: Computed modulated Jovian electron spectra (dotted lines) at Earth with respect to three source functions (solid lines) at Jupiter (5 AU), in comparison with observations for different times as indicated in the legend. The emphasis is on the spectral shapes below ~ 20 MeV.

5.4.4 An alternative source function

Simnett and McDonald (1969), motivated by IMP IV electron observations, reported a spectral index of $\gamma = 1.8$ for the energy range 3-20 MeV. They, however, seemed to have believed that these electrons had mostly a galactic origin which is unlikely and is as such another example of how controversial these observations and their interpretation can be. As mentioned, Moses (1987) preferred $\gamma = 1.5$ while Ferrando et al. (1991) reported $\gamma = 2.5$ at these low energies. Recently, Kühl et al. (2013), using electron observations near Earth from SOHO/EPHIN, reported even lower values, mainly consistent to what Moses (1987) reported. Lopate (1991), on his part motivated by the Pioneer 10 observations over two decades, calculated $\gamma = 1.8 \pm 0.2$ in the energy range $2 \leq E \leq 17$ MeV as shown in Figure 5.8. He found that γ changed from 1.2, close to Earth, in 1973 to 1.8 ± 0.2 from 1975 onwards as a function of the Earthôs position with respect to Jupiter.

It must be mentioned at this point that the Pioneer 10 electron data at these low energies as well as the Voyager 1 and 2 electron data have been somewhat controversial because of the possibility that these kind of electron detectors also measured electrons as background caused counts, as produced by proton interactions with the metal frames of the spacecraft.

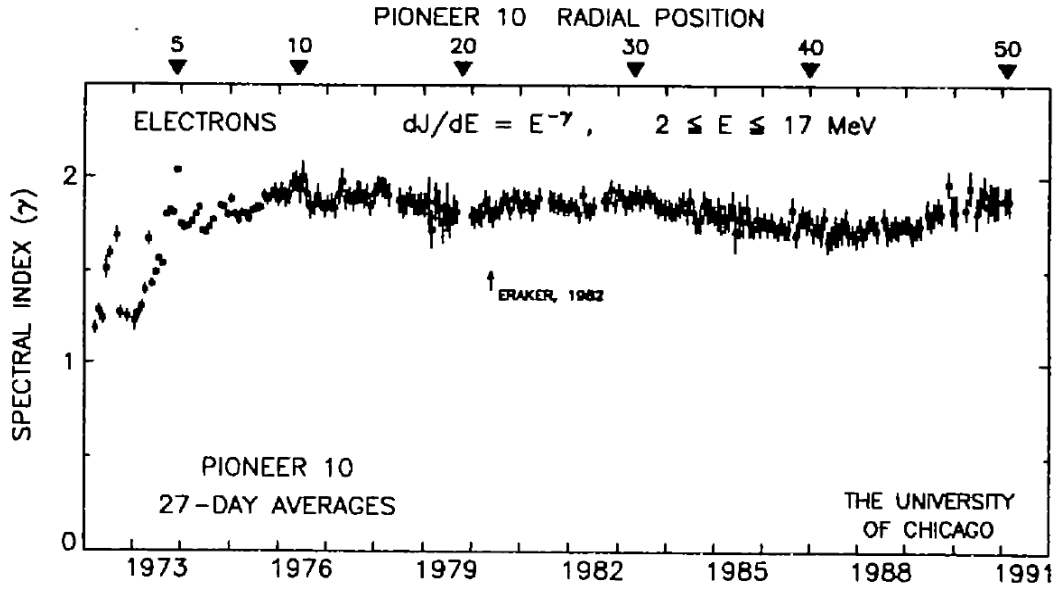

Figure 5.8: Computed spectral index for the 27 day averages from Pioneer 10 for electrons between $2 \leq E \leq 17$ MeV while Pioneer 10 had moved from the Earth to ~50 AU over a period of 20 years. Figure is adapted from Lopate (1991).

But, this becomes an issue only when the spacecraft is far away from the strong Jovian source, in other words, when the electron fluxes drop below the assumed experimental threshold of the detector. This issue was never raised by Lopate (1991) and comes mainly from private communications with team members of the Voyager mission. An obvious open question is what will become of the spectral index if low electron fluxes were to be corrected for such a background 'contamination', which has not yet been published. From a modeling point of view this data issue is most frustrating and will be discussed again in a later chapter; see also Potgieter and Nndanganeni (2013a). However, Lopate's result is close to $\gamma \sim 2$ as given by Chenette (1980). Gómez-Herrero et al. (2000, 2001) and Rodriguez-Frias et al. (2000), making use of SOHO/EPHIN observations, claim that the electrons in the energy range of 150 keV to 10 MeV observed during the quiet time period in 1996, were indeed of Jovian origin with a spectral index ranging from 1.5 to 1.7, consistent to what Lopate (1991) and others reported for observations closer to the Earth.

In what follows, an attempt is made to construct two new alternative source functions with the assumption that the Voyager 1 data set obtained from Webber (2014, private communication) as shown in Figure 5.2 is trustworthy because it had been observed close enough to Jupiter (that is, the intensity is high enough so that background electron counts become negligible). However, it is rather disturbing that these date sets differ so much, contributing to the frustration mentioned above.

In order to make progress, and based on the above insight, the first alternative source function is constructed as a simple combination of two power-laws: $j(E) \propto E^{-3.0}$ and $j \propto E^{-12.0}$. It is therefore assumed that the source function must roll over sharply at some energy, as reported by Moses (1987). This new source function is given by:

$$Q = j_{\text{alternative1}} = 30\left(\frac{c_k j_{3.0} d_k j_{12.0}}{c_k j_{3.0} + d_k j_{12.0}}\right), \tag{5. 11}$$

with

$$j_{3.0} = 1.5\times 10^{3}\left(\frac{E}{E_0}\right)^{-3.0}, j_{12.0} = 10^{16}\left(\frac{E}{E_0}\right)^{-12.0}, \tag{5. 12}$$

$$c_k = 5.0, d_k = 5.0,$$

with $j_{\text{alternative1}}$ in units of particles $\text{m}^{-2}\ \text{s}^{-1}\ \text{sr}^{-1}\ \text{MeV}^{-1}$.

Making use of new observations close to Earth from Voyager 1, namely V1-77 BSe (Webber 2015, private communication) a second alternative function is constructed and is given as:

$$Q = j_{\text{alternative2}} = 1.5\left(\frac{c_k j_{1.5} d_k j_{12.0}}{c_k j_{1.5} + d_k j_{12.0}} \right), \tag{5. 13}$$

$$j_{1.5} = 4\times 10^3 \left(\frac{E}{E_0} \right)^{-1.5} ; j_{12.0} = 10^{12.0} \left(\frac{E}{E_0} \right)^{-12.0} \tag{5. 14}$$

$$c_k = 0.6,\ d_k = 5.0$$

with $j_{\text{alternative2}}$ also in units of particles m^{-2} s^{-1} sr^{-1} MeV^{-1}.

In Figure 5.9, these constructed source functions are shown together with a corresponding computed spectrum at Earth for solar minimum conditions. Evidently, they are completely different, as intended. Shown together with them are data from Voyager 1 (V1-77 BSe), as observed in 1977 and from ISEE 3 as observed in 1979 and 1984 at Earth. Essentially, both of these observations are used to determine the roll over and spectral shape above ~20 MeV. As noted before, in this model the DCs that are independent of rigidity were used, with the consequence that the modulated spectrum at Earth maintains the shape of the source function. This is considered to be the case at least during solar minimum whereas the ISEE 3 data was not obtained at solar minimum.

It follows from this figure that below 10 MeV, based on the solution given by Eqs. (5.13) and (5.14), the power law shape of the Jovian electrons is quite prominent, with flux of ~5905 m^{-2} s^{-1} sr^{-1} MeV^{-1} at 10 MeV. Above 20 MeV, the intensity decreases rapidly, so that the Jovian electrons subside quickly. Considering the solution given by Eqs. (5.11 to 5.12), it follows that below 25 MeV, the power-law shape of the Jovian electrons dominates, with a flux of ~500 electrons m^{-2} s^{-1} sr^{-1} MeV^{-1} at 10 MeV. Above 25 MeV, the intensity decreases rapidly so that the Jovian electrons subside quickly. One thus expects to see a rapid fall-off as the Jovian electron contribution dissipates, eventually yielding a negligible flux of Jovian electrons. Then, galactic electrons should progressively dominate with increasing energy, so that a turnover in spectral shape, from being Jovian electron dominated to galactic electron dominated, is expected between 10 and 20 MeV if the green curve is considered, and they will dominate between 20 MeV and 50 MeV, if the black curve is considered consistent to what was shown in Figure 5.1.

Figure 5.10 shows the comparison between Ferreira's source function and the two new alternative sources as given by Eqs. (5.11 to 5.14), together with their modulated spectra at

Earth. The observations are the same as in Figure 5.9. The differences illustrate the implication of using a much steeper source function at all energies.

Qualitatively, Ferreira's source function is thus seen as underestimating the intensity at low energies, but vastly over-predicting the intensity at higher energies so that in his case the Jovian electrons would dominate up to much higher energies than what is argued here. Because of the complexity of low-energy electron observations, and taking into account all the solar and other phenomena that may influence these observations, it is conceded that there is no conclusive reason to say that Ferreira's function is incorrect. It is merely argued that the new alternative source functions are preferred and will be used as such in later chapters. Of course, it could be that the shape of the Jovian source function is changed by propagation conditions towards the Earth, and that the assumption that the diffusion coefficients for electrons are independent of energy at these low energies could be an oversimplification.

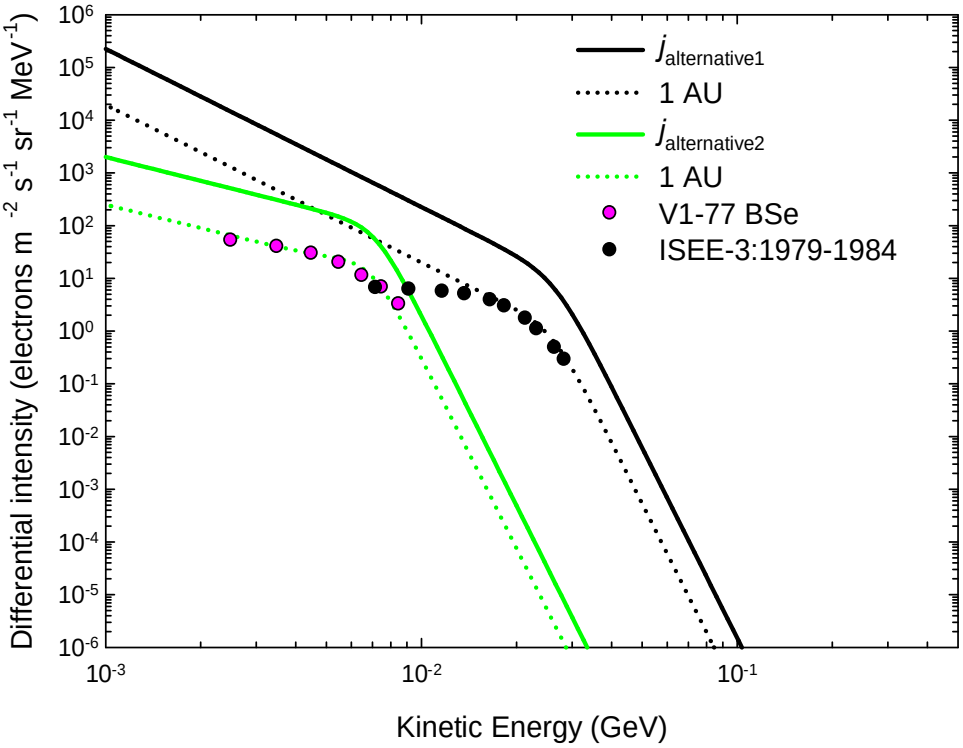

Figure 5.9: The two newly constructed source functions (solid black curve and green curve) for Jovian electrons together with computed corresponding modulated spectrum (black dotted curve and green dotted curve) at Earth for solar minimum conditions. This is compared to Voyager 1 (V1-77 BSe) observations (Webber 2015, private communication) and the ISEE 3 observations from 1979 to 1984 at Earth as reported by Moses (1987; see his Figure 13).

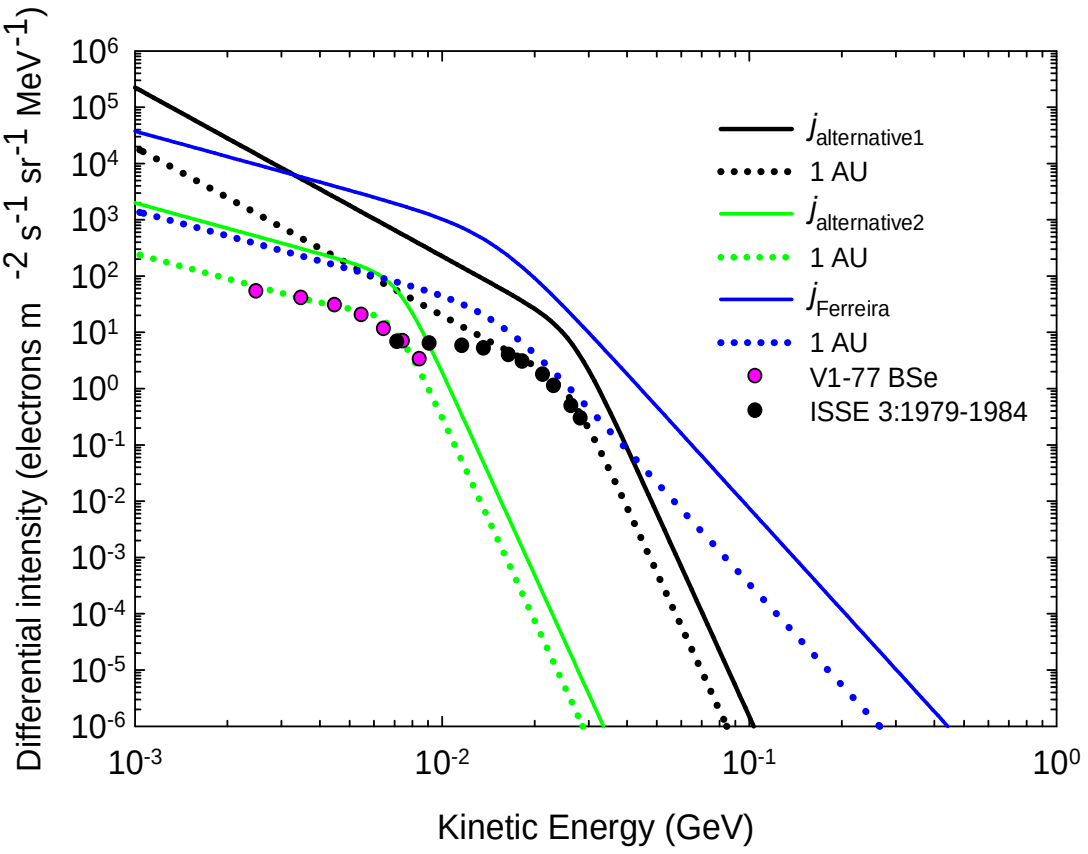

Figure 5.10: A comparison of the two new alternative source functions (black and green solid line) for Jovian electrons with the source function of Ferreira (2002) (blue solid line). The dotted lines are the corresponding modulated spectra at Earth (1 AU). The observations are the same as in Figure 5.9.

However, the theory (see e.g. Potgieter 1996) seems rather solid about this aspect. The impact and effect on the modulated spectra of these Jovian source functions, together with the galactic electron contribution, will be addressed specifically in Chapter 8.

5.5 Radial dependence of Jovian electron intensities

In this section the radial profiles of Jovian electrons for several energies are computed as a function of radial distance between Earth at 1 AU and 40 AU, in the equatorial plane with $\theta = 90^{\circ}$. The computation is based on the Ferreira and $j_{\text{alternative1}}$ source functions shown in Figure 5.10. The DCs used for these computations are given by Eqs. (5.2 to 5.5). The radial profiles shown are computed at 8 MeV, 10 MeV and 28 MeV respectively. The red curves represent the radial profiles computed with Ferreira's source function and the black curves are

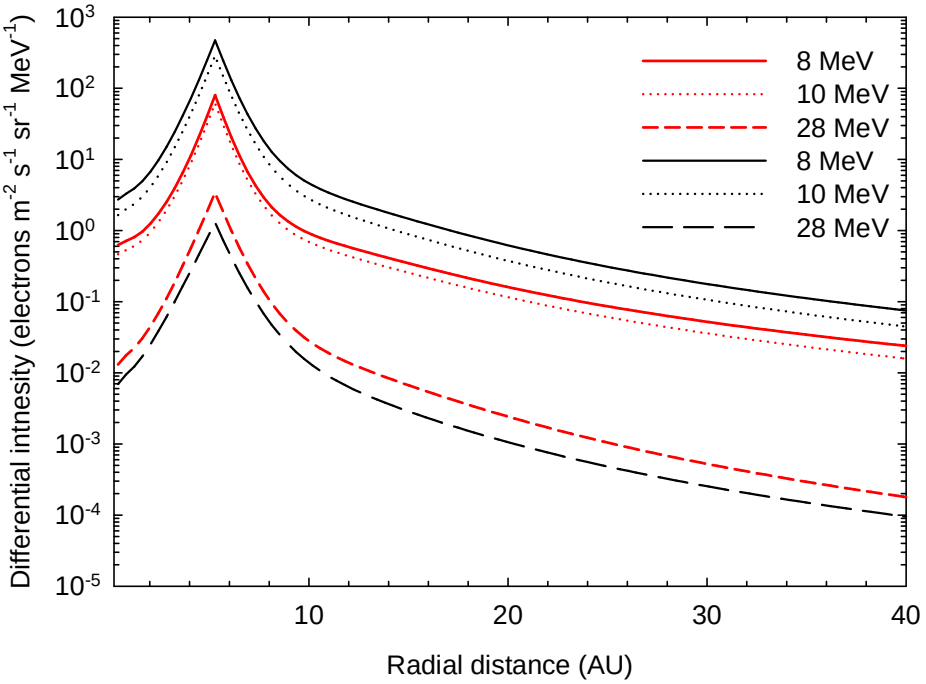

Figure 5.11: Computed radial dependence of 8 MeV, 10 MeV and 28 MeV Jovian electrons using the Ferreira source function (red curves) and the $j_{\text{alternative1}}$ source function (black lines) as shown in Figure 5.10.

for the new alternative source functions. The global picture is quite similar, with the difference mainly in the absolute values of the intensity.

Evidently, the profiles computed with the alternative source function produce higher intensities than the one computed with Ferreira's source function at 8 MeV and 10 MeV but not at 28 MeV. The main feature is that there is a relatively sharp increase from 1 AU up to the source at 5 AU, and then an equally rapid decrease beyond the source to subside relatively quickly beyond 15 AU. The higher the energy, the faster this happens. This means that the Jovian electrons cannot dominate far out in the heliosphere. This was also the conclusion made by Ferreira et al. (2001a, b), and more recently by Potgieter and Nndanganeni (2013a).

The latter aspect is followed up in Figure 5.12 which shows the computed radial profile of 10 MeV Jovian electrons in comparison with the 6-14 MeV observations from Voyager 1 since its launch in 1977 (Webber 2006; Webber 2014, private communication). The computation is shown only up to 40 AU. This illustrates that the model can indeed reproduce the observed radial profile relatively close to the Jovian source, that is, within the first ~15 AU of the inner

heliosphere, using the alternative source function. Beyond 20 AU, the model clearly shows that the observed intensities as shown here cannot be just Jovian electrons. This again emphasizes that although Jovian electrons dominate in the inner heliosphere, they subside rather quickly as a function of increasing radial distance and energy, so that very few Jovian electrons would be observed at the TS (see also, Potgieter and Ferreira 2002; Potgieter and Nndanganeni 2013a). This aspect will again be shown and discussed in Chapter 8.

The relative contribution of galactic to Jovian electrons at these low-energies throughout the heliosphere is an important modulation issue, and will be discussed later again in an effort to estimate the galactic electron intensities at these low energies at Earth.

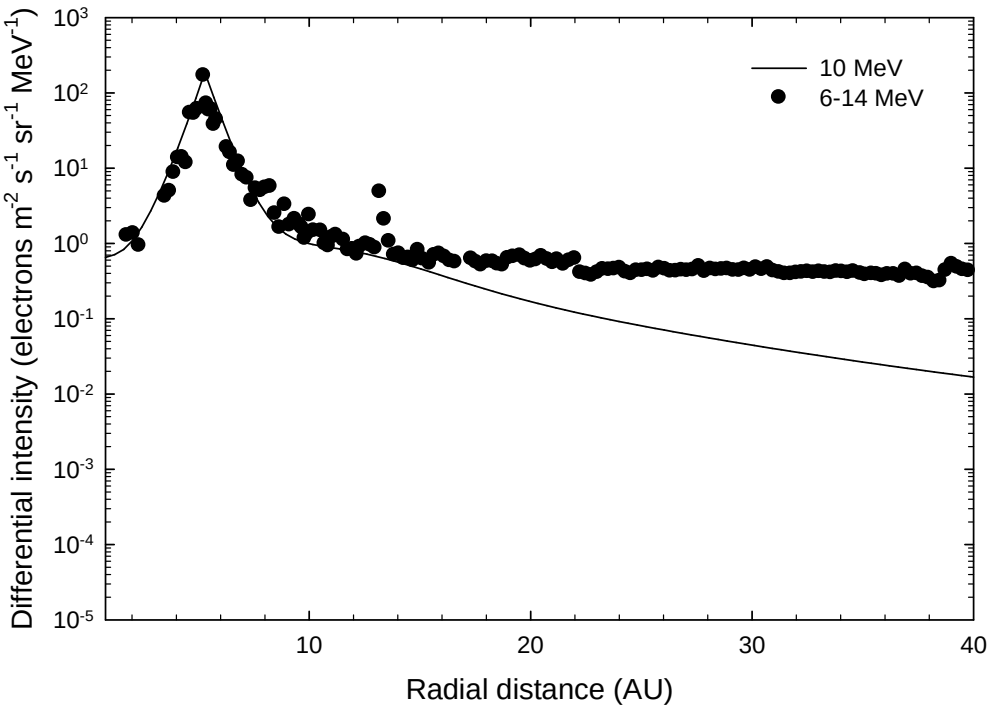

Figure 5.12: The computed radial dependence of 10 MeV Jovian electrons together with Voyager 1 observations (Webber 2014, private communication) between 6-14 MeV since its launch in 1977. The conspicuous peak at 5 AU shows the intensity at the Jovian source when Voyager 1 encountered the Jovian magnetosphere. Beyond 15 AU, the model indicates that the observed intensities must have an increasing contribution from galactic electrons.

5.6 Summary and conclusions

There are three distinct electron populations in the inner heliosphere; the solar particles originating from the Sun, the Jovian electrons from Jupiterôs magnetosphere and the galactic electrons produced from astrophysical sources far outside the heliosphere. This chapter focused on the modeling of Jovian electrons in the inner heliosphere. The challenge regarding this lies in determining a source function for Jovian electrons, which on its part will influence up to where and to what energy exactly these electrons dominate in the heliosphere. If this can be reasonably answered, it becomes possible to compute what the intensity of galactic electrons is at these rather low energies at Earth. This is especially relevant because Voyager 1 is presently measuring galactic electrons in the local interstellar medium as was discussed in the previous chapter. Many electron observations are available but since it is so difficult to measure them, there are large uncertainties, even discrepancies, that are not always mentioned in publications.

Based on modeling results, it is found that Jovian electrons surely dominate in the inner heliosphere up to at least 25 MeV. This energy will be re-evaluated in Chapter 8. Above ~25 MeV, the contribution from the galactic electrons should therefore become progressively larger. Of course, it is expected that at much lower energies (below ~0.5 MeV), solar electrons would make a contribution as solar activity varies; see e.g. Kühl et al. (2013), and the interesting features that follow from their investigation. The contribution from solar electrons was not studied for this thesis.

Figure 5.1 shows a compilation of observed electron spectra at Earth from different spacecraft and balloon flights as an illustration of the characteristic spectral forms of electrons between 1 MeV and 1 GeV. Even though these observations were obtained at different times of the solar cycle, they exhibit the same general characteristics in terms of their spectral slope. The roll (turn)-over in the spectra from being Jovian electron dominated to galactic electron dominated is clearly seen around ~50 MeV. This energy value will be determined more accurately in later chapters.

In Figure 5.2 the observed radial intensity profiles from Voyager 1 for five different electron energy channels are shown. The emphasis is on the energy dependence of the Jovian electron source (at ~5 AU) and not so much on the radial profiles. It does illustrate the point that the Jovian electron intensity exhibits a power-law spectral shape, at least up to 10 MeV. Where exactly in terms of energy the Jovian source function rolls over from being a power-law to an

expected exponential drop-off remains rather elusive, but what is presented here is considered, in this context, as progress.

Another controversial issue is what the spectral index of these Jovian electrons should be, from the lowest to the highest energies of relevance here. It is well-known that the source function can be influenced by solar events such as CIRs and solar flares, but most electron observations were reported for solar quiet times, so that it is likely that the spectral index will change significantly as the particles move from Jupiter to the point of observations at or close to the Earth. However, these observations are mostly chosen for relatively quiet times.

Based on the literature as given throughout this chapter, the Jovian electron source function may have a spectral index ranging from 1.5 to 3.0, based mostly on observations away from Jupiter. Theoretical arguments, however, preclude an electron accelerated spectrum to have an index less than 2.0. In the previous chapter it was shown that the HPS, or very LIS, (Stone et al. 2013) can have a spectral slope between $E^{-1.35}$ and $E^{-1.55}$ because cosmic propagation over the vast distances in the Galaxy may indeed change the shape of the source indices from larger than 2.0 into the observed value (see e.g. Bisschoff and Potgieter 2014). This is unlikely to happen over just 5 AU in the inner heliosphere. If so, it means that the assumption that the diffusion coefficients for electrons are independent of energy at these low energies, could be an oversimplification. However, the theory seems rather solid about this, so if this assumption is valid, it may mean that the flattening of the observed electron spectra below ~80 MeV close to Earth (see Figure 5.1) is probably caused by a larger than anticipated contribution of galactic electrons above 10-20 MeV. This is particularly further investigated in Chapter 8.

The spectral shape and value of the Jovian source function were thus investigated using observations, and the modulation model which is based on the work of Ferreira et al. (2001a, b), but modified for the purpose of this study. The diffusion coefficients used here are similar to those from Nndanganeni (2012), with some modifications. The source function from Ferreira et al. (2001a, b) was used as a departure point and a reference. Two new alternative source functions were constructed as shown in Figures 5.9 and 5.10, given by Eqs. (5.11-5.14). Modifying the source functions improved the compatibility between the modeling results and the observations. However, although arguments were presented why Ferreira's function should not be used, they are not considered as conclusive, so it is a matter of preference as applied in Chapter 8.

Chapter 6

Drift effects in the modulation of galactic electrons in the heliosphere

6.1 Introduction

Particle drifts play an important role in the modulation of cosmic rays (CRs), in particular during solar minimum activity period. During solar maximum, the heliospheric magnetic field (HMF) has a complex structure, and as such particle drifts play a smaller role and the modulation is additionally determined by large scale distributions in the solar wind (e.g. McKibben et al. 1995; Heber and Potgieter 2006). The most characteristic feature of drifts is their sensitivity to the polarity of the HMF. Particle drifts also cause profound and fundamental changes in the characteristics of the solar modulation of galactic and Jovian electrons. Unlike protons, where the effect of drifts could extend down to very low energies, drift effects for electrons only extend to ~100 MeV, because below this energy the diffusion process dominates the transport of these particles (Potgieter 1996) as explained in previous chapters.

The fundamental process of global curvature, gradient and current sheet drifts in the heliosphere is still not fully understood, especially how HMF turbulence could affect the magnitude of drifts on a global scale; as examples, see Engelbrecht and Burger (2013a, b) and Ngobeni (2015) for recent detailed discussions on turbulence theory as applied to the modulation studies. General consensus is that weak scattering drifts, as discussed in Chapter 3, give too large drift effects, as follows from the application of numerical drift models to solar modulation when compared to observations from the Earth to the outer heliosphere (e.g. Ngobeni and Potgieter 2014). In this chapter, an empirical (phenomenological) approach is followed to illustrate how reducing drifts, in a straightforward manner, affects the solar modulation of galactic electrons. The effects of drifts on the global modulation of these electrons are revisited by studying different modulation scenarios using the numerical model as described in Chapter 3. Only solar minimum conditions with the tilt angle $\breve{U} = 5^{o}$ are considered. Computations are done for the both magnetic polarity epochs. The termination shock (TS) is specified at 94 AU, and the heliopause (HP) as heliospheric modulation

boundary, assumed to be the heliopause, is specified at 122 AU. All computations are shown in the heliospheric equatorial plane with $\theta = 90^{\circ}$, at radial distances of 1 AU, 5 AU, 60 AU, 90 AU and 110 AU with respect to the electron heliopause spectrum (HPS) as described and discussed in Chapter 4 (see section 4.4).

In the next section, ways of reducing drifts explicitly are illustrated and discussed, and the effects that this has on the modulated spectra will be shown. In section 6.3, ways of reducing drifts implicitly are discussed.

6.2 Reducing drifts explicitly

Potgieter et al. (1989) were the first to recognize that applying the weak scattering drift approach unconditionally to solar modulation was an over-simplification. But it was only when the Ulysses space mission could not confirm the large latitudinal gradients predicted by these early drift dominated models that serious theoretical studies started to gain better understanding of this process. For overviews of how this process historically developed, see e.g. Heber and Potgieter (2006, 2008); Potgieter (2013a), and references therein.

6.2.1 Weak scattering and modified drifts.

In this section, the focus is on the rigidity dependence of the drift coefficient. The main aim is to illustrate the effects of changing the rigidity dependence of the drift coefficient, and the effects that this will have on the computed modulated spectra. This is done by comparing computations done under the assumption of weak scattering to a modified drift coefficient.

Cosmic ray modeling done by Potgieter et al. (1989) and Webber et al. (1990) already showed that weak scattering drifts gave excessive drift-modulation effects at lower energies, not at neutron monitor energies, and that some reduction is necessary. This also followed from later studies by Langner et al. (2003, 2006) and more recently from Ngobeni and Potgieter (2014, 2015). Burger et al. (2000) showed that by approximating the scattering parameter $\omega\tau$ as discussed in Chapter 3 (see Eqs. 3.52 to 3.55) as being $\omega\tau \propto P$, gave reasonable agreement with CRs observations. Additional theoretical motivations and discussions of the reduction of drifts were given in previous studies by Minnie et al. (2007); Burger et al. (2008); Visser (2009); Burger and Visser (2010); Engelbrecht and Burger (2013a, b). Recently, Ngobeni (2015) revisited this issue of the reduction of the drift

coefficient based on changing the rigidity dependence of $\omega\tau$. The relevant drift coefficient from Chapter 3 is repeated here as

$$\left(K_A\right)=\frac{\beta P}{3B_m}f_s, \tag{6.1}$$

so that with $f_s=1.0$ weak scattering is assumed, and when modified in terms of rigidity, this expression becomes

$$\left(K_A\right)=\left(K_A\right)_0\frac{\beta P}{3B_m}\frac{\left(P/P_0'\right)^2}{1+\left(P/P_0'\right)^2}. \tag{6.2}$$

As shown in Chapter 3, this reduces the drift coefficient significantly at lower energies (see Figure 3.8). It follows that the explicit reduction of Eq. (6.1) can be accomplished through changing the HMF, the rigidity dependence and/or the constant $\left(K_A\right)_0$. In terms of its rigidity dependence, which is emphasized here, the very small latitudinal gradients as observed by Ulysses (Heber and Potgieter 2006, 2008 and De Simone et al. 2011) conclusively required that the drift magnitude must be reduced at lower energies, as in Eq. (6.2). In addition, the drift magnitude needs to be reduced over the heliospheric poles, the exact reason why the Parker HMF is replaced by a modified HMF, B_m. In this regard, see also Langner (2004), and Raath (2014) for a more recent investigation.

Figure 6.1 shows the rigidity dependence at Earth of the three main DCs together with the drift coefficient for both weak scattering and for modified drift based on Eqs. (6.1) and (6.2). The DCs used here are described in Chapter 3 (see Eqs. (3.44) to (3.47) and also Figure 3.6), and are not repeated here. As explained in Chapter 3, *a* and *b* are constants which determine the values of $K_{\perp r}$ and $K_{\perp\theta}$ in terms of $K_{\parallel}$ respectively, and *d* is the enhancement factor which enhances $K_{\theta\theta}=K_{\perp\theta}$ toward the poles. The top panel shows the drift coefficient with weak scattering (Eq. (6.1) with $f_S=1.0$) where $K_A\propto\beta P$, and the bottom panel shows the modified version (Eq. (6.2) with f_S given by Eq. (3.57)).

Evidently, the modified version gives a drift reduction from below 1 GV, at first very moderately, but it gets significantly larger with lower rigidities. This means that as drifts get progressively less, diffusion gets to be more and more dominant, so that drift effects should dissipate for electrons with decreasing energies. This will be illustrated below with computed spectra. This approach is similar to what Potgieter (1996) and Potgieter and Ferreira (1999)

used to reduce drifts as a function of rigidity. The work on turbulence theory by Engelbrecht and Burger (2013a, b), and the application thereof by Ngobeni (2015), gives quantitatively a similar result but differs in the sense that the drift reduction is less strong below ~ 500 MeV. The approach is also consistent with the work of Potgieter et al. (1989); Webber et al. (1990); Ferreira and Potgieter (2004a, b) and Ndiitwani et al. (2005) which called for a reduction of drifts, also with increasing solar activity.

Figure 6.2 shows the corresponding computed electron spectra as a function of kinetic energy based on the rigidity dependence shown in Figure 6.1. The spectra are computed at 1 AU, 5 AU, 60 AU, 90 AU and 110 AU in the equatorial plane ($\theta = 90^{\circ}$) for both $A > 0$ and $A < 0$ magnetic polarity epochs and with a tilt angle $\alpha = 5^{\circ}$ and with $(K_A)_0 = 1.0$ in Eq. (6.2). The latter confirms that only the rigidity dependence is modified.

The top panel shows the spectra for the weak scattering case for the $A > 0$ polarity epoch (black lines) and for $A < 0$ (red lines). It follows that the effects of drifts (here shown as the difference between the two polarity epochs) are still present below ~10 MeV throughout the heliosphere, so that the diffusion process only starts to dominate below ~3 MeV, but at somewhat higher energies further out in the heliosphere. The bottom panel shows the spectra done with Eq. (6.2) for the same radial distances as in the top panel. It now follows that drift effects end at higher energies throughout the heliosphere so that the extent to which drifts have an effect, decreases as a function of increasing energy for both $A > 0$ and $A < 0$ solutions. Diffusion therefore comes to play a dominant role at higher energies than in the previous case. However, drift effects are quite prominent in the mid-energy range throughout the heliosphere; even at very large radial distance, between ~100 MeV and ~600 MeV. Increasing the rigidity dependence of K_A at lower energies thus very effectively reduces the extent to which drifts dominate the modulation process in the heliosphere.

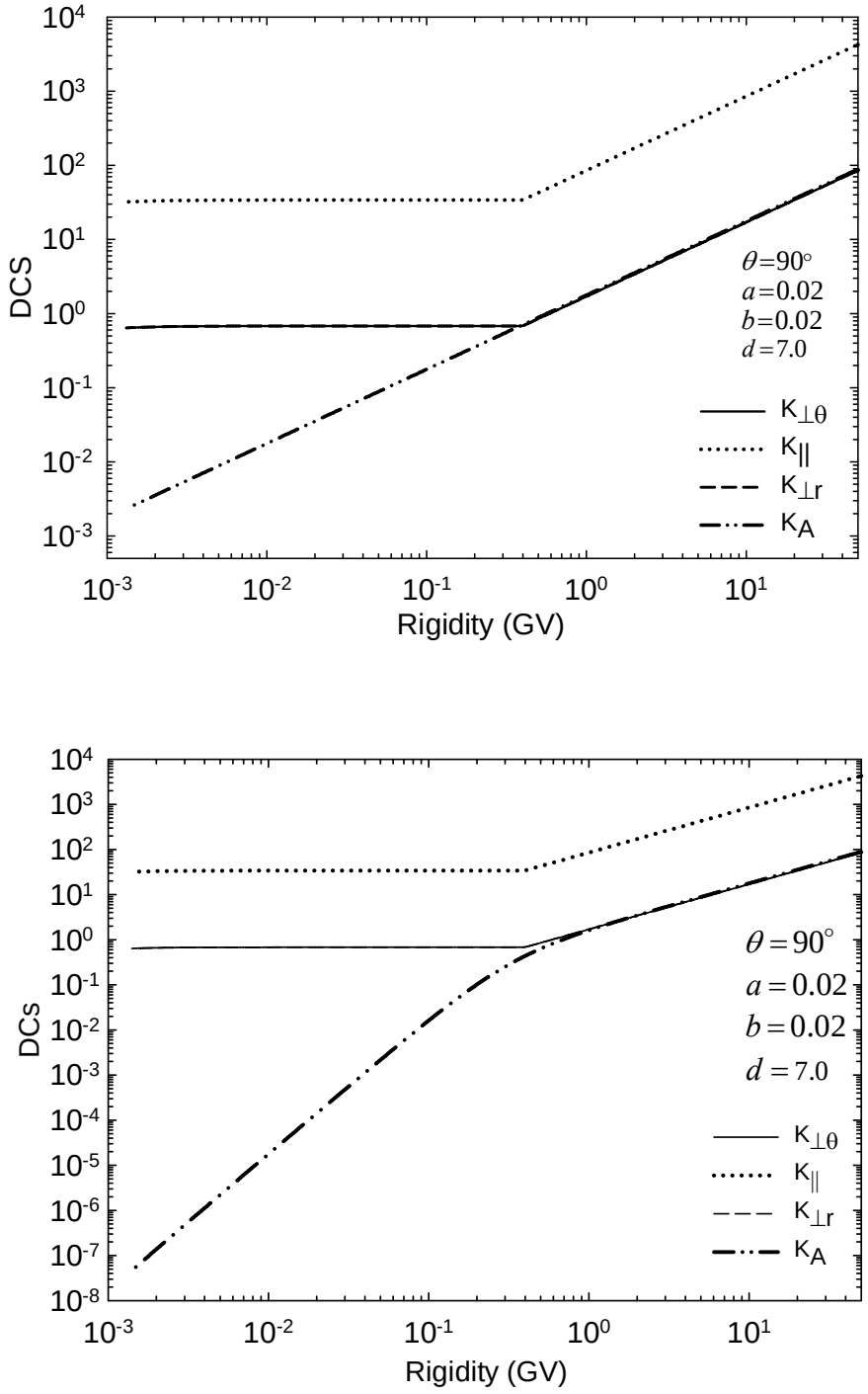

Figure 6.1: A comparison of the rigidity dependence of $K_{\parallel}, K_{\perp r}, K_{\perp\theta}$ and K_A for 12 MeV galactic electrons at Earth where $\theta = 90^{\circ}$. The top panel is obtained when Eq. (6.1) is used for the drift coefficient and the bottom panel for Eq. (6.2). The DCs are in units of 6×10^{20} cm^2 s^{-1}. The meaning of the constants *a*, *b* and *d*, is described in the text. Here, $\left(K_A\right)_0 = 1.0$ in Eq. (6.2). Note that $K_{\perp r}$ and $K_{\perp\theta}$ coincide because the computations are done for the equatorial plane with *a* = *b* = 0.02

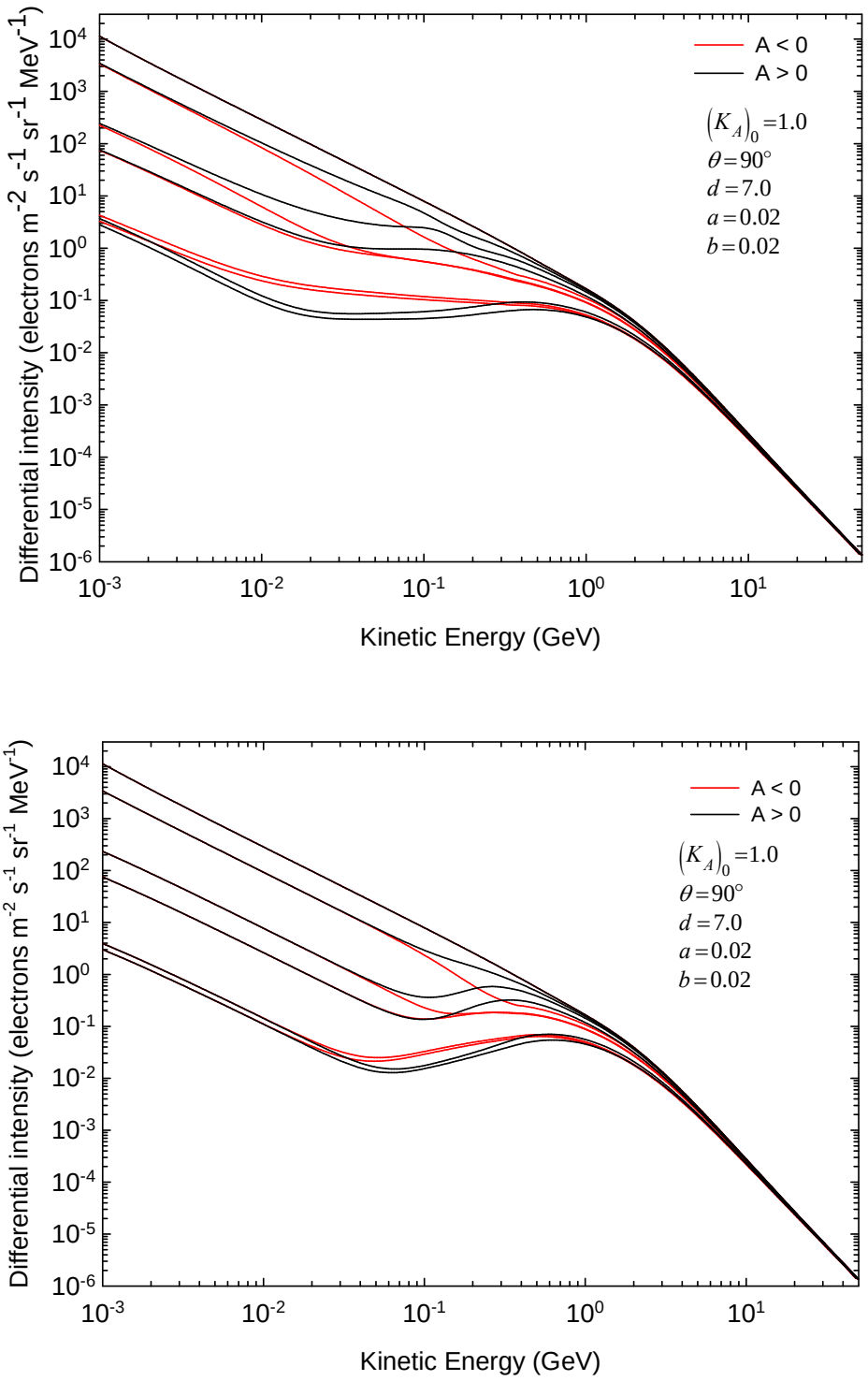

Figure 6.2: The computed electron spectra are shown, respectively, from the bottom to the top at 1 AU, 5 AU, 60 AU, 90 AU and 110 AU with $\theta = 90^{\circ}$ as a function of kinetic energy for the $A > 0$ epoch (black lines) and for $A < 0$ (red lines). The top panel is for weak scattering drifts and the bottom panel is for reduced drifts given by Eqs. (6.1 and 6.2), respectively, as shown in Figure 6.1. The HPS is specified at 122 AU as the top black line in every figure.

6.2.2 Damping drifts with the scaling factor $(K_A)_0$

In this section the effects of the reduction of drifts on electron modulation is further investigated and illustrated. The reduction is done through changing the drift scaling factor $\left(K_A\right)_0$ in Eq. (6.2). Several values have been studied, but only two case are shown here, with $\left(K_A\right)_0$ = 1.0 and 0.2, which represents 100% drifts (as in Figure 6.2) and 20 % drifts, respectively. The main objective here is to show how changing the value of $\left(K_A\right)_0$ affects electron modulation as a function of kinetic energy at different radial distances. This is a far more drastic reduction process, compared to only modifying the rigidity dependence at low energies shown above. Effectively, this means that the scattering parameter $\omega\tau$ in Eq. (3.55) is no longer much larger than 1.0 but is reduced in relation to which $\left(K_A\right)_0$ is reduced. Modulation effects are illustrated for both the weak scattering drift coefficients and the modified drift coefficients as discussed above. Instead of showing all the computed spectra as done in the previous section, only the computed ratios between the $A>0$ and $A<0$ magnetic polarity epochs are shown.

Figure 6.3 shows the computed ratios for 100% (top panel) and 20% (bottom panel) drifts, under the assumption of a weak scattering drift coefficient (Eq. 6.1). Generally, the ratio in the inner heliosphere (1 AU and 5 AU) drops below unity for E < ~5 GeV with the smallest ratio (~0.3) around ~20 MeV. The ratio then again increases rapidly towards unity with decreasing energy as the effects of drift subside but are still present, even at energies around 1 MeV. The ratio less than unity obviously implies that the $A>0$ epoch is producing less intensities at a given energy (more modulation) than the $A<0$ solutions, which is a characteristic of electron modulation in the inner heliosphere. Above ~ 10 GeV the ratio converges to unity because there is progressively less modulation (smaller spatial gradients) at these higher energies, despite the fact that the drift coefficient scales proportional to rigidity. However, at larger radial distances, the ratio exceeds unity meaning the $A>0$ spectra are higher than the $A>0$ ones. This cross-over of spectra with increasing distance has been reported before (Reinecke and Potgieter 1994). The maximum ratio shifts towards lower energies with increasing distance, illustrating that drift effects change as one moves outwards, and that drifts could be as large in the far outer heliosphere than at the Earth.

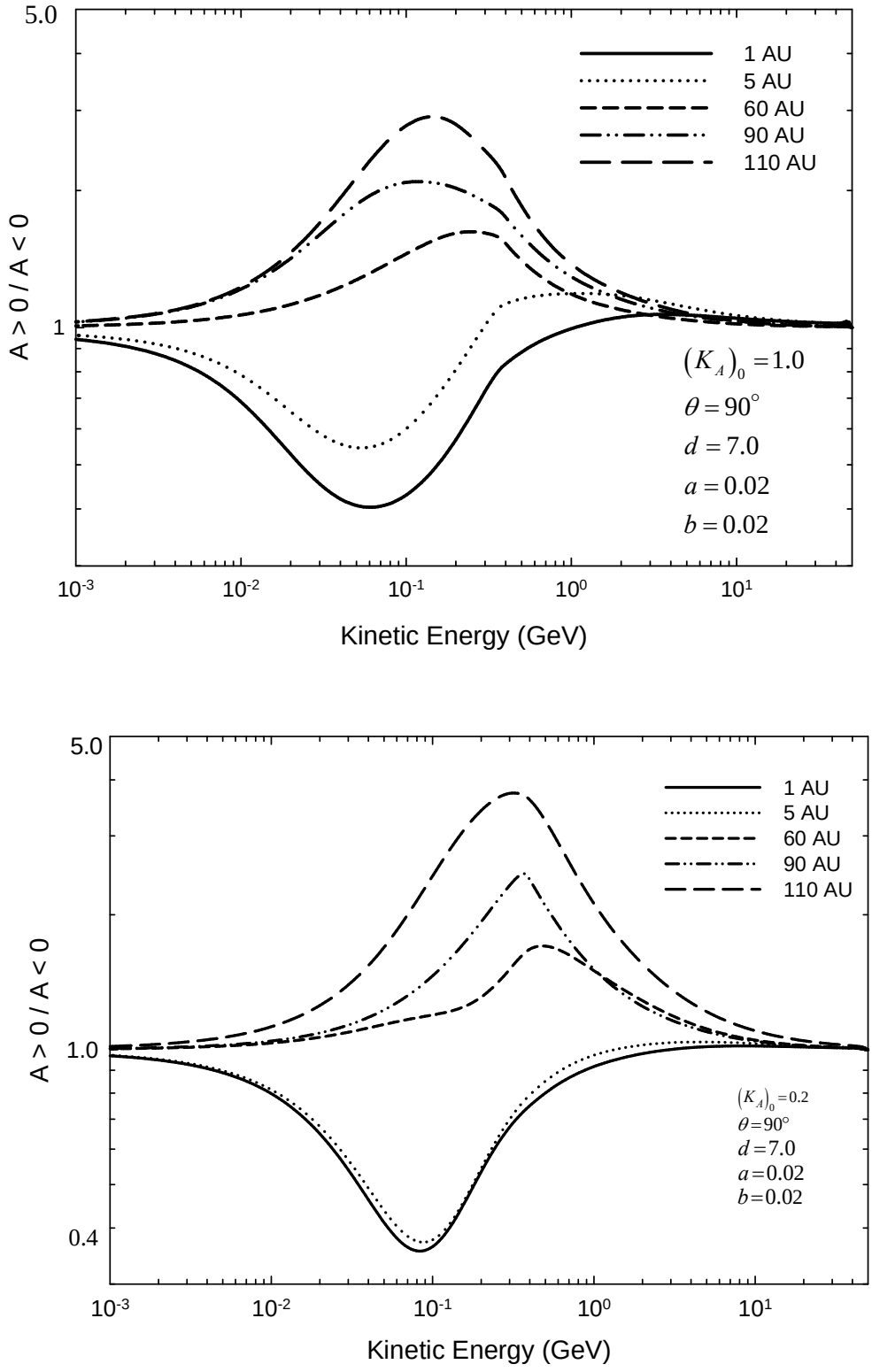

Figure 6.3: The ratio of modulated electron spectra computed with 100% and 20% drifts, shown at 1 AU, 5 AU, 60 AU, 90 AU and 110 AU, with the HPS specified at 122 AU. This is done for the weak scattering drift coefficient as in Eq. (6.1) for both magnetic polarity epochs. Deviation from unity is indicative of how large drift effects are.

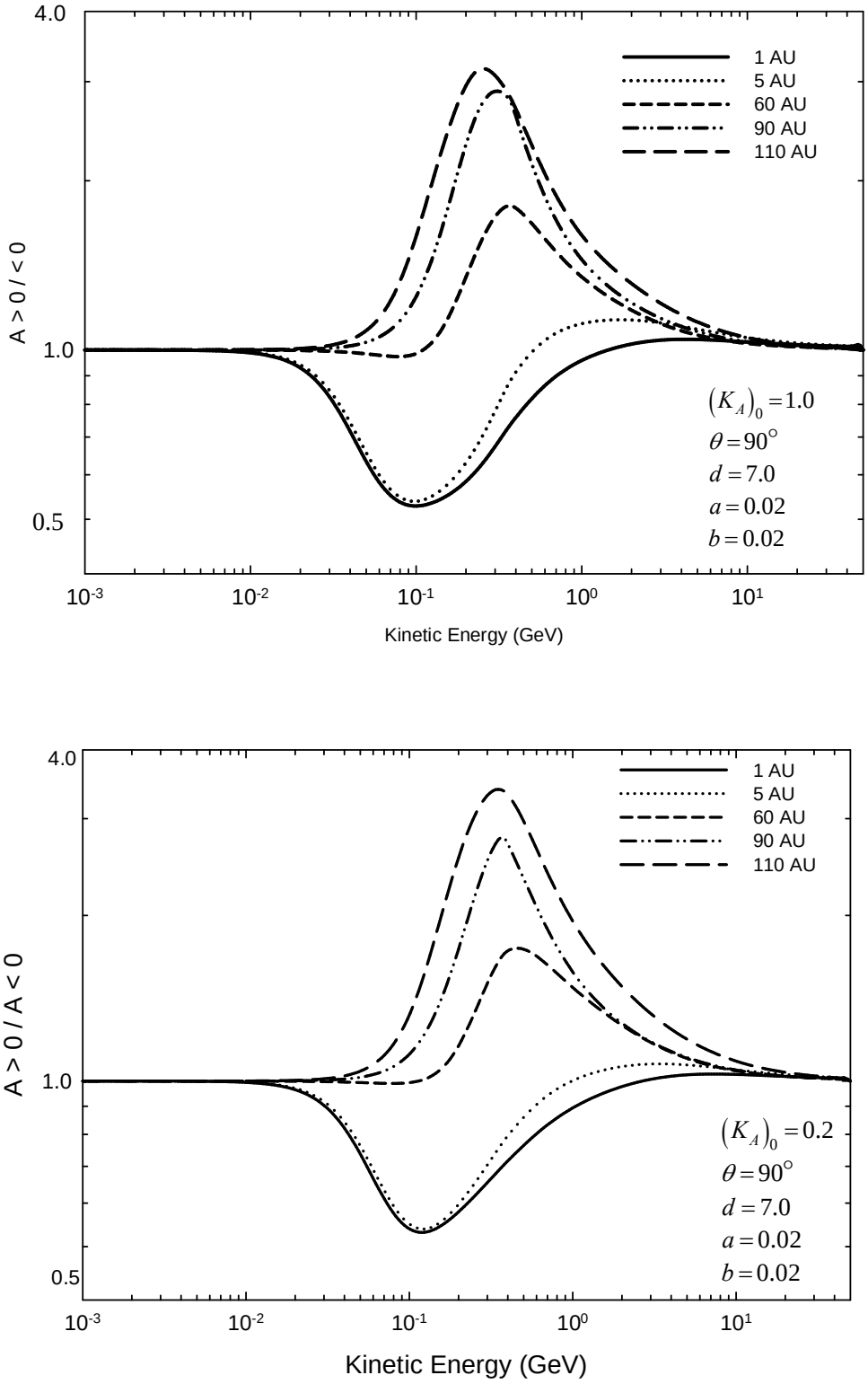

Figure 6.4: Similar to Figure 6.3 but for the modified drift coefficient as given by Eq. (6.2).

The bottom panel shows the ratio computed for 20% drifts. The general quantitative features are much the same as for the 100% drifts, but the drift effects now diminish much sooner with decreasing energy when compared to the top panel. The maximum effect in the inner heliosphere is shifted to a high energy, from around ~20 Me to ~100 MeV; similarly for larger radial distances. The drift effects again dissipate rather quickly with increasing energy. Comparing the top and the bottom panel, it is evident from the value of the ratios that full drifts give higher spectra compared to the 20% drifts. Clearly, the energy range over which drifts dominate as well as the total global effect is effectively reduced by decreasing the value of $(K_A)_0$. Despite having only 20% drifts, the drift effects are still surprisingly large.

In Figure 6.4 the computed ratios are shown again for 100% and 20% drifts, respectively in the top and bottom panels, but now for the modified drift coefficient as in Eq. (6.2). The main difference here is that K_A decreases much stronger as a function of decreasing rigidity and this is clearly evident from the computed ratio as illustrated in this figure. Below 10 MeV, at all radial distances, the ratio is unity, and this happens at a higher energy than in Figure 6.3. This illustrates that at these low energies, the modulation process for electrons is dominated by diffusion, and as such, drifts become negligible. A similar trend is seen above ~10 GeV, but for a different reason: there is little modulation, and as such the drift effects become quite small, they are not completely absent.

Comparing the top panels of Figure 6.3 and 6.4, it is clear that there is a significant difference in terms of the energy dependence of this ratio as expected. In the inner heliosphere the ratio is still less than unity, but the energy dependence of the drift contribution is shifted to a higher energy with the minimum in the ratio at 100 MeV and the maximum at ~250 MeV for larger distances. Similar remarks can be made when comparing the two bottom panels. Below 15 MeV there are no drift effects and the ratio is unity at all radial distances. Comparing the top panel with the bottom panel in Figure 6.4, the differences are not as large as between the two panels in Figure 6.3. This means that with the significantly stronger rigidity dependence of K_A, the drift effects are already significantly reduced at these lower energies, so that an additional reduction in the total value of K_A is not as effective anymore. So, the conclusion can be made that changing the drift scaling factor $(K_A)_0$ has a significant effect on electron modulation, but less so when the rigidity dependence of K_A is already changed. Both these phenomenological procedures can be used effectively to suppress the drift effects on low energy electrons to bring drift models in line with observations. However, it should be noted

that changing the value of K_A alone, could not reproduce the observed latitudinal gradients for Ulysses (Potgieter 1997; Webber et al. 1990; Langner et al. (2003); Langner (2004); Ferreira and Potgieter (2004a, b). In order to do so, the reduction of K_A at lower energies was absolutely required.

Recently, Engelbrecht and Burger (2013a, b) illustrated that this rigidity reduction followed rigorously from the way that they applied turbulence theory, but at the same time they argued that full drifts as described by the weak scattering approach are also too large. See also Ngobeni (2015). At this stage it is apparent that it is a matter of time before turbulence and drift theory will be refined to the point that the exact reduction can be determined and motivated from first principles (ab initio) while reproducing major observations, which so far has not been the case.

6.3 Reducing drifts implicitly

Reducing drifts implicitly is a far more subtle process than the strong handed approach of decreasing the drift coefficient directly. Inspection of Parker's transport equation (Eq. 3.1), clearly shows that drift effects depend on the product of the drift velocity and the cosmic ray density gradients; for example, if the spatial gradients are to be very large (meaning the cosmic ray intensity decreases significantly from the HP to the Earth), drift effects on the computed spectra will also become very large without touching the drift velocity field, as described by Eq. (3.52). On the other hand, with very small spatial gradients, drift effects also become very small, as apparently happened in the 2007-2009 solar minimum period; see Potgieter et al. (2014c). Distinction is therefore made between the magnitude of drifts (essentially given by value of the drift coefficient in Eq. 6.1) and drift effects as the consequences of these assumptions on modulated spectra throughout the heliosphere. It should also be noted that electrons experience far less adiabatic energy changes than protons so their spectra are not exhibiting the characteristic E^{+1} spectral shape at the Earth.

It is first noted that perpendicular diffusion, in general, plays an important role in the heliospheric modulation of galactic cosmic rays, so that changing its value and rigidity dependence also affects the effectiveness of drifts. Additionally, Potgieter (1996) illustrated that large perpendicular diffusion in the polar regions of the heliosphere could suppress most effectively the strong latitude effects generated by strong global drifts; see also Ferreira et al. (2001b). For the first time it was realized that perpendicular diffusion in the radial direction

could be different from perpendicular diffusion in the polar direction, especially away from the equatorial regions. Many studies (e.g. Potgieter 1996, 2000; Burger et al. 2000; Ferreira 2002; Langner 2004; Moeketsi 2004; Ngobeni 2006; Strauss 2010) support this concept, but unfortunately cannot yet give how exactly these diffusion coefficients differ as a function of energy and space, so that it is determined empirically. As an example of the theoretical controversies surrounding this approach, see the study of Engelbrecht and Burger (2013a, b). However, the issue of how large the two perpendicular diffusion coefficients are with respect to the parallel diffusion coefficient, is very important to electron modulation as they respond directly to the rigidity dependence of all three diffusion coefficients. In this section, reducing drifts implicitly is revisited, illustrated and discussed for electron modulation in particular.

6.3.1 Effects of changing $K_{\perp r} / K_{\parallel}$ on modulated spectra

In this section the effects of increasing the ratio $K_{\perp r} / K_{\parallel}$ on electron modulation is shown, illustrating the role of $K_{\perp r}$ in the implicit reduction of drifts. This is done independently of the ratio $K_{\perp \theta} / K_{\parallel}$, which is kept constant at 0.02. As before, the computations are carried out for both $A > 0$ and $A < 0$ magnetic polarity epochs, for solar minimum conditions with $\alpha = 5^{\circ}$ and for 100 % drifts. As before, the computed spectra are shown at 1 AU, 5 AU, 60 AU, 90 AU and 110 AU in the equatorial plane with respect to the HPS $\left(E^{-1.55}\right)$ specified at 122 AU. A straight forward rigidity dependence is used as shown in the bottom panel of Figure 6.1, which means that all three DCs have the same rigidity dependence which is constant below 0.4 GV (see also Figure 3.6). This aspect is important for electron modulation because it causes the total modulation at a given position in the heliosphere to become constant at $E <$ ~50 MeV, which in this study is considered an important feature of electron modulation (see also Potgieter and Nndanganeni 2013a).

As a reference solution, the spectra shown in Figure 6.2 are repeated in Figure 6.5, but shown only down to 10 MeV to emphasize the difference in the drift solutions. Spectra are computed with $K_{\perp r} / K_{\parallel} = 0.02$, which will be changed in the figures to come. Details of the spectra shown in this figure have already been discussed in section 6.2.1 and are not repeated here, except to emphasize that the spectra conserve the spectral shape of the HPS at lower energies where drift effects are negligible. Note the total modulation between the HPS (upper curve) and the spectrum at the Earth (lowest curve), at 10 MeV is a factor of ~3000.

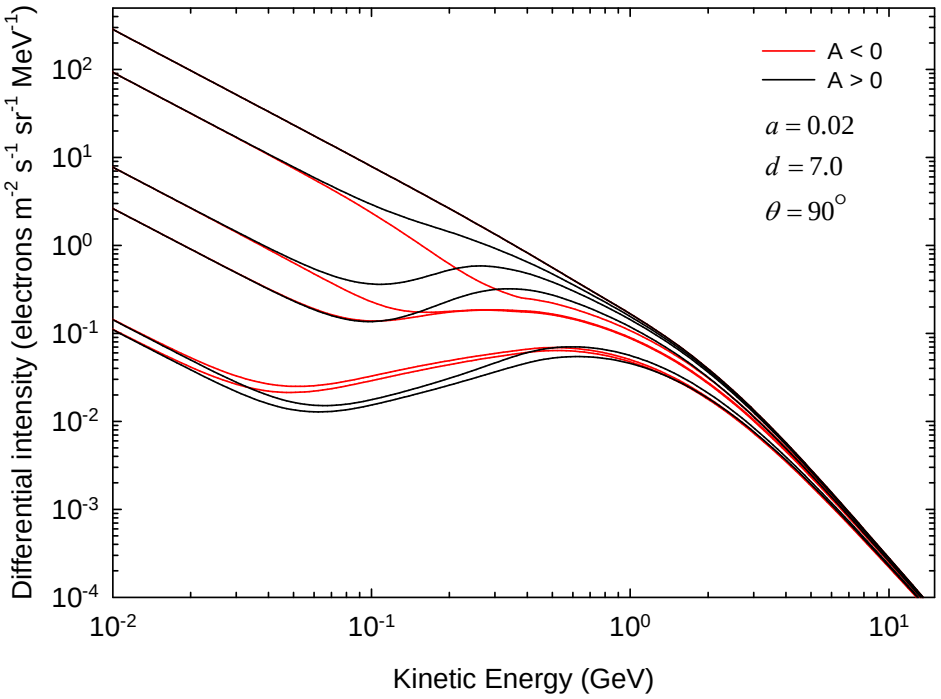

Figure 6.5: Similar to the bottom panel of Figure 6.2, but with the spectra only shown down to 10 MeV. The HPS is specified at 122 AU. For this case, $K_{\perp r} / K_{\parallel} = a = 0.02$. Note that the intensity drops from the HP to the Earth by a factor of ~3000.

Figure 6.6 shows the spectra again but now computed with $K_{\perp r} / K_{\parallel} = 0.03$ in the top panel and $K_{\perp r} / K_{\parallel} = 0.05$ in the bottom panel. It follows by comparing these results with those in Figure 6.5, that there is a clear difference between the two drift solutions ($A > 0$ vs. $A < 0$) that is, in terms of the energy dependence of the drift effects. First, note how the total modulation between the HPS and the Earth at 10 MeV reduced, from an intensity of 1.0×10^{-1} m^{-2} s^{-1} sr^{-1} MeV^{-1} to 4.5×10^{-1} m^{-2} s^{-1} sr^{-1} MeV^{-1} for $K_{\perp r} / K_{\parallel} = 0.03$ and from 1.0×10^{-1} m^{-2} s^{-1} sr^{-1} MeV^{-1} to 3.5 m^{-2} s^{-1} sr^{-1} MeV^{-1} for $K_{\perp r} / K_{\parallel} = 0.05$. The reduced total modulation means that the spatial gradients are correspondingly reduced, the higher this ratio becomes.

To emphasize the modulation effects caused by these changes, the computed ratios between the $A > 0$ and $A < 0$ spectra as in Figure 6.6 are computed and shown in Figure 6.7. In both cases, the energy dependence of the maximum drift contribution is shifted toward a higher energy, while less drift effects occur at lower energies. At all radial distances similar features

are observable; the difference between the solutions based on the two magnetic polarity epochs becomes narrower as compared to Figure 6.5. Striking is that for the $K_{\perp r} / K_{\parallel} = 0.05$ case, the drift effects become almost negligible at the Earth, whereas in the outer heliosphere the effects are still there, but with a much reduced ratio. This is emphasizing the point that, as $K_{\perp r} / K_{\parallel}$ increases, the spectra ratios become progressively less implying that the drift effects diminish relatively quickly. Increasing $K_{\perp r} / K_{\parallel}$ does indeed reduce drift effects very effectively, making it a most effective way of reducing drift effects indirectly (implicitly) without changing the drift coefficient at all.

The question arises as to what extent can $K_{\perp r} / K_{\parallel}$ be changed because too little modulation can easily be caused, as is already apparent in the lower panel of Figure 6.6. Unfortunately, diffusion theory cannot yet give a definitive answer. Modeling work found values between 0.005 (Ferreira et al. 2001a, b) and 0.05, but values approaching 0.10 are avoided. For example, Vos (2011) and Potgieter et al. (2014c) could reproduce PAMELA proton spectra at Earth from 2006 to 2009, using a ratio of $K_{\perp r} / K_{\parallel} = 0.02$ throughout the heliosphere in their model. To complicate the issue even further, updated diffusion theories indicate that this ratio may not be a constant throughout the heliosphere, and also not a constant with rigidity as is assumed here. See e.g. earlier work by Burger et al. (2000) and more recent work by Strauss (2010, 2013), Ngobeni and Potgieter (2011) and Manuel et al. (2013, 2014). This issue is not pursued further because such refinements will not change the qualitative picture and conclusions that are presented here, but may indeed be required when the modeling is applied to reproducing specific observations over a wide range of energies.

In the next section the ratio of $K_{\perp \theta} / K_{\parallel}$ will be investigated, which in its turn will further complicate matters.

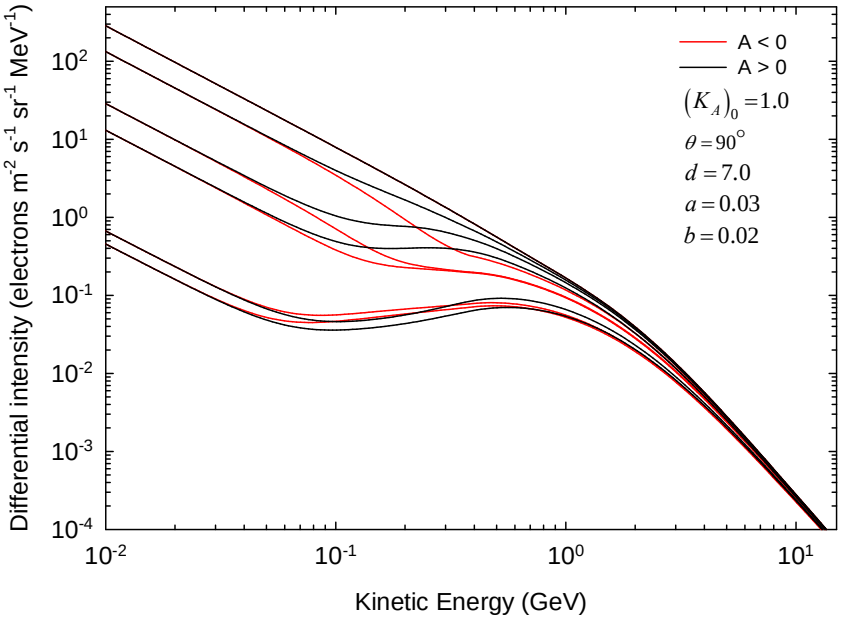

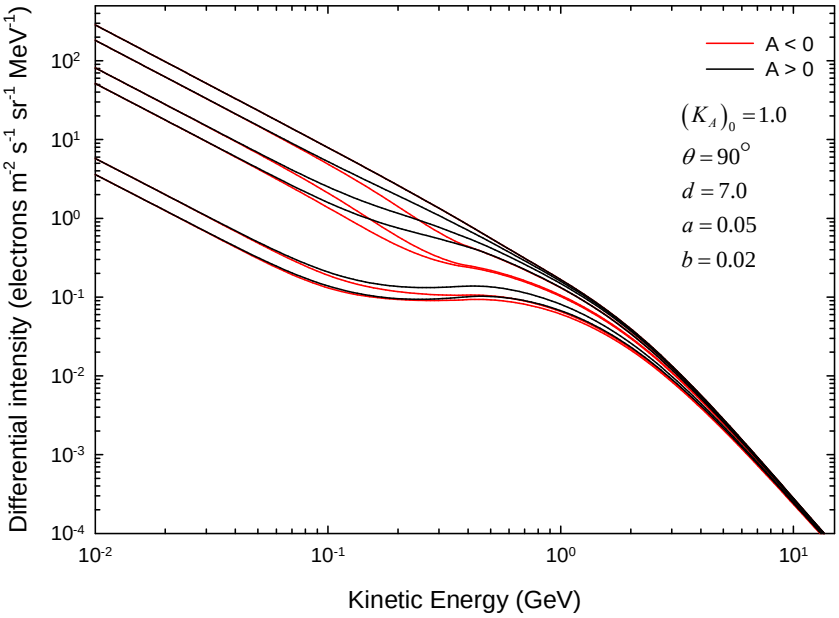

Figure 6.6: Computed spectra as a function of kinetic energy from the inner to the outer heliosphere with $\theta = 90^\circ$ at 1 AU, 5 AU, 60 AU 90 AU and 110 AU (bottom to top) for both magnetic polarity epochs. The top panel shows spectra computed for $K_{\perp r} / K_{||} = a = 0.03$ and the bottom panel for $K_{\perp r} / K_{||} = a = 0.05$. Note the reduction in the total modulation; at 10 MeV the drop in intensity for the upper panel is by a factor of ~600 and in the lower panel only ~75.

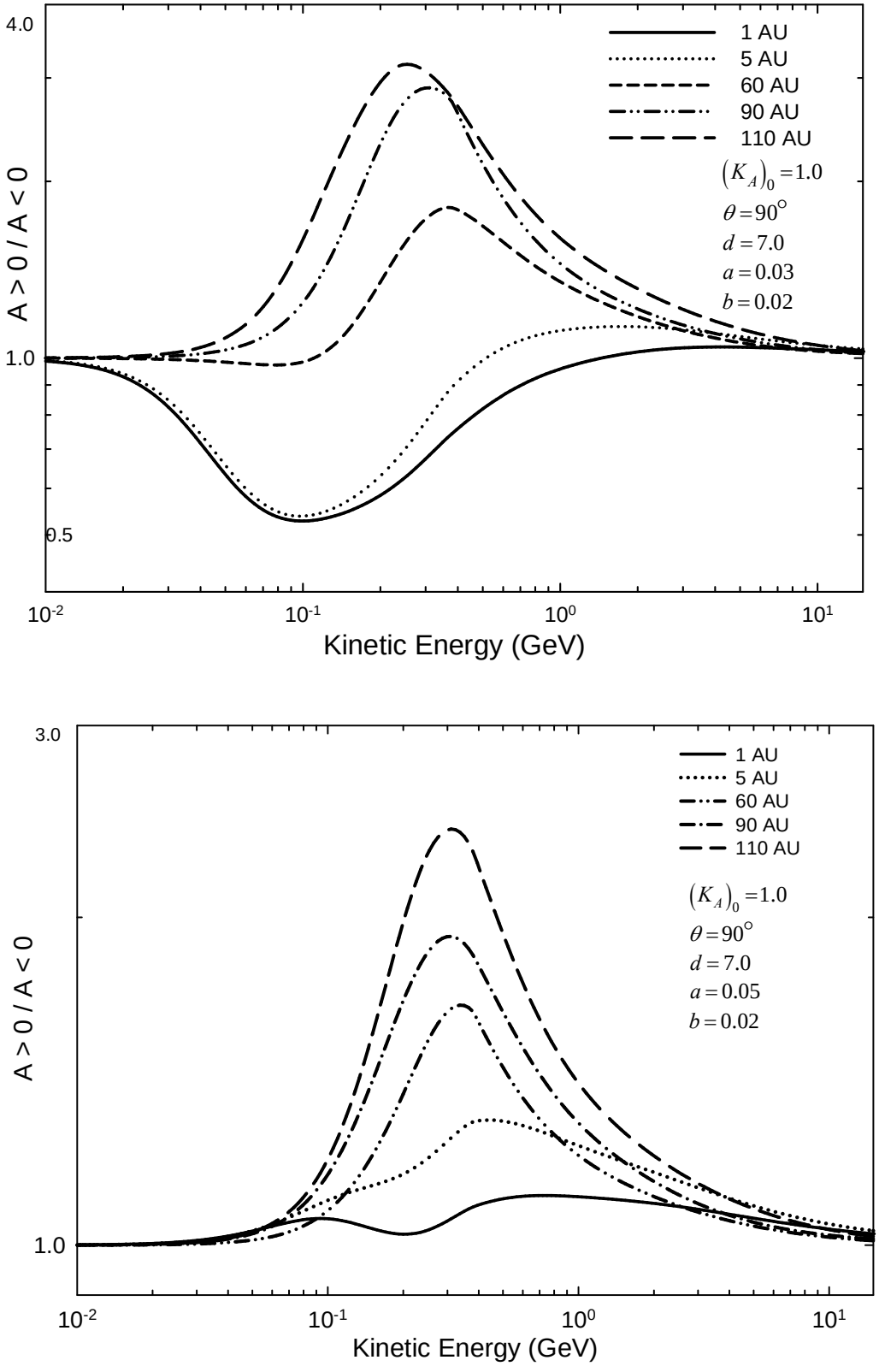

Figure 6.7: Computed ratios of $A > 0$ to $A < 0$ based on the spectra shown in Figure 6.6.

6.3.2 Effects of enhancing $K_{\perp\theta}$ on modulated spectra

Increasing $K_{\perp\theta}$ as a function of polar angle (co-latitude) results in reducing the latitudinal dependence of cosmic rays intensities in the heliosphere for both magnetic both polarity epochs at almost all energies. Potgieter (1996, 1997, 2000) and Ferreira et al. (2000, 2001a) emphasize the importance of this enhancement of $K_{\perp\theta}$ towards the heliospheric poles and argue it is essential to explain the small latitudinal gradients observed by Ulysses (Heber and Potgieter 2006). This enhancement is thus particularly effective in reducing drift effects in the heliospheric polar regions, and is therefore of importance for this study. This approach is revisited and studied in more detail as applied to electron modulation. The equation for $K_{\perp\theta}$ with the function $F(\theta)$ which incorporates the enhancement factor d is given by Eq. (3.43), with Figure 3.3 showing this function for $d = 1.0,\ 3.5,\ 7.0$ and 13.0 in the equatorial plane. To emphasize the modulation effects caused by these changes, the spectra are computed for both $A > 0$ and $A < 0$ respectively.

In what follows, only the computed ratio of $d = 1/d = 7$ is shown for the $A < 0$ and $A > 0$ cycles at 1 AU, 5 AU, 60 AU, 90 AU and 110 AU. This will show how making this enhancement changes the modulation. The impact on drift effects will be done afterwards. The computations are done for full drifts, for solar minimum condition with $\alpha = 5^{\circ}$, and in the equatorial plane. The main aim is to show the effects that the enhancement factor d has on the computed modulated electron spectra throughout the heliosphere. The reason why only the $d = 1/d = 7$ is shown is because the electron modulation results are qualitatively very similar, and for the rest of this study only $d = 7$ will be used as required to reproduce observations.

Figure 6.8 shows the computed ratios of $d = 1.0$ to $d = 7.0$ intensities for both magnetic polarity epochs. The top panel is for $A < 0$ at different radial distances as given in the figure legend. A ratio less than 1.0 at ~ 200 MeV implies that the $d = 1.0$ solutions produced higher intensities (less modulation) than the $d = 7.0$ solutions. In the inner heliosphere, at 1 AU and 5 AU, the ratio changes significantly, being larger than unity at all energies, with a maximum effect around 200 MeV, and only converges to unity at very high energies. Further out in the heliosphere, at larger distances, the tendency is that the ratio is almost constant, and then increases to reach the maximum effect around ~ 200 MeV to subside again.

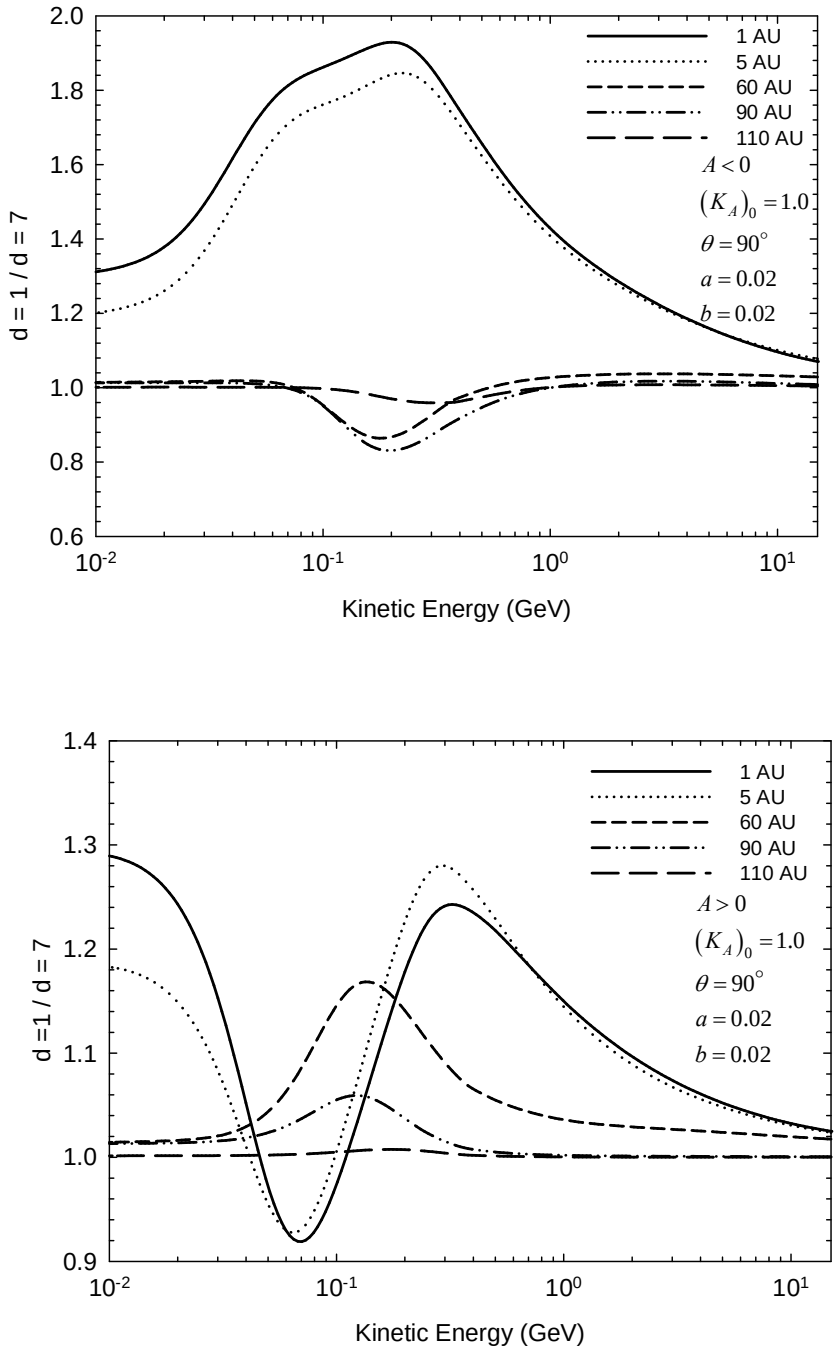

Figure 6.8: Computed ratio of $d=1/d=7$ intensities at various radial distances for the $A<0$ (top panel) and the $A>0$ (bottom panel) polarity epochs, where $d=1.0$ represents no enhancement of $K_{\perp\theta}$ to $d=7.0$ which is a significant enhancement towards the heliospheric poles, as shown in Figure 3.3. The other parameters were kept unchanged.

At 60 AU, the ratio is almost constant throughout the heliosphere. At 90 AU and 110 AU, the ratio is unity for $E \leq 80$ MeV and for $E \geq 700$ MeV, but between 80 MeV and 700 MeV the ratio is less than unity. For this polarity cycle, the enhancement factor has larger effects in the inner heliosphere where the ratio is almost a factor of two, as compared to the outer heliosphere.

The bottom panel shows the ratio computed for $A > 0$. Compared to the top panel, the picture is completely different and more complicated, with the largest effect for the spectra in the inner heliosphere; with a ratio of 1.18 and 1.29 at 1 AU and 5 AU, respectively. At larger distance the effects are much reduced. At 60 AU for $E \leq 40$ MeV ratio is very close to unity then increases above this energy to give the maximum intensity at ~150 MeV, then decreases rapidly to converge to become constant above 1 GeV. At 90 AU, the ratio is unity for $E \leq 40$ MeV and above $E \geq 300$ MeV, but larger than unity for $20 \geq E \leq 300$ MeV. At 110 AU the ratio is unity throughout the heliosphere.

Evidently, this enhancement has the largest effects on modulated spectra in the inner heliosphere. In the $A > 0$ cycle, the effects are subsiding with increasing radial distance, with almost no contribution in the middle heliosphere, but somewhat larger in the outer heliosphere. In the $A < 0$ cycle, the effects are different in terms of energy, but overall smaller than in the $A > 0$ cycle, even in the inner heliosphere. This means that this enhancement will reduce drifts in different ways, depending on the magnetic polarity.

In what follows, the spectra computed with different values of d are shown for the two polarity epochs to illustrate what this reduction does to drift effects, as presented by the differences between the spectra for the two polarity epochs, from the Earth to the heliopause.

Figure 6.9 shows the computed spectra at 1 AU, 5 AU, 60 AU, 90 AU and 110 AU in the equatorial plane for $d = 1.0$ and $d = 3.5$. These computations are carried out for both $A > 0$ and $A < 0$ for full drifts, and for solar minimum conditions with $\alpha = 5^{\circ}$. These computations illustrate the effectiveness of the enhancement factor d in reducing drifts. The top panel shows the spectra with $d = 1.0$ that are without an enhancement. Note that the drifts effects are more pronounced in the inner heliosphere at 1 AU and 5 AU between 10 MeV $\geq E \leq$ 1 GeV. In the middle and outer heliosphere, the drift effects are evident, but with the energy where the drifts start to contribute shifted to the higher values as compared to the inner heliosphere. The bottom panel shows the spectra for $d = 3.5$. Compared to the top panel where there was no enhancement, the drift effects are reduced, especially at 1 AU and 5

AU, with the energy dependence of the contribution of drifts shifted to higher energy. Changing to $d = 3.5$ seems to be less effective in terms of drift reduction in the outer heliosphere because the drift effects are still pronounced at 60 AU, 90 AU and 110 AU.

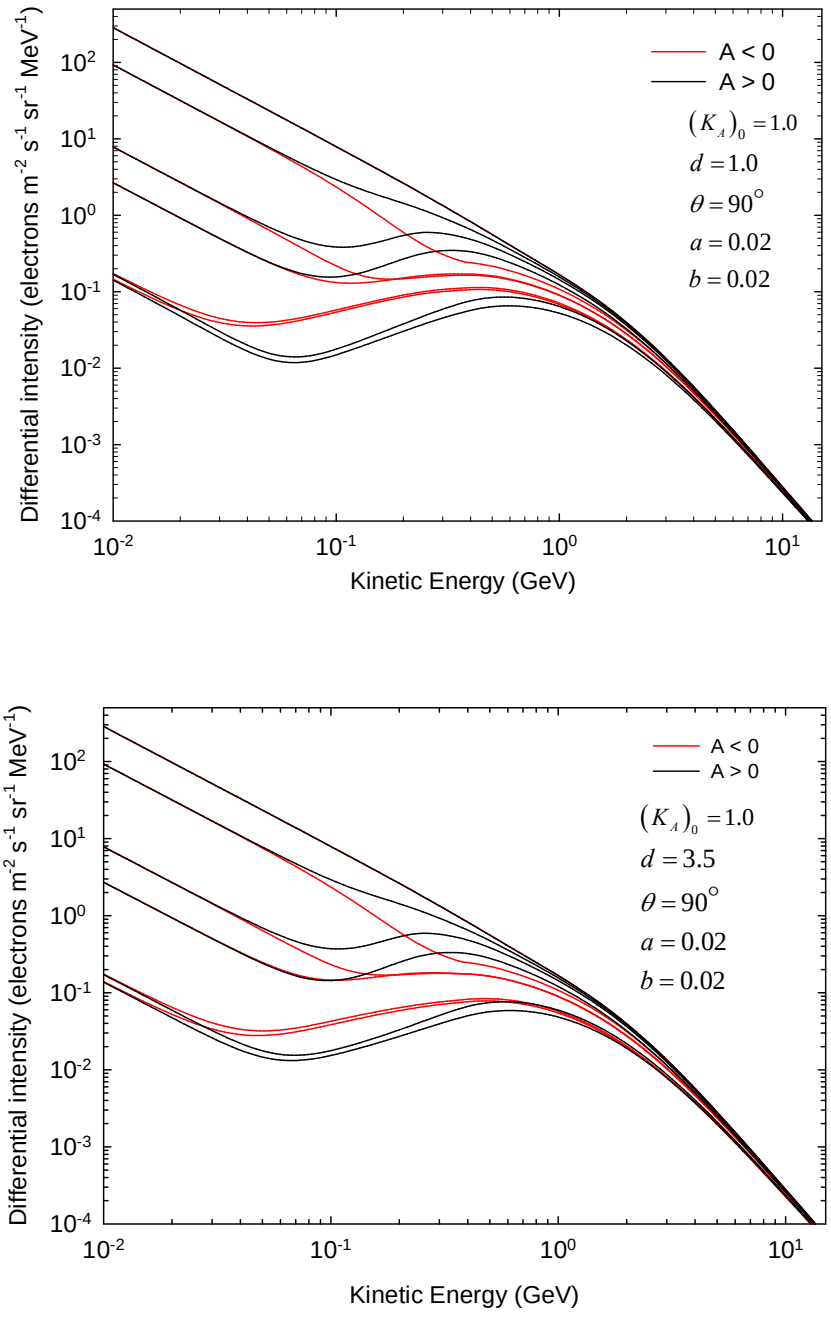

Figure 6.9: Computed spectra as a function of kinetic energy at 1 AU, 5 AU, 60 AU, 90 AU and 110 AU for both magnetic polarity cycles with $\theta = 90^\circ$. This is done for $d = 1.0$ (upper panel) and $d = 3.5$ (lower panel) illustrating the effects of enhancing $K_{\perp\theta}$ on the modulated electron spectra computed from the inner and the outer heliosphere.

Figure 6.10 shows similar computations but now for $d = 7.0$ and $d = 13.0$. The top panel is for $d = 7.0$ and the bottom panel is for $d = 13.0$. The trends are similar to what was evident in Figure 6.9; drift effects are meaningfully reduced in the inner heliosphere but not in the outer heliosphere. There are smaller differences between the solutions for $d = 7.0$ and $d = 13.0$ than between d =1.0 and d = 3.5, indicating that there is an optimal value for this enhancement factor.

Figure 6.11 shows the computed ratios of the $A > 0$ and $A < 0$ spectra at five different radial distances as described in the figure caption. The ratios are computed for $d = 1.0$, $d = 7.0$ and $d = 13.0$ respectively. This summarises the impact that this enhancement has on drift effects as a function of energy and radial distances in the equatorial plane, indicating how this enhancement factor suppresses drift effects in the heliosphere. Comparing the three solid lines, all for spectra at the Earth, it becomes clear that the maximum drift effects occur for $d = 1.0,$ and gets reduced with increasing d. The same applies for 5 AU, with the ratios are less than unit for all energies between ~ 10 MeV and ~10 GeV. This means that the $A < 0$ spectra for electrons are higher than the $A > 0$ spectra. The energy at which the maximum drift effects occur moves to somewhat higher values with increasing d, indicating that drift effects are first reduced at lower energies. At larger distances from the Sun, the ratios are larger than unity, indicating that the A < 0 spectra are lower than the A > 0 spectra. Here, the difference between the blue (d = 7.0) and green lines (d = 13.0) are indistinguishable, indicating that d = 7.0 is already causing an optimal reduction in this region of the heliosphere. Changing d from 1.0 to 13.0 reduces drifts effectively in the inner heliosphere. It follows from these computational results that enhancing $K_{\perp\theta}$ through the factor d is quite effective in reducing drift effects in the inner heliosphere but not in the middle to the outer heliosphere.

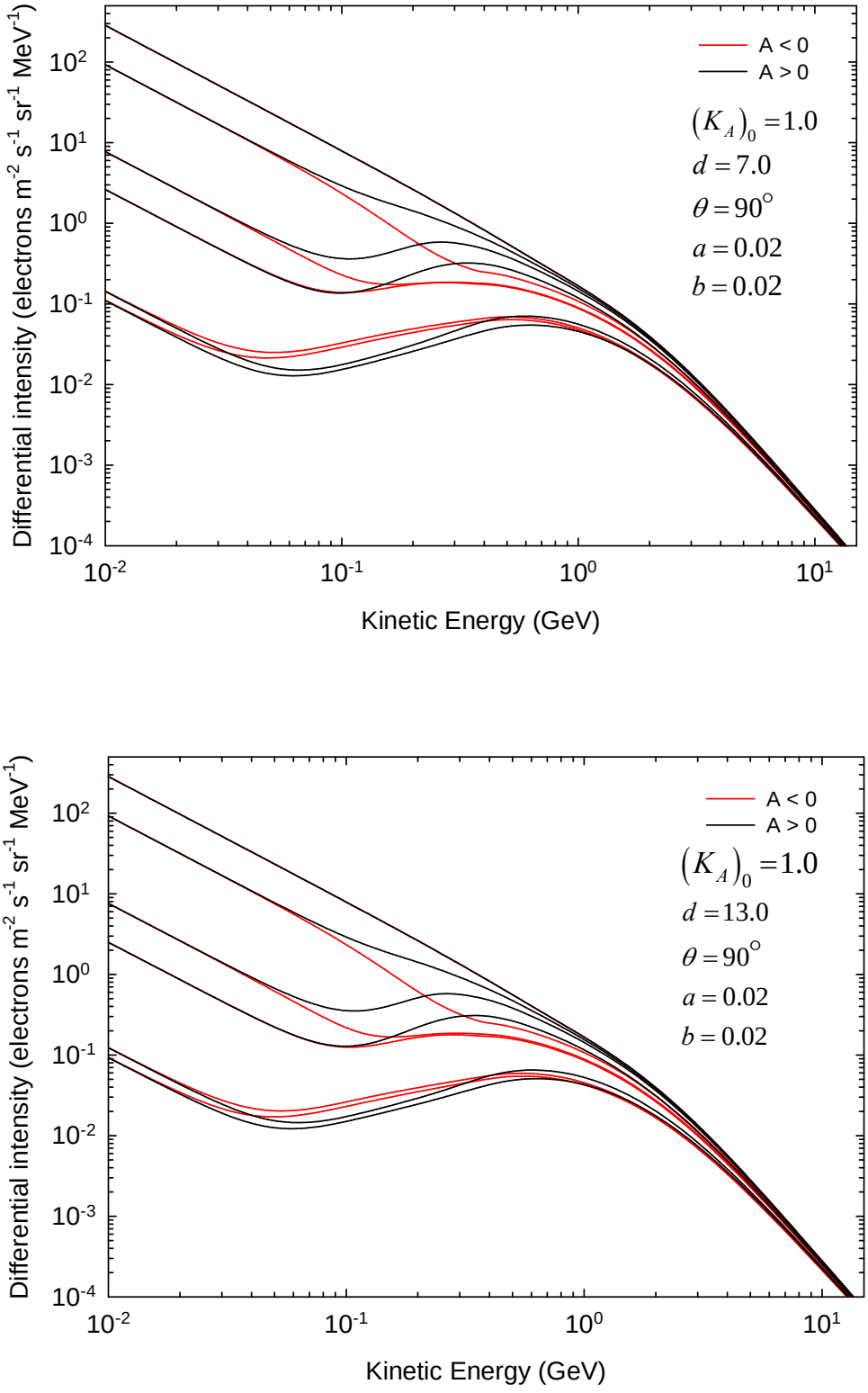

Figure 6.10: Similar to Figure 6.9 but for $d = 7.0$ (upper panel) and $d = 13.0$ (lower panel), with the latter as the maximum enhancement. Note how the drift effects are reduced with increasing d.

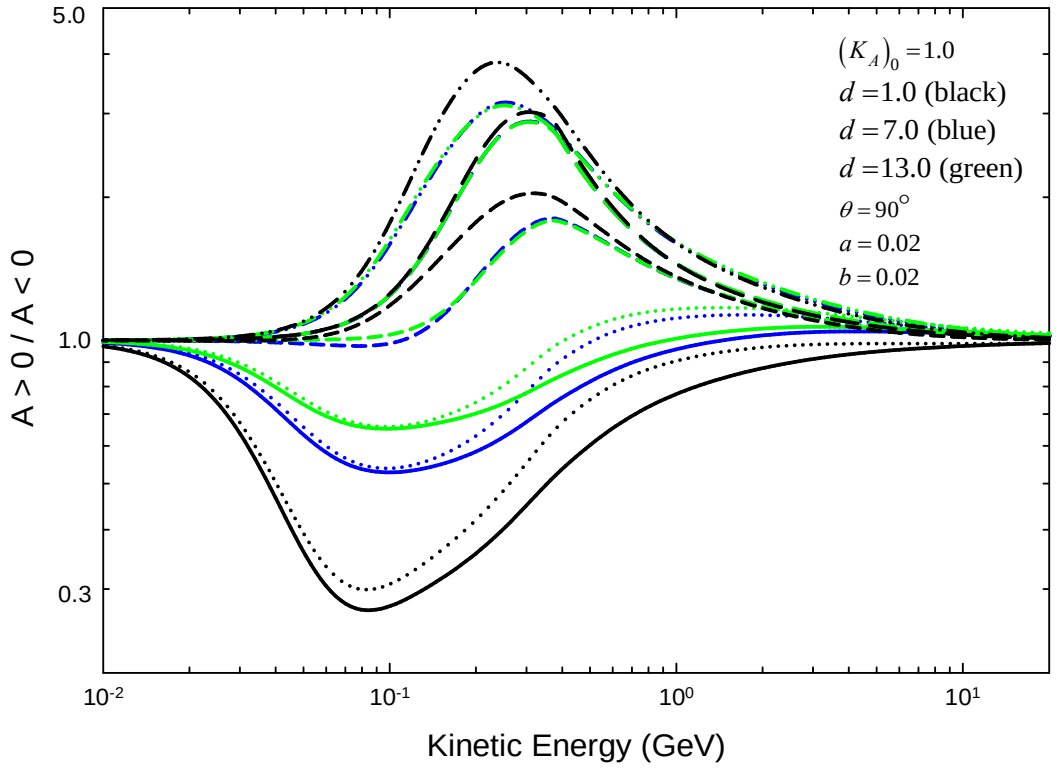

Figure 6.11: The computed ratios of $A>0$ and $A<0$ spectra, shown at 1 AU (solid), 5 AU (dotted), 60 AU (shot-dashed), 90 AU (long-dashed) and 110 AU (dashed double dotted) in the equatorial plane with 100% drifts. Ratios are computed with $d=1.0$ (black lines), $d=7.0$ (blue lines), and for $d=13.0$ (green lines). Deviation from unity is indicative of how large drift effects are. Note how increasing d (black to blue to green) effectively reduces drift effects in the inner heliosphere.

6.4 Summary and conclusions

Drift effects were neglected until Jokipii et al. (1977), and others, pointed out that particle drifts are an important mechanism in cosmic ray modulation. The fundamental process of global curvature, gradient and current sheet drifts in the heliosphere is, however, still not fully understood, especially how HMF turbulence could affect the magnitude of drifts on a global scale, and over a full solar activity cycle. General consensus is that implementing weak scattering drift in modulation models gives too large drift effects. This follows from the application of these numerical drift models to solar modulation and comparison with observations from the Earth to the outer heliosphere.

Particle drifts had been recognized as a major modulation process and overshadowed development of advanced diffusion theories until in the early 2000s, when major efforts were made to understand diffusion theory better, together with the underlying heliospheric turbulence theory (Bieber 2003 and McKibben 2005). It was then realized that particle drifts do not dominate solar modulation over a complete solar cycle, but that it is a part of a compelling interplay among the four basic mechanisms, and that this play-off can change over a solar cycle and from one cycle to another (e.g. Potgieter et al. 2013a). How the reduction of drifts should occur from a fundamental theoretical point of view is a work in progress.

The effects of drifts on the global modulation of electrons, and how its reduction influences these effects, were revisited by studying different modulation scenarios, using the numerical model as described in Chapter 3. Ways of reducing drifts explicitly and implicitly were illustrated and the consequences were discussed. Reducing drifts explicitly was done in two ways, firstly by changing the rigidity dependence of the drift coefficient, in which the solutions for weak scattering and the modified drifts are computed and compared. Secondly, by reducing the scaling factor $\left(K_A\right)_0$. Reducing drifts implicitly is a far more subtle process than the strong-handed approach of decreasing the drift coefficient directly. This was done firstly by varying the ratio of $K_{\perp r} / K_{\parallel}$. It is an effective way of reducing drift effects, through changing diffusion. It was found that this ratio should be between 0.005 and 0.05, since making it too large can easily produce too little modulation. To complicate the issue, some updated theories indicate that this ratio may not be constant throughout the heliosphere and also not constant with rigidities as was assumed here. Secondly, the effects of enhancing the diffusion coefficient perpendicular to the HMF in the polar direction were also investigated by studying different enhancement scenarios. The conclusion that can be drawn is that enhancing this perpendicular diffusion coefficient does indeed reduce drifts effectively in the inner heliosphere.

The next chapter is devoted to the electron modulation in the heliosheath.

Chapter 7

Modulation of galactic electrons in the heliosheath

7.1 Introduction

The heliosphere seems to move through the interstellar medium with a velocity of between ~23 km.s^{-1} and more likely ~26 km.s^{-1} (see e.g. Zieger et al. 2013), so that a heliospheric interface is formed by the interaction of the solar wind and interstellar plasma as discussed in Chapter 2. This interface consists of a termination shock (TS), a heliopause (HP) and a bow wave or bow shock (BS). The region between the TS and HP is defined as the inner heliosheath and the region between the HP and BS as the outer heliosheath. In cosmic ray (CRs) modulation studies, the term heliosheath is frequently used to refer to the inner heliosheath.

The TS can be considered as the first heliospheric boundary away from the Sun, with the main feature that the Sunôs supermagnetosonically expanding solar wind abruptly slows down. Voyager 1 found the position of the TS to be at 94 AU in 2004 when it crossed into the heliosheath region (Stone et al. 2005), and Voyager 2 did the same in 2007 at 84 AU (Stone et al. 2008). This indicated that the position of the TS is dynamic, moving in and out with the solar activity cycle, which affects the modulation of CRs; see e.g. Manuel et al. (2015).

The HP is the second boundary of the heliosphere, and is regarded as a contact discontinuity which separates the solar and interstellar media. It has been widely considered as the outer boundary of the heliosphere and is mostly applied as such in CRs modulation models. However, based on MHD modeling it is known and expected that a BS or perhaps just a bow wave should occur well beyond the HP in the nose direction of the heliosphere. Whether a BS or bow wave exists in reality, has become somewhat controversial as argued by McComas et al. (2012) and Scherer and Fichtner (2014). In this work, the HP is assumed to be the CRs modulation boundary so that no further attention is given to the outer heliosheath and BS.

The heliosheath is different from the region up-wind of the TS, and several theoretical and observational publications, since the launch of the two Voyager spacecraft, have emphasised

the importance of this region to CRs modulation. Voyager 1 crossed the HP at ~ 121.7 AU in August 2012 (e.g. Krimigis et al. 2013; Gurnett et al. 2013) and is now ~132 AU from the Sun. Remarkably, the magnetic field on both sides of the HP was found to be similar, although theoretically they are assumed to be independent of each other (Burlaga et al. 2013). This delayed the identification of the boundary as the HP and led to many alternative explanations and controversy, created mostly by Fisk and Gloeckler (2014) and Gloeckler and Fisk (2014). Recent publications by Gurnett et al. (2013), Burlaga et al. (2014) and Burlaga and Ness (2014a, b) have largely settled these arguments, so that it is now widely accepted that Voyager 1 is well beyond the HP in the very local interstellar medium (LISM). What will happen when Voyager 2 crosses the TS is eagerly awaited.

Taking this into account, the heliosheath may have an average width of ~28 AU from Voyager 1's point of view. Obviously, this number changes over the solar cycle because the TS is not stationary (e.g. Manuel et al. 2015, and references there-in). Voyager 2 has not yet reached the HP so that only estimates are made, based on assumptions that the heliosheath may be less wide along the Voyager 2 trajectory (see also Ngobeni and Potgieter 2011), influenced by MHD modeling (e.g. Opher et al. 2009). Considering the present position of Voyager 2, the thickness of the heliosheath in that direction could be ~25 AU or less with an uncertainty of ~2.5 AU caused by possible solar wind pressure differences. If this kind of prediction is correct, Voyager 2 might reach the HP as early as in the second semester of 2015; see e.g. Webber and Intriligator (2014) for these estimates and mostly speculative arguments.

The importance of the heliosheath as a steady diffusion barrier for the modulation of CRs was realised in the 1980s (Quenby et al. 1990), and the modeling of this type of modulation was included in some numerical models (see e.g. Potgieter and Le Roux 1989a, b and Jokipii et al. 1993). The question of what happens at and beyond the TS was addressed in several observational papers (McDonald et al. 2000, 2002; Webber and Lockwood 2001a, b; Webber et al. 2001). These authors concluded that the modulation in the outer heliosphere dominates the overall modulation at lower energies, even at solar minimum, and that there is a clear difference between the $A > 0$ and $A < 0$ magnetic polarity cycles for most of the heliosphere.

The heliosheath, from a modeling point of view, has also been recognized as a very important feature of the heliosphere that contributes significantly to the overall modulation of galactic CRs, especially for low energy galactic electrons (Ferreira and Potgieter 2002; Potgieter and Langner 2004; Ferreira et al. 2004; Caballero- Lopez et al. 2010; Nkosi et al. 2011; Ngobeni and Potgieter 2014; Manuel et al. 2015). This will be illustrated further in this chapter.

Both Voyager spacecraft provided fascinating low-energy electron intensity profiles while approaching the TS, and have continued to do so. When Voyager 1 crossed the HP it returned data from which two electron spectra, as very LIS, were later calculated (Stone et al. 2013) as discussed in Chapter 4. The heliopause spectrum (HPS), or very LIS, as discussed in that chapter, is utilised here to compute modulated electron spectra and intensity profiles in the heliosheath.

It has become clear that the role of the heliosheath is different for galactic cosmic rays (GCRs) than for the anomalous cosmic rays (ACRs). The TS did not have a significant effect on the ACRs so that the expected drastic changes in the ACRs intensity was not observed (Stone et al. 2005). It has turned out that they originate and get accelerated inside the heliosheath (e.g. Strauss et al. 2010) so that their intensity drops to very low values beyond the HP, whereas the GCRs intensities increase across the HP, significantly for lower energies (Webber et al. 2012; Stone et al. 2013) as will be shown below. For GCRs the sources are well outside the heliosphere, and as such the size (width) of the heliosheath contributes to their total modulated reduction towards the Sun.

In this chapter the focus is on the modulation of galactic electrons in the heliosheath, especially at low energies (~1 MeV to ~50 MeV). Modulated electron spectra and corresponding radial intensity profiles are computed. The modeling results are then compared to electron observations made by Voyager 1. But first some observations from Voyager 1 for ACRs, GCRs helium (He) and protons will be shown and briefly discussed, ending the section with observations for electrons as observed by the two Voyager spacecraft since 2007. It will also be shown what observationally happened to CRs of different species and energies, ahead of the HP, across and beyond it.

7.2 Cosmic ray observations at the TS and beyond

In this section observations from Voyager 1 for ACRs, GCRs protons and He are shown together with galactic electrons to illustrate how differently these particles get modulated in the heliosheath as compared to the inner heliosphere. A compilation of intensity-time profiles observed by Voyager 1 will be shown for the different CRs species to illustrate the regions of the heliosphere and especially how different the modulation is in the heliosheath.

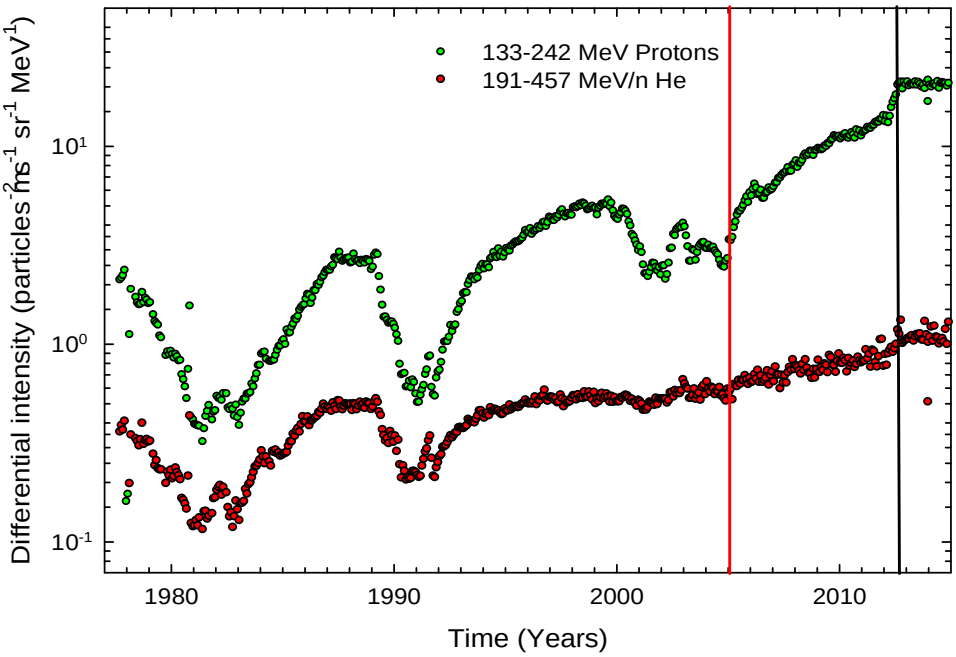

Figure 7.1: The observed intensity for GCRs protons (133-242 MeV) and He (191-457 MeV/n) as a function of time as observed by Voyager 1 since its launch until recently. This illustrates how these particles were modulated with the solar activity cycle until Voyager 1 reached the TS at 94 AU in December 2004 (red vertical line) and up to the HP at 121.7 AU (black vertical line) in August 2012. See http://voyager.gsfc.nasa.gov/heliopause/data.html/.

Figure 7.1 shows the observed GCRs protons (133-242 MeV) together with GCRs He (191-457 MeV/n) as observed by Voyager 1 since 1977 and until recently. For the protons, and to some extent for the higher rigidity He, the solar cycle dependence is evident, exhibiting the 11-year solar cycle until it disappeared around 2009, whereafter there was just a steady increase in the observed intensity. When Voyager 1 crossed the TS, the observed proton intensity showed a relatively fast but steady increase, then a small-step decrease over a short period of time, followed by a very steady increase for several years, until the HP position was reached. When Voyager 1 crossed the HP, a relatively large intensity increase was evident for the GCRs protons, after which the intensity remained essentially constant, assumingly already at the local interstellar values. For these protons, there was almost a factor of 2 increase compared to the factor ~10 from the TS to the HP crossing.

The He intensity shows smaller changes after the TS crossing with much smaller periodicity in the intensities so that the effect of crossing into the heliosheath is less spectacular for these

higher rigidity CRs. The observed intensity for the He also exhibits the same features mentioned above, but much less significantly.

Clearly, the heliosheath acts as a large modulation barrier for lower energy GCRs, and as the place of creation for the ACRs. The process is, however, highly dependent on energy and seems related to the solar cycle.

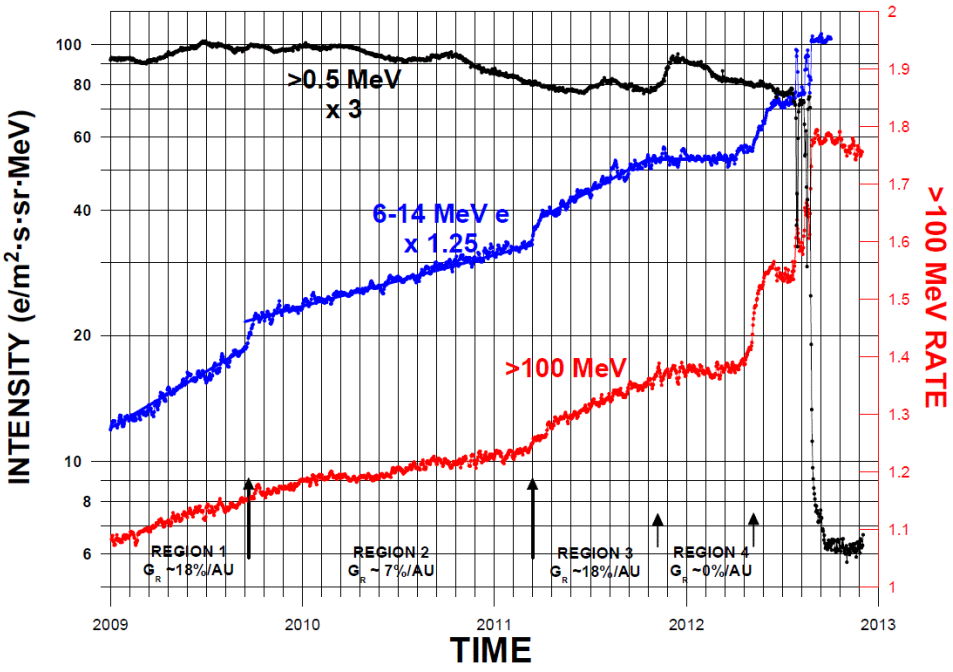

Figure 7.2: Five day running average intensities (x3) of ACRs dominated protons with kinetic energy $E > 0.5\,\mathrm{MeV}$, GCRs electron intensity (x1.25) for 6-14 MeV and the GCRs proton count rate for E > 100 MeV, from 2009 until the beginning of 2013, as observed by Voyager 1. Figure taken from Webber et al. (2012).

Figure 7.2 shows how differently ACRs dominated protons $(E > 0.5\ \mathrm{MeV})$ behaved over the period 2009 to 2013 in comparison with GCRs (6-14 MeV) electrons and protons (count rates with E > 100 MeV) as observed by Voyager 1 (Webber et al. 2012). The ACRs protons reached a maximum early in 2010, while the GCRs electrons and protons kept increasing. A drastic decrease occurred in the ACRs intensities at ~121.7 AU coinciding with the crossing of the HP. This drop in intensity was more than 90% which is well below the intensities that was observed at the TS and since its launch (Stone et al. 2013; Webber and McDonald 2013). This huge decrease occurred over a short period and was an indication that Voyager 1 crossed the HP. In contrast, both GCRs electrons and protons show large intensity increases, starting

mid-2012 but then even larger and quicker increases in August 2012; in total a factor of ~2 for electrons and ~40% for the protons. From this it can be deduced again that the HP region is more extended than previously thought, and acts by itself as a modulation barrier contributing to the total effect of the full inner heliosheath.

Figure 7.3 shows five-day running averages of the 6-14 MeV electrons together with GCRs protons with E > 200 MeV as measured by Voyager 1 from the time when the spacecraft crossed the TS in 2004 to the end of 2011. It should be noted that before the TS crossing between 1992 and 2001, the electron intensity was mainly dominated by background, and as such the intensity profile then exhibited almost constant intensities (not shown here; see Potgieter and Nndanganeni 2013a). The main feature is that the 6-14 MeV electron intensity and the E > 200 MeV protons had increased rapidly and irregularly beyond the TS in 2004, but after mid-2008 the increases were more smoothly, and as such the radial intensity gradient could be determined. Evident for the electrons, but not for the protons, is the relatively large temporal event in 2004, which could easily be associated with the TS and consequently be interpreted as the effect of the TS on these electrons (see also Prinsloo 2015). Soon after, beyond the TS as shown here, there was a large intensity increase for the both electrons and protons over almost a year. This was followed by a period of clear periodic modulation for both electrons and protons which disappeared late in 2008 to be followed by relatively smooth steady increases for longer periods for both, but with clearly defined changes in the associated intensity gradients. This occurred for electrons when Voyager 1 was already ~17 AU beyond the TS, which resulted in ~ 20% increase in intensities over a short period, accompanied by a sudden decrease in the radial gradient from ~19 AU/% to 8 %/AU (Webber et al. 2012). Another sudden increase was observed in 2011 when Voyager 1 was 22 AU away from the TS.

Figure 7.4 shows the mentioned changes in the radial intensity gradients for both electrons and protons. Between 2008.5 and 2009.7, the averaged radial gradient was determined by Webber et al. (2012) to be ~18.5 %.AU^{-1},which corresponds to an intensity increase of ~20% over a short period of time. Since the end of 2009, a smaller radial gradient (8 %.AU^{-1}) was observed until the beginning of 2012, when it increased again to 18 %.AU^{-1}. The smoother increases were also evident for the protons, but with a much smaller radial gradient, between 2008.5 and 20009.7, it was ~2.7 %.AU^{-1} which decreased to 0.97 %.AU^{-1} after 2009.7, increasing again to ~3 %.AU^{-1} after 2011, which corresponds to the sudden intensity increase of ~5 %. These changes indicate that Voyager 1 went through regions with different

modulation/propagation conditions. See also Opher et al. (2015) for a discussion of these changes.

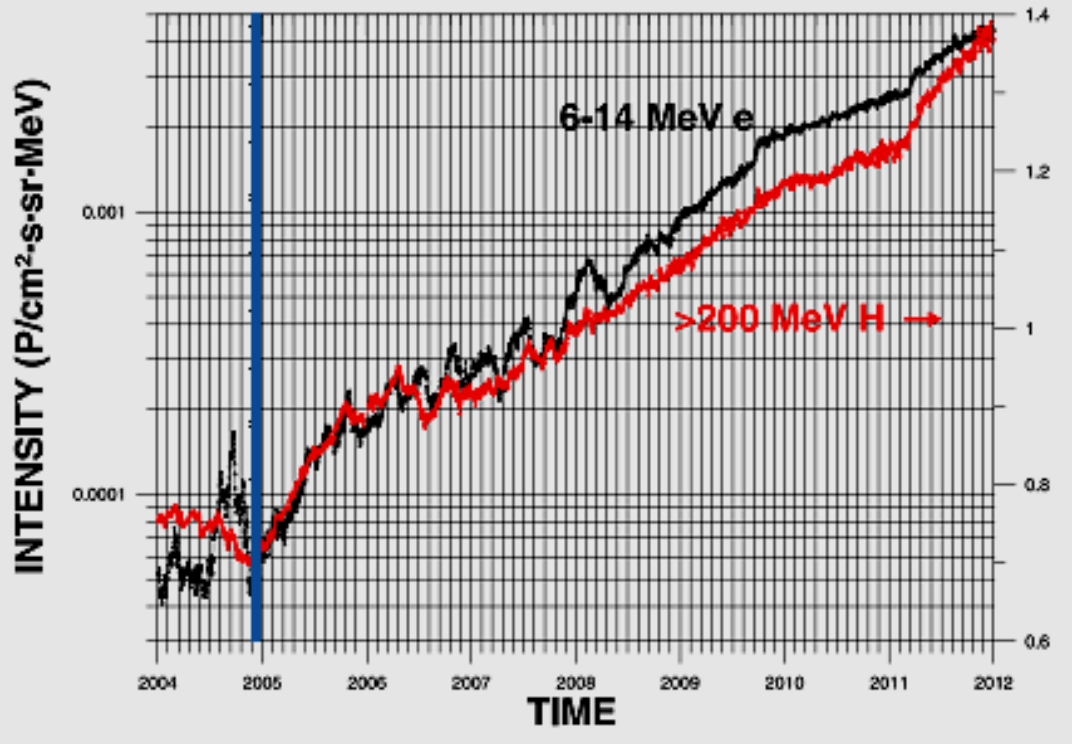

Figure 7.3: The running averages of daily intensities of 6-14 MeV electrons (black curve) and $E >$ 200 MeV protons (red curve) as observed by Voyager 1 since 2004 until the end of 2011. Note that there are some similarities in the temporal variations despite the much higher energy of the protons. Voyager 1 crossed the TS at 94 (blue solid line) in December 2004 (Stone et al. 2005). Figure taken from Webber et al. (2012).

In Figure 7.5 the observed 5-12 MeV electron intensity is shown from the beginning of 2007 to 2014 for Voyager 2, and to mid-2015 for Voyager 1. Note that the time profile of Voyager 1 is shifted by 2.7 years to make this direct comparison possible (Webber and Intriligator 2014). This is shown to emphasize the difference in the observed electron intensities for the two Voyager spacecraft. Evidently, there are clear time variations (periodicities) in the observed intensities, but relatively large solar cycle related changes only for the Voyager 2 observations. This means that Voyager 2, being ~20 AU closer to the Sun than Voyager 1, was still subjected to changes caused by solar activity while Voyager 1 was too far away and too deep inside the inner heliosheath (see also the modeling done by Manuel et al. 2014). The Voyager 2 intensities also show a large temporal event in mid-2007, correlating with the time when this spacecraft crossed the TS. Evident from this figure is that the electron intensity, as

observed by Voyager 1, increased significantly from the time of the TS crossing up to the HP position resulting in the total modulation between the TS and HP, to be more than a factor of 100 at these energies.

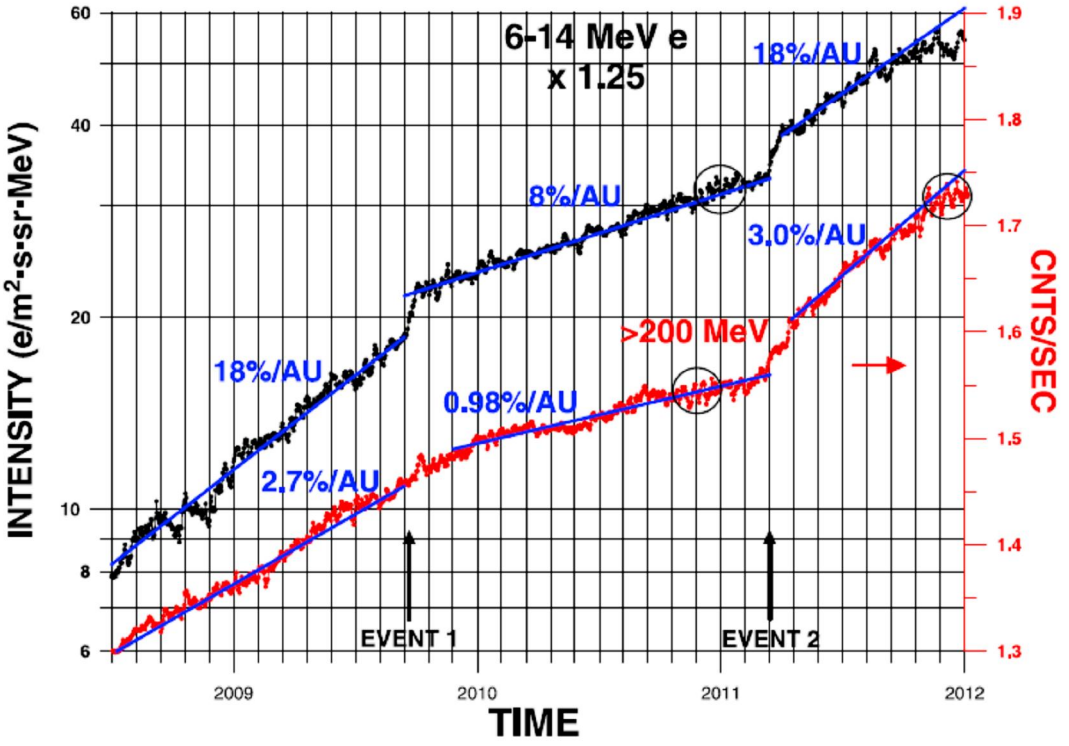

Figure 7.4: The five-day running averages of the 6-14 MeV electrons (black curve) and $E > 200$ MeV protons intensities (red curve) measured at Voyager 1 from 2008.5 to the end of 2011. Note the changes in the corresponding radial gradients as indicated. Figure taken from Webber et al. (2012).

After the HP crossing, the intensity reached a maximum value and has been steady since. The Voyager 2 picture is clearly different.

In this thesis, the interest is on the global features of electron modulation in the outer heliosphere, in particular the inner heliosheath related to what had been observed by Voyager 1. Since Voyager 2 is experiencing large time variations and is still not at the HP, these observations, although very interesting, are not used for comparative studies in this thesis. The model being utilised here is a steady state model which will not be able to reproduce all the aspects of the observed time dependence. Turning to Voyager 1 observations, there are also short variations and periodicities in the data but not as large and as many as observed at

Voyager 2, which makes the Voyager 1 data suited for a global study, focussing on the total increase beyond the TS, up to the HS.

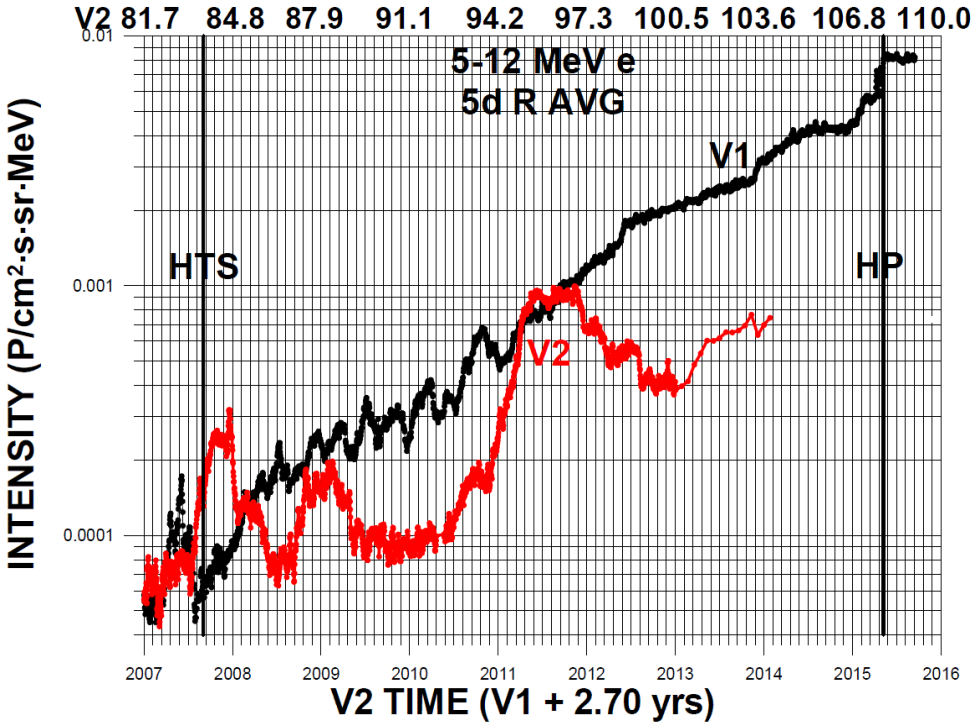

Figure 7.5: The five-day running averages of 5-12 MeV electron intensity measured at Voyager 1 (V1, black curve) and Voyager 2 (V2, red curve) from 2007 to mid-2015. The TS and HP crossings are indicated by vertical lines. The radial position of Voyager 2 is indicted at the top. Figure taken from Webber and Intriligator (2014).

The overall conclusion that can be made based on Figure 7.1 to Figure 7.5 is that the heliosheath acts as a modulation barrier for GCRs, especially so for lower energies. The question for global modeling is what is responsible for this.

7.3 Previous modeling and predictions for electrons in the heliosheath

From a modeling point of view, it worth noticing that the mentioned global trends in the behaviour of electrons observed at Voyager 1 were predicted by Potgieter and Ferreira (2002) and Ferreira et al. (2004). They illustrated that, besides the physical extent of the inner heliosheath and the different modulation conditions that may persist in this region, the value

of the galactic electron spectrum (or LIS) at these low energies plays a significant role in how large the radial gradient can be inside the heliosheath. At that time, they had to study several scenarios with different positions assumed for the TS and HP, and also for the values of the LIS at these low energies. The three modulation issues then were: What is the LIS at $E < 1$ GeV, where is the TS located and where is the HP located in the nose direction of the heliosphere. These issues have all now been settled to a large extent, although we still await what Voyager 2 may find.

Figure 7.6 shows examples of modeling results as computed by Potgieter and Ferreira (2002) and compared to 16 MeV electron observations from Pioneer 10, which stopped at ~70 AU. The top panel illustrates the effect of different positions of the TS (r_s) while keeping the HP position (r_b) fixed, whereas the bottom panel illustrates the effect of changing the HP position while keeping the TS position fixed. It follows that the effects of changing r_s on the electron radial profile are quite prominent for all three scenarios. The effect on the radial gradients is more pronounced with $r_s = 80$ AU than for the other two scenarios. In all these cases the modulation in the inner heliosheath was predicted to be large. These results show that the effects of the TS position on the radial profile become smaller, close to the TS, if the width of the inner heliosheath is decreased by moving the TS position but keeping the position of the HP unchanged. Overall, it was found that increasing the width of the heliosheath resulted in an increase in the modulation that occurs in the inner heliosheath, with the effects of the TS more pronounced the wider the heliosheath is made.

Figure 7.7 shows the modulation effects on the radial intensity profile of the 16 MeV electrons of using three different LIS values with the positions of the TS and the HP fixed at $r_s = 90$ AU and $r_b = 120$ AU, respectively. It follows that the higher the LIS value is at these low energies, the larger the modulation becomes and the more prominent the effect of the TS is as follows from the peaks in the intensity at the TS. Evidently, they illustrated that the assumed value of the LIS was a very important issue. Furthermore, in order to reduce the LIS intensity to the observations, the diffusion coefficients used in their model had to be changed significantly. With the newest observations this aspect can also be improved.

Potgieter and Langner (2004) also studied the effects of the heliosheath and the TS on cosmic ray electrons and positrons. They concluded that the modulation in the heliosheath is strongly dependent on these CRs species and is enhanced by the inclusion of the TS. It was also

possible to determine the total amount of modulation that occurs in the heliosheath and also between 1 AU (Earth) and the HP.

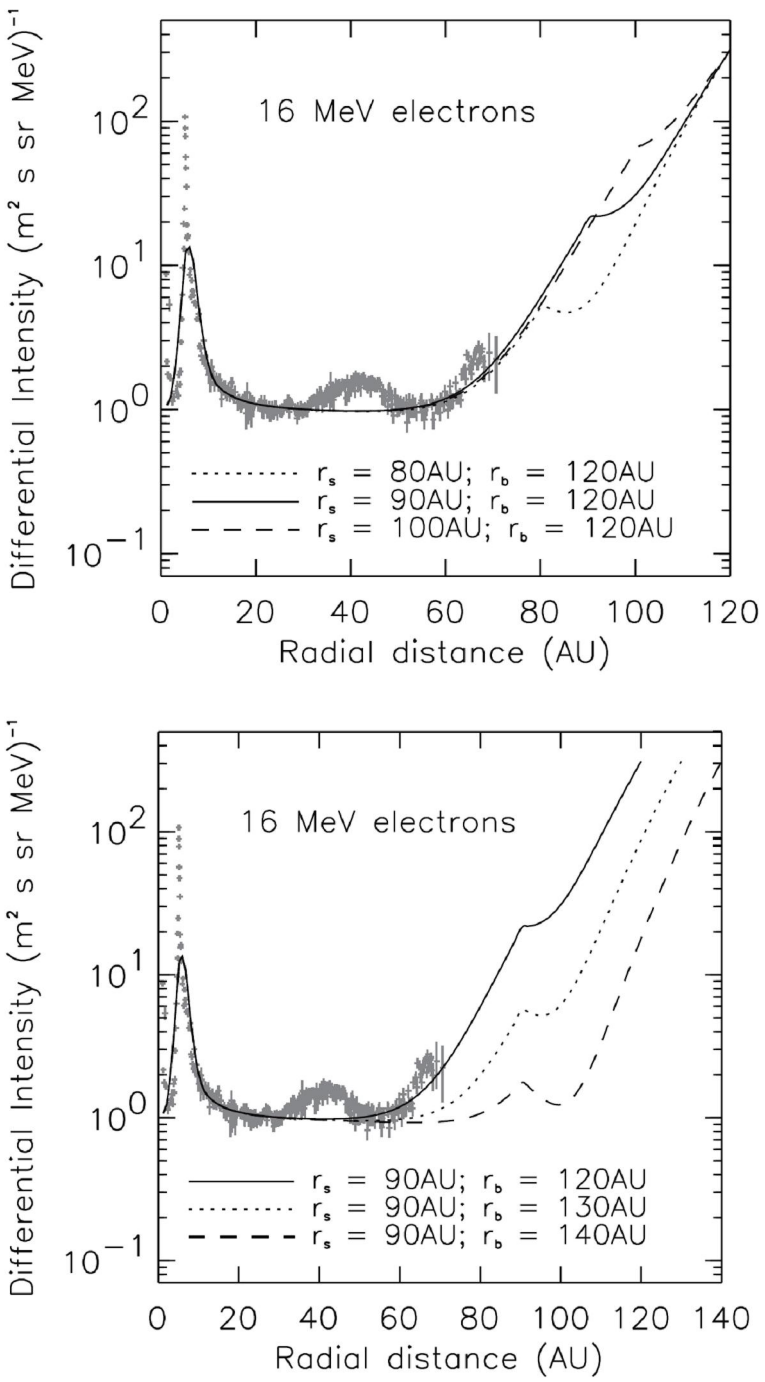

Figure 7.6: The computed intensity radial profile for 16 MeV electrons. The top panel shows the profiles with a varying TS position, from 80 AU to 100 AU, with the HP fixed at 120 AU, whereas the bottom panel is for a fixed TS position, 90 AU, while varying the HP position from 120 AU to 140 AU. Electron observations at ~16 MeV from Pioneer 10 are shown for comparison. Figures taken from Potgieter and Ferreira (2002).

An illustrative example of their work is given in Figure 7.8, emphasizing the level of modulation occurring in the heliosheath as the ratio of the LIS intensity to the computed intensity at 90 AU, $j_{LIS} / j_{90\,\mathrm{AU}}$, in comparison with what happens between the TS and Earth, $j_{90\,\mathrm{AU}} / j_{1\mathrm{AU}}$, and in total between the HP and the Earth $\left(j_{\mathrm{LIS}} / j_{1\mathrm{AU}}\right)$. At low energies the modulation from the TS, at 90 AU, to 1 AU is comparable to the modulation that occurs between the TS and the LIS, with the HP at 120 AU at low energies. The ratio is smallest at 500 MeV for the computation done between the LIS and the spectra at 90 AU, emphasizing the point that the amount of modulation is getting smaller, the higher the energy is. In this case also because of the re-acceleration of these galactic electrons at the TS. For this modeling approach, the ratio computed as $j_{90\,\mathrm{AU}} / j_{1\mathrm{AU}}$ exceeds the ratio $j_{\mathrm{LIS}} / j_{1\mathrm{AU}}$ with $E \geq 200$ MeV because of the TS acceleration. It was found that this effect is not equally pronounced for all species, and that it depends on the drift direction.

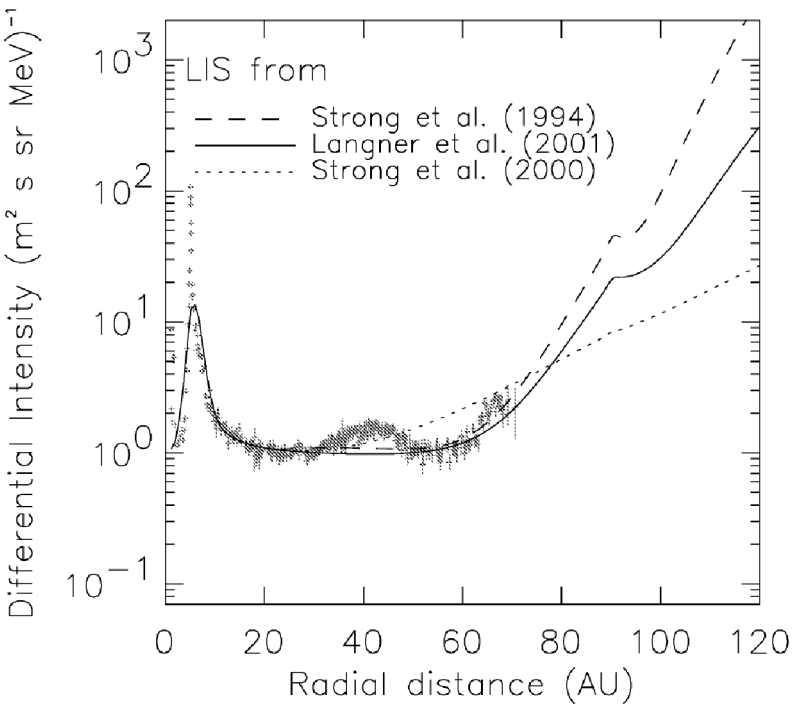

Figure 7.7: The computed intensity profiles for 16 MeV electrons as a function of radial distance for three different LIS values, with $r_s = 90$ AU and $r_b = 120$ AU, this keeping the width of the inner heliosheath as fixed. The dashed line is the scenario for the high LIS from Strong et al (1994), the dotted line for the lowest LIS from Strong et al. (2000) and the solid line for the LIS from Langner et al. (2001). Figure taken from Ferreira et al. (2001).

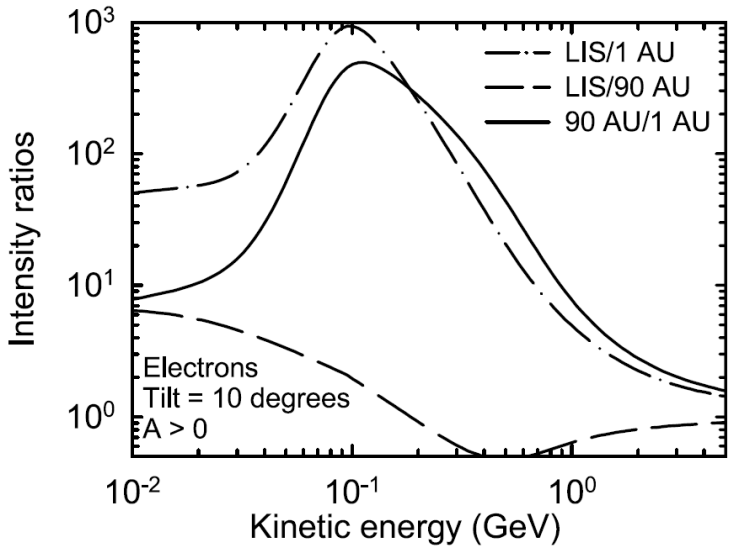

Figure 7.8: The computed intensity ratios $j_{LIS} / j_{1AU,}$ j_{LIS} / j_{90AU} and j_{90AU} / j_{1AU} and j_{90AU} / j_{1AU} for galactic electrons as a function of kinetic energy in the equatorial plane with $\alpha = 10^{\circ}$, for an $A > 0$ polarity cycle. The LIS is specified at 120 AU and the TS is at 90 AU. For this modeling the galactic electrons were re-accelerated at the TS. Figure taken from Potgieter and Langner (2004).

Nkosi et al. (2011) studied the modulation of galactic electrons in the heliosheath with the emphasis on the role of the perpendicular diffusion coefficient as the main cause of the extra-ordinarily large increase in the observed intensities of these low-energy electrons in the heliosheath. They computed the radial intensity profile as well as the modulation effects of varying the extent of the heliosheath by changing the location of the TS, HP and the value of the LIS. At the time when this work was done, Voyager 1 was already beyond ~112 AU in the heliosheath. However, there was still a significant uncertainty about the actual spectral shape (energy dependence) of the LIS (or HPS) of these low-energy galactic electrons and about the actual position of the HP. Figure 7.9 shows their computed radial intensity profiles of low energy electrons in the heliosheath. These computations are done with respect to the highest Webber and Higbie (2008) LIS (top panel), together with Langner et al. (2001) LIS (bottom panel) respectively. The main aim of this approach was to show the global modulation effects of the thickness of the heliosheath and the effects of a high and a lower LIS on the modulation in the heliosheath. The position of the TS was changed from 84 AU to 100 AU, and the HP was changed from 120 AU and 130 AU respectively. They found that changes in the radial intensity profiles are influenced by the position of the TS, and

subsequently by how wide the inner heliosheath is made. This is then influenced by what the value of the LIS is at these energies. This means that the assumed diffusion coefficients play a crucial role in changing this profile inside the heliosheath.

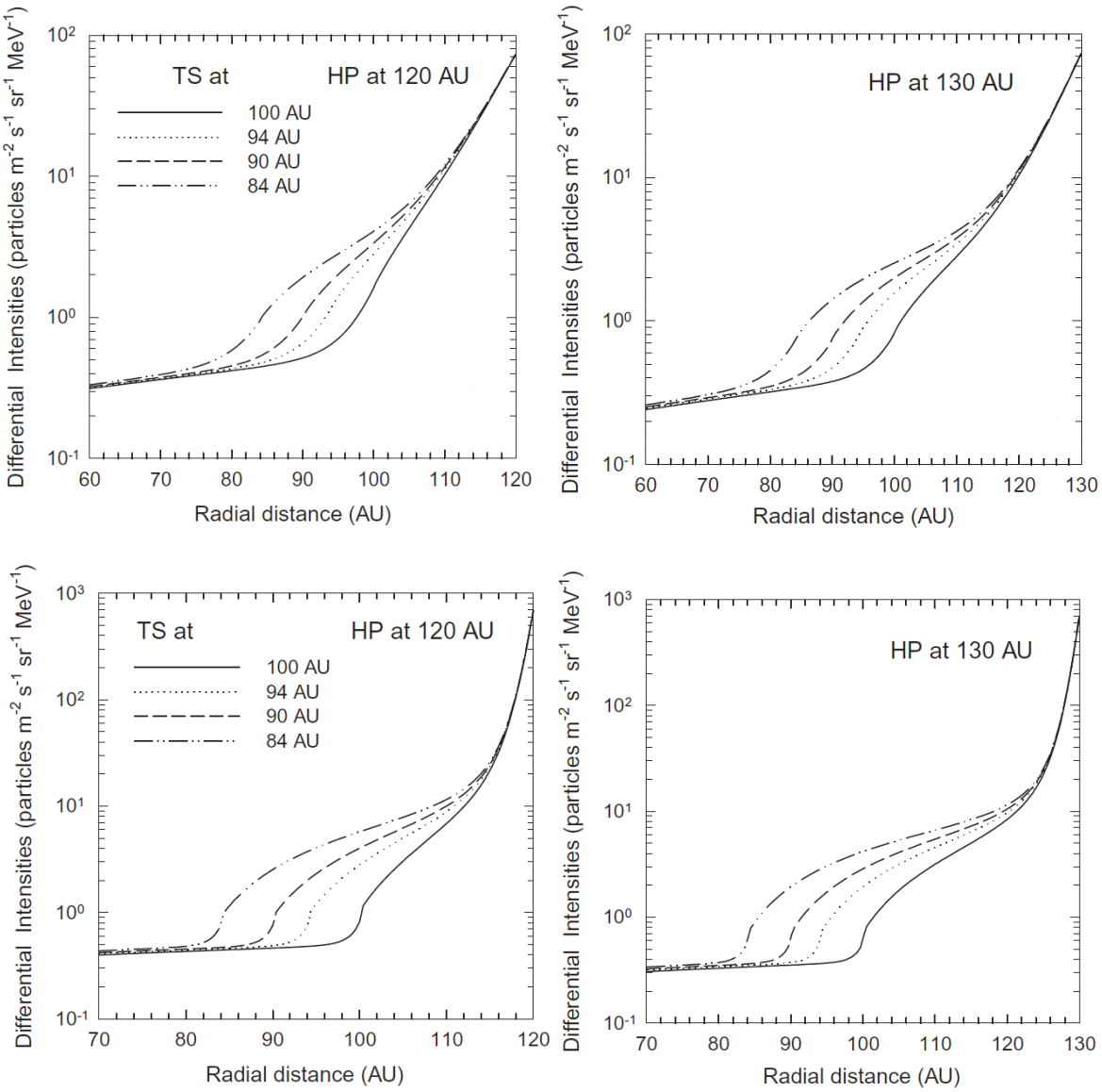

Figure 7.9: Computed 10 MeV galactic electron intensities as a function of radial distance at a polar angle of $\theta = 55^{\circ}$, approximating the Voyager 1 heliolatitude. Computations are shown for four TS positions, varying from 84 AU to 100 AU, with the HP fixed at 120 AU and 130 AU, respectively. The top panel is computed with respect to the highest LIS from Webber and Higbie (2008) and the bottom panel with respect to the LIS by Langner et al. (2001). Figure taken from Nkosi et al. (2011).

They also came to the conclusion that indeed the heliosheath acts as a very effective modulation barrier for these low energy electrons, causing intensity radial gradients of up to 20% AU^{-1}. This will be further investigated below by making use of the new insight concerning the location of the HP and the LIS (or HPS).

The subsequent section is about the modeling work done for this study by utilizing the HPS which was computed and discussed in detail in Chapter 4, with the focus on the modulation that occurs in the heliosheath.

7.4 New modeling results

7.4.1 Spectra and the total modulation in the heliosphere

Shown in Figure 7.10, is an illustrative example of computed modulated spectra with $\theta = 60^{\circ}$ and at 90 AU, 110 AU and 119 AU, resulting from the two choices for the HPS, taken as the very LIS and described in Chapter 4: $\mathrm{HPS}\left(E^{-1.55}\right)$ and $\mathrm{HPS}\left(E^{-1.35}\right)$, respectively. The spectra are computed for an $A>0$ magnetic polarity epoch with a tilt angle $\alpha = 5^{\circ}$ assuming full drifts. As mentioned before, the interesting fact about studying low energy electrons is that they respond directly to the energy dependence of the diffusion coefficients at low energies as opposed to protons which experience large adiabatic energy losses (Potgieter 1996, 2000). It is therefore expected that the slope of the HPS will be maintained at low energies, even at the Earth, as long as the diffusion coefficients remain independent of energy at these energies, as assumed in Chapter 3, section 3.3. It follows from the figure that the modulated spectra indeed keep the same slopes as that of the two HPS, respectively. Note that for E > ~700 MeV the two HPS are the same because they are normalised to the PAMELA data, and between ~5 MeV and ~20 MeV the two are again the same because in this range they are normalised to the Voyager 1 observations. Qualitatively, the spectra computed with the above mentioned two HPS show the same modulation features, but quantitatively the results are different.

Figure 7.11 shows computed electron spectra at 90 AU, 110 AU, and 119 AU, with respect to the $\mathrm{HPS}\left(E^{-1.55}\right)$ and $\mathrm{HPS}\left(E^{-1.35}\right)$ specified at 122 AU, and with $\theta = 60^{\circ}$, now for both $A>0$ and $A<0$ magnetic polarity epochs. This figure illustrates the solar cycle related changes caused by drifts (see also Chapter 6). The top panel shows the computations with

respect to HPS$\left(E^{-1.35}\right)$ and the bottom panel with respect to HPS$\left(E^{-1.55}\right)$. Evidently, the drifts effects (considered as the differences between the two polarity cycles) subside with increasing radial distance with the maximum effect shifting to higher energies with increasing distance. At 90 AU the drifts effects are still quite prominent between ~40 MeV and ~300 MeV. At larger distances the drift effects are smaller and more prominent between ~200 MeV and ~2 GeV. The overall picture remains the same for both HPS scenarios with some quantitative differences.

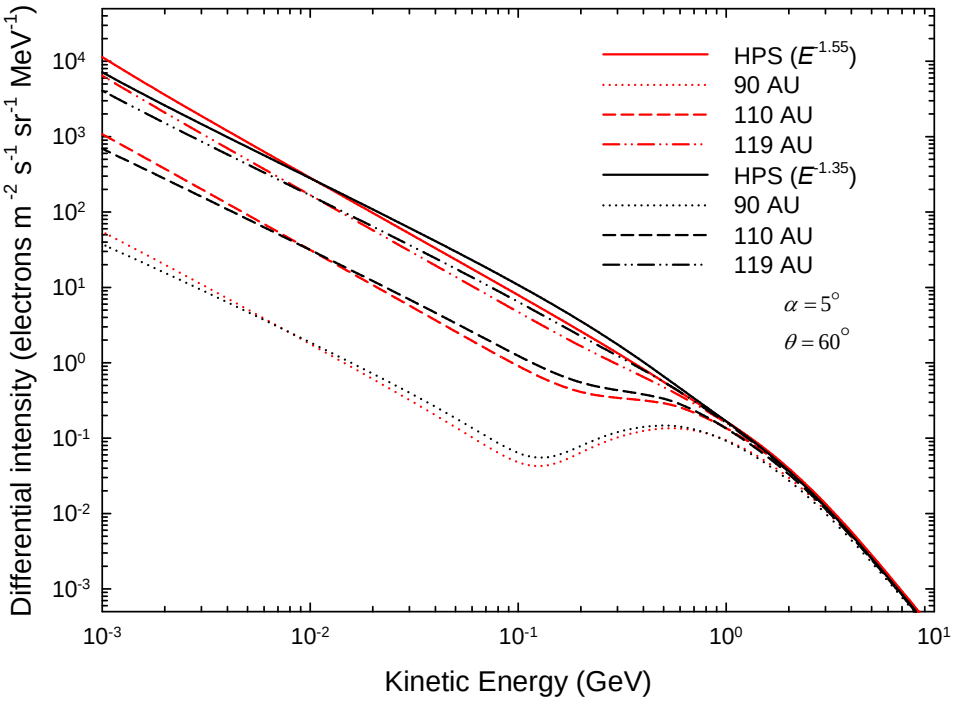

Figure 7.10: Computed electron spectra at 90 AU, 110 AU, and 119 AU (which is deep in the heliosheath) with $\theta = 60^{\circ}$ approximating the Voyager 1 trajectory. These spectra are computed with respect to the two choices for the HPS (as LIS): (1) HPS$\left(E^{-1.55}\right)$ and (2) HPS$\left(E^{-1.35}\right)$, for the $A < 0$ magnetic polarity cycle, with the TS at 94 AU and the HP at 122 AU.

Furthermore, drift effects still can occur inside the heliosheath. Ngobeni (2015) studied galactic Carbon modulation with his numerical model, and came to the conclusion that drifts effects are over-estimated in the outer heliosphere when using the weak scattering approach as is done here. However, this is not pursued further in this thesis.

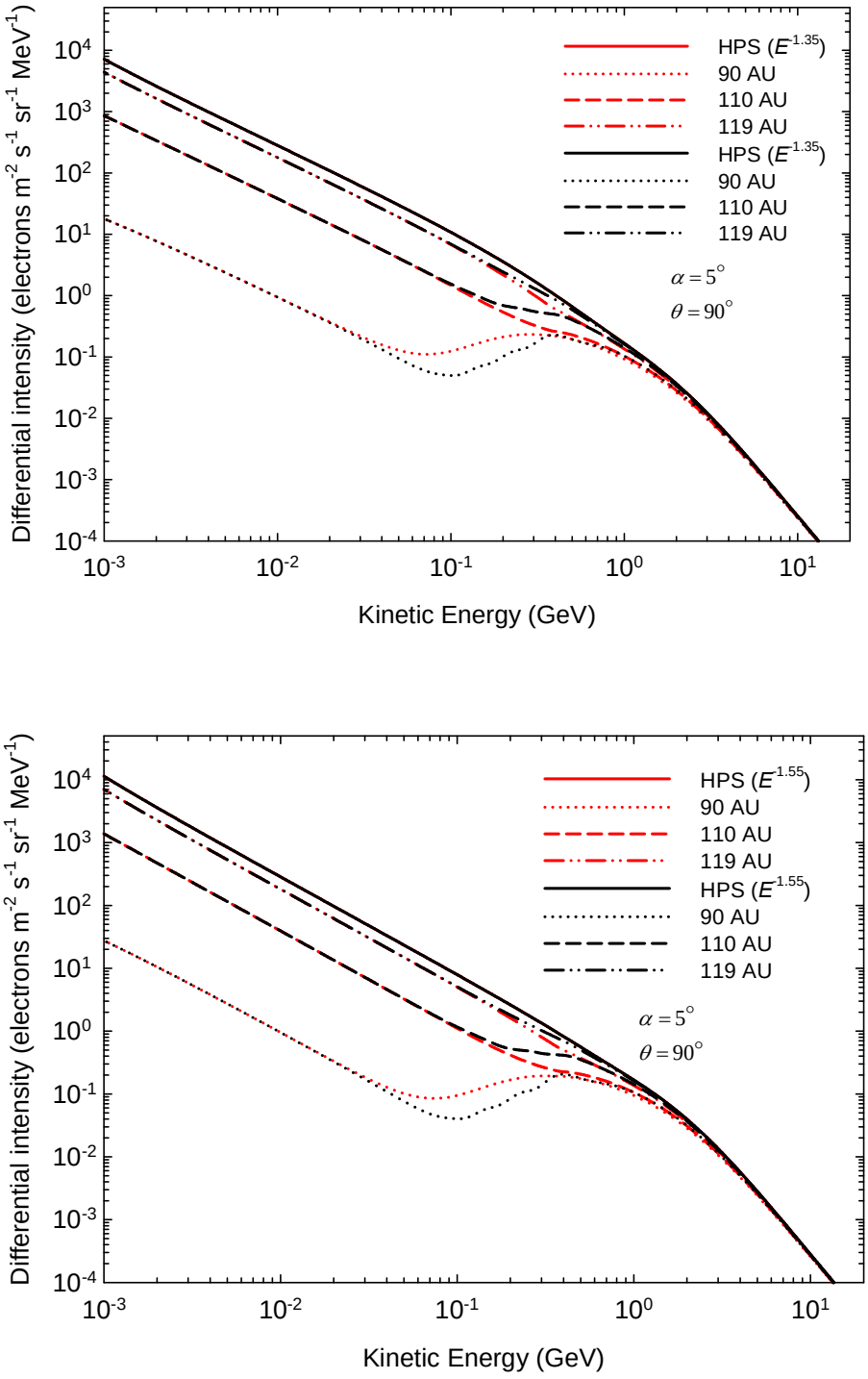

Figure 7.11: Computed electron spectra with $\theta = 60^\circ$, at 90 AU, 110 AU, 119 AU and at 122 AU, where the HPS is specified. This is done for solar minimum conditions with $\alpha = 5^\circ$ and for the two magnetic polarity epochs, $A > 0$ (black curves) and $A < 0$ (red curves) to illustrate the solar cycle related changes caused by drifts. The top panel shows the results as computed with respect to the $\mathrm{HPS}\left(E^{-1.35}\right)$ and in the bottom panel with respect to the $\mathrm{HPS}\left(E^{-1.55}\right)$.

Figure 7.12 illustrates the modulation in the heliosphere in terms of intensity ratios between two HPS (or LIS) scenarios and the intensity at 119 AU, 110 AU, 90 AU and 1 AU, respectively for both HMF polarity epochs. The TS is specified at 94 AU and the HP is at 122 AU. This is done for solar minimum conditions with $\alpha = 5^{\circ}$ and at $\theta = 60^{\circ}$. The top panel, is with respect to $\mathrm{HPS}\left(E^{-1.55}\right)$ with the rigidity dependence of the diffusion coefficients as used above, is independent of energy at lower energies. This ratio can also be interpreted as a modulation factor, the total modulation between the HP and other distances closer to the Sun. It follows that: (1) The ratio is constant at lower energies at all radial distances, indicative of the energy independence of the diffusion coefficients, thus retaining the spectral shape of the HPS. It is also happening because electrons experience less adiabatic energy losses, and as such their modulation is diffusion dominated at E < 100 MeV. (2) Overall, the ratio at all distances decreases with increasing energy as it should; less modulation occurs the higher the energy becomes. At $E > 30\,\mathrm{GeV}$, the modulation factor becomes unity as modulation subsides. (3) As expected, the maximum amount of modulation occurs between the HP and the Earth, a factor of ~1200 at the lowest energies. (4) In this case, there is also a significant amount of modulation between the HPS and 90 AU at these low energies (almost a factor of 200) which subsides significantly with larger radial distances. (5) The drift effects as discussed above are again quite evident.

In the bottom panel of Figure 7.12, the computed ratios are based on the spectra shown in Figure 4.5 to illustrate the effects of using diffusion coefficients that are increasing as a function of decreasing energy based on the LIS approach of Langner et al. (2001), and the diffusion coefficient from Ndiitwani (2005) and the diffusion coefficients from Potgieter and Langner (2004). The consequence is that the total modulation at E < 100 MeV is much less compared to what was shown in the top panel. The drift effects in this case are somewhat diminished, especially in the outer heliosphere. This happens because the less modulation causes smaller intensity gradients which inherently diminish the drift effects.

Comparing these results to those shown in Figure 7.8, it follows that qualitatively the global picture is similar. The quantitative differences are mainly caused by the fact that Langner et al. (2001) also utilised diffusive shock acceleration at the TS in a 2D model, and the diffusion coefficients from Burger et al. (2000).

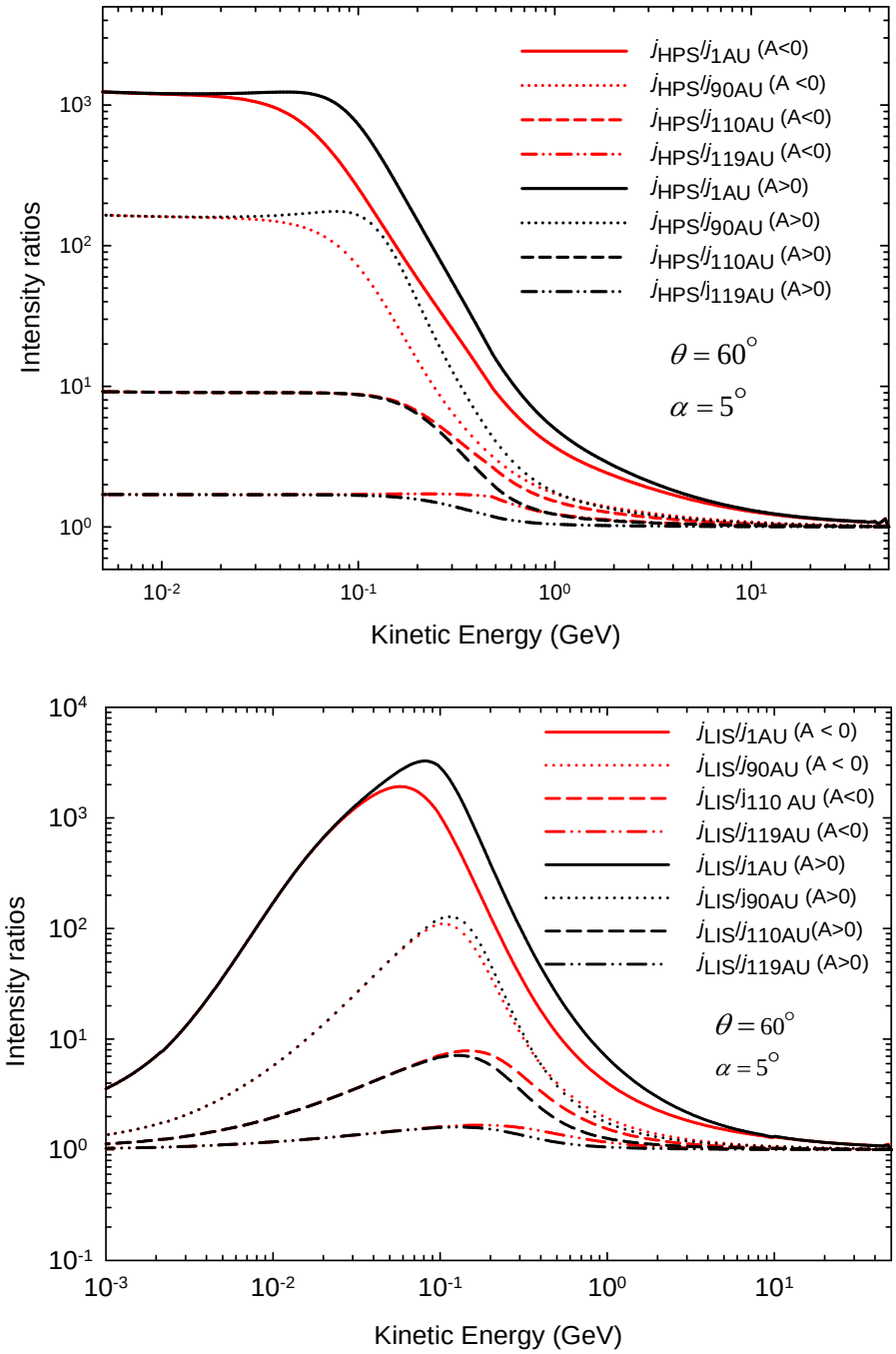

Figure 7.12: Computed intensity ratios for different radial distances as a function of kinetic energy with $\alpha = 5^{\circ}$ for both HMF polarity epochs and at $\theta = 60^{\circ}$. Ratios are computed with respect to two HPS scenarios, in the top panel for $\mathrm{HPS}\left(E^{-1.55}\right)$ and in the bottom panel is the ratio computed based on spectra shown in Figure 4.5 which is computed with respect to the LIS from Langner et al. (2001) and a completely different energy dependence of the diffusion coefficients, as used given by Ndiitwani (2005). In both panels the ratios are between the relevant HPS value and the intensity at different radial distances indicated as $j_{\mathrm{HPS}} / j_{1\mathrm{AU}}$, $j_{\mathrm{HPS}} / j_{90\mathrm{AU}}$, $j_{\mathrm{HPS}} / j_{110\mathrm{AU}}$ and $j_{\mathrm{HPS}} / j_{119\mathrm{AU}}$ and $j_{\mathrm{LIS}} / j_{1\mathrm{AU}}$, $j_{\mathrm{LIS}} / j_{90\mathrm{AU}}$, $j_{\mathrm{LIS}} / j_{110\mathrm{AU}}$, and $j_{\mathrm{LIS}} / j_{119\mathrm{AU}}$ respectively. The black curves are for $A > 0$ polarity cycles and the red curves for $A < 0$.

7.4.2 Modulation effects of varying the extent of the heliosheath

In this section the effects of varying the extent of the heliosheath by changing the location of the TS, the HP and the value of the HPS are illustrated. It follows on the work that was done by Nkosi et al. (2011), but with the difference that the HPS is based on the latest Voyager 1 observations (Stone et al. 2013) and the fact that the position of the HP has been established at ~122 AU in the Voyager 1 direction. The HPS used are those computed and discussed in Chapter 4, section 4.5. The other difference is in the modulation parameters assumed for this computation, which are based on the diffusion coefficients similar to those used by Potgieter and Nndanganeni (2013a) but with small adjustments in order to obtain improved compatibility between the model and observations; see Eq. (3.44 to 3.47).

Figure 7.13 shows the effects of changing the TS position from $r_s = 80$ AU to $r_s = 100$ AU on the electron spectra computed at 90 AU and 110 AU, for the two HPS scenarios, HPS$\left(E^{-1.55}\right)$ and HPS$\left(E^{-1.35}\right)$. The HPS is specified at 122 AU and the computations are done with $\theta = 60^{\circ}$ and $\alpha = 5^{\circ}$ for an $A > 0$ magnetic polarity epoch.

The top panel shows the modulated spectra at 90 AU and 110 AU, computed with respect to the HPS$\left(E^{-1.55}\right)$. At 90 AU, the intensity decreases by a factor of ~30 when $r_s = 100$ AU is changed to $r_s = 80$ AU, with the effect much smaller at 110 AU.

The bottom panel shows the modulated spectra at the same radial distances as mentioned above, but with HPS$\left(E^{-1.35}\right)$. Again the results are qualitatively different with accountable quantitative differences. As the TS position increases (less wide heliosheath), the intensity increases at a given radial distance with the effects dissipating at radial distances close to the HPS. Computations were also done for $r_b = 130$ AU, but are not shown here since no additional insight was gained. For the same reason the computations were not repeated for an $A < 0$ polarity cycle.

Evidently, by reducing the width of the heliosheath, the amount of modulation in the outer heliosphere decreases significantly with little or no modulation close to the HP in contrast to what Voyager 1 observed. The relatively large and sharp increases measured for galactic electrons across the HP region clearly present an additional effect to be taken into account, implying that apart from the heliosheath as effective modulation barrier, the HP region also

serves as a moderate modulation barrier. This is an aspect that can be incorporated in the model for future studies.

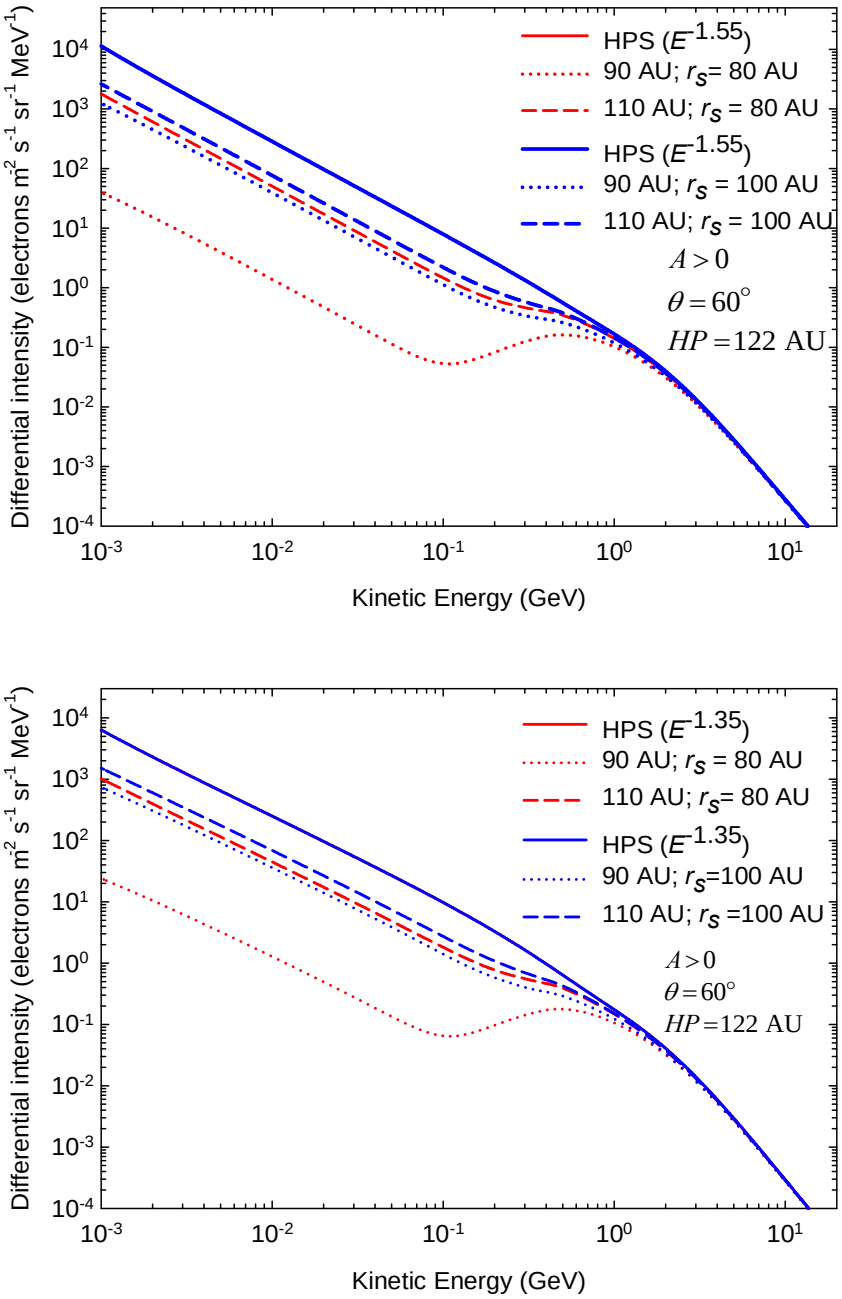

Figure 7.13: Modulated spectra for an $A>0$ polarity cycle for galactic electrons computed at 90 AU and 110 AU in the heliosheath with $\theta=60^\circ$ and $\alpha=5^\circ$, for two different r_s positions, changing it from $r_s=80$ AU (red lines) to $r_s=100$ AU (blue lines) but with the HP position fixed at r_b= 122 AU. For the top panel $\mathrm{HPS}\left(E^{-1.55}\right)$ is used and for the bottom panel $\mathrm{HPS}\left(E^{-1.35}\right)$.

7.5 Radial dependence of 12 MeV electron intensities

Figure 7.14 shows the computed differential intensities for 12 MeV electrons, which are shown as a function of radial distance between 70 AU and 122 AU, again with $\theta = 60^{\circ}$. This illustrates the effect on the radial intensity profile of moving the position of the TS from $r_s = 80$ AU to $r_s = 100$ AU while keeping the HP position fixed at $r_b = 122$ AU. This is done for the two HPS scenarios; the blue curves show the profile computed with HPS$\left(E^{-1.35}\right)$ and the red curves with HPS$\left(E^{-1.55}\right)$.

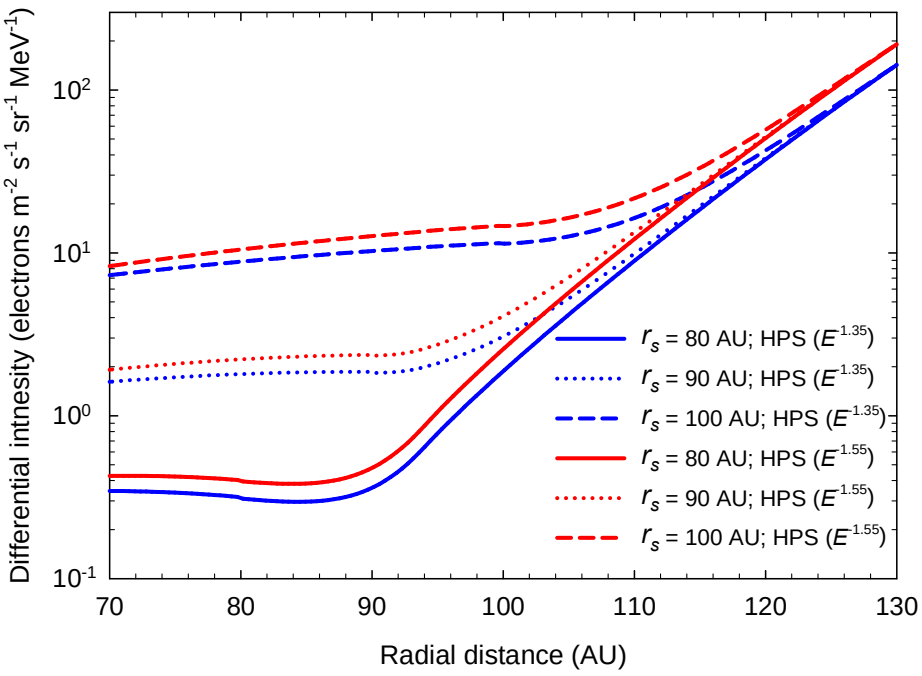

Figure 7.14: Computed 12 MeV galactic electron intensity as a function of radial distance again with $\theta = 60^{\circ}$. The computations are shown for three TS positions, varying from $r_s = 80$ AU to $r_s = 100$ AU with the HP fixed at $r_b = 122$ AU **,** where the two HPS are specified; red curves are for HPS$\left(E^{-1.55}\right)$, blue curves for HPS$\left(E^{-1.35}\right)$.

Qualitatively, the results look similar for the two HPS scenarios, with the only difference being in the level of the intensities. Changing the TS position, so that the heliosheath is

getting wider, causes the intensity profiles between 70 AU and r_s to become somewhat flatter. The difference amongst the three scenarios becomes progressively less with increasing radial distance, to be negligible once $r > \sim 110$ AU. These results indicate that, closer to the HP the effect on electron modulation of the position of the TS becomes insignificant.

Comprehensively, these results for galactic electrons indicate that when the HP is ~10 AU away from an observer, the position of the TS becomes irrelevant. Increasing the HPS makes the heliosheath effects on the radial profile for these 12 MeV electrons to be more noticeable.

7.6 Comparison with Voyager 1 electron observations

Figure 7.15 shows the computed galactic electron spectra computed in the outer heliosphere at 90 AU, 110 AU and 119 AU with respect to the two HPS scenarios, $\mathrm{HPS}\left(E^{-1.55}\right)$ and $\mathrm{HPS}\left(E^{-1.35}\right)$, respectively specified at the HP with $r_b = 122$ AU. The computed spectra are compared to the six sets of Voyager 1 observations at corresponding radial distances with the time of observations as indicated in the legend (V1 2010; Webber 2014, private communication; Caballero et al. 2010; then V1 2011/274, V1 2012/121, V1 2012/303 and V1 2012/366, respectively, from Stone et al. 2013). Clearly, the model reproduces the Voyager 1 observed spectra at 110 AU, 119 AU and 122 AU for the shown energy range in detail.

Qualitatively, both HPS give good compatibility with the observations and as such there is no compelling reason why one should be selected above the other, although the scenario $\mathrm{HPS}\left(E^{-1.55}\right)$ is subjectively preferred as discussed in Chapter 4. See also Bisschoff and Potgieter (2014).

Since the beginning of this study, the 6-14 MeV Voyager 1 observations were the only energy channel made available (Webber 2010-2013, private communication) and have been used as a guideline in verifying the modeling results. In late 2014, new 5-12 MeV electron observations were made available (Webber 2014, private communications) based on a different technique used in the data analysis that modified the electron observations as mentioned by Stone et al. (2013). Unfortunately, some normalization issues remain so that the latter set of observations has not been used for this study.

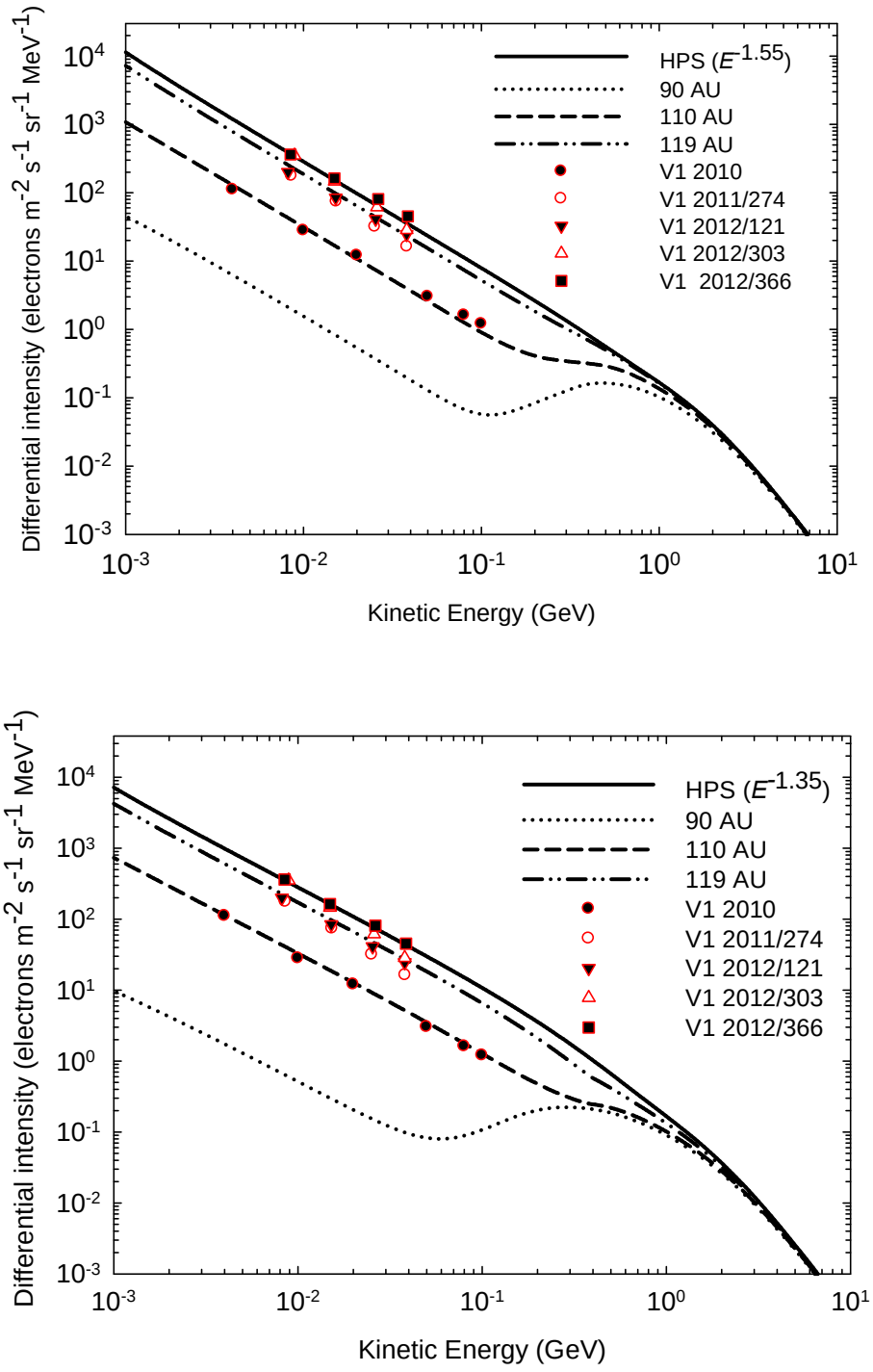

Figure 7.15: Computed electron spectra at 90 AU, 110 AU and 119 AU, compared with Voyager 1 (V1) observations at 112 AU (Webber 2010, private communication), 119 AU and 122 AU (Stone et al. 2013) respectively, with the time of observations as indicated. These spectra are computed with $\theta = 60^{\circ}$, approximating the Voyager 1 trajectory, with respect to the two HPS scenarios: $\mathrm{HPS}\left(E^{-1.55}\right)$ in the top panel and $\mathrm{HPS}\left(E^{-1.35}\right)$ in the bottom panel. The HPS are specified at the HP with $r_b = 122$ AU.

Figure 7.16 shows the computed radial profile between 70 AU and 122 AU of the 12 MeV electron intensity compared to the observed 6-14 MeV from Voyager 1. The focus here is on the global trend that is depicted in the increasing intensity, which is extraordinary. The model can indeed produce a snap-shot of this global modulation picture. The short-term features seem moderate compared to the total increase, although on shorter time scales the intensity did vary when Voyager 1 approached the TS. What is also evident is that as Voyager 1 approached the HP the intensity kept on increasing and in the process these short-term changes diminished. There is clearly a good compatibility between this observation and the computed profile using $\mathrm{HPS}\left(E^{-1.55}\right)$.

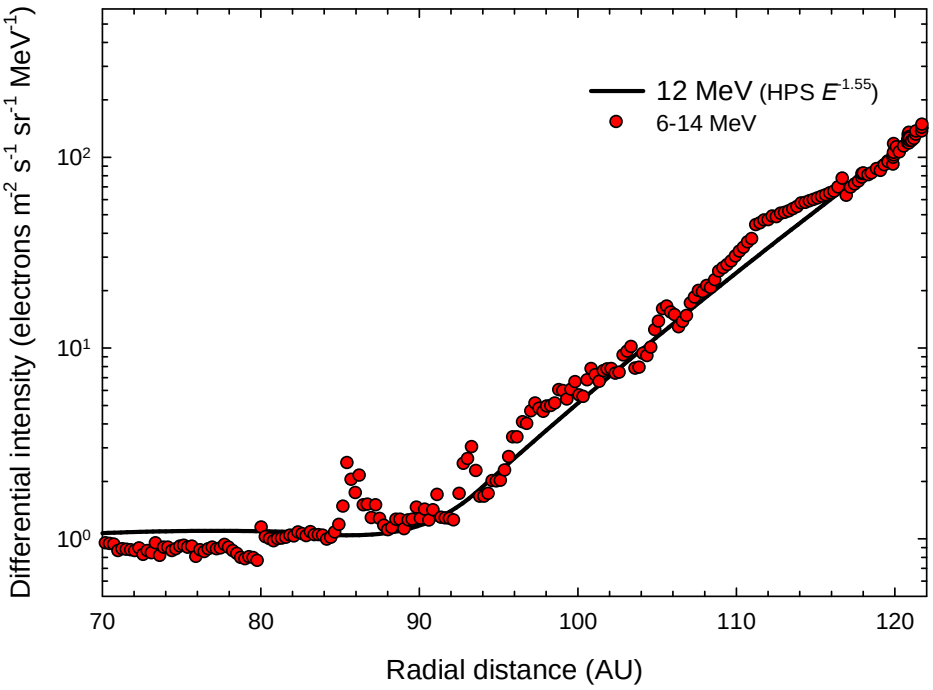

Figure 7.16: Computed radial dependence of 12 MeV galactic electrons (solid black line), between 70 AU and the HP at 122 AU, together with Voyager 1 observations (red filled circles; Webber, 2012, private communication) for 6-14 MeV electrons. This is done with $\mathrm{HPS}\left(E^{-1.55}\right)$.

Finally, the most prominent modulation feature shown in Figure 7.15 is that in order to reproduce the spectral shape of the observed spectra from 110 AU to 122 AU, the HPS must have a simple power law form below ~0.8 GeV. Concerning the diffusion coefficients, they must be rigidity independent at these low energies as predicted by turbulence theory and

discussed by Potgieter and Nndanganeni (2013a); see also Figure 3.6. To reproduce the observed radial intensities observed by Voyager 1 beyond the TS, a significant drop in the diffusion coefficient is also necessary; see Figure 3.7. This is due to the fact that the turbulence beyond the TS and inside the heliosheath increases, causing the diffusion coefficients to drop significantly over the TS to stay smaller up to the HP. Similar conclusions were made by Nkosi et al. (2011), Strauss (2010), Strauss et al. (2010, 2011) and Nndanganeni (2012).

7.7 Summary and conclusions

This chapter is focussed on the total modulation that occurs in the heliosheath, motivated by the electron observations from Voyager 1. The main purpose is to gain a better understanding of how low-energy electrons get modulated in this region which is different than the rest of the heliosphere. This is done by comparing a comprehensive 3D model to the observations.
Modulation in the heliosheath has become most relevant since the crossing of the TS by Voyager 1 (Stone et al. 2005, Richardson et al. 2009). It became evident that this region affects the transportation of the CRs differently than in the rest of the heliosphere and has been recognised as an eminent feature of the heliosphere that contributes to the overall modulation of CRs, especially at lower energies. The Voyager spacecraft had returned some unexpected observations such as the strength of the TS and its varying position and eventually the location of the HP which was predicted much further out by MHD models. See the review on challenges to cosmic ray from beyond the solar wind termination shock by Potgieter (2008b).

The relevance of modulation beyond the TS was discussed already by Quenby et al. (1990) and the numerical models that included some aspects of this type of modulation were developed then by Potgieter and le Roux (1989a, b). Here, only a brief review was given regarding the modulation of ACRs and GCRs (see the review on ACRs by Strauss et al. 2011). Modeling studies which motivated this work were from Ferreira and Potgieter (2002); Potgieter and Ferreira (2002); Ferreira et al. (2004); Langner and Potgieter (2004) and Nkosi et al. (2011). These efforts were shown in Figure 7.6 to Figure 7.9. Their main conclusion was that the heliosheath should act as an effective modulation barrier for low-energy electrons and its significance depends on the thickness of the heliosheath and on how high the LIS was made, all unknowns at that time. Their diffusion coefficients were based mostly on

the theoretical work of le Roux and Fichtner (1999) and Matthaeus et al. (2003) which utilised slab turbulence theory. Most encouraging was that for these low-energy electrons the observations did confirm most of the predictions of earlier models (e.g. Ferreira and Potgieter 2002; Ferreira et al. 2004a, b).

In this Chapter the observations for GCRs He and protons were shown in Figure 7.1 and briefly discussed as an illustration of the effects that the heliosheath has on GCRs. The heliosheath clearly acts as a modulation barrier for these particles, the more so, the lower the energy.

Figure 7.2 showed how differently ACRs dominated protons $(E > 0.5\ \mathrm{MeV})$ behaved over the period 2009 to 2013 in comparison with GCRs (6-14 MeV) electrons and protons (count rates with E > 100 MeV) as observed by Voyager 1 (Webber et al. 2012). In contrast, both GCRs electrons and protons show large intensity increases, starting mid-2012 but then even larger and quicker increases in August 2012; in total a factor of ~2 for electrons and ~40% for the protons. From this it can be deduced that the HP region is more extended than previously thought, and acts by itself as an additional modulation barrier contributing to the total effect of the full inner heliosheath.

Figure 7.3 showed the running averages of 6-14 MeV electrons and protons as observed by Voyager 1 since 2004 until the end of 2011. The main feature is that the 6-14 MeV electron intensity and the E > 200 MeV protons had increased rapidly and irregularly beyond the TS in 2004, but after mid-2008 the increases were more smoothly and as such the radial intensity gradient could be determined. Evident for the electrons, but not for the protons, is the relatively large temporal event in 2004 (e.g. shown in Figure 7.16), which could easily be associated with the TS and consequently be interpreted as the effect of the TS on these electrons (see also Prinsloo 2015).

Figure 7.4 showed the changes in the radial intensity gradients for both electrons and protons. These changes indicate that Voyager 1 went through regions with different modulation/propagation conditions.

Figure 7.5 showed 5-12 MeV electron intensities as observed by Voyager 1 and 2 as an illustration of how differently it has evolved. This is not too surprising because Voyager 2 is ~ 20 AU closer to the Sun and is exploring a different region of the heliosphere. In this study Voyager 2 observations were not pursued since this requires a time dependent model to reproduce the relatively large periodicity in the observed intensities. For Voyager 1, the focus

is on the global (total) variation which can be utilised in a steady state approach to the modeling.

In this thesis, what is new is that the position of the HP has become known, at least in the Voyager 1 direction, and the important issue regarding the value and the spectral shape of the HPS at lower energies has been largely resolved when Voyager 1 crossed the HP. Some uncertainty still exist as was discussed in Chapter 4.

The diffusion coefficients utilised were based on the approach that was first used by Potgieter (1984) which gave the diffusion coefficients independent of rigidity at low energy as was predicted by turbulence theory later in the 1990's. Making use of this insight, the modeling of 12 MeV galactic electrons in the heliosheath was computed by utilising the new HPS and a set of appropriate diffusion coefficients as discussed in Chapter 3. This straightforward approach was adequate to reproduce the observations from Voyager 1, both for the flux and the radial intensity profile. This is not to say that the approach by e.g. Nkosi et al. (2011) is less suitable but the approach followed here is less complicated and quantitatively they yield almost the same results. This was illustrated in Figure 7.14.

The spectra in the heliosheath were computed along the Voyager 1 trajectory followed by studying the effects of the thickness of the heliosheath and the effects of using different HPS. The modulation effects of varying the extent of the heliosheath by changing the location of the TS, the position of the HP and the value of the HPS were illustrated in Figure 7.13.

It was reconfirmed that the heliosheath acts as a very large modulation barrier for low-energy galactic electrons. Then the radial intensity profile of these low energy electrons was studied and the modelled results were compared to the observations (see Figures 7.15 and 7.16). The spectra were computed at 90 AU, 110 AU and 119 AU with $\theta = 60^{\circ}$. The conclusion made was that modifying the spectral index of the HPS only changes the radial profile quantitatively but not qualitatively.

The HP region could also form an outermost zone for low energy electrons to be modulated differently. This has not been done in this thesis since it requires a new and detailed modeling study. The outer heliosheath might also contribute in reducing intensities as electrons propagate from the LIS medium to the disturbed region around the HP.

Finally, the radial intensity profile of the 12 MeV was computed. This was compared to the Voyager 1 observations and it was found that the new HPS together with the appropriate set of diffusion coefficients produced compatibility between the model results and the observations evident from Figure 7.16.

The most prominent modulation feature shown in Figure 7.15 is that in order to reproduce the spectral shape of the observed spectra at 110 AU and 122 AU respectively, the HPS must have a simple power law form below ~0.8 GeV and that the diffusion coefficients must be rigidity independent at these low energies as predicted by turbulence theory and discussed by Potgieter and Nndanganeni (2013a). To reproduce the observed radial intensities observed by Voyager 1 beyond the TS, a significant drop in the diffusion coefficient is required. This is due to the fact that the turbulence beyond the TS and inside the heliosheath increases, causing the diffusion coefficients to drop significantly over the TS to stay smaller up to the HP.

In the next chapter the focus will be on the combined modulation of galactic and the Jovian electrons in the heliosphere.

Chapter 8

The combined modulation of Jovian and galactic electrons in the heliosphere.

8.1 Introduction

It was discussed in the previous chapters how the modulation of cosmic rays (CRs) in the heliosphere is simulated by using numerical models, such as the 3D Jovian electron model based on the numerical solution of Parker's (1965) transport equation. In order to execute these simulations, a heliopause spectrum (HPS) or very local interstellar spectrum (LIS) for galactic electrons was introduced as an initial condition at the heliopause (HP). For this work, the HP is considered as the heliospheric modulation boundary, specified at 122 AU. For the Jovian electrons, alternative source functions were introduced into the model which influences the energy range where these particles, when modulated, dominate in the heliosphere.

When Voyager 1 crossed the HP, it gave an answer to the long outstanding question about the spectral shape (energy dependence) of the very LIS at these low energies, as well as where the modulation boundary is. As described in Chapter 4, these observations made it possible to determine a realistic HPS and as such makes it possible to study with confidence the total modulation of galactic electrons in the heliosphere. When combined with a Jovian electron source function, as described in Chapter 5, a global view of the modulation of both galactic and Jovian electrons can be obtained. The model described in previous chapters is used to do so, specifically including the assumption that the diffusion coefficients are independent of rigidity at lower energies.

The main focus of this chapter is on the study of the overall modulation when combining Jovian and galactic electrons in the heliosphere and also to determine the intensity contribution of the two populations to the total electron intensity in the heliosphere. The computational results are compared to selected set of observations at or close to the Earth and in the outer heliosphere. These observations are used then to determine the energy range where the Jovian electrons dominate over the galactic electrons and also to estimate what the intensity of the galactic electrons can be at the Earth.

Nndanganeni (2012), by studying the radial dependence of the intensity of 12 MeV galactic electrons, was able to predict from a modeling point of view what the highest and the lowest plausible intensity of galactic electrons can be at the Earth. The highest possible value was found as 2.5 x 10^{-1} electrons m^{-2} sr^{-1} s^{-1} MeV^{-1} and the lowest as 3 x 10^{-3} electrons m^{-2} sr^{-1} s^{-1} MeV^{-1}. Potgieter and Nndanganeni (2013a) did a follow-up, including also the radial dependence of the Jovian electrons at this energy. They compared their results to the observed radial intensity profile for 6-14 MeV electrons from Voyager 1 since its launch and until it was at ~117 AU. It was shown that the Jovian electrons dominate in the inner heliosphere, for $r < 20$ AU, at these energies. It was shown how quickly the Jovian contribution dissipates as a function of increasing radial distance so that a negligible flux of Jovian electrons reaches the TS shock region. Similar conclusions were made by Potgieter and Ferreira (2002). Taking into account the controversy regarding the Voyager 1 electron data between 40 AU and 80 AU, Potgieter and Nndanganeni (2013a) computed three different scenarios to predict what intensity the galactic electrons may have at Earth. They found similar results as those from Nndanganeni (2012). This aspect will be reinvestigated in this chapter using the energy dependence of the combined modulation of galactic and Jovian electrons from a spectral point of view.

8.2 Modeling parameters

The 3D steady state modulation model discussed in Chapter 3, which includes the Jovian electron source, is used to compute the combined modulation of Jovian and galactic electrons. In order to achieve compatibility with the observations, a phenomenological approach is mostly followed to establish the basic diffusion coefficients which relate mostly to quasi linear theory (QLT: see e.g. Bieber et al. 1994) as explained in previous chapters. This requires that the spatial dependence of the diffusion coefficients be specified differently in the inner heliosphere than in the outer heliosphere and specifying the rigidity dependence differently above and below 0.4 GV as explained before; see Figure 3.6. The diffusion coefficients are given by Eqs. (3.44 to 3.47) and the drift coefficient is given by Eq. (3.56).
In Chapter 4 the issue pertaining to the HPS (or very LIS) of galactic electron, and the effects it has on the modulated spectra were illustrated. The modulation of Jovian electrons was computed in Chapter 5, mainly addressing the issue relating to the source function, as to how it should look like and what the spectral index of this source function could be at these low

energies. The general modulation features of drifts were illustrated and discussed in Chapter 6.

Up to what energies the Jovian electrons may dominate depends strongly on what is assumed in the first place for the Jovian source function and then what the spectral shape of the HPS is, so that here the combined modulation of the Jovian and the galactic electrons is studied and illustrated. Only the HPS with $E^{-1.55}$ below ~1 GeV, as discussed in Chapter 4 (see Eqs. 4.2 and 4.3), is used and illustrated. For the Jovian electrons the three source functions as discussed in Chapter 5 are used; see Figure 5.10 and Eqs. (5.9), (5.11) and (5.13). Again only solar minimum modulation conditions are assumed with the tilt angle $\alpha = 5^{\circ}$ and with full drifts. Keep in mind that particle drifts dissipate with decreasing energy to become negligible for Jovian electrons as noted before.

8.3 Modeling results

First, Figure 8.1 shows the electron spectra at Earth (1 AU) computed separately for Jovian (blue curves) and galactic (magenta curves) electrons with respect to a source function at Jupiter (5 AU) and the HPS (or very LIS) specified at the modulation boundary (heliopause at 122 AU). This illustrates how different these two populations are in terms of their spectral shapes and the consequent modulation. In terms of their intensities, the Jovian electrons clearly dominate at the lower energies, of which the details will be further illustrated and discussed in the next two figures. Note that the slope of the Jovian electron source is maintained at the Earth, as well as that of the HPS as the consequence of the assumed constant rigidity dependence of the diffusion coefficient (DCs) used in the modulation model (see e.g. Figure 3.6). Also note that the two slopes at these very low energies are very similar, which is coincidental.

In Figure 8.2 the combined modulation of Jovian and galactic electrons are shown. The modulated spectra at the Earth (1 AU) are based on the HPS ($E^{-1.55}$) and the three alternative Jovian source functions, respectively, as defined in Chapter 4 and Chapter 5. In the top panel the DCs are assumed to be large with the immediate implication that less modulation occurs whereas for the bottom panel smaller DCs are assumed and hence a larger amount of modulation is found. Consider the three cases as shown in the top panel: First, note the light-green (dash-dotted) curve as the combined modulated spectrum at 1 AU which is based on $j_{\text{alternative2}}$ as shown in Figure 8.1 and given by Eq. (5.13).

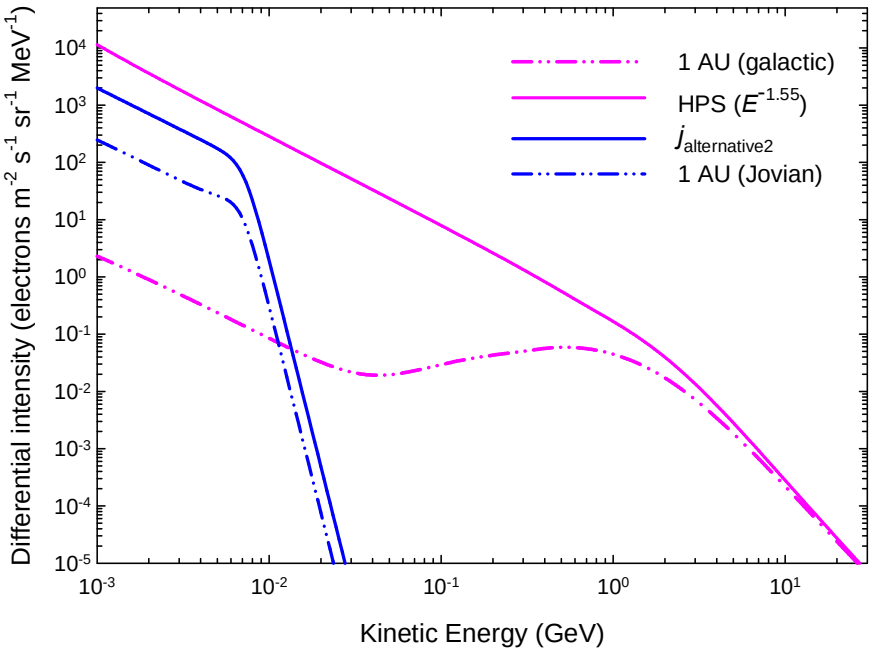

Figure 8.1: Computed galactic electron spectrum at Earth (1 AU) with respect to the HPS ($E^{-1.55}$) at 122 AU together with the modulated Jovian electron spectrum at Earth (1 AU) with respect to a Jovian source function $j_{\text{alternative2}}$ as defined in Chapter 5; see Eq. (5.13).

It exhibits four significant changes in the spectral slope. For $E < 10$ MeV this spectrum preserves the slope of the Jovian source function. Above ~10 MeV the intensity drops sharply as the contribution from the Jovian source falls away so that the slope changes to that of the HPS, up to ~100 MeV. This means the galactic electrons in this case begin to dominate at the Earth from between 10 to 20 MeV. As emphasized before, the slope of the source function and that of the HPS is preserved because the DCs are independent of rigidity at these low energies. Above ~ 100 MeV the usual modulation features are applicable to galactic electrons as discussed in Chapter 6.

Second, the red (dotted) curve is the modulated spectrum based on the Jovian electron source function $\left(j_{\text{alternative1}}\right)$ in Eq. (5.11). This combined spectrum looks different because the spectral index of the function was changed from γ =1.5 to γ =3.0; see Eqs. (5.9 & 5.11). In contrast to the one discussed above this gives a much higher intensity up to ~30 MeV. As before the Jovian electrons dissipate quickly with increasing energy but in this case over a wider energy range. The consequence is that the Jovian electrons can dominate up to ~50 MeV. Again the spectral slope of the source function is preserved at the lower energies.

Third, consider the blue (dashed) curve as the combined spectrum at the Earth computed with the source function j_{Ferreira} in Eq. (5.9), which gives a different intensity contribution from the Jovian electrons up to ~100 MeV. Evidently the shape of the Jovian electron source function plays a significant role in determining up to what energies the Jovian electrons can dominate over the galactic electrons in the inner heliosphere.

Because of the complexity (and reliability) of low-energy electron observations, also taking into account all the solar and other phenomena that may influence these observations, there is not a compelling reason to choose between these source functions but to illustrate their effects on modulation. Comparison with observations will be done in the next section.

The bottom panel of Figure 8.2 is similar to the top panel, but computed with smaller DCs, to give larger modulation, with the consequence that the energy range where the galactic electron dominate over the Jovian electrons is shifted to a lower energy. Clearly, this energy range thus also depends on the level of solar modulation; increased solar modulation causes the Jovian electrons to dominate to higher energies.

These aspects are emphasized in the two panels of Figure 8.3 by plotting the appropriate intensity ratios. The top panel illustrates the intensity ratios of the combined spectra obtained by using small and large DCs as shown in the top and bottom panel of Figure 8.2 for the three alternative Jovian source functions, respectively. As expected the largest ratio is found for the solid black curve $\left(j_{\text{alternative2}}\text{ scenario}\right)$ at ~ 15 MeV. This ratio decreases and shifts to higher energies for the other source functions. The ratio becomes unity eventually as the modulation dissipates. The bottom panel gives the ratios of the HPS and the three modulated spectra at Earth as displayed in the top panel of Figure 8.2 for the three source scenarios $\left(j_{\text{Ferreira}}, j_{\text{alternative1}}, j_{\text{alternative2}}\right)$. This illustrates the amount of modulation between the HPS and the modulated spectra at Earth for the three source scenarios. Above ~100 MeV the solutions are indistinguishable because then the galactic electrons surely dominates the intensity levels. Obviously, all these ratios converge to unity at high enough energy where it is assumed that no modulation occurs.

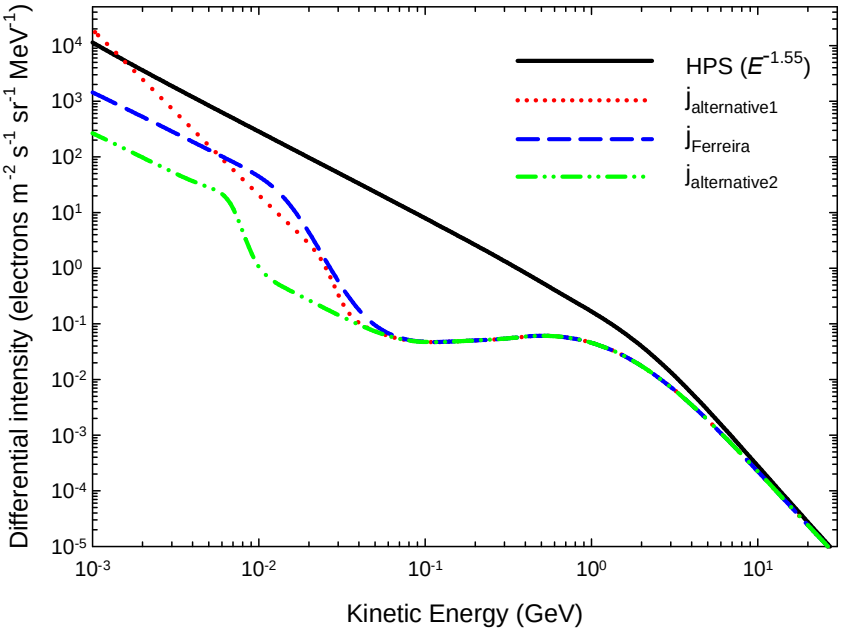

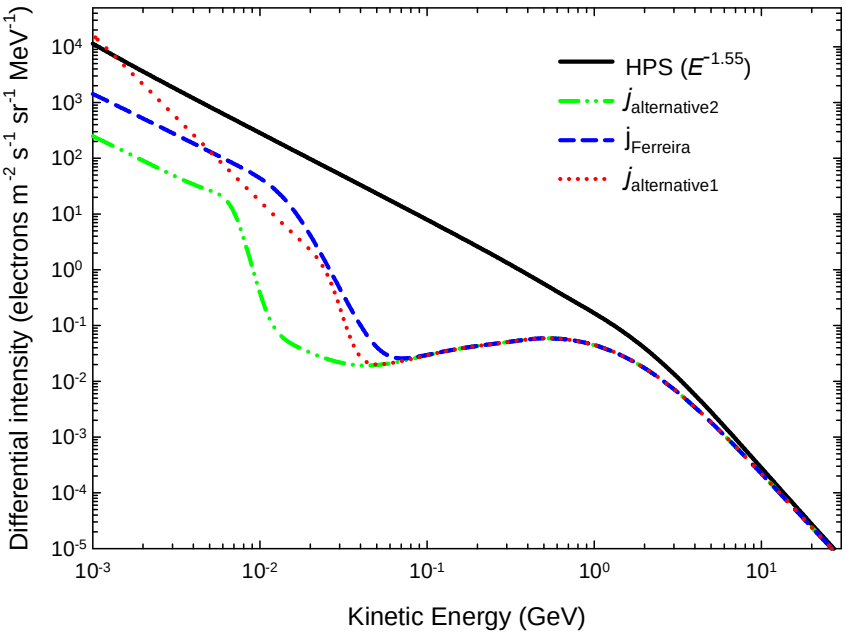

Figure 8.2: Three combined modulated spectra for Jovian and galactic electrons at Earth (1 AU), with respect to $\mathrm{HPS}\left(E^{-1.55}\right)$ specified at 122 AU (black solid line) and three spectra based on the three different source functions ($\left(j_{\mathrm{alternative1}}, j_{\mathrm{alternative2}}\right.$ and $\left.j_{\mathrm{Ferreira}}\right)$ as shown in Figure 5.10. The difference between the two panels is in the assumed diffusion coefficients (DCs); in the top panel large DCs are assumed which results in relatively less modulation whereas in the bottom panel smaller DCs are used which produce larger modulation.

Evidently, the choice of a Jovian source function, a HPS and the choice of DCs influence the total modulation that occurs between the Earth and the heliospheric boundary (HP).

Switching to radial profiles, Figure 8.4 shows a comparison of the computed 6 MeV and 20 MeV Jovian and galactic electron intensities from the Earth to the HP. In the top panel it is separately computed for Jovian and galactic electrons, using the source function and the HPS shown in Figure 8.1. As expected, for the Jovian electrons a sharp increase occurs from 1 AU up to the source at 5AU and then an equal rapid decrease beyond the source, dropping by a factor of ~1000 over a relatively short distance in the inner heliosphere. Very few of these electrons would be able to reach the TS (see also Potgieter and Ferreira 2002). Turning to the galactic component, it is found that for r < ~10 AU their intensity is much lower than for the Jovian electrons. For 6 MeV, the galactic electron intensity equals the Jovian electron intensity at ~16 AU but for 20 MeV the Jovian electrons have essentially disappeared because of the spectral shape of this particular source function. For the j_{Ferreira} source function this energy will be higher as found by Strauss et al. (2013). The intensity for the galactic electrons increases steadily as a function of increasing radial distance up to the TS where after there is a sudden intensity increase up to the HP in order to match the HPS at these energies (see also Chapter 7). The bottom panel shows the combined radial intensity profiles and re-emphasizes what was mentioned above.

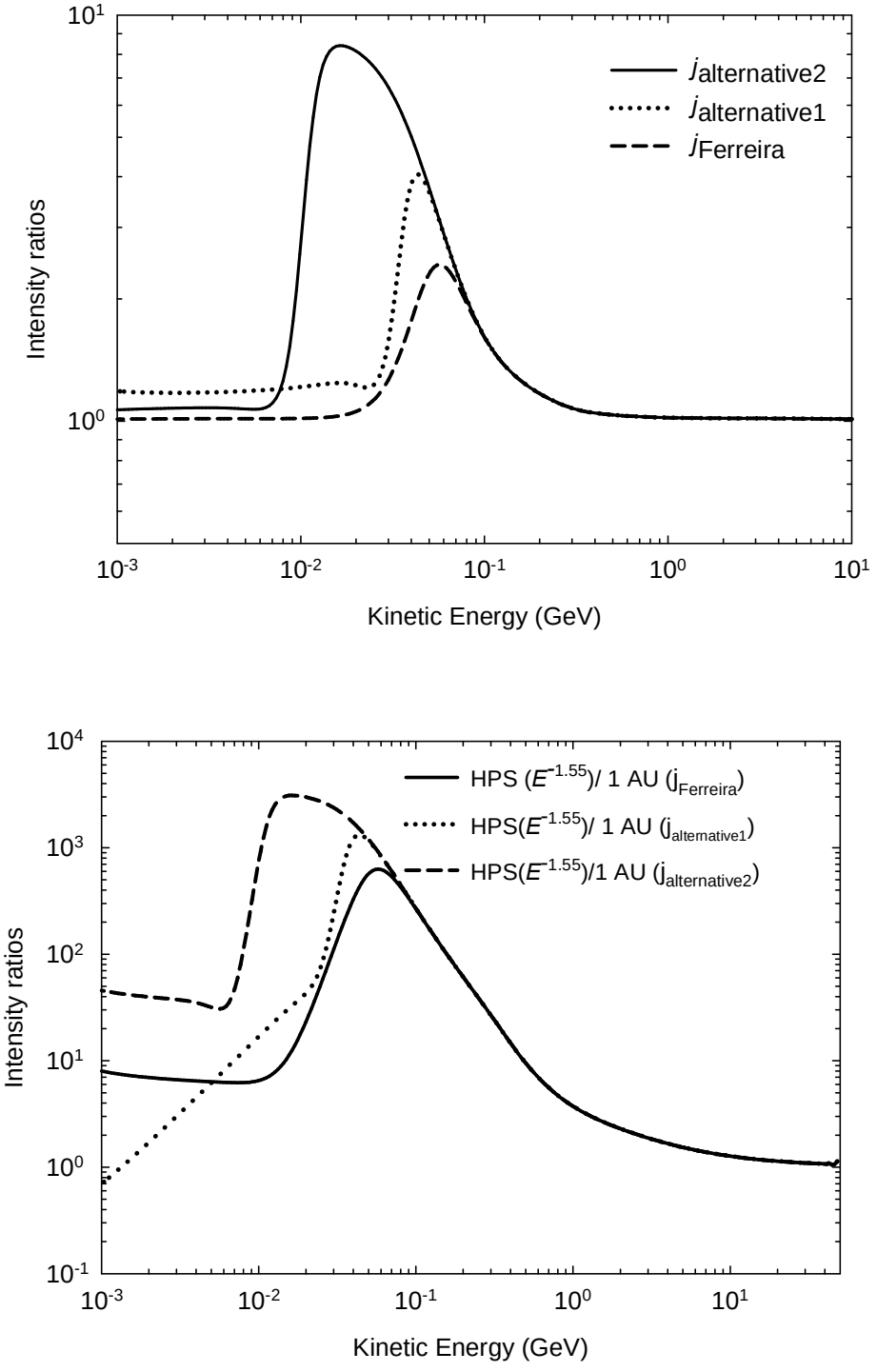

Figure 8.3: The top panel shows the intensity ratios of the modulated spectra, as in the top and bottom panels of Figure 8.2, to illustrate the effect of increased solar modulation. The bottom panel gives the ratios of the $\mathrm{HPS}\left(E^{-1.55}\right)/1\ \mathrm{AU}\left(j_{\mathrm{Ferreira}}\right)$, $\mathrm{HPS}\left(E^{-1.55}\right)/1\ \mathrm{AU}\left(j_{\mathrm{alternative1}}\right)$ and $\mathrm{HPS}\left(E^{-1.55}\right)/1\mathrm{AU}\left(j_{\mathrm{alternative2}}\right)$ respectively, emphasizing what was displayed in the top panel of Figure 8.2. This gives the total modulation between the HP and the Earth.

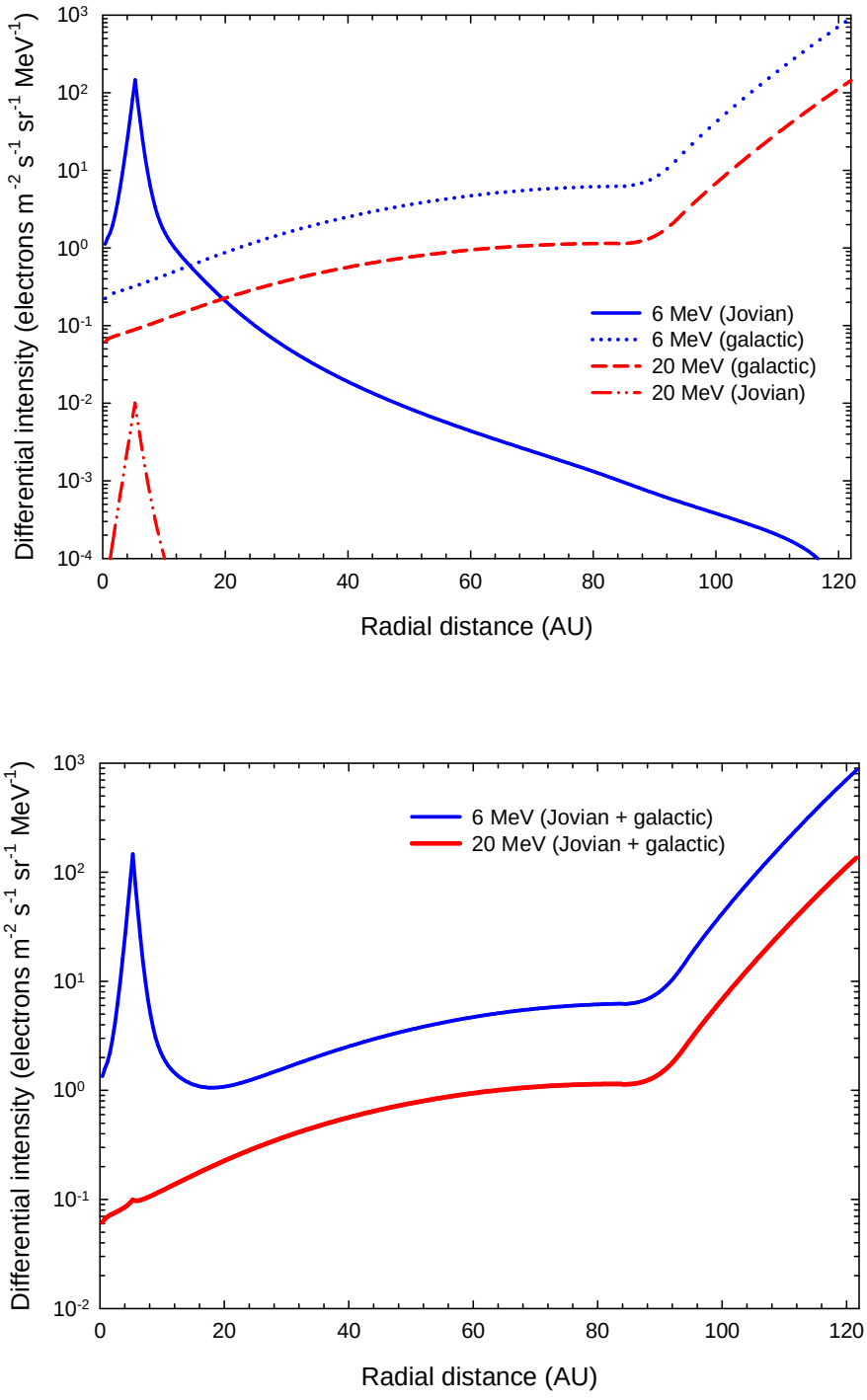

Figure 8.4: Computed radial profiles of 6 MeV and 20 MeV Jovian and galactic electron intensities, separately done in the top panel and combined for the bottom panel. These intensities are computed with respect to the Jovian source function $\left(j_{\text{alternative2}}\right)$ and the HPS$\left(E^{-1.55}\right)$ as shown in Figure 8.1.

8.4 Comparison with the electron observations

Figure 8.5 shows the recently published PAMELA electron spectrum at Earth between ~80 MeV up to ~40 GeV for the 2009 solar minimum (Adriani et al. 2015). Two sets of unpublished observations from Voyager 1 are shown below ~50 MeV, indicated as V1-77 BSe and V1-77 corr (Webber 2015, private communication). As the numbers indicated, these observations were made in 1977 when Voyager 1 was still relatively close to the Earth and were made with two different detectors on board this spacecraft. At least, they were made during the solar minimum period centred around 1976-77, which was classified as a so-called A > 0 solar magnetic cycle. Together with the PAMELA data, this illustrates the characteristic spectral forms of modulated Jovian and galactic electrons. At this stage, it is safe to assume that above ~100 MeV the observations are of galactic origin which will be further investigated in this chapter. A fourth data set is also shown, from ISEE 3 (Moses 1987), observed in the period 1979-1984, that is, before and after solar maximum conditions.

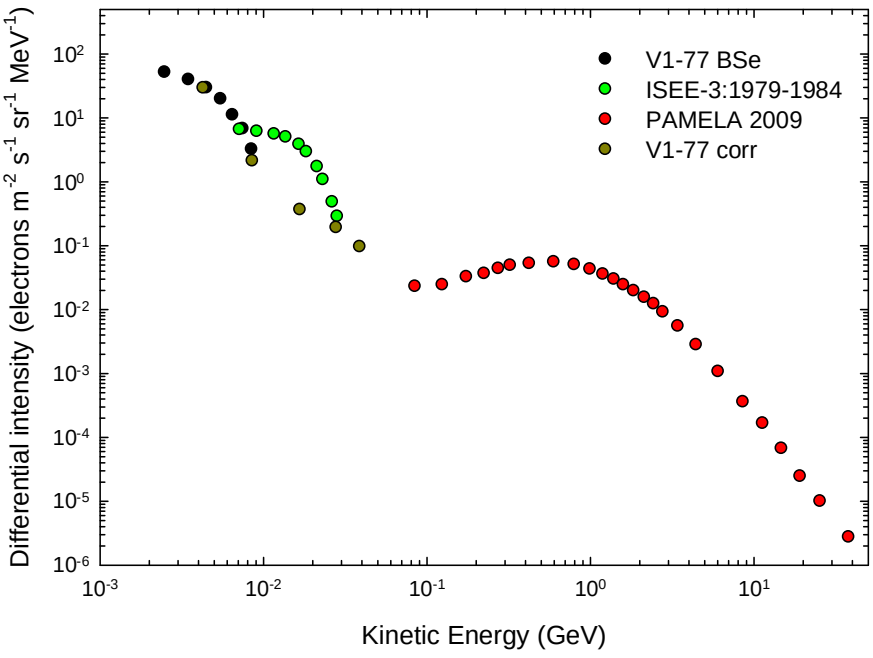

Figure 8.5: Electron spectra observed at or close to the Earth for the energy range from ~2 MeV to ~50 GeV. These spectra illustrate a transition below 100 MeV from galactic electrons to Jovian electrons with decreasing energy. The observations are for 2009 from PAMELA (Adriani et al. 2015), for 1979-1984 from ISEE-3 (Moses 1987), and for 1977 from Voyager 1, indicated as V1-77 BSe and V1-77 corr, which come from two different detectors on board this spacecraft (Webber 2015, private communication).

Evidently, there is a significant difference between the V1 and ISEE 3 observations in terms of their energy distribution, which is most puzzling. This shift might be due to the difference in the times of these observations, but it is difficult to understand why the shift is only in the energy range and not in the level of the modulated intensity. Since systematic errors of observations are rarely published (and unknown for these V1 data sets), it is not possible to judge the accuracy of these observations, so that no attempt is made to do so in this thesis about numerical modeling. Because the V1 data were obtained during a solar minimum period, these two sets are used further on in combination with the PAMELA spectrum. By inspecting these observations, it follows that a transition occurs below ~100 MeV, assumingly as the contribution of the Jovian electrons becomes increasingly dominant with decreasing energy. The numerical modeling solutions can give additional insight into what happens below 100 MeV.

Next, the modulation model results are compared to observations, from the inner to the outer heliosphere. The main purpose is to illustrate the total global modulation of these electrons, especially at low energies, and to illustrate that the combined model can reproduce the main features of observations at Earth and in the outer heliosphere.

Figure 8.6 shows the computed combined modulation of Jovian and galactic electrons from the HP at 122 AU to the Earth (see also Figure 8.2). A computed spectrum is shown at 110 AU to illustrate the significant modulation inside the heliosheath (see also Figure 7.15). These computed spectra are compared to observations as indicated in the legend and figure caption. At Earth two modulation scenarios are shown for which the reason is as follows: It is not possible to reproduce simultaneously the PAMELA electron spectrum below ~200 MeV and the Voyager 1 data, shown as V1-77 corr, using one set of modulation parameters and a rigidity dependence for the diffusion coefficients that can be related to any reasonable diffusion theory. Scenario 1 (green dotted line) satisfactorily reproduces the PAMELA observations from the highest to the lowest observational data points but cannot match the V1-77 corr data in the energy range from 10 MeV to 50 MeV, while doing so below 10 MeV. Both the V1-77 BSe and V1 -77 corr observations are reproduced below this energy because they are quite similar. Consequently, the model has been tuned to the effect that scenario 2 can reproduce the V1-77 corr data set at all energies but then ends up too high in intensity to reproduce the PAMELA observations reasonably below ~200 MeV. The logical conclusion is that either the PAMELA data are too low for E < ~200 MeV or the V1-77 corr data are too high between 10 MeV and 50 MeV. The difference is in the order of a factor of 2 which from an instrumental point of view may not be bad at all. Unfortunately, the data sets are not

overlapping because of the designs of the detectors. Obviously, the PAMELA electron data, which is now published, have superior statistics and does detect only electrons, not including positrons as the Voyager 1 instrument is doing. If both sets of observations at these energies are considered to be reliable, then drastic changes need to be implemented in the rigidity dependence of the DCs for electrons. This will require that the rigidity dependence has to increase below ~100 MeV which is not supported beyond doubt by turbulence models (e.g. Teufel and Schlickeiser 2002; Engelbrecht and Burger 2013a, b); these turbulence models do support a flat rigidity dependence in this energy range, with an increase at much lower rigidities for electrons.

Using other electron measurements at these energies as shown in Chapter 5 (see Figure 5.1), do not help much so this data reliability issue is set aside, remaining to be investigated thoroughly from an observational point of view. Of course, it may be that different modulation conditions existed in 1977 than in 2009, as the work on protons of Vos (2011) indicated; see also Potgieter et al. (2014a). However, from a particle drift point of view, electron intensities should be higher in A < 0 cycles (around 2009) than in A > 0 cycles (around 1976-77). The remaining and important issue of up to what energies the Jovian electrons can dominate over the galactic electrons will be addressed with the next figure.

Turning to the outer heliosphere where the spectra at 110 AU and the HPS are shown together with the observations in Figure 8.6, it is necessary to recap. As discussed in Chapter 4, the HPS must have a power law form below ~1 GeV with $E^{-(1.55\pm0.05)}$, where E is kinetic energy, if the observations at 110 AU to 122 AU are to be reproduced. This power law form was observed first by Voyager 1 in 2010 and it was re-affirmed in 2012 when the spacecraft crossed the HP at 122 AU (even when a different technique was used to analyse the electron data; see Stone et al. 2013). Clearly the model reproduces the observed Voyager 1 spectra at 110 AU and 122 AU quite satisfactorily. The computed spectra show how galactic electrons get modulated quite significantly in the heliosheath. Even the additional observations shown as V1-BSe LIS and V1-77 IS (Webber 2015, private communication) are consistent to the observations reported by Stone et al. (2013) and as such give good compatibility with the modeling results for the outer heliosphere.

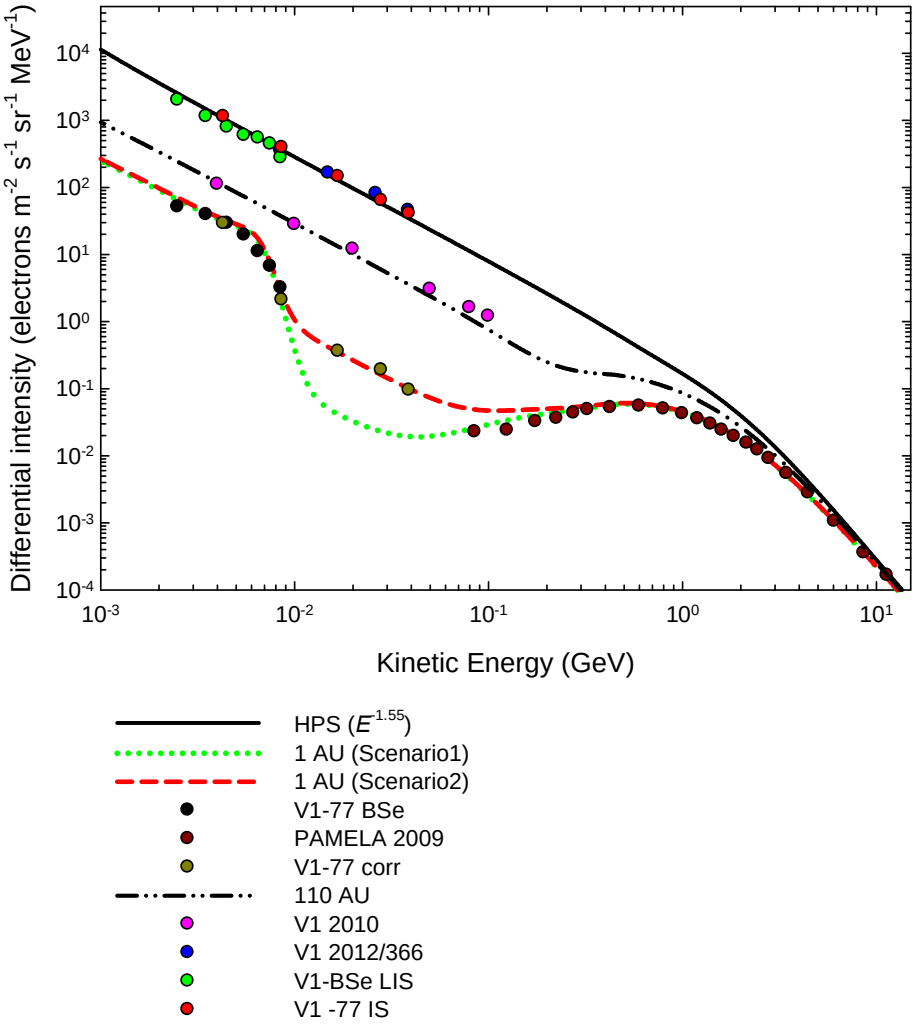

Figure 8.6: Computed electron spectra at the Earth (1 AU) for two different modulation scenarios (red dashed and green dotted lines), and at 110 AU as a function of kinetic energy using the $\mathrm{HPS}\left(E^{-1.55}\right)$ at 122 AU and the Jovian source function $j_{\mathrm{alternative2}}$ at Jupiter (~5 AU). This is compared to the PAMELA 2009 spectrum (Adriani et al. 2015; see also Potgieter et al. 2015) and the V1-77 corr and V1- 77 BSe observations as shown in Figure 8.5. The observations in the heliosheath are from Voyager 1 observed during different periods; V1 2012/366 (Stone et al. 2013), V1 2010 (Webber 2010, private communication), V1-BSe LIS and V1-77 IS (Webber 2015, private communication).

Figure 8.7 shows in the top panel the computed spectra for galactic and Jovian electrons separately at the Earth (1 AU), then with their intensities multiplied by the E^2 in the bottom panel for illustrative purposes. The differential intensity in the top panel is in units of

electrons m^{-2} s^{-1} sr^{-1} MeV^{-1} whereas in the bottom panel the intensities are in units of electrons m^{-2} s^{-1} sr^{-1} GeV. The spectrum for Jovian electrons is computed with respect to the source function $j_{\text{alternative2}}$ from Figure 8.1. The two galactic spectra are computed with respect to $\text{HPS}\left(E^{-1.55}\right)$ and are done for the two modulation scenarios shown in Figure 8.6. These spectra are compared again with electron observations at or close to Earth from PAMELA 2009, V1-77 corr and V1-77 BSe.

The aim is to determine the energy range up to which the Jovian electrons dominate the galactic electrons and then determine what the galactic electron intensity can be at this low energy at Earth.

The two panels in Figure 8.7 illustrate in the first place how the Jovian electrons sharply decrease from ~10 MeV to fall below the two galactic spectra for E < ~15 MeV. Their intensity is already matching the galactic electron intensity for modulation scenario 1 at ~12 MeV and for scenario 2 at ~9 MeV. The observations in the energy range between 16 MeV and 40 MeV must then be interpreted as of galactic of origin, as the slope of the HPS is reproduced. Secondly, it is shown that according to scenario 1, where the PAMELA spectrum for 2009 is used, the predicted intensity of the galactic electrons at Earth is 5.5 electrons m^{-2} s^{-1} sr^{-1} MeV^{-1} at E = 1 MeV. According to scenario 2, where the Voyager 1 data for 1977 is used, the predicted intensity of the galactic electrons at Earth at this energy is 20 electrons m^{-2} s^{-1} sr^{-1} MeV^{-1}. An alternative way of showing these results is given in the bottom panel where the computed spectra for both the Jovian and galactic electrons are shown but now with their intensities multiplied by E^2. This emphasizes the conclusions made from the top panel.

Previously, in an attempt to predict the intensity of galactic electrons at Earth, Potgieter and Nndanganeni (2013a) computed a value of 2.5×10^{-1} electrons m^{-2} s^{-1} sr^{-1} MeV^{-1} at 12 MeV. This was based on radial intensity profiles for 6-14 MeV electrons from Voyager 1 observed over two decades. From Figure 8.7 follows that the galactic intensity at the Earth for scenario 1 (based on the PAMELA observations) at 12 MeV is 1.7×10^{-1} electrons m^{-2} s^{-1} sr^{-1} MeV^{-1} where as for the scenario 2 (based on the V1-77 corr observations) is 5.5×10^{-1} electrons m^{-2} s^{-1} sr^{-1} MeV^{-1}. Since these observations were made during solar minimum periods, they are indicative of what the maximum intensity of galactic electrons may be at the Earth.

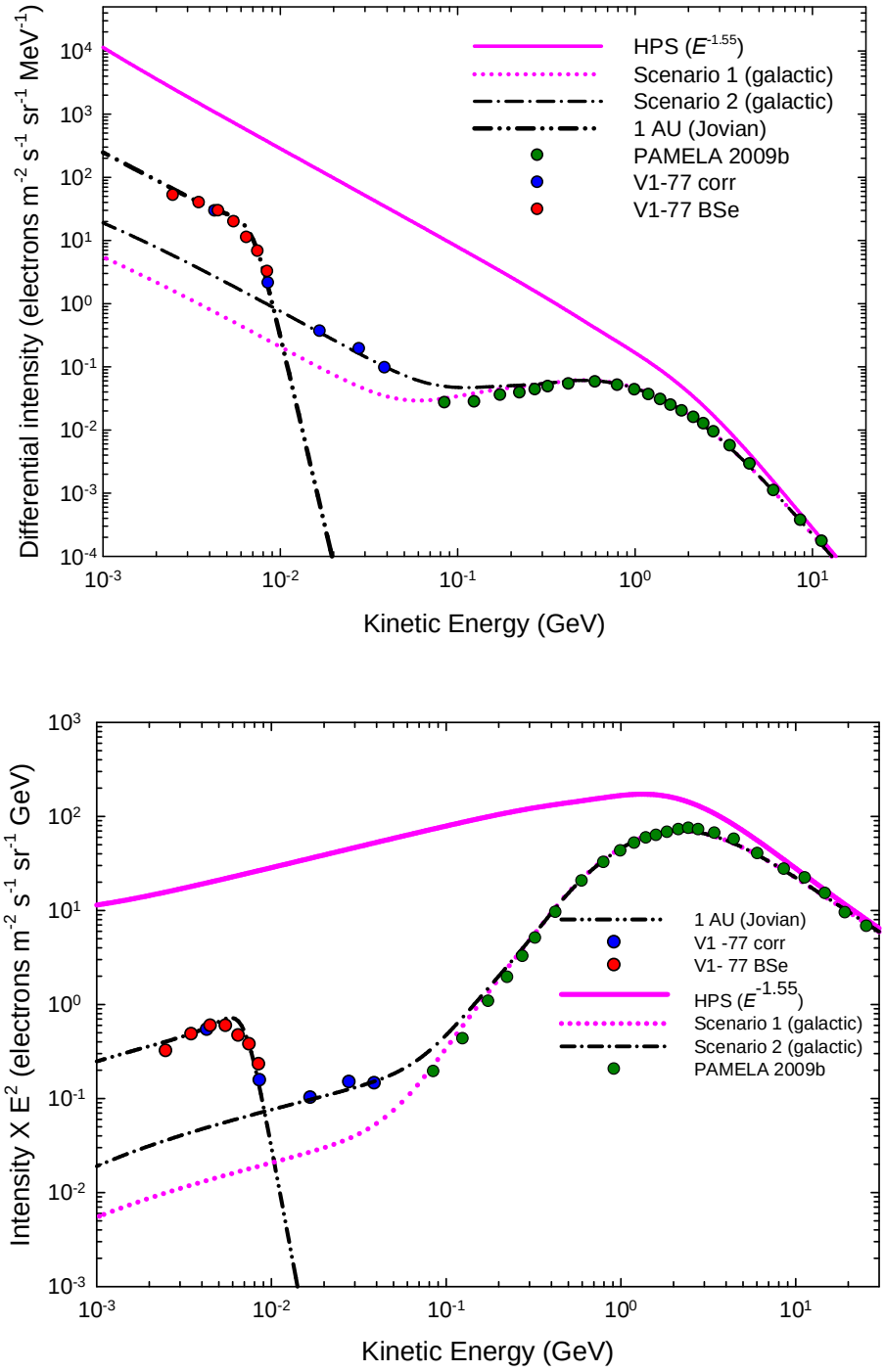

Figure 8.7: Computed Jovian (dash-double-dotted line) electron spectrum and two galactic electron spectra (scenarios 1 and 2 as dotted and dash-dotted lines) at Earth (1 AU) as a function of kinetic energy E. The top panel shows the computed spectra similar to those shown in Figure 8.1, now compared to observations. The bottom panel shows the intensity multiplied by E^2 for illustrative purposes. The Jovian electron spectrum is computed using the source $j_{\text{alternative2}}$ and the galactic electron spectra using $\text{HPS}\left(E^{-1.55}\right)$. The observations are for 2009 from PAMELA (Adriani et al. 2015; Potgieter et al. 2015), and for 1977 from Voyager 1, indicated as V1-77 corr and V1-77 BSe (Webber 2015, private communication).

8.5 Summary and conclusions

This chapter is focused on the total and combined modulation of galactic and Jovian electrons that occurs in the heliosphere, motivated by observations at the Earth and also in the outer heliosphere. The main aim is to gain a better understanding of how these low energy electrons get modulated throughout the heliosphere and the effects of combining the intensities of the two populations on the modulated spectra. The other objective is to see if the galactic electron intensity at Earth can be predicted from this work by comparing different scenarios which are supported by the observations at or close to Earth. This is done by combining the spectra calculated with different source function for Jovian electrons together with the galactic spectra computed with respect to the $\mathrm{HPS}\left(E^{-1.55}\right)$.

The modulation in the heliosphere especially for low energy electrons with $E<50$ MeV has always been controversial especially the issue about the energy range where the Jovian electrons dominate the galactic electrons at these energies (the reliability of the electron observations has always been a discouraging factor). As shown here, this depends on the spectral shape (energy dependence) of the galactic spectrum and that of the source function for Jovian electrons. Previous modeling attempts relevant to this work was done by Ferreira (2002) and revisited by Moeketsi (2005) and Nkosi (2006) but they were not able to resolve the issues about the spectral shape of the galactic electrons and the Jovian source function. This is mainly because observations were not then available close to the HP. For the Jovian electrons it seems to be a tedious process to analyse the Jovian electron data and as such only the data from ISEE 3:1979-1984 (Moses 1987) was used by the mentioned authors. In this work significant improvements have been made because the HPS is settled. With regard to the Jovian source function, the new Voyager 1 observations from Webber (2015, private communication), and the insight from the literature, suggested a source function with a different spectral index. Apart from Ferreira's (2002) work, two alternative source functions were computed and investigated. The energy range in which these Jovian electrons dominate the low energy electron intensities in the heliosphere, was also determined and the intensity that the galactic electron can have at Earth was estimated. This was illustrated first from a modeling point of view as shown in Figures 8.2 and 8.3. The radial intensity profiles for both Jovian and galactic electrons for 6 MeV and 20 MeV were also computed (see Figure 8.4), but based on only the Voyager 1 data. This gives a clear indication of the range, in terms of both radial distance and energy, where the Jovian dominates the galactic electrons.

Model predictions were compared with the observations as shown in Figures 8.6 and 8.7, addressing the issue about the global modulation of the low energy electrons throughout the heliosphere. First from the spectra computed at Earth in comparison with the observations it is clear that it is not possible to reproduce simultaneously the PAMELA electron spectrum below ~200 MeV and the Voyager 1 data, shown as V1-77 corr, using one set of modulation parameters and a rigidity dependence for the diffusion coefficients that can be related to any reasonable diffusion theory. The logical conclusion that can be made from this is that either the PAMELA data are too low for E < ~200 MeV or the V1-77 corr data are too high between 10 MeV and 50 MeV. The difference is in the order of a factor of 2, which from an instrumental point of view may not be bad. Since there is no straightforward answer that can be given in addressing these issues, this study then resorted into studying two scenarios possible with the model. Based on the modeling results, the following conclusion was made: if both sets of observations at these energies were considered to be reliable, a drastic change is needed to be implemented in the rigidity dependence of the DCs for electrons. This requires that the rigidity dependence has to increase below ~100 MeV, which is not supported beyond doubt by turbulence models (e.g. Teufel and Schlickeiser 2002); these turbulence models do support a flat rigidity dependence in this energy range for electrons, with an increase at much lower rigidities.

The model could reproduce the observed Voyager 1 spectra at 110 AU and 122 AU quite satisfactorily. Even the additional observations, shown as V1-BSe LIS and V1-77 IS (Webber 2015, private communication), are consistent to the observations reported by Stone et al. (2013) and as such give good compatibility with the modeling results for the outer heliosphere.

Concerning the Jovian source function and its spectral shape, the issue is still open for debate and the choice of using a source function defined as $j_{\text{alternative2}}$ is only a matter of preference.

As far as predicting the galactic electron intensity at Earth is concerned, it was found and shown in Figure 8.7 that the intensity at 1 MeV is 5.5 electrons m^{-2} s^{-1} sr^{-1} MeV^{-1}, based on scenario 1, which reproduced the 2009 PAMELA electron spectrum, and 20 electrons m^{-2} s^{-1} sr^{-1} MeV^{-1} based on scenario 2 which reproduced the 1977 Voyager 1 observations.

Chapter 9

Summary and conclusions

Modulation of cosmic ray electrons in the heliosphere plays a crucial role in improving our understanding and evaluation of the processes applicable to low energy Jovian and galactic electrons. This provides a useful tool in understanding and estimating the diffusion tensor applicable to heliospheric modulation. Modulated electron intensities in the lower energy range (1-100 MeV) give a direct indication of the average parallel and perpendicular mean free path, in contrast to protons that experience large adiabatic energy changes below ~300 MeV. In this study, utilising the observations from the selected spacecraft, two new HPS for the galactic electrons and two new alternative Jovian electron source functions were developed and applied to study the modulation of these electrons. This is done by using a full 3D steady state model based on Parker's transport equation including a Jovian source function.

The background on CRs modulation and the heliosphere was discussed, including the solar wind, the HMF and the geometry of the heliosphere. A brief discussion was also given about selected spacecraft missions. The mathematical and numerical model was described together with aspects of the diffusion tensor which had to be assumed in order to solve the transport equation.

The rigidity and the spatial dependence of these diffusion coefficients are of special interest because this determines how the computed spectra get modulated throughout the heliosphere. The rigidity and the spatial dependent for $\lambda_{||}$ at the Earth is primarily based on the theoretical work of Teufel and Schlickeiser (2002), on which the rest followed. But, first the work done on these diffusion coefficients and implemented in the numerical models by Ndiitwani (2005) and by Nkosi (2006) was evaluated. It was found that the rigidity dependence that they applied had to be changed to find compatibility with recent Voyager 1 electron observations which form an integral part of this study. Consequently, the rigidity and spatial dependence for the diffusion coefficients from Nndanganeni (2012) were implemented in the 3D model. Regarding the drift coefficient, the weak scattering assumption was assumed but modified according to Burger et al. (2000).

Voyager 1 crossed the HP in August 2012 and measured CRs spectra which can be regarded as HPS, also for galactic electrons. In this work a HPS is considered to be close to what can be called a very LIS as were also discussed by Potgieter and Nndanganeni (2013b) and Potgieter et al. (2014b). Two new HPS were constructed with different spectral indices $\left(E^{-1.35}\right.$ and $\left.E^{-1.55}\right)$ at low energies (E < 100 MeV). This difference is mainly the result of the different techniques that were used in the process of analysing the Voyager 1 observations as reported by Stone et al. (2013). These HPS, normalized to the PAMELA electron spectrum of 2009 at energies above 50 GeV, were subsequently implemented to perform a computational modulation study for the whole heliosphere.

Jovian electron modulation was investigated, first by revisiting the controversial issue regarding their source function and what the spectral index and intensity level could be, from the lowest to the highest energies of relevance to solar modulation. In the process two new alternative source functions were computed and implemented in the model. Their effect on Jovian electron modulation and subsequently on the total electron modulation was investigated and a preferred source function was selected.

The issue concerning drift effects on the global modulation of electrons and how its reduction influences these effects were revisited by studying different scenarios using the numerical modulation model. The general consensus is that weak scattering drifts give too large drift effects as follows from the application of numerical drift models when compared to observations from the Earth to the outer heliosphere, and that reduction at E < ~1 GeV is required as originally suggested by Potgieter et al. (1989) and formalized by Burger et al. (2000). Similar approaches were followed in recent work by Vos (2011), Raath (2014) and Ngobeni (2015). It was found that particle drifts cause profound and fundamental changes in the characteristics of the solar modulation of galactic electrons. However, drifts for electrons extend down to only ~100 MeV, because below this energy the diffusion process dominates the transport of these particles as originally reported by Potgieter (1996). Studying electron modulation, ways of reducing drifts explicitly and implicitly, were investigated and illustrated, and the consequences were discussed. It was then concluded that reducing drifts implicitly is far more a subtle process than the strong-handed approach of decreasing the drift coefficient directly. Enlarging the rigidity dependence of the drift coefficient at lower energies reduces very effectively the extent to which drifts dominate the modulation process. Drifts effects also subside with increasing energy throughout the heliosphere for both HMF polarities. The issue pertaining to how drift reduction occurs from a fundamental theoretical

point of view is a work in progress and beyond the scope of this work. For a recent discussion of this issue, see Ngobeni and Potgieter (2015).

Aspects of galactic electron modulation in the heliosheath were addressed by comparing Voyager 1 observations and modeling results. It was found that this region affects the transport of these electrons quite differently than in the rest of the heliosphere, especially below 100 MeV. This became evident when Voyager 1 crossed the HP in August 2012. The heliosheath clearly acts as a modulation barrier for GCRs in general; the extent of the effect depends on the energies considered. At lower energies (1-100 MeV), and especially for galactic electrons, the effect becomes quite spectacular. Reducing the width of the heliosheath decreases the amount of modulation in the outer heliosphere significantly. See also the work of Manuel et al. (2015) on how the time-dependence of the heliosheath width affects proton modulation over an 11-year cycle.

Finally, the combined modulation of Jovian and galactic electron were computed with the first objective to determine the energy range where the Jovian electrons may dominate in the inner heliosphere. Secondly, the intensity that galactic electrons could have at Earth, being predicted from a spectra point of view as motivated by the PAMELA observations in 2009 and the Voyager 1 observations close to the Earth in 1977.

The main results and conclusions of this study are:

- Concerning the applicability of heliospheric diffusion theory for low-energy electrons, a robust conclusion is drawn. It is evident that the basic theoretical prediction that the diffusion process for electrons is independent of energy below ~ 0.5 GeV and above ~ 0.001 GeV is essentially correct, and this is also applicable to the heliosheath. Applying this in the model is the only way how the Voyager 1 electron spectra observed between 6 to ~100 MeV at 110 AU, 119 AU and 122 AU could be reproduced while reproducing the PAMELA spectra observed between ~80 MeV and 50 GeV at Earth.
- The mentioned two HPS were implemented in the modulation model and evaluated specifically a low energies (E < ~100 MeV). First, it must be emphasized that it is now firmly established that the electron HPS follows a power law shape at these energies, as determined by Potgieter and Nndanganeni (2013a, b). It was found that both HPS could reproduce the observed Voyager 1 spectra so that it was not possible to distinguish between the two, primarily limited by the accuracy of the observational data. However, preference is given to the HPS indicated as $\mathrm{HPS}\left(E^{-1.55}\right)$. This is also the preference of Bisschoff and Potgieter

(2014) who studied electron modulation from a galactic propagation point of view. A similar electron HPS was found by Potgieter et al. (2015).

- With the HPS established, electron spectra from 50 GeV down to 1 MeV were computed from the inner to the outer heliosphere to establish how the total modulation of electrons evolves over a distance of 122 AU from the Sun. Comparison between these computed electron spectra for the outer heliosphere and Voyager 1 observations, required the use of a modified set of diffusion coefficients in the 3D model. The rigidity dependence of previously used diffusion coefficients could be simplified while maintaining the basics of turbulence theory applied to heliospheric conditions. The observed electron spectrum for 2009 from PAMELA at the Earth was also reproduced from 50 GeV down to 80 MeV. This study therefore reported on the total modulation of galactic electrons, using a well motivated HPS or very LIS.
- Concerning electron modulation in the heliosheath, the Voyager spacecraft returned some unexpected observations such as the strength of the TS and its varying position and eventually the location of the HP which was predicted much further out by MHD models.

(1) The modulation effects of varying the extent of the heliosheath by changing the location of the TS, the position of the HP and the value of the HPS were illustrated. Then the conclusion was made that modifying the spectral index of the HPS as mentioned above changes the radial profile quantitatively but not qualitatively. (2) The model reproduced Voyager 1 spectra observed between 110 AU and 122 AU in detail as long as the HPS has a simple power law form below ~0.8 GeV and the diffusion coefficients are independent of rigidity at these low energies, as predicted by turbulence theory. (3) To reproduce the significant increase in the observed intensities beyond the TS by Voyager 1, a significant drop in the diffusion coefficients is required. From a global modulation point of view, this implies that the turbulence beyond the TS and inside the heliosheath must be different from upstream of the TS, causing the diffusion coefficients in the process to drop significantly over the TS to stay smaller up to the HP, where it must increase to match the very local interstellar values (see e.g. Lou et al. 2015).

- Two new Jovian electron source functions were determined by comparing modeling with observations and subsequently applied in the model. From this study it became clear that: (1) The reliability of these low energy electron observations severely hampered a conclusive finding about what exactly the spectral slope of this source function could be and especially how it subsides with increasing energy. (2) That the slope with which the source function

decreases as the electron energy increases, typically between 1 and 30 MeV, plays an important role in determining the energy range over which the Jovian electrons could dominate over the galactic electrons in the innermost heliosphere. In one case the range stretch up to only ~20 MeV and in the other case up to ~50 MeV. Because of the complexity and reliability of low energy electron observations and other phenomena that may influence these observations, there is not a compelling reason to choose amongst the three source functions, but to illustrate their effects on modulation in the inner heliosphere. Preference was given to the source function indicated as $\left(j_{\text{alternative2}}\right)$ simply because it was based on recently obtained Voyager 1 data for 1977 (Webber 2015, private communication). According to this scenario Jovian electron intensity could dominate in the inner heliosphere only up to ~25 MeV above which the contribution from galactic electrons becomes progressively larger. This value is lower than what was previously reported e.g. by Ferreira et al. (2002) and recently by Strauss et al. (2013). The discrepancy between the Voyager 1 data and the observations reported by Moses (1987) needs to be further investigated.

- Investigating ways of reducing drifts explicitly and implicitly was done and it was found that the ratio $K_{\perp r} / K_{\parallel}$ plays an important role in the implicit reduction of drift effects. This ratio should be between 0.005 and 0.05; making it any larger easily produces too little modulation in the inner heliosphere. Conceptually this means that when the intensity gradients get smaller, the modulation between the HPS and the spectrum at Earth becomes less, so that drift effects become reduced. Making this ratio smaller enhances drift effects, that is, without touching the drift coefficient.
- The effects of enhancing $K_{\perp\theta}$, the diffusion coefficient perpendicular to the HMF in the polar direction, were also investigated, and it was found that its enhancement is one of the most effective ways of reducing drift effects, in particular over the polar regions of the inner heliosphere, but not in the middle to the outer heliosphere. A similar conclusion was made by Ngobeni and Potgieter (2015) who studied galactic cosmic ray Carbon.
- The choice of Jovian source function, a HPS and the choice of DCs influence the total modulation that occurs between the Earth and the heliospheric boundary. Observationally the galactic electron intensity below ~50 MeV is not known at Earth because of the dominance of the Jovian electrons at these energies in the inner heliosphere. This has been improved by making use of the modeling results, and it was found that the observations in the energy range between 16 MeV and 40 MeV at Earth could be interpreted as of galactic of origin, as the slope of the HPS is reproduced. The model was subsequently used to make estimates of

the galactic intensity at Earth; at 1 MeV a differential intensity of 5.5 electrons m^{-2} s^{-1} sr^{-1} MeV^{-1} is predicted, based on modeling the 2009 PAMELA electron spectrum, but if the 1977 Voyager 1 observations were considered, this value could be as high as 20 electrons m^{-2} s^{-1} sr^{-1} MeV^{-1}.

The following aspects of the comprehensive modeling of electron modulation, to mention only a few, are considered to be beyond the scope of the present study and will need further investigation:

- Implementing diffusion coefficients and a drift coefficient in the model based on basic turbulence theory to study modulation effects over a full solar activity cycle in order to establish to what extent such an approach is an improvement over the more phenomenological approach followed here and by many others.
- The approach followed here did not consider the re-acceleration of galactic electrons at the TS which is an aspect that needs a thorough investigation. It is not to say that diffusive shock acceleration at the TS does not influence these low energy electrons, as illustrated by Langner et al. (2004). Studies in this regard, using a completely different modulation code, have been started by Prinsloo (2015).
- New modeling studies are required for the HP region, which seems to create a relatively large modulation barrier, highly dependent on the energies considered. This could be used as a platform for understanding how come these low energy electrons in the inner heliosheath seem to be affected somewhat differently than in the rest of the heliosphere. This relates to how turbulence in the heliosheath region actually evolves.
- A time dependent 3D model should be used to do a study of the Voyager 2 electron observations in the inner heliosheath which seems to vary far more with time than the Voyager 1 observations. This is the reason why the present steady state approach is not suited for comparison with Voyager 2 electron observations. Informative studies for protons were performed by Manuel et al. (2014, 2015) with a 2D model. In this context the use of very stable SDE based 3D models (e.g. Lou et al. 2015) could be a huge step forward.

References

Adriani, O., Barbarino, G. C., Bazilevskaya, G. A., et al., The PAMELA Space Mission, Nuc. Phys. B Proc. Supp., 188, 296-298, 2009.

Adriani, O., Barbarino, G. C., Bazilevskaya, G. A., et al., Cosmic- ray electron flux measured by the PAMELA experiment between 1 and 625 GeV, Phys. Rev. Lett. 106, 201101:1-5, 2011.

Adriani, O., Barbarino, G. C., Bazilevskaya, G. A., et al., Time dependence of the proton flux measured by PAMELA during the 2006 July -2009 December solar minimum, Astrophys. J., 765, 91:1-8, 2013.

Adriani, O., Barbarino, G. C., Bazilevskaya, G. A., et al., The PAMELA Mission: Heralding a new era in precision cosmic ray physics, Phys. Rep., 544, 323-370, 2014.

Adriani, O., Barbarino, G. C., Bazilevskaya, G. A., et al., Time dependence of the e^- flux measured by PAMELA during the July 2006- December 2009 solar minimum, Astrophys. J., 810, 142:1-13, 2015.

Aguilar, M, Aisa, D., Alvino, A., et al., Electron and positron fluxes in primary cosmic rays measured with the Alpha Magnetic Spectrometer on the international Space Station., Phys. Rev., Lett., 113, 121102, 2014.

Alcaraz, J., Alvisi, D., Alpat, B., et al., Protons in the near Earth orbit, Phys. Lett., 472, 215-226, 2000.

Baker, D. N., and Van Allen, J. A., Energetic electrons in the Jovian magnetosphere, J. Geophys. Res., 81, 617-632, 1976.

Balogh, A., and Smith, E. J., The heliospheric magnetic field at solar maximum: Ulysses observations, Space Sci. Rev., 97, 147-160, 2001.

Balogh, A., and Erdõs, G., The heliospheric magnetic field, Space Sci. Rev., 176, 177-215, 2013.

Balogh, A., Smith, E. J., Tsurutani, B. T., et al., The heliospheric magnetic field over the south polar region of the Sun, Science, 268, 1007-1010, 1995.

Bazilevskaya, G. A., Cliver, E. W., Gennady, A., et al., Solar cycle in the heliosphere and cosmic rays, Space Sci. Rev., 409-435, 2015.

Bieber, J. W., Matthaeus, W. H., Smith, C. W., et al., Proton and electron mean free paths: The Palmer consensus revisited, Astrophys. J., 420, 294-306, 1994.

Bieber, J. W., and Matthaeus, W. H., Perpendicular diffusion and drift at intermediate cosmic ray energies, Astrophys. J., 485, 655ï 659, 1997.

Bieber, J. W., Transport of charged particles in the heliosphere: Theory, Adv. Space, Res., 32, 549-560, 2003.

Bisschoff, D., and Potgieter, M. S., Implications of Voyager 1 observations beyond the heliopause for the local interstellar electron spectrum, Astrophys. J., 749,166:1-9, 2014.

Boezio, M., Pearce, M., Picozza, P., et al., PAMELA and indirect dark matter searches, New J. Phys., 11, 105023: 1-25, 2009.

Boezio, M., Adriani, O., Barbarino, G. C., et al., The cosmic ray electron flux measured by the PAMELA experiment between 1 and 625 GeV, Phys. Rev. Lett., 106, 201101:1-5, 2011.

Burger, R. A., and Potgieter, M. S., The calculation of neutral sheet drift in two-dimensional cosmic ray modulation models, Astrophys. J., 339, 501-511, 1989.

Burger, R. A., and Visser, D. J., Reduction of drifts effects due to solar wind turbulence, Astrophys. J., 725, 1366ï 1372, 2010.

Burger, R. A., Potgieter, M. S., and Heber, B., Rigidity dependence of cosmic ray proton latitudinal gradients measured by the Ulysses spacecraft: Implications for the diffusion tensor, J. Geophys. Res., 105, 27447-27455, 2000.

Burger, R. A., Kruger, T. P. J., Hattingh, M., et al., A Fisk-Parker hybrid heliospheric magnetic field with a solar cycle dependence, Astrophys. J., 674, 511-519, 2008.

Burlaga, L. F., and Ness, N. F., Large-scale distant heliospheric magnetic field: Voyager 1 and 2 observations from 1986 through 1989, J. Geophys. Res., 98, 17451-17460, 1993.

Burlaga, L. F., and Ness, N. F., Interstellar magnetic field observed by Voyager 1 beyond the heliopause, Astrophys J., Lett., 795, L19:1-5, 2014a.

Burlaga, L. F., and Ness, N. F., Voyager 1 observations of the interstellar magnetic field and the transition from the heliosheath, Astrophys. J., 784, 146:1-14, 2014b.

Burlaga, L. F., Ness, N. F., and Stone, E. C., Magnetic field observations as Voyager 1 entered the heliosheath depletion region, Science, 341, 147-150, 2013.

Burlaga, L. F., Ness, N. F., Florinski, V., and Heerikhuisen, J., Magnetic field fluctuations observed in the heliosheath and interstellar magnetic field by Voyager 1 at 115.7-124.9 AU during 2011-2013, Astrophys. J., 792, 134:1-10, 2014.

Caballero-Lopez, R. A., Moraal, H., and McDonald, F. B., The modulation of galactic electrons in the heliosheath, Astrophys. J., 725, 121-127, 2010.

Carlson, P. A., Centuary of cosmic rays, Phys. Today., 65, 30-36, 2012.

Chenette, D. L., Colon T. F., and Simpson, J. A., Burst of relativistic electrons from Jupiter observed in interplanetary space with the time variation of the planetary rotation period, J. Geophys. Res., 79, 3551-3558, 1974.

Chenette, D. L., The propagation of Jovian electrons to Earth, J. Geophys. Res., 85, 2243-2256, 1980.

Clette, F., Svalgaard, L., Vaquero, J. M., and Cliver, E. W., Revisiting the Sunspot number: A 400 year perspective on the solar cycle, Space Sci. Rev., 53, 35-103, 2015.

Cline, T. L, Ludwig, G. H., and McDonald, F. B., Detection of interplanetary 3 to 12 MeV electrons, Phys. Rev. Lett.,13, 786-789, 1964.

Cliver, E. W., Solar energetic particles: Acceleration and transport, Proc. 26th Inter. Cosmic Ray Conf. (Salt Lake city, Utah, USA), 516, 103-119, 2000.

Cliver, E. W., History of research on solar energetic particle (SEP) events: The evolving paradigm, Proc. IAU Symp., 257, 401-412, 2008.

Cliver, E. W., Richardson, I. G., Ling, A. G., Solar drivers of 11-yr and long term cosmic ray modulation, Space Sci. Rev., 176, 3-19, 2013.

Cliver, E. W., The extended cycle of solar activity and the Sunôs 22-year magnetic cycle, Space Sci. Ser., 53, 169-189, 2015.

Colon, T. F., and Simpson, J. A., Modulation of Jovian electron intensity in interplanetary space by corotating interaction regions, Astrophys. J., 211, L45-L49, 1977.

Cranmer, S. R., Self-consistent models for the solar wind, Space Sci. Rev., 172, 145-156, 2012.

Cranmer, S. R., van Ballegooijen, A., and Richard, E. J., Self-consistent coronal heating and solar wind acceleration from anisotropic magnetohydrodynamic turbulence, Astrophys. J. Supp. Series, 171, 520-551, 2007.

De Simone, N., Di Felice, V., Gieseler, J., et al., Latitudinal and radial gradients of galactic cosmic ray protons in the inner heliosphere -PAMELA and Ulysses observations, Astrophys. Space Sci. Trans., 7, 425-434, 2011.

del Peral, L., Gómez-Herrero, R., Rodriguez-Frias, M. D., et al., Jovian electrons in the heliosphere: New insights from EPHIN on board SOHO, Astropart. Phys., 20, 235-245, 2003.

Dröge, W., Particle scattering by magnetic field, Space Sci. Rev., 93, 121-151, 2000.

Dröge, W., Probing heliospheric diffusion coefficients with solar energetic particles, Adv. Space Res., 35, 532-542, 2005.

Dunzlaff, P., Kopp, A., and Heber, B., Propagation of Jovian electrons jets in heliospheric flux tube structure, J. Geophys. Res., 115, A10106:1-15, 2010.

Dunzlaff, P., Heber, B., and Kopp, A., Ulysses observations of Jupiterôs 10 h modulation in interplanetary space in 2004, J. Geophys. Res., 118, 4021-4032, 2013.

Earl, J. A., The diffusive idealization of charged particle transport in random magnetic fields, Astrophys. J., 193, 231-242, 1974.

Effenberger, F., Fichtner, H., Scherer, K., A generalized diffusion tensor for fully anisotropic diffusion of energetic particles in the heliospheric magnetic field, Astrophys. J., 750, 108: 1-8, 2012.

Engelbrecht, N. E., On the heliospheric diffusion tensor and its effect on the 26-day recurrent cosmic ray variations, M.Sc. dissertation, North-West University, South Africa, 2008.

Engelbrecht, N. E., On the development and applications of three-dimensional ab initio cosmic ray modulation model, Ph.D. thesis, North-West University, South Africa, 2012.

Engelbrecht, N. E., and Burger, R. A., An ab initio model for cosmic ray modulation, Astrophys. J., 772, 46:1-12, 2013a.

Engelbrecht, N. E., and Burger, R. A., An ab initio model for the modulation of galactic cosmic ray electrons, Astrophys. J., 779, 158:1-14, 2013b.

Eraker, J. H., Origins of the low-energy relativistic interplanetary electrons, Astrophys. J., 257, 862-880, 1982.

Eraker, J. H., and Simpson, J. A., Jovian electron propagation close to the Sun (< 0.5 AU) Astrophys. J., 232, L131-L134, 1979.

Evenson, P., and Clem, J., Observations of cosmic ray electrons and positrons during the early stages of the A- magnetic polarity epoch, J. Geophys. Res., 109, A07107:1-4, 2004.

Evenson, P., and Clem, J., Cosmic ray electron spectrum in 2009, Proc. 32nd Inter. Cosmic Ray Conf., (Beijing, China),11, 52-56, 2011.

Evenson, P., Meyer, P., and Nandkumar, R., The energy spectrum of cosmic ray electrons 5-150 MeV in late 1978 and early 1979, Proc. 16th Inter. Cosmic Ray Conf. (Kyoto, Japan), 1, 462-466, 1979.

Evenson, P., Garcia-Munoz, M., Meyer, P., A quantitative test of solar modulation theory: the proton, helium and electron spectra from 1965 through 1979, Astrophys. J., 275, L15-L18, 1983.

Fahr, H. J., Kausch, T., and Scherer, H., A 5-fluid hydrodynamic approach to model the solar system-interstellar medium interaction, Astron. Astrophys., 357, 268-282, 2000.

Ferrando, P., Müller-Mellin, R., Sierks, H., The Kiel electron telescope on board Ulysses, Proc. 22nd Inter. Cosmic Ray Conf. (Dublin, Ireland), 3, 366-369, 1991.

Ferrando, P., Ducros, R., Rastoin, C., and Raviart, A., Jovian electron jets in interplanetary space, Plan. Space Sci., 41, 839-843, 1993.

Ferreira, S. E. S., The heliospheric transport of galactic cosmic ray and Jovian electrons, Ph.D. thesis, Potchefstroom University, South Africa, 2002.

Ferreira, S. E. S., The transport of galactic and Jovian cosmic ray electrons in the heliosphere, Adv. Space Res., 35, 586-596, 2005.

Ferreira, S. E. S., and Potgieter, M. S., The modulation of 4-16 MeV electrons in the outer heliosphere: Implications of different local interstellar spectra, J. Geophys. Res., 107, SSH 12:1-10, 2002.

Ferreira, S. E. S., and Potgieter, M. S., Modulation over a 22-year cosmic ray cycle: on the tilt angles of the heliospheric current sheet. Adv. Space Res., 32, 657-662, 2003.

Ferreira, S. E. S., and Potgieter, M. S., Galactic cosmic rays in the heliosphere, Adv. Space Res., 34, 115-125, 2004a.

Ferreira, S. E. S., and Potgieter, M. S., Long-Term cosmic-ray modulation in the heliosphere, Astrophys. J., 603, 744-752, 2004b.

Ferreira, S. E. S., and Scherer, K., Time evolution of galactic and anomalous cosmic ray spectra in a dynamic heliosphere, Astrophys. J., 642, 1256-1266, 2006.

Ferreira, S. E. S., Potgieter, M. S., Burger, R. A., and Heber, B., Modulation effects of anisotropic perpendicular diffusion on cosmic ray electron intensities in the heliosphere, J. Geophys. Res., 105, 305-314, 2000.

Ferreira, S. E. S., Potgieter, M. S., Burger, R. A., et al., Modulation of Jovian and galactic electrons in the heliosphere 1. Latitudinal transport of few MeV electrons, J. Geophys. Res., 106, 979-987, 2001a.

Ferreira, S. E. S., Potgieter, M. S., Burger, R. A., et al., Modulation of Jovian and galactic electrons in the heliosphere: 2 Radial transport of few MeV electrons, J. Geophys. Res., 106, 313-321, 2001 a.

Ferreira, S. E. S., Potgieter, M. S., Heber, B., et al., Transport of a few-MEV jovian and galactic electrons at solar maximum, Adv. Space Res., 32, 669-674, 2003a.

Ferreira, S. E. S., Potgieter, M. S., and Heber, B., Particle drift effects on cosmic ray modulation during solar maximum, Adv. Space Res., 32, 645-650, 2003b.

Ferreira, S. E. S., Potgieter, M. S., Heber, B., et al., Charge-sign dependent modulation in the heliosphere over a 22-year cycle, Ann. Geophys., 21, 1359-1366, 2003c.

Ferreira, S. E. S., Potgieter, M. S., and Lopate, C., Effects of the termination shock on 16 MeV electron modulation, Proc. Conf. 27th ICRC, Hamburg, Germany, 2001c.

Ferreira, S. E. S., Potgieter, M. S., and Webber, W. R., Modulation of low energy cosmic ray electrons in the outer heliosphere, Adv. Space Res., 34, 126-131, 2004.

Fichtner, H., Anomalous cosmic rays: Messengers from the outer heliosphere, Space Sci. Rev., 95, 639-754, 2001.

Fichtner, H., Potgieter, M. S., Ferreira, S. E. S., et al., On the propagation of Jovian electrons in the heliosphere: transport modeling in 4-D phase space, Geophys. Res. Lett., 27, 1611-1414, 2000.

Fichtner, H., Potgieter, M. S., Ferreira, S. E. S., et al., Time dependent 3D modeling of the heliospheric propagation of few-MeV electrons, Proc. 27th Inter. Cosmic Ray Conf. (Hamburg, Germany), 8, 3666-3669, 2001.

Fisk, L. A., Solar modulation of galactic cosmic rays, 2, J. Geophys. Res., 76, 221-226, 1971.

Fisk, L. A., Solar modulation of galactic cosmic rays. IV. Latitude-dependent modulation, J. Geophys. Res., 81, 4646-4650, 1976.

Fisk, L. A., Motion of the footprints of heliospheric magnetic field lines at the Sun: Implications for recurrent energetic particle events at high heliographic latitudes, J. Geophys. Res., 101, 15547-15553, 1996.

Fisk, L. A., and Gloeckler, G., On whether or not Voyager 1 has crossed the heliopause, Astrophys. J., 789, 41:1-9, 2014.

Fisk, L. A., Gloeckler, G., The global configuration of the heliosheath inferred from recent Voyager 1 observations, Astrophys. J., 776,79:1-10, 2013.

Fisk, L. A., Kozlovsky, B., and Ramaty, R., An interpretation of the observed Oxygen and Nitrogen enhancements in low-energy cosmic rays, Astrophys. J., 190, L35-L37, 1974.

Florinski, V., On the transport of cosmic rays in the distant heliosheath, Adv. Space Res., 48, 308-313, 2011.

Flückiger, E. O., and Bütikofer, R., Swiss neutron monitors and cosmic ray research at Jungfraujoch, Adv. Space Res., 44, 1155-1159, 2009.

Fujii, Z., and McDonald, F. B., Study of the properties of the step decreases in galactic and anomalous cosmic rays over solar cycle 21, J. Geophys. Res., 100, 17043-17052, 1995.

Gaggero, D., Maccione, L., Grasso, D., et al., Three dimensional modeling of CR propagation, arxiv:1306.6850[astro-ph.HE], 2013.

Gaggero, D., Maccione, L., Grasso, D., et al., PAMELA and AMS-02 e+ and eī spectra are reproduced by three-dimensional cosmic-ray modeling, Phys. Rev., 8, 0083007:1-9, 2014.

Garcia-Munoz, M., Mason G. M., and Simpson, J. A., The abundance of galactic cosmic ray carbon, Nitrogen and Oxygen and their astrophysical implications, Astrophys. J. Lett., 184, 967-994, 1973.

Giacalone, J., Drake, J. F. and Jokipii, J. D., The acceleration mechanism of anomalous cosmic rays, Space Sci. Rev., 173, 283-307, 2012.

Gil, A., and Alania, M. V., 27 day variations of cosmic rays or the minima epochs of solar activity: Experimental and 3-D drift modeling results, Proc. 27th Inter. Cosmic Rays Conf. (Hamburg, Germany), 9, 3725-3728, 2001.

Gleeson, L. J., and Axford, W. I., Cosmic ray in the interplanetary medium, Astrophys. J. Lett., 149, L115-L118, 1967.

Gleeson, L. J., and Axford, W. I., The Compton-Getting effect, Astrophys. Space Sci., 2, 431-440, 1968.

Gloeckler, G., and Fisk, L. A., A test whether or not Voyager 1 has crossed the heliopause, Geophys. Res. Lett., 41, 5325-5330, 2014.

Gómez-Herrero, R., Rodriguez-Frias, M. D., del Peral, L., et al., Quite-time periods observed by EPHIN/SOHO during the minimum of the 22nd solar cycle, Solar Phys., 194, 405-413, 2000.

Gómez-Herrero, R., Rodriguez-Frias, M. D., del Peral, L., et al., Heliospheric electrons from Jupiter, Proc. 27th Inter. Cosmic Ray Conf. (Hamburg, Germany), 3601-3604, 2001.

Guo, X., and Florinski, V., Galactic cosmicï ray modulation near the heliopause, Astrophys. J., 793, 1-18, 2014.

Gurnett, D. A., Kurth, W. S., Burlaga, L. F., and Ness, N. F., In situ observations of interstellar plasma with Voyager 1, Science, 341, 1489-1492, 2013.

Haasbroek, L. J., The transport and acceleration of charged particles in the heliosphere, Ph.D. thesis, Potchefstroom University, South Africa, 1997.

Haasbroek, L. J., and Potgieter, M. S., The modulation of cosmic rays in the high latitude heliosphere: A computer simulation, Space Sci. Rev., 72, 385-390, 1995.

Hamilton, D. C., and Simpson, J. A., Jovian electron propagation out of the solar equatorial plane-Pioneer 11 observations, Astrophys. J., 228, L123-L127, 1979.

Hasselmann, K., and Wibberenz, G., A note on the parallel diffusion coefficient, Astrophys. J., 162, 1049-1051, 1970.

Hathaway, D. H., The solar cycle, Living Rev. Solar Phys., 7, 1-65, 2010.

Hattingh, M., The modulation of galactic cosmic rays in a three-dimensional heliosphere, Ph.D. thesis, Potchefstroom University, South Africa, 1998.

Heber, B., Cosmic rays through the solar hale cycle: Insight from Ulysses, Space Sci. Rev., 176, 265-278, 2013.

Heber, B., and Marsden, R. G., Cosmic ray modulation over the poles at solar maximum: observations, Space Sci. Rev., 97, 309-319, 2001.

Heber, B., and Potgieter, M. S., Cosmic rays at high heliolatitudes, Space Sci. Rev., 127, 117-194, 2006.

Heber, B., Potgieter, M. S., Galactic and anomalous cosmic rays through the solar cycle: New insights from Ulysses, the Heliosphere through the Solar Activity Cycle, Springer Praxis Books. Praxis Publishing Ltd, Chichester, UK, 195, 2008.

Heber, B., Ferrando, P., Raviart, A., Propagation of 3-10 MeV electrons in the inner heliosphere: Ulysses observations, Adv. Space Res., 27, 547-552, 2001.

Heber, B., Sarri, G., Wibberenz, G., et al., The Ulysses fast latitude scans: COSPIN/KET results, Ann. Geophys., 21, 1275-1288, 2003a.

Heber, B., Ferrando, P., Raviart, A., et al., Quite time MeV electron increases at solar maximum: Ulysses COSPIN/KET observations, Adv. Space Res. 32, 663-668, 2003b.

Heber, B., Potgieter, M. S., Ferreira, S. E. S., et al., An overview of Jovian electrons during the distant Ulysses Jupiter flyby, Planet. Space Sci., 55, 1-11, 2007.

Heber, B., Kopp, A., Gieseler, J., et al., Modulation of galactic cosmic ray protons and electrons during an unusual solar minimum, Astrophys. J., 699, 1956-1963, 2009.

Hoeksema, J. T., Large structure of heliospheric magnetic field: 1976-1991, Solar wind Seven Colloquium, 191-196, 1992.

Intriligator, D. S., and Webber, W. R., Voyager 1 and 2 in a shrunken and squashed heliosphere, J. Geophys. Res., 116, 06105:1-8, 2011.

Jokipii, J. R., Cosmic-ray propagation. I. Charged particles in a random magnetic field, Astrophys. J., 146, 480-487, 1966.

Jokipii, J. R., Propagation of cosmic rays in the solar wind, Rev. Geophys. Space Phys., 9, 27-87, 1971.

Jokipii, J. R., and Kopriva, D. A., Effects of particle drift on the transport of cosmic rays. III. Numerical model of galactic cosmic-ray modulation, Astrophys. J., 234, 384-392, 1979.

Jokipii, J. R., and Kóta, J., Effects of drift on the transport of cosmic rays. IV: A three dimensional model including diffusion, Astrophys. J., 265, 573-581, 1983.

Jokipii, J. R., and Kóta, J., The polar heliospheric magnetic field, Geophys. Res. Lett., 16, 1-4, 1989.

Jokipii, J. R., Levy, E. H., and Hubbard, W. B., Effects of particle drift on cosmic-ray transport. I. General properties, application to solar modulation, Astrophys. J., 213, 861-868, 1977.

Jokipii, J. R., and. Parker, E. N., On the convection, diffusion, and adiabatic deceleration of cosmic rays in the solar wind, Astrophys. J., 160, 735ï 744, 1970.

Jokipii, J. R., Kóta, J., and Merényi, E., The gradient of galactic cosmic rays at the solar wind termination shock, Astrophys. J., 405, 782-786, 1993.

Jokipii, J. R., and Thomas, B., Effects of drift on the transport of cosmic rays. IV. Modulation by a wavy interplanetary current sheet, Astrophys. J., 243, 1115-1122, 1981.

Jones, F. C., and Ellison, D. C., the plasma physics of shock acceleration, Space Sci. Rev., 58, 259-346, 1991.

Jones, H. P., Chapman, G. A., Harvey, K. L., et al., A comparison of feature classification methods for modeling solar irradiance variation**,** Solar Phys.**,** 248, 323-337, 2008.

Kissmann, R., PICARD: A novel code for the galactic cosmic ray propagation problem, Astropart. Phys., 55, 37-50, 2014.

Klecker, B., Kunow, H., Cane, H. V., Energetic particle observations, Space Sci. Rev., 123, 217-250, 2006.

Kopp, A., Büsching, I., Strauss, R. D., et al., A stochastic differential equation code for multidimensional Fokker-Planck type problems, Comp. Phys. Comm., 183, 530-542, 2012.

Kopp, A., Büsching, I., Strauss, R. D., et al., A stochastic approach to galactic proton propagation: Influence of the spiral arm structure, New Astron., 30, 32-37, 2014.

Kóta, J., Theory and modeling of galactic cosmic rays: trends and prospects, Space Sci., Rev., 176, 391-403, 2013.

Kóta, J., and Jokipii, J. R., Effects of drift on the transport of cosmic rays VI: A three dimensional model including diffusion, Astrophys. J., 265, 573-581, 1983.

Kóta, J., and Jokipii, J. R., Are cosmic rays modulated beyond the heliopause? Astrophys. J., 782, 24-29, 2014.

Krimigis, K. S., Roelof, E. C., Decker, R. B., and Hill, M. E., Zero outward flow velocity for plasma in a heliosheath transition layer, Nature., 477, 359-361, 2011.

Krimigis, S. M., Decker, R. B., Roelof, E. C., et al., Search for the exit: Voyager 1 at heliosphere border with the galaxy, Science, 341, 144-147, 2013.

Kühl, P., Dresing, N., Dunzlaff, P., et al., Spectrum of galactic and Jovian electrons, Proc. 33rd Inter. Cosmic ray Conf. (Rio de Janeiro, Brazil), icrc2013-0072, 2013.

LõHeureux, J. and Meyer, P., Quite-time increases of low-energy electrons: The Jovian origin, Astrophys. J., 209, 955-960, 1976.

LõHeureux, J., Fan, C. Y., and Meyer, P., The quite time spectra of cosmic ray electrons of energies between 10 and 200 MeV observed on OGO-V, Astrophys. J., 171:363-376, 1972.

Langner, U. W, The effects of the termination shock acceleration on cosmic rays in the heliosphere, Ph.D. thesis, Potchefstroom University, South Africa, 2004.

Langner, U. W., and Potgieter, M. S., Heliospheric modulation of cosmic ray positrons and electrons: Effects of the heliosheath and the solar wind termination shock, Astrophys. J., 602, 993-1001, 2004.

Langner, U. W., de Jager, O. C., and Potgieter, M. S., On the local interstellar spectrum for cosmic ray electrons, Adv. Space Res., 27, 517-522, 2001.

Langner, U. W., Potgieter, M. S., and Webber, W. R., Modulation of cosmic ray protons in the heliosheath, J. Geophys. Res., 108, A10:1-9, 2003.

Langner, U. W., Potgieter, M. S., and Webber, W. R., Modelling of barrier modulation for cosmic ray protons in the outer heliosphere, Adv. Space. Res., 34, 138-143, 2004.

Langner, U. W., Potgieter, M. S., Fichtner, H. and Borrmann, T., Effects of different solar wind speed profiles in the heliosheath on the modulation of cosmic ray protons, Astrophys. J., 640, 1119-1134, 2006.

Lapidus, L., and Pinder, G., Numerical solution of partial differential equations in science and engineering, New York: Wiley-Interscience, 1982.

le Roux, J. A., and Potgieter, M. S., The simulation of Forbush decrease with time-dependent cosmic ray modulation models varying complexity, Astron. Astrophys. J., 234, 531-545, 1991.

le Roux, J. A., and Potgieter, M. S., The simulation of complete 11 and 22 year modulation cycles for cosmic ray in the heliosphere using a drift model with global merged interaction regions, Astrophys. J., 442, 847-851, 1995.

le Roux, J. A., and Fichtner, H., The simulation of step decreases in the cosmic ray intensity with a cosmic-ray-hydrodynamic model, Adv. Space Res., 23, 501-504, 1999.

le Roux, J. A., Potgieter, M. S., and Ptuskin, V. S., A transport model for the diffusive acceleration and modulation of anomalous cosmic rays in the heliosphere, J. Geophys. Res., 101, 4791-4804, 1996.

Leske, R. A., Cummings, A. C., Mewaldt, R. A., and Stone E. C., Anomalous and galactic cosmic rays at 1 AU during the cycle 23/24 solar minimum, Space Sci. Rev., 176, 253-263, 2013.

Li, H., Wang, C., and Richardson, J. D., Properties of the termination shock observed by Voyager 2, Geophys. Res. Lett., 35, L19107:1-4, 2008.

Lodders, K., Solar system abundances and condensation temperature of the elements, Astrophys. J., 591, 1220-1247, 2003.

Lopate, C., Jovian and galactic electrons (2-30 MeV) in the heliosphere from 1 to 50 AU, Proc. 22nd Int. Cosmic Ray Conf., (Dublin, Ireland), 2, 149-152, 1991.

Lou, X., Zhang, M., Feng, X., and Mendoza-Torres, J. E., Investigation of the transient cosmic ray decreases observed by voyagers in 2007: A numerical approach, J. Geophys. Res., 118, 7517-7524, 2013.

Lou, X., Zhang, M., Potgieter, M. S., et al., A numerical simulation of cosmic-ray modulation near the heliopause, Astrophys. J., 808, 82: 1- 7, 2015.

Malama, Y. G., Izmodenov, V. V., and Chalov, S. V., Modelling of the heliospheric interface multi-component nature of the heliospheric plasma, Astron. Astrophys. 445, 693-701, 2006.

Malandraki, O. E., Marsden, R. G., Lario, D., Energetic particle observations and propagation in the three-dimensional heliosphere during the 2006 December Events, Astrophys. J., 704, 469-476, 2009.

Manuel, R., Ferreira, S. E. S., and Potgieter, M. S., Time-dependent cosmic ray modulation in the outer heliosphere: Signatures of a heliospheric asymmetry and model predictions along Voyager 1 and Voyager 2 trajectories, Proc. 33rd Inter. Cosmic ray Conf. (Rio de Janeiro, Brazil), icrc2013-0186, 2013.

Manuel, R., Ferreira, S. E. S., and Potgieter, M. S., Time dependent of cosmic rays in the heliosphere, Solar Phys., 289, 2207-2231, 2014.

Manuel, R., Ferreira, S. E. S., Potgieter, M. S., The effects of a dynamic inner heliosheath on cosmic ray modulation, Astrophys. J., 799, 223:1-7, 2015.

Marsden, R. G., The heliosphere after Ulysses, Astrophys. Space Sci., 277, 337-347, 2001.

Marsh, N., and Svensmark, H., Cosmic rays, clouds and climate, Space Sci. Rev., 94, 215-230, 2000.

Matthaeus, W. H., Gray, P. C., Pontius, D. H., et al., Spatial structure and filed line diffusion in transverse magnetic turbulence, Phys. Rev. Lett., 75, 2136-2139, 1995.

Matthaeus, W. H., Qin, G., Bieber, J. W., and Zank, G. P., Nonlinear collisionless perpendicular diffusion of charged particles, Astrophys. J., 590, L53-L56, 2003.

McComas, D. J., Goldstein, R., and Gosling, J. T., Ulyssesô second orbit: Remarkably different solar wind, Space Sci. Rev., 97, 99-103, 2001.

McComas, D. J., Elliot, H. A., Gosling, J. T., et al., Ulyssesô second fast latitude scan: Complexity near solar maximum and the reformation of polar coronal holes, Geophys. Res. Lett., 29, 1-4, 2002.

McComas, D. J., Velli, M., Lewis, W. S., et al., Understanding coronal heating and solar wind acceleration: case for In Situ near-Sun measurements, Rev. Geophys., 45, RG1004: 1-26, 2007.

McComas, D. J., Ebert, R. W., Elliott, H. A., et al., Weaker solar wind from the polar coronal holes and the whole Sun., Geophys Res. Lett., 35, L18103:1-5, 2008.

McComas, D. J., Alexashov, D., Bzowski, M., The heliosphereôs interstellar interaction: No bow shock, Science, 336, 1291-1293, 2012.

McComas, D. J., Alexander, N., Angold, N., Integrated Science Investigation of the Sun (ISIS): Design of the Energetic Particle Investigation, Space Sci. Rev., 177, 4-70, 2014.

McDonald, F. B., Cline, T. L., and Simnett, G. M., Multifarious temporal variations of low energy relativistic cosmic ray electrons, J. Geophys. Res., 77, 2213-2231, 1972.

McDonald, F. B., Heikkila, B., Lal, N., and Stone, E. C., The relative recovery of galactic and anomalous cosmic rays in the distant heliosphere: Evidence for modulation in the heliosheath, J. Geophys. Res., 105, 1-8, 2000.

McDonald, F. B., Klecker, B., McGuire, R. E., et al., Relative recovery of galactic and anomalous cosmic rays in a distant heliosphere: Further evidence for modulation in the heliosheath, J. Geophys. Res., 107, A5:SSH 2-1, 2002.

McDonald, F. B., Webber, W. R., Stone, E. C., et al., Voyager observations of galactic cosmic ray electrons in the heliosheath, EoS trans. AGU., 3992-3995, 2007.

McDonald, F. B., Webber, W. R., Stone, E. C., et al., Galactic cosmic rays in the distant heliosphere, Centenary Symposium 2012, Discovery of Cosmic rays, AIP Conf. Proc., 1516, 85-88, 2013.

McKibben, R. B., Pyle, K. R., and Simpson J. A., Changes in radial gradients of low energy cosmic rays between solar minimum and maximum observations from 1 to 31 AU, Astrophys. J., 289, L35-L39, 1985.

McKibben, R. B., Connell, J. J., Lopate, C., et al., Cosmic ray modulation in the 3D heliosphere, Space Sci. Rev., 72, 367-378, 1995.

McKibben, R. B., Cosmic ray diffusion in the inner heliosphere, Adv. Space Res., 35, 518-531, 2005.

Mewaldt, R. A., Davis, A. J., Lave, K. A., et al., Record setting cosmic rays intensities in 2009 and 2010, Astrophys. J. Lett., 723, L1-L6, 2010.

Mewaldt, R. A., Cosmic rays in the heliosphere: requirements for future observations, Space Sci. Rev., 176, 365-390, 2013.

Minnie, J., Bieber, J. W., Matthaeus, W. H., and Burger, R. A., Suppression of particle drifts by turbulence, Astrophys. J., 670, 1149-1158, 2007.

Mocchiutti., E., Adriani, O., Barbarino, G. C., et al., The PAMELA experiment, arXiv: 0905.225, 2009.

Moeketsi, D. M., Modeling of galactic and Jovian electrons in the heliosphere, M.Sc. dissertation, Potchefstroom University, South Africa, 2004.

Moeketsi, D. M., Potgieter, M. S., Ferreira, S. E. S., et al., The heliospheric modulation of 3-10 MeV electrons: Modeling of changes in the solar wind speed in relation to perpendicular polar diffusion, Adv. Space Res., 35, 597-604, 2005.

Moraal, H., Gleeson, L. J. and Webb, G. M., Effects of charged particle drifts on the modulation of the intensity of galactic cosmic rays, Proc.16th Inter. Cosmic Ray Conf. (Kyoto, Japan), 3, 1-6, 1979.

Moses, D., Jovian electrons at 1 AU, 1978-1984, Astrophys. J., 313, 471-486, 1987.

Moskalenko, I. V., Strong, A. W., Ormes, J. F., and Potgieter, M. S., Secondary antiprotons and propagation of cosmic rays in the galaxy and heliosphere, Astrophys. J., 565, 280-296, 2002.

Ndiitwani, D. C., A study of modulation of galactic time dependent cosmic rays in the heliosphere, M.Sc. dissertation, North-West University, South Africa, 2005.

Ndiitwani, D. C., Ferreira, S. E. S., Potgieter, M. S., and Heber, B., Modelling cosmic ray intensities along the Ulysses trajectory, Ann. Geophys., 23, 1061-1070, 2005.

Ngobeni, M. D., Aspects of the modulation of cosmic rays in the outer heliosphere, M.Sc. dissertation, North-West University, Potchefstroom, South Africa, 2006.

Ngobeni, M. D., Modeling of galactic cosmic rays in the heliosphere, Ph.D. thesis, North-West University, South Africa, 2015.

Ngobeni, M. D., and Potgieter, M. S., The heliospheric modulation of cosmic rays: effects of a latitude dependent solar wind termination shock, Adv. Space Res., 46, 391-401, 2010.

Ngobeni, M. D., and Potgieter, M. S., Modulation of galactic cosmic rays in a north-asymmetrical heliosphere, Adv. Space Res., 48, 300-307, 2011.

Ngobeni, M. D., and Potgieter, M. S., A study of the global heliospheric modulation of galactic carbon, Adv. Space Res., 53, 1634-1646, 2014.

Ngobeni, M. D., and Potgieter, M. S., Modelling the effects of scattering parameters on particle-drift in the solar modulation of galactic cosmic rays, Adv. Space Res., 56, 1525-1537, 2015.

Nkosi, G. S., A study of cosmic ray anisotropies in the heliosphere, M.Sc. dissertation, North-West University, South Africa, 2006.

Nkosi, G. S., Potgieter, M. S., and Ferreira, S. E. S., Electron anisotropies in the inner heliosphere, Planet. Space Sci., 56, 501-509, 2008.

Nkosi, G. S., Potgieter, M. S. and Webber, W. R., Modelling of low energy galactic electrons in the heliosheath, Adv. Space Res., 48, 1480-1489, 2011.

Nndanganeni, R. R., Modelling of galactic cosmic ray electrons in the heliosphere, M.Sc. dissertation, North-West University, South Africa, 2012.

Nndanganeni, R. R., and Potgieter, M. S., The solar modulation of electrons in the heliosphere, In proc. 33rd inter. Cosmic Ray. Conf. (Rio de Janeiro, Brazil), icrc2013-0033, 2013.

Opher, M., Richardson, J. D., Toth, G., et al., Confronting observations and modeling: The role of the interstellar magnetic field in Voyager 1 and 2 asymmetries, Space Sci. Rev., 143, 43-55, 2009.

Opher, M., Drake, J. F., Zieger, B., et al., Magnetized Jets driven by the Sun: the structure of the heliosphere revisited, Astrophys. J. Lett., 800, L28: 1-7, 2015.

Parker, E. N., Dynamics of the interplanetary space and magnetic fields, Astrophys. J., 128, 664-676, 1958.

Parker, E. N., The stellar wind regions, Astrophys. J., 134, 20-27, 1961.

Parker, E. N., Interplanetary dynamic processes, Interscience Publishers, New York, 1963.

Parker, E. N., The passage of energetic charged particles through interplanetary space, Planet. Space Sci., 13, 9-49, 1965.

Pesses, M. E., Jokipii, J. R., and Eichler, D., Cosmic ray drift, shock wave acceleration and the anomalous component of cosmic rays, Astrophys. J., 246, L85-L88, 1981.

Philips, J. L., Bame, J., Barnes, B., et al., Ulysses solar wind plasma observations from pole to pole, Geophys. Res. Lett., 22, 3301-3304, 1995.

Picozza, P., Galper, A. M., Castellini, G., et al. PAMELA: A payload for antimatter matter exploration and light nuclei astrophysics, Astropart. Phys., 27, 296-315, 2007.

Pogorelov, N. V., Zank, G. P., Ogino, T., MHD modeling of the outer heliosphere: achievements and challenges., Adv. Space Res., 41, 306-317, 2008.

Pogorelov, N. V., Heerikhuisen, J., Zank, G. P., et al., Heliospheric asymmetries due to the action of the interstellar magnetic field, Adv. Space Res., 44, 1337-1344, 2009.

Pogorelov, N. V., Sues., S. T., Borovikov, S. N., et al., Three-dimensional features of the outer heliosphere due to coupling between the interstellar and interplanetary magnetic fields. IV. Solar cycle model based on Ulysses observations, Astrophys. J., 772, 1-17, 2013.

Potgieter, M. S., The modulation of cosmic rays as described by the three dimensional drifts model, Ph.D. thesis, Potchefstroom University, South Africa, 1984.

Potgieter, M. S., The long- term modulation of galactic cosmic rays in the heliosphere, Adv. Space Res., 16, 191-203, 1995.

Potgieter, M. S., Heliospheric modulation of galactic electrons: Consequences of new calculations for the mean free path of electrons between 1 MeV and 10 GeV, J. Geophys. Res., 101, 24411-24422, 1996.

Potgieter, M. S., The heliospheric modulation of galactic cosmic rays at solar minimum, Adv. Space Res., 19, 883-892, 1997.

Potgieter, M. S., The modulation of galactic cosmic rays in the heliosphere: Theory and models, Space Sci. Rev., 83,147-158, 1998.

Potgieter, M. S., Heliospheric modulation of cosmic ray protons: Role of enhanced perpendicular diffusion during periods of minimum solar modulation, J. Geophys. Res., 105, A8, 18295-18303, 2000.

Potgieter, M. S., Solar cycle variations and cosmic rays, J. Atmos. Solar Terr. Phys., 70, 207-218, 2008a.

Potgieter, M. S., Challenges to cosmic ray modeling from beyond the solar wind termination shock, Adv. Space Res., 41, 245-258, 2008b.

Potgieter, M. S., The dynamic heliosphere, solar activity and cosmic rays, Adv. Space Res., 46, 402-412, 2010.

Potgieter, M. S. , Solar modulation of cosmic rays, Living Rev. Solar Phys., 10, 1-66, 2013a.

Potgieter, M. S., Cosmic rays in the heliosphere: Insights from observations, theory and Models, Space Sci. Rev., 176, 165-176, 2013b.

Potgieter, M. S., Very local interstellar spectra for galactic electrons, protons and helium, Braz. J. Phys., 44, 581-588, 2014a.

Potgieter, M. S., The charge-sign dependent effect in the solar modulation of cosmic rays, Adv. Space Res., 53, 1415-1425, 2014b.

Potgieter, M. S., and Moraal, H., A drift model for the modulation of galactic cosmic rays, Astrophys. J., 294, 425-440, 1985.

Potgieter, M. S., and le Roux, J. A., A numerical model for a cosmic ray modulation barrier in the outer heliosphere, Astron. Astrophys., 209, 406-410, 1989a.

Potgieter, M. S., and le Roux, J. A., More on a possible modulation barrier in the outer heliosphere, Adv. Space Res., 9, 121-124, 1989b.

Potgieter, M. S., and Ferreira, S. E. S., The importance of perpendicular diffusion in the heliospheric modulation of cosmic ray electrons, Adv. Space Res., 23, 463-466, 1999.

Potgieter, M. S., and Ferreira, S. E. S., Modulation of cosmic rays in the heliosphere: theory and models, Highlight paper of 27th Int. Cosmic Ray Conf. (Hamburg, Germany), 217-225, 2001.

Potgieter, M. S., and Ferreira, S. E. S., Effects of the solar wind termination shock on the modulation of Jovian and galactic electrons in the heliosphere, J. Geophys. Res., 107, SHH1, 2002.

Potgieter, M. S., and Langner, U. W., Heliospheric modulation of cosmic ray positron and electrons: effects of the heliosheath and the solar wind termination shock, Astrophys. J., 602, 2993-1001, 2004.

Potgieter, M. S., and Nndanganeni, R. R., The solar modulation of electrons in the heliosphere, Astrophys. Space Sci., 345, 33-40, 2013a.

Potgieter, M. S., and Nndanganeni, R. R., A local interstellar spectrum for galactic electrons, Astropart. Phys., 48, 25-29, 2013b.

Potgieter, M. S., and Strauss, R., du T., Heliospheric physics: shock acceleration in the heliosphere and the anomalous cosmic rays, Nigerian J. Space Res., 8, 144-160, 2010.

Potgieter, M. S., Le Roux, J. A., and Burger R. A., A numerical model for a cosmic ray modulation barrier in the outer heliosphere, Astron. Astrophys., 209, 406-410, 1989.

Potgieter, M. S., Ferreira, S. E. S., Heber, B., et al., Implications of the heliospheric modulation of cosmic ray electron observed by Ulysses, Adv. Space Res., 23, 467-470, 1999.

Potgieter, M. S., Ferreira, S. E. S., Burger, R. A., Modulation of cosmic rays in the heliosphere from solar minimum to maximum: a theoretical perspective, Space Sci. Rev., 97, 295-307, 2001.

Potgieter, M. S. Vos, E. E., Boezio, M., et al., Modulation of galactic protons in the heliosphere during the unusual solar minimum of 2006 to 2009, Solar Phys., 289, 391-406, 2014a.

Potgieter, M. S., Vos, E. E., Nndanganeni, R. R., The first very local interstellar spectra for galactic protons, helium and electrons. Proc. 14th ICATPP Conference on Cosmic Rays for Particle and Astroparticle Physics, (Como, Italy), 8, 204-211, 2014b.

Potgieter, M. S., Vos, E. E., Boezio, M., et al., Modulation of galactic protons in the heliosphere during the unusual solar minimum of 2006 to 2009, Solar Phys., 289, 391-406, 2014c.

Potgieter, M. S., Vos, E. E., Munini, R., et al., Modulation of galactic electrons in the heliosphere during the unusual solar minimum of 2006 to 2009: A modeling approach, Astrophys. J., 810,141:1-10, 2015.

Prinsloo, L., Acceleration of cosmic rays in the outer heliosphere, M.Sc. dissertation, North-West University, South Africa, 2015.

Ptuskin, V. S., Moskalenko, I. V., Jones, F. C., et al., Dissipation of magnetohydrodynamic waves on energetic particles: The impact on the interstellar turbulence and cosmic ray transport, Astrophys. J., 642, 902-916, 2006.

Quenby, J. J., Lockwood, J. A., and Webber, W. R., Cosmic ray gradient measurements and modulation beyond the inner solar wind termination shock, Astrophys. J., 365-371, 1990.

Raath, J. L., A comparative study of cosmic ray modulation models, M.Sc. dissertation, North-West University, South Africa, 2014.

Raath, J. L., Potgieter, M. S., Strauss, R. D., and Kopp, A., The effects of magnetic field modifications on the modulation of cosmic rays in the heliosphere, arXiv:1506.07305, 2015.

Rastoin, C., Jovian and galactic electrons in the heliosphere: Observations of the KET experiment on board the Ulysses spacecraft, Ph.D. thesis, University of Paris VII, France, 1995.

Reinecke, J. P. L., and Potgieter, M. S., An explanation for the difference in cosmic ray modulation at low and neutron monitor energies during consecutive solar minimum periods, J. Geophys. Res., 99, 14761-14767, 1994.

Richardson, J. D., and Burlaga, L. F., The solar wind in the outer heliosphere and heliosheath, Space Sci. Rev., 176, 217-235, 2011.

Richardson, J. D., Wang, C., and Paularena, K. I., The solar wind: From solar minimum to solar maximum, Adv. Space Res., 27, 427-479, 2001.

Richardson, J. D., Kasper, J. C., Wang, C., et al., Cool heliosheath plasma and deceleration of the upstream solar wind at the termination shock, Nature, 454, 63-66, 2008.

Richardson, J. D., Stone, E. C., Kasper, J. C., et al., Plasma flows in the heliosheath, Geophys. Res. Lett., 36, L10102:1-4, 2009.

Rodriguez, M. D., Gómez-Herrero, R., del Peral, L., et al., Observation with EPHIN/SOHO of electrons during quite time periods, Proc. 1st Solar and Space Weather Euroconf., ESA SP 463, 415-418, 2000.

Scherer, K., and Fichtner, H., The return of the bow shock, Astrophys. J., 782, 1-5, 2014.

Scherer, K., Fichtner, H., Fahr, H. J., and Marsch, E., The outer heliosphere: The Next Frontiers, Edited by Scherer, H., Fichtner, H., and Marsch, E., COSPAR Colloquiua Series, 11, Elsevier Science, 2001.

Scherer, K., Fichtner, H., Borrmann, T., et al., Interstellar terrestrial relations: variable cosmic enviroments the dynmic heliosphere and their imprints on terrrestrial archive and climate, Space Sci. Rev., 127, 327-465, 2006a.

Scherer, K., Ferreira, S. E. S., Potgieter, M. S., and Fichtner, H., Time- and latitude dependence of compression ratio and the injection rate at the heliospheric termination shock, AIP Conf. Proc. 858: Physics of the inner heliosheath, 20-26, 2006b.

Scherer, K., Fichtner, H., Heber, B., Cosmic ray flux at the Earth in a variable heliosphere, Adv. Space Res., 41, 1171-1176, 2007.

Scherer, K., Fitchtner, H., Ferreira, S. E. S., et al., Are anomalous cosmic rays the main contribution to the low energy galactic cosmic ray spectrum? Astrophys. J., 680, L105-L108, 2008.

Scherer, K., Fichtner, H., Strauss, R. D., et al., On cosmic ray modulation beyond the heliopause: Where is the modulation boundary? Astrophys. J., 735, 1-5, 2011.

Schrijver, C. J., Kauristie, K. A., Alan, D., et al., Understanding space weather to shield society: A global road map for 2015-2025 commissioned by COSPAR and ILWS, Adv. Space Res., 55, 12, 2745-2807, 2015.

Schröter, J., Heber, B., Steinhilber, F., and Kallenrode, M. B., Energetic particles in the atmosphere: A Monte-Carlo simulation, Adv. Space Res., 37, 1597-1601, 2006.

Shalchi, A., Extended nonlinear guiding center theory of perpendicular diffusion, Astron. Astrophys., 453, L43-L46, 2006.

Shalchi, A., Nonlinear cosmic ray diffusion theories, Astrophys. Space Sci. Lib., 362, Springer, Berlin, 2009.

Shalchi, A., A unified particle diffusion theory for cross-field scattering: Sub-diffusion, recovery of diffusion and diffusion in three-dimensional turbulence, Astrophys. J., Lett., 720, L127-L130, 2010.

Shea, M. A., and Smart, D. F., Space weather and ground level solar proton events of the 23rd solar cycle, Space Sci. Rev., 171, 161-188, 2012.

Simnett, G. M., and McDonald, F. B., Observations of cosmic ray electrons between 2.7 MeV and 21.5 MeV, Astrophys. J., 157, 1435-1448, 1969.

Simpson, J. A., Hamilton, D., Lentz, G., et al., Protons and electrons in Jupiterôs magnetic field: Results from the university of Chicago experiment on Pioneer 10, Science, 183, 306-309, 1974.

Simpson, J. A., Smith, D. A., and Zhang, M., Jovian electron propagation in three dimensions of the heliosphere: The Ulysses investigation, J. Geophys. Res., 98, 21129-21144, 1993.

Simpson, J. A., The cosmic radiation: Reviewing the present and future, Proc. 29th Inter. Cosmic Ray Conf. (Durban, South Africa), 8, 4-23, 1997.

Smith, E. J., The heliospheric current sheet, J. Geophys. Res., 106, 15819-15832, 2001.

Smith, E. J., The global heliospheric magnetic field in the heliosphere through the solar activity cycle, edited by A. Balogh, Lanzerotti, and Suess, S.T., 79-150, Berlin: Springer, 2008.

Smith, E. J., Balogh, A., Forsyth, R. F., et al., Recent observations of the heliospheric magnetic field at Ulysses: Return to low latitude, Adv. Space Rev., 26, 823-832, 2000a.

Smith, E. J., Jokipii, J. R., Kóta, J., et al., Evidence of a North-South asymmetry in the heliosphere associated with a southward displacement of the heliospheric current sheet, Astrophys. J., 533, 1084-1089, 2000b.

Snyman, J. L., Modeling of the heliosphere and cosmic ray transport, M.Sc. dissertation, North-West University, South Africa, 2007.

Solanki, S. K., Inhester, B., and Schüssler, M., The solar magnetic field, Rep. Prog. Phys., 69, 563-668, 2006.

Steenberg, C. D., Modelling of anomalous and galactic cosmic ray modulation in the outer heliosphere, Ph.D., Potchefstroom University, South Africa, 1998.

Sternal, O., Engelbrecht, N. E., Burger, R. A., et al., Possible evidence for a Fisk-type heliospheric magnetic field. I. Analyzing the Ulysses /KET electron observations, Astrophys. J., 741, 1-12, 2011.

Stone, E. C., Cumming, A. C., and Webber, W. R., The distance to the solar wind termination shock in 1993 and 1994 from observations of anomalous cosmic rays, J. Geophys. Res., 101, 11017-11026, 1996.

Stone, E. C., Cummings , A. C., McDonald, F. B., et al., Voyager 1 explores the termination shock region and the heliosheath beyond, Science, 309, 2017-2020, 2005.

Stone, E. C., Cummings, A. C., McDonald, F. B., et al., An asymmetric solar wind termination shock, Nature, 454, 71-74, 2008.

Stone, E. C., Cummings, A. C., McDonald, F. B., et al., Voyager 1 observes low energy galactic cosmic rays in the region depleted of heliospheric ions, Science, 341, 6142,150-153, 2013.

Strauss, R. D., Modelling of anomalous cosmic rays, M.Sc. dissertation, North-West University, Potchefstroom, South Africa, 2010.

Strauss, R. D., Modelling of cosmic rays in the heliosphere by stochastic processes, Ph.D. thesis, North-West University, Potchefstroom, South Africa, 2013.

Strauss, R. D., and Potgieter, M. S., Where does the heliospheric modulation of galactic cosmic rays starts?, Adv. Space Res., 53, 1015-1023, 2014.

Strauss, R. D., Potgieter, M. S., and Ferreira, S. E. S, the heliospheric transport and modulation of multiple charged anomalous oxygen revisited, Astron. Astrophys., 513, A24:1-6, 2010.

Strauss, R. D., Potgieter, M. S., Ferreira, S. E. S., and Hill, M. E., Modelling anomalous cosmic ray oxygen in the heliosheath. Astron. Astrophys, 522, A35:1-8, 2010.

Strauss, R. D., Potgieter, M. S., Ferreira, S. E. S., Modeling the acceleration and modulation of anomalous cosmic ray oxygen, Adv. Space Res., 48, 65-75, 2011.

Strauss, R. D., Potgieter, M. S., Büsching, I, and Kopp, A., Modelling heliospheric current sheet drift in stochastic cosmic ray transport models, Astrophys. Space Sci., 339, 223-236, 2012.

Strauss, R. D., M. S. Potgieter, and S. E. S. Ferreira, Cosmic ray modulation beyond the heliopause: A hybrid modeling approach, Astrophys. J., 765, 1-6, 2013a.

Strauss, R. D., Potgieter, M. S., and Ferreira, S. E. S., Modeling and observing Jovian electron propagation times in the inner heliosphere, Adv. Space Res., 51, 339-349, 2013b.

Strong, A. W., Bennet, K., Bloemen, H., et al., Diffuse continuum gamma rays from the galaxy observed by COMPTEL, Astron. Astrophys, 292, 82-91, 1994.

Strong, A. W., Moskalenko, I. V., and Reimer, O., Diffuse continuum gamma rays from the Galaxy, Astrophys. J., 537, 763-784, 2000.

Strong, A. W., Moskalenko, I. V., and Ptuskin, V. S., Cosmic ray propagation and interaction in the galaxy, Annul. Rev. Nucl. Part. Sci., 57, 285-327, 2007.

Strong, A. W., Orlando, E., and Jaffe, T. R., The interstellar cosmic-ray electron spectrum from synchrotron radiation and direct measurements, Astron. Astrophys., 534, A54:1-13, 2011.

Teegarden, B. J., McDonald F. B., Trainor, J. H., et al., Interplanetary MeV electrons of Jovian origin, J. Geophys. Res., 79, 3615-3622, 1974.

Teufel, A., and Schlickeiser, R., Analytic calculation of the parallel mean free path of heliospheric cosmic rays. I. Dynamical magnetic slab turbulence and random sweeping slab turbulence, Astron. Astrophys., 393, 703-715, 2002.

Teufel, A., and Schlickeiser, R., Analytic calculation of the parallel mean free path of heliospheric cosmic rays. II. Dynamical magnetic slab turbulence and random sweeping slab turbulence with finite wave power at small wave numbers, Astron. Astrophys., 397, 15-25, 2003.

Usoskin, I. G., History of solar activity over millennia, Liv. Rev. Solar Phys., 10, 1-94, 2013.

Visser, D. J., The effects of turbulence-modified drift on the modulation of cosmic rays in the heliosphere, M.Sc. dissertation, North-West university, South Africa, 2009.

Vos, E. E., Cosmic ray modulation processes in the heliosphere, M.Sc. dissertation, North-West, South Africa, 2011.

Vos, E. E., Potgieter, M. S., Boezio, M., et al. Modulation of galactic electrons during the unusual solar minimum of 2009, Proc. 33rd Inter. Cosmic Ray Conf., (Rio de Janeiro, Brazil), icrc2013-0273, 2013.

Wang, Y. M., Coronal holes and open magnetic flux, Space Sci. Rev., 144, 383-399, 2009.

Wang, Y. M., Semi empirical models of the slow and fast solar wind, Space Sci. Rev., 172, 123-143, 2012.

Webber, W. R., Monte Carlo calculations of cosmic rays in the galaxy. Effect of the source distribution on the age and matter distribution, Astrophys. J., 402, 185-187, 1993.

Webber, W.R., Voyager measurements of galactic cosmic rays and implications for modulation in the heliosheath and beyond, AIP Conf. Proc. 858, 135-140, 2006.

Webber, W. R., and Higbie, P. R., Limits on the interstellar cosmic ray electron spectra below ~1-2 GeV derived from the galactic polar radio spectrum and constrained by new Voyager 1 Measurements, J. Geophys. Res., 113, A11106:1-10, 2008.

Webber, W. R., and Higbie, P. R., Galactic propagation of comic ray nuclei in a model with an increasing diffusion coefficient at low rigidities: A comparison of the new interstellar

spectra with Voyager data in the outer heliosphere, J. Geophys. Res., 114, A02103:1-6, 2009.

Webber, W. R., and Intriligator, D. S., Voyager 1 and 2 observations of cosmic ray intensities in the North-South heliosheath implications for the latitude extent of the heliospheric current sheet and radial structure in the heliosheath , arXi:1403.3322, 2014.

Webber, W. R., and Lockwood, J. A., Voyager and Pioneer spacecraft measurements of cosmic ray intensities in the outer heliosphere: Toward a new paradigm for understanding the global modulation process:1. Minimum solar modulation (1987 and 1997), J. Geophys. Res., 106, 29323-29332, 2001a.

Webber, W. R., and Lockwood, J. A., Voyager and Pioneer spacecraft measurements of cosmic ray intensities in the outer heliosphere: Toward a new paradigm for understanding the global modulation process: 2. Maximum solar modulation (1990-1991), J. Geophys. Res., 106, 29333-29340, 2001b.

Webber, W. R., and McDonald, F. B., Recent Voyager 1 data indicate that on August 25, 2012 at a distance of 121.7 AU from the Sun, sudden and unprecedented intensity changes were observed in anomalous and galactic cosmic rays, Geophys. Res. Lett., 40, 1665-1668, 2013.

Webber, W. R., Potgieter, M. S., and Burger, R. A., A comparison of predictions of a wavy neutral sheet drift model with cosmic ray data over a whole modulation cycle: 1976-1987, Astrophys. J., 349, 634-640, 1990.

Webber, W. R., Lockwood, J. A., McDonald, F. B., et al., Using transient decreases of cosmic ray observed at Voyagers 1 and 2 to estimate the location of the heliospheric termination shock, J. Geophys. Res., 106, 253-260, 2001.

Webber, W. R., Cumming, A. C., McDonald, F. B., et al., Passage of large interplanetary shock from the inner heliosphere to the termination shock and beyond: Its effects on cosmic rays at V1 and V2, Geophys. Res. Lett., 34, L20107:1-4, 2007.

Webber, W. R., Cummings, A. C., McDonald, F. B., et al., Transient intensity changes of cosmic rays beyond the heliospheric termination shocks as observed at Voyager 1, J. Geophys Res., 114, A07108:1-6, 2009.

Webber, W. R., McDonald, F. B., Cumming, A. C., et al., Sudden intensity increases and radial gradient changes of cosmic ray MeV electrons and protons observed at Voyager 1 beyond 111AU in the heliosheath, Geophys. Res. Lett., 39, 1328-1332, 2012.

Wenzel, K. P., Marsden, R. G., Page, D. E., and Smith, E. J., The Ulysses mission, Astron. Astrophys., 92, 207-219, 1992.

Whang, Y. C., and Burlaga, L. F., Anticipated Voyager crossing of the termination shock, Geophys. Res. Lett., 27, 1607-1610, 2000.

Wilcox, J. M., and Ness, N. F., Quasi-stationary Corotating structure in the interplanetary medium, J. Geophys. Res., 70, 5793-5805, 1965.

Williams, T., The influence of the wavy heliospheric current sheet on the modulation of cosmic rays (in Afrikaans), M.Sc. dissertation, Potchefstroom University, South Africa, 1990.

Zank, G. P., Pauls, H. L., Williams , L. L., et al., Interaction of the solar wind with the local interstellar medium: A multi-fluid approach, J. Geophys. Res., 101, 21639-21656, 1996.

Zank, G. P., Matthaeus, W. H., Smith, C. W., et al., Heating of the solar wind beyond 1 AU by turbulent dissipation, AIP Conf. Proc. 471, 523-526, 1999.

Zank, G. P., Li, G., and Verkhoglyadova, O., Particle at interplanetary shock, Space Sci. Rev., 130, 255-272, 2007.

Zieger, B., Opher, M., Schwadron, N. A., A slow bow shock ahead of the heliosphere, Geophys. Res., Lett., 40, 2923-2928, 2013.

Zurbuchen, T. H., A new view of the coupling of the Sun and the heliosphere, Ann. Rev. Astron. Astrophys., 45, 297-338, 2007.

Acknowledgements

I would like to thank the following persons and institutions for support:

- God for His divine Favour, Mercy and His Grace that has brought me this far.
- Prof Marius Potgieter, my supervisor for assistance, his excellent leadership, and motivation throughout this study. I also thank him for giving me more insight about the subject.
- Mr Etienne Vos for his assistance with the model and for useful discussions we had.
- Mrs Petro Sieberhagen, Mrs Lee- Ann van Wyk and Mrs Elanie van Rooyen for all their administrative assistance.
- The Centre for Space Research at the North-West University, the South African National Research Foundation (NRF), South African National Space Agency (SANSA) and the Department of Labour of South Africa for financial support in the form of bursaries throughout my studies.
- Mr Katlego Moloto, Mrs Sannet Taylor, Mrs Elanie van Rooyen and Dr Wilma Baloyi for their friendship, motivation and support.
- I also thank Prof W R Webber for making unpublished Voyager 1 electron data available for this study.

A special thanks to:

- My parents, Gerson and Elisah Nndanganeni, for their unconditional love and support throughout my studies and their love for education.
- My daughter, Zwivhuya, for her love and for inspiring me to want to do more.
- My brother-in law, Mr Thiemuli Nemavhola, for his love and support.
- My sisters, Rudzani Nemavhola and Takalani Nndanganeni, for their love and support.
- My grandmother, Mrs Maria Lithudzha, for all her wisdom and love for education.
- The Letsosa Family in Potchefstroom for your love, support and prayers.

I dedicate this thesis to my whole Family